University of Alberta

Modeling and Mitigation of Transformer Inrush Currents

by

Sami Gabr Abdulsalam ©

A thesis submitted to the Faculty of Graduate Studies and Research
in partial fulfillment of the requirements for the degree of

Doctor of Philosophy

Electrical and Computer Engineering Department

Edmonton, Alberta
Fall, 2007

Library and
Archives Canada

Published Heritage
Branch

395 Wellington Street
Ottawa ON K1A 0N4
Canada

Bibliothèque et
Archives Canada

Direction du
Patrimoine de l'édition

395, rue Wellington
Ottawa ON K1A 0N4
Canada

Your file Votre référence
ISBN: 978-0-494-32907-8
Our file Notre référence
ISBN: 978-0-494-32907-8

NOTICE:
The author has granted a non-exclusive license allowing Library and Archives Canada to reproduce, publish, archive, preserve, conserve, communicate to the public by telecommunication or on the Internet, loan, distribute and sell theses worldwide, for commercial or non-commercial purposes, in microform, paper, electronic and/or any other formats.

The author retains copyright ownership and moral rights in this thesis. Neither the thesis nor substantial extracts from it may be printed or otherwise reproduced without the author's permission.

AVIS:
L'auteur a accordé une licence non exclusive permettant à la Bibliothèque et Archives Canada de reproduire, publier, archiver, sauvegarder, conserver, transmettre au public par télécommunication ou par l'Internet, prêter, distribuer et vendre des thèses partout dans le monde, à des fins commerciales ou autres, sur support microforme, papier, électronique et/ou autres formats.

L'auteur conserve la propriété du droit d'auteur et des droits moraux qui protège cette thèse. Ni la thèse ni des extraits substantiels de celle-ci ne doivent être imprimés ou autrement reproduits sans son autorisation.

In compliance with the Canadian Privacy Act some supporting forms may have been removed from this thesis.

While these forms may be included in the document page count, their removal does not represent any loss of content from the thesis.

Conformément à la loi canadienne sur la protection de la vie privée, quelques formulaires secondaires ont été enlevés de cette thèse.

Bien que ces formulaires aient inclus dans la pagination, il n'y aura aucun contenu manquant.

Canada

Abstract

Transformer inrush currents have always been a concern in the power industry. Over the last decades, a few methods have been proposed to limit transformer inrush currents. The deregulation of the electricity market and the increased awareness of power quality have re-ignited interest in finding more effective and practical methods for controlling inrush currents.

One of this thesis' main objectives was to investigate sequential phase energization aided with a single neutral or series resistor as an effective inrush current mitigation technique. Transformer non-linear characteristics play an essential role in the accurate representation of transformers under inrush and highly nonlinear conditions. A transformer modeling and simulation technique was developed for the stable and accurate simulation of transformer behavior during inrush current conditions. Moreover, a novel technique was developed for estimating transformer saturation characteristics from measured terminal voltages and currents during transformer energization.

The effectiveness of the sequential energization inrush mitigation technique was verified through experimental, simulation, and sensitivity studies. With the neutral-resistor-based scheme, it was found that the neutral grounding resistor acts similarly to a series resistor during sequential phase energization and that the first phase energization leads to the highest inrush level. The single, series-resistor scheme provides a solution for inrush current mitigation in transformers with un-grounded primaries. Both schemes were found to be capable of reducing inrush current magnitude by 80-90%, depending on the application and

transformer type. A detailed analysis of the techniques transient performance led to the development of a solid design guide for the size of the resistor involved.

The study of the sequential energization technique was further extended to capacitor energization application. With optimally-sized neutral impedance, sequential energization was found to be capable of achieving close-to-synchronous energization conditions. The scheme performance is presented together with the design guidelines for the neutral grounding impedance.

Acknowledgements

First and foremost, I would like to thank and Praise Allah almighty for enlighting my way and directing me through each and every success I have or may reach.

I would like to thank and express my deep appreciation to my supervisor, Prof. Wilsun Xu, for all his encouragement, support, guidance and patience during my study at the University of Alberta. It has been my honor and privilege to work under his supervision. His enthusiasm, guidance and insight throughout the duration of this study were invaluable to me.

I would also like to thank Dr. Washington Neves, Brazil, for all of his guidance and fruitful discussions. His advice and encouragement have been invaluable to me during the one year period he spent with us at the power lab.

It has been a great opportunity to work with my colleagues in the power quality research group. I would like to thank all of them especially Dr. Tarek Kandil, Dr. Emad Ahmed, Yu Cui, Jacek Kliber and Ali Arefifar for their cooperation and valuable discussions, providing a great environment in the power lab. My thanks also go to Albert Terhide for all his help during my experimental work.

Thanks are due to Enppi, Egypt, for their support in giving me the opportunity to pursue my Ph.D. degree. The financial support I received from the University of Alberta throughout my program is highly appreciated.

Words cannot express my sincere gratitude, thanks and love to my father and mother for all their endless encouragement, support and love for my entire life. I got from my father, Dr. Gabr Abdulsalam the strength, inspiration and the spirit of challenge that enabled me to complete this work.

Finally, I would like to express my appreciation to my wife, Heba. Without her endless support, patience and encouragement, this work would have never been completed. I am indebted to her for standing beside me while I spent these years working on this project. To her, my son Youssef and my daughter Sana, I dedicate this work.

Table of Contents

1. Introduction 1

    1.1 Transformer Inrush Currents and Impact on System Performance 1

    1.2 Available Mitigation Techniques 4

    1.3 The Sequential Switching Mitigation Technique 9

    1.4 Research Objectives 13

    1.5 Thesis Contributions and Outline 14

2. Transformer Inrush Current Phenomena and Its Analysis 18

    2.1 Introduction 18

    2.2 Characteristics of the Saturable Inductor 20

    2.3 Factors affecting inrush current magnitude 23

        2.3.1 Instant of Switching 24

        2.3.2 Residual Flux and Saturation Characteristics 28

        2.3.3 Series Impedance 31

    2.4 Single Phase and Simultaneous Three Phase Energization Inrush Current 32

    2.5 Conclusions 43

3. Transformer Modeling and Simulation for Inrush Current Studies 44

    3.1 Introduction 44

    3.2 Transformer Model Description 47

    3.3 Transformer Model Implementation 50

        3.3.1 Model Linearization 50

        3.3.2 Representation of Reluctance Curves 53

        3.3.3 Solution Methodology 55

    3.4 Simulation Results 58

    3.5 Conclusions 63

4. Estimation of Transformer Saturation Characteristics from Inrush Waveforms 64

4.1 Introduction 64

4.2 Parameter-Estimation Algorithm 67

4.3 Calculation of Magnetizing Current 71

4.4 Residual Flux Estimation 74

4.5 Model Verification and Simulation Results 77

4.5.1 Estimated Reluctance-Flux Curves 78

4.5.2 No-Load Operation 83

4.5.3 Single-Pole Switching 83

4.5.4 Simultaneous three-pole switching 84

4.6 Conclusions 87

5. Performance of the Sequential Energization Scheme 88

5.1 Introduction 88

5.2 Scheme Performance 90

5.2.1 Experimental Results 90

5.2.2 Simulation Results 102

5.3 Sensitivity Analysis 108

5.4 Conclusions 116

6. Transient Analysis of the Sequential Energization Scheme and Design Guide 120

6.1 Introduction 121

6.2 Analysis of First-Phase Energization 123

6.3 Expression for Inrush Current Peak 127

6.4 Investigation of Second Phase Switching Inrush Current 133

6.4.1 Three Single Phase Units Connected in Yg-Y 134

6.4.2 Three single Phase Units Connected in Yg-Δ or 3 Limb, Yg-Y or Yg-Δ 142

6.4.3 Effect of Delta Winding Connection 147

6.5 Neutral Resistor Sizing 154

6.6 Neutral Voltage Rise 157

6.6.1 IEEE/ANSI Standards for the Neutral Terminal Insulation 161

6.6.2 Surge Arrester Application to limit Neutral Voltage Rise 164

6.6.3 Saturable-Inductor Grounding Application to limit Neutral Voltage Rise 170

6.7 Energy Requirements for the Neutral Grounding Resistor/Arrester Scheme ... 173

6.7.1 Literature Review and Industry Practice 174

6.7.2 Energy Requirements for Neutral Grounding Resistor 178

6.8 Considerations on Ferroresonance 181

6.9 Conclusions 183

7. Single Pre-Insertion Resistor with Sequential Switching 184

7.1 Introduction 184

7.2 Experimental and Simulation Results 186

7.2.1 Y-Δ Connection (energizing from Y side) 187

7.2.2 Δ-Y Connection (energizing from Δ side) 188

7.2.3 Yg-Δ Connection (energizing from Yg side) 190

7.3 Theoretical Analysis and Resistor Sizing 192

7.3.1 Y-Δ Connection (energizing from Y side) 192

7.3.2 Δ -Y Connection (energizing from Delta side) 197

7.3.3 Yg -Δ Connection (energizing from Yg side) 199

7.4 Considerations on Ferroresonance 200

7.5 Conclusions 206

8. Application for Capacitor Switching Transients Mitigation 207

8.1 Introduction 207

8.2 Scheme Arrangement and Theoretical Analysis 209

8.3 Neutral Impedance Sizing 215

8.3.1 Single-stage R-L neutral impedance 215

8.3.2 Dual-stage R-L neutral impedance 217

8.4 Scheme Performance and Transient Simulation Study 219

8.4.1 Instantaneous Switching with solid ground: 221

8.4.2 Sequential switching with single-stage neutral impedance: 222

8.4.3 Sequential switching with dual-stage neutral impedance: 224

8.5 Impact on Voltage Magnification 225

8.6 Conclusions 229

9. Conclusions and Recommendations 230

10. References 238

List of Figures

Figure 1.1 The sequential phase energization scheme aided with an optimally-sized grounding resistor (top) and with a single pre-insertion resistor (bottom). 10

Figure 2.1 Nonlinear Flux-Current characteristics. 19

Figure 2.2 Saturation Curve of Iron, Showing "Regions" and the Corresponding Fictitious Equivalent of a Saturable Reactor, [49]. 21

Figure 2.3 Influence of the switching angle α on the flux build up in the core. 24

Figure 2.4 Calculation of the maximum inrush current magnitude using the maximum flux build-up and simplified saturation characteristics. 26

Figure 2.5 Theoretical maximum flux build-up limit and the corresponding peak inrush current as affected by the instant of switching, α. $\phi_s = 1.2(p.u.)$ 27

Figure 2.6 Influence of the residual flux ϕ_r on the flux build up in the core. 28

Figure 2.7 Theoretical maximum flux build-up limit and the corresponding peak inrush current as affected by the residual flux $\phi_r = +0.7(p.u.)$ and the instant of switching, α. $\phi_s = 1.2(p.u.)$ 30

Figure 2.8 Supply voltage 'top' and the theoretical induced flux assuming zero-residual pattern 'middle' and with residual flux 'bottom' in the transformer cores during energization of Yg-Δ bank. 35

Figure 2.9 Distribution of current among 3-phase bank, Y-Δ windings due to saturation of Phase A with phases B and C unsaturated (low residual flux pattern). 36

Figure 2.10 Maximum inrush condition, 3-Phase Transformer, Y-Δ connection. Terminal Phase voltage 'top', Inrush Currents 'middle' and Neutral Voltage 'bottom'. 39

Figure 2.11 Distribution of current among 3-phase bank, Δ -Y windings due to saturation of Phase A with phases B and C unsaturated (zero residual flux pattern). 40

Figure 2.12 Maximum inrush condition, 3-Phase Transformer, Δ–Y connection. Terminal line voltage 'top', Line Inrush currents 'middle' and Phase Inrush currents 'bottom'. 42

Figure 3.1 Transformer electrical equivalent circuit (per-phase) referred to the primary side. 47

Figure 3.2 Equivalent magnetic circuit and flux distribution for a three-limb, three-phase transformer. 47

Figure 3.3 The fitted $\mathcal{R} - \phi$ curve for a typical three limb transformer. 54

Figure 3.4 Phase inrush currents for instantaneous three phase switching using the predictor corrector scheme 'shadowed' and the Newton Raphson scheme 'solid' for the transformer given in [53] and [56]. 59

Figure 3.5 Instantaneous three phase switching of Yg-Δ transformer described in appendix. 60

Figure 3.6 Instantaneous switching of the transformer described in [54] using 9-segment piecewise reluctance-flux curves. 62

Figure 4.1 Approximate equivalent magnetic circuit for the three limb, E core, three-phase transformer. 68

Figure 4.2 Equivalent electric circuit for a Wye-Delta transformer. 73

Figure 4.3 Flux-Current characteristics obtained for different cases assuming zero residual flux. 75

Figure 4.4 Estimating the residual flux value from No-Load Flux-Current curve and calculated flux-current curve during inrush conditions. 76

Figure 4.5 Calculated Hysteresis loop for the transformer under test. 78

Figure 4.6 Reluctance-Flux characteristics obtained for the transformer under test using No-Load waveforms. 79

Figure 4.7 Flux-Current characteristics obtained for the highest recorded inrush peak considering the calculated residual fluxes. 79

Figure 4.8 Reluctance-Flux characteristics obtained for the highest recorded inrush peak considering the calculated residual fluxes. 80

Figure 4.9 Flux-Current characteristics obtained for Wye-Delta connection and using simultaneous three-pole switching. 81

Figure 4.10 Reluctance-Flux characteristics obtained for Wye-Delta connection and using simultaneous three-pole switching. 81

Figure 4.11 Reluctance-Flux characteristics obtained for central and outer limbs of the transformer given in Appendix. 82

Figure 4.12 Measured and simulated No-Load current. 83

Figure 4.13 Simulated 'solid' and Measured 'dotted' highest inrush waveforms using the obtained Reluctance-Flux characteristics. 84

Figure 4.14 The first cycle of the simulated 'solid' and recorded 'dotted' mid-range inrush using single phase switching. 84

Figure 4.15 Recorded 'dotted' and simulated 'solid' energizing inrush currents for Wye-Delta connection. 85

Figure 4.16 Recorded 'dotted' and simulated 'solid' energizing inrush currents for Wye-Wye connection. 86

Figure 5.1 Recorded simultaneous energizing phase voltages for Yg-Y transformer. 91

Figure 5.2 Recorded simultaneous energizing phase currents for Yg-Y transformer 92

Figure 5.3 Magnitude of inrush current as affected by the neutral resistor, for Yg-Δ connection, positive sequence switching order. 92

Figure 5.4 Magnitude of inrush current as affected by the neutral resistor, for Yg-Δ connection, positive sequence switching order. (Enlarged Portion) 93

Figure 5.5 Extended 2nd and 3rd $I_{max}(R_n)$ curves, for Yg-Δ connection, positive sequence switching order. 94

Figure 5.6 Flux distribution after energizing phases A and B. 95

Figure 5.7 Magnitude of inrush current as affected by the neutral resistor, for Yg-Δ connection, negative sequence switching order. 96

Figure 5.8 Magnitude of inrush current as affected by the neutral resistor, for Yg-Δ connection, negative sequence switching order. (Enlarged Portion) 96

Figure 5.9 Typical inrush current waveform during 1st phase energization, R_n=2.0Ω. 97

Figure 5.10 Typical inrush current waveforms (top) and the neutral current (bottom) during 2nd phase energization, R_n = 2.0 Ω. 98

Figure 5.11 Inrush current waveforms (top) and the neutral current (bottom) during 2nd phase energization, R_n = 0.25Ω. 99

Figure 5.12 Inrush current waveforms (top) and the neutral current (bottom) during 2nd phase energization, R_n = 0.5Ω. 99

Figure 5.13 Inrush current waveforms (top) and the neutral current (bottom) during 2nd phase energization, R_n =50Ω. 100

Figure 5.14 Inrush current waveforms (top) and the neutral current (bottom) during 3rd phase energization, R_n = 2.0 Ω. 101

Figure 5.15 Sequential energization scheme performance through simulation for; First (Top), Second (Center) and Third (Bottom) energizing stages, R_n=2.0Ω. 103

Figure 5.16 Magnitude of inrush current as affected by the neutral resistor, for Yg-Δ connection, positive sequence switching order. 104

Figure 5.17 Magnitude of inrush current as affected by the neutral resistor, for Yg-Δ connection, positive-sequence switching order. (Enlarged Portion) 105

Figure 5.18 Extended $I_{max}(R_n)$ performance curves for a positive-sequence switching order. 105

Figure 5.19 Magnitude of inrush current as affected by the neutral resistor, for Yg-Δ connection, negative-sequence switching order. (Enlarged Portion) 105

Figure 5.20 $I_{max}(R_n)$ performance curves for the 138MVA, 72/13.8 kV, Yg-Δ transformer with a positive -sequence switching order. 106

Figure 5.21 $I_{max}(R_n)$ performance curves for the 138MVA, 72/13.8 kV, Yg-Δ transformer with a positive -sequence switching order. (Enlarged Portion) 106

Figure 5.22 Maximum inrush current as affected by the neutral resistor, for 3x300MVA, 199.2/13.8kV, Yg-Δ connection, positive-sequence switching order. 107

Figure 5.23 Maximum inrush current as affected by the neutral resistor, for 3x300MVA, 199.2/13.8kV, Yg-Y connection, positive-sequence switching order. 108

Figure 5.24 Measured saturation curve for 1 MVA, Yg-Δ 3-Limb transformer, [32]. 109

Figure 5.25 First and Second phase switching $I_{max}(R_n)$curves for saturation starting at 1.35 p.u (Top). Enlarged portion (Bottom) showing the intersection points of the curves (around 80 Ohms) 110

Figure 5.26 First and Second phase switching $I_{max}(R_n)$curves for saturation starting at 1.25 p.u. 112

Figure 5.27 First and Second phase switching $I_{max}(R_n)$curves for saturation starting at 1.25 p.u (Top). Enlarged portion (Bottom) showing the intersection points of the curves (around 30-40 Ohms). 112

Figure 5.28 $I_{max}(R_n)$curves for saturation starting at 1.25 p.u. First phase energization (Top) and second phase (Bottom). 114

Figure 5.29 $I_{max}(R_n)$curves for saturation starting at 1.35 p.u. First phase energization (Top) and second phase (Bottom). 115

Figure 6.1 Simplified equivalent circuit for the energization of the first phase and the corresponding characteristics. 123

Figure 6.2 Simplified equivalent circuit for the energization of the first phase 125

Figure 6.3 (a) Magnetic circuit with flux distribution during first-phase switching and (b) Simplified equivalent magnetic circuit. 125

Figure 6.4 Normalized exponential (top) and complete inrush waveforms for a saturation angle of 45 electrical degrees. 129

Figure 6.5 Normalized exponential (top) and complete inrush waveforms for a saturation angle of 70 electrical degrees. 130

Figure 6.6 Normalized inrush current waveforms showing exponential and sinusoidal components for saturation angles of 70 and 45 electrical degrees. 131

Figure 6.7 $I_{Pk}(R)$ compared to the experimental inrush peak current for the 30 kVA, 208/208 Yg-Δ, three limb transformer. 132

Figure 6.8 Sequential energization of a 3-phase transformer consisting of three Single-Phase units with a neutral grounding resistor. 135

Figure 6.9 Equivalent electric circuit for three phase transformers, Yg-Δ connection. 143

Figure 6.10 Simulation of the 3x300MVA, Yg-Y transformer, [10], during second phase switching for $R_n = 150$ [Ω]. 147

Figure 6.11 Electrical equivalent circuit for the transformer during second phase switching and under saturation condition of un-energized phase C. 148

Figure 6.12 Modeling of the Delta winding during saturation condition of Phase C. 151

Figure 6.13 Simulation of the 30kVA, 208/208V, E-Core transformer for the second phase switching condition showing the effect of Delta winding current for $R_n = 0.1$ (Ω). 153

Figure 6.14 Neutral voltage peak as function of R_n during the first and second switching stages for the 132.8 MVA transformer. 158

Figure 6.15 Phase currents, neutral current and neutral voltage during complete switching sequence for the 132.8, Yg-Δ transformer, $R_n = 50\Omega$. 159

Figure 6.16 first phase energization $I_{max}(R_n)$performance curves with different residual flux levels for the Hyundai, 72/13.8 kV, 132.8 MVA transformer. 160

Figure 6.17 Neutral voltage rise curves for the first switching stage with different residual flux levels for the Hyundai, 72/13.8 kV, 132.8 MVA Transformer. 160

Figure 6.18 Modeling of surge arresters before and after saturation. 165

Figure 6.19 First phase energization $I_{max}(R_n)$curves with different arrester saturation voltages for the 132.8, Yg-Δ transformer. 166

Figure 6.20 First and second phase energization $I_{max}(R_n)$curves with different arrester saturation voltages for the 132.8, Yg-Δ transformer. 167

Figure 6.21 Phase currents, neutral current, and neutral voltage during complete switching sequence $R_n = 50\Omega$. Arrester saturation voltage is 0.5 (p.u.) for the 132.8MVA, Yg-Δ transformer. 168

Figure 6.22 First phase energization $I_{max}(R_n)$curves showing the effect of arrester 50%saturation voltage with different residual flux levels for the 132.8, Yg-Δ transformer. 169

Figure 6.23 Inrush currents $I_{max}(R_n)$ performance curves during 1st and 2nd switching phases. Reactor series resistor designed of ~0.55pu rise during first switching for the 30kVA, laboratory transformer. 171

Figure 6.24 Neutral voltage magnitudes during 1st and 2nd switching phases. Reactor series resistor designed for ~0.55pu rise during first switching phase Inrush currents for the 30kVA, laboratory transformer. 171

Figure 6.25 Saturable Reactor performance during the first phase switching. (please note the magnitude of the neutral voltage after the first cycle and the duration of the overvoltage). 172

Figure 6.26 Saturable Reactor performance during the second phase switching. (please note the magnitude of the neutral voltage before switching phase 2 and after switching 2nd phase. 173

Figure 6.27 Accumulated energy during different switching stages. Results are for the 132.8 MVA transformer with infinite system. 178

Figure 6.28 Accumulated energy during different switching stages [J]. Arrester set at 0.5 [p.u.] saturation voltage with 1000MVAsc system. 180

Figure 6.29 Voltage at the primary side of a 22/0.48, 160kVa, Y-Δ transformer due to energizing Phase A. Top: Isolated neutral. Bottom: Neutral grounding. 181

Figure 7.1 Single pre-insertion resistor sequential energization technique for inrush current reduction. 185

Figure 7.2 The performance of the pre-insertion scheme as applied to a 208/208, 30kVA, E-core,Y/Δ transformer. (Energizing from Y side). 187

Figure 7.3 The performance of the pre-insertion scheme as applied to a 208/208, 30kVA, E-core, Δ/Yg transformer. 189

Figure 7.4 The performance of the pre-insertion scheme as applied to a 208/208, 30kVA, E-core, Yg/Δtransformer. 190

Figure 7.5 Equivalent circuit for the analysis of the pre-insertion resistor scheme during first stage switching. (Energizing from Y side). 192

Figure 7.6 Equivalent circuit for the analysis of the pre-insertion resistor scheme during first stage switching. (Energizing from Δ side). 197

Figure 7.7 Development of ferroresonance in delta connected winding. (Energizing from Δ side). 202

Figure 7.8 Damped fundamental Ferroresonance condition during sequential energization and a series resistor of 4.0 (Ω). From top to bottom; terminal voltage, inrush current, core flux and the V-ϕ loops. 203

Figure 7.9 Experimental $I_{max}(R_s)$performance curve trials during second phase energization with a single series resistor. (Energizing from Yg side). 204

Figure 7.10 Sub-harmonic ferroresonance condition during sequential energization and a series resistor of 4.0 (Ω). From top to bottom; terminal voltage, inrush current, core flux and the loops. 205

Figure 8.1 The sequential energization scheme for capacitor switching transients mitigation. 209

Figure 8.2 Open circuit voltage as affected by the neutral impedance for (top) second phase switching ΔV_{2-}, (middle) second phase switching ΔV_{2+} and (bottom) Third phase switching ΔV_3. 214

Figure 8.3 Open circuit voltages ΔV_{2-} , ΔV_3, and the objective function f_{Voc}. 217

Figure 8.4 Scheme 2 for mitigating capacitor switching transients using dual stage neutral impedance. 218

Figure 8.5 IEEE 13-Bus industrial test system. 220

Figure 8.6 Instantaneous switching performance: (a) Phase voltage, transient voltage and phase currents during a complete switching sequence. (b) Transient overvoltage magnitude V_d against disturbance duration, τ_d. 221

Figure 8.7 Single-stage neutral impedance mitigation technique: (a) Phase voltage, transient voltage and phase currents during a complete switching sequence. (b) Transient overvoltage magnitude V_d against disturbance duration, τ_d. 223

Figure 8.8 Dual-stage neutral impedance mitigation technique: (a) Phase voltage, transient voltage and phase currents during a complete switching sequence. (b) Transient overvoltage magnitude V_d against disturbance duration, τ_d. 225

Figure 8.9 Voltage at the utility capacitor bus (top) and magnified voltage at customer bus 13 (bottom). 227

1. Introduction

This chapter presents an introduction to inrush current phenomena in power transformers, and a review of available mitigation techniques. The chapter starts with a discussion of the diverse effect of inrush currents on power system performance and their impact on transformer reliability and lifetime. A brief introduction to the mechanism of inrush current development in power transformers is presented, followed by a thorough review of the available inrush current mitigation techniques and the present state-of-the-art in the field. The sequential energization scheme is also presented, and the thesis' main research objectives are explained. The chapter concludes by presenting this thesis' main contributions and an outline of the thesis, with a brief description of each of the chapters to follow.

1.1 Transformer Inrush Currents and Impact on System Performance

Power transformers are critical components in power-system networks and are the most expensive equipment in substations. These transformers are used for different purposes and configurations and they may be energized either occasionally (yearly) or frequently (daily). The Un-controlled energization of transformers produces high inrush currents, which can reduce the transformers' residual life due to the high mechanical stresses involved, and can also lead to the unexpected operation of protective relays and power-quality reduction [1] and [2].

Normally, during energization, the core flux is non-sinusoidal, being saturated in one polarity which results in a direct current component. The high non-linearity of the iron core reflects into a current waveform that is rich in harmonics. The typical harmonic content of a transformer inrush waveform includes 62% of 2nd harmonic and 55% of DC component of the fundamental power frequency [3]. In addition, inrush currents caused by transformer energization can reach magnitudes of 10 or 20 times the nominal Full-Load current of a transformer [4], [5], [6] [7], [8], [9] and [10]. Inrush current levels as high as 26 to 40 times the rated current has been reported in [4] and [8], respectively. As well, inrush currents can approach 70 to 90% of the short circuit current level [9] and [15]. Moreover, the duration of inrush currents may last from tens of cycles up to few minutes for large power transformers [1].

The nature of inrush currents which include a high current magnitude rich in harmonics coupled with relatively a long duration as compared to that of the short circuit current level, leads to adverse effects on the transformer itself as well on to the protection system's performance and power quality. On the transformer side, the mechanical stresses imposed on the windings approach those caused by short-circuit currents [11], [12] and [9]. Transformers are more subjected to switching operations, and, consequently, inrush currents. The compression of transformer windings during inrush conditions increases the risk of insulation failure [11].

One of the major problems with transformer inrush currents is the false operation of protection during inrush conditions. This subject has been of great interest to many researchers [3], [4], [13], [14], [16], [17], [18], and [19]. As well, winding movement due to inrush current can cause the operation of over-pressure protection [20].

The Power-quality consequences of inrush currents can be quite serious [21]. Examples include the overrating of fuses and difficulties with fuse coordination, temporary over-voltages (TOV's), voltage sags and motor tripping. High current magnitudes drawn from the energizing system side will cause voltage sags of long duration on nearby busses. Voltage sag levels of 20% on a system's bus were reported in [4]. The reduced voltage magnitude might result in motor and sensitive load tripping. Additionally, voltage sag during inrush conditions might lead to sympathetic inrush phenomena in nearby transformers during voltage recovery [22], [23], [24], [25] and [26].

In the power-system industry, two different strategies have been implemented to tackle the problem of transformer inrush currents. The first strategy focuses on adapting to the effects of inrush currents by desensitizing the protection elements when transformer units are energized. Other approaches go further by 'over-sizing' the magnetic core to achieve higher saturation flux levels. These partial countermeasures impose downgrades on the system's operational reliability, result in considerable increases in the unit cost, expose the transformer to high mechanical stresses and lead to a lower quality of power. As mentioned earlier, higher mechanical stresses can lead to displacement in the transformer core windings and the possibility of a fire hazard in the transformer.

The second strategy focuses on reducing the inrush current magnitude itself during the energization process. Minimizing the inrush current will extend the transformer's lifetime and provide better system performance and lower maintenance and down-time costs. As well, an effective mitigation technique will increase the reliability of operation, since the problem of protection-system malfunction is eliminated during transformer energization.

1.2 Available Mitigation Techniques

Over the past several decades a few methods have been proposed to control transformer inrush currents. Representative examples are the pre-insertion of closing resistors and the controlled closing of circuit breakers. Other methods tend to reduce inrush currents indirectly by reducing the residual flux magnitude in the transformer core. Generally, in order to limit transformer inrush currents, the transformer core should be kept from reaching high levels of flux during the energization process. In this section, a review of the available inrush current mitigation techniques will be presented together with the industry practice.

Closing Resistors for Inrush Current Reduction:

The pre-insertion scheme, which is a classical control strategy, is based on temporarily inserting series impedance(s) in-series-with the switched equipment during energization. Circuit breakers equipped with closing resistors initially insert these impedances in series with each phase of the switched equipment and after some time delay, in the order of several milliseconds are bypassed through additional shunting switches. Switching devices for transmission lines' overvoltage reduction, capacitor energization, and harmonic filters energization are commonly equipped with closing resistors [27]. Closing pre-insertion resistors have also been used as well for transformer inrush current reduction [28], [13] and [30]. However, the resistance size required to achieve an acceptable reduction in inrush current is generally higher and requires longer insertion time than that used for line energization applications, [13], [18] and [28]. Typically, pre-insertion resistor size of 300-400 ohms with insertion times of 8 ms is implemented for transmission line energization applications, [7]. Insertion times of 7 to 12 cycles are typical for capacitor-energizing applications [27] and

[29]. For transformer-energization applications, pre-insertion resistor values from 3,000 to 7,000 ohms and insertion times of 15 to 25 ms have been reported in the literature [18].

The closing resistor scheme, although it can effectively reduce inrush current with a sufficiently sized resistor, has two major drawbacks. First, the closing resistors need to be shorted-out after the energization process is complete. Doing so requires three additional breaker contacts, which increase the complexity of the moving mechanism and maintenance costs [31]. In addition, the increased number of the switching elements and the fault-current tolerance of the resistors reduce the breaker's reliability [27] and [31]. The second drawback is related to cost, for a breaker equipped with closing resistors costs 20-25% more than breakers with no closing resistors [6] and [27].

Controlled Closing of Circuit Breaker:

Since the early nineties and due to the developments in high-speed circuit-breaker technology, controlled closing has been successfully implemented in the power industry for capacitor, reactor and transmission line energization applications [7] and [27]. Basically, individual pole contacts are precisely controlled to close at a certain instant on the supply voltage waveform, at which energizing transients are eliminated or, at least, minimized. The application of controlled closing to capacitor and transmission line energization is quite straightforward and depends directly on the speed and mechanical scatter characteristics of the circuit breaker used [22], [27], [32], [33] and [34].

However, for applications with transformer energization, the problem is much more difficult due to the existence of an unknown residual flux magnitude and polarity in the transformer magnetic core. If a transformer is energized at an instant where its flux waveform does not reach the saturation level, inrush currents will not be produced. Accordingly, with an accurately known residual flux pattern in the core, the instant of switching of each phase could be optimized to achieve an induced steady-state flux and, consequently, eliminate the inrush current. This process is the basis of the controlled switching schemes to mitigate inrush currents [34], [35], [36] and [37].

In the past, the development of such a scheme was limited by the speed and accuracy of the available circuit-breaker technology as well as the lack of an efficient method to measure or estimate the residual flux at the instant of energization. It was stated in [35] that due to the delay introduced by the mechanical breaker, a small shift in the switching angle might result. Developments in circuit-breaker technology resulted in fast and reliable circuit-breaker operation, which eliminated the problem of speed. Recent studies showed that this delay can be in the range of 0.28 ms, which causes a shift of about 6 electrical degrees for modern high-speed circuit breakers [21]. A lower reduction rate of the inrush currents might be achieved if the amount of residual flux were not accounted for in the control scheme. Since no accurate means was available to determine the residual flux in the transformer core, the energization instants were not optimally selected [6] and [27].

Although, no efficient way has been found to measure residual flux directly, the microprocessor-based computational power available today can provide means of estimating the amount of residual flux resulting from the previous de-energizing process. In [38], a method for estimating the residual flux level from the de-energization voltage waveforms measured across the windings closest to the core was presented. However, due to the effect of grading and system capacitance, the amount of the residual flux in the core during the following energization process could be smaller than that estimated from the previous de-energization event [34] and [39]. Accordingly, the actual residual flux in the transformer core at the following energization event will be different than the estimated value, and, hence, the scheme will be inaccurate.

Applying controlled de-energization and energization was proposed in [6] to overcome the problem of residual flux estimation. It was shown that controlling the de-energization event could lead to a pre-determined residual flux pattern and, accordingly, eliminate the problem of measuring or estimating it. The implemented method controls the switching-off instant to achieve the lowest possible residual flux in the transformer core, and, hence, its effect can be neglected while optimizing the following switching event based on the assumption of zero residual. However, controlled de-energization could not be implemented in forced outages due to protective relay operation. Current chopping while interrupting the low excitation current can prevent the controlled de-energization solution from being successful [7] and [40].

Even though synchronous switching can be theoretically implemented with the knowledge of the residual flux to completely eliminate inrush currents, some conditions can exist where the full control of the breaker-switching instant cannot be adopted. The presence of slow circuit breakers and breakers with staggered pole closing could prevent the application of controlled closing. Moreover, for transformers with multi-limb cores, more details about the magnetic structure and characteristics of each core leg should be known and considered when applying controlled closing. This information is necessary for completing the switching of the second and third pole closures as the flux will be forced into the un-energized core legs depending on the core topology [35] and [36].

Reduction of Residual flux

A number of methods have been reported in the literature for reducing the residual flux and, consequently, limiting the maximum flux build-up leading to a reduction in inrush current magnitude.

One of the common known methods for lowering the residual flux in the core is the use of a variable source to gradually decrease the supply voltage across the transformer's terminals and, consequently, the flux in the core [41]. However, this method is applicable only at research laboratories and is not of interest for practical application.

Another strategy is to allow the transformer's magnetizing current and, consequently, the core flux, to slowly discharge in parallel connected capacitors after de-energization [4], [7], [27] and [41]. The minimum kVA rating of such capacitor banks was found to be in the order of 40% to 100% of the magnetizing kVA of the transformer [27], [41]. Regardless of the method implemented, the elimination of residual flux lowers the maximum flux to just 2.0 (p.u.). As a result, this scheme is not an attractive solution for inrush reduction unless combined with other inrush-control schemes.

Neutral Resistors for Inrush Current Reduction

The neutral resistance's impact on the magnitude of inrush currents in transformers was studied earlier in [30]. As a minimum, the neutral resistor was expected to have some reduction on the inrush current duration. After several experimental and simulation tests, it was found that a neutral resistor of a few ohms together with '*simultaneous*' switching didn't have any effect on either the magnitudes or the time constant of inrush currents. The pre-insertion resistors were recommended as the most effective means of controlling inrush currents. The impact of the neutral resistor on transformer inrush currents was briefly investigated in [28]. Through simulations, it was found that the neutral resistor had little effect on reducing the inrush current peak or even the rate of decay as compared to the cases without a neutral resistor. The use of neutral impedances was concluded to be ineffective compared to the use of pre-insertion resistors. This finding was explained by the low neutral current value as compared to that of high phase currents during inrush. It was mentioned that due to the cancellation effect of the three phase currents in the neutral, insufficient voltage was present across the neutral resistance to have any effect on either the inrush magnitude or the rate of decay. It has never been reported in the literature that inrush currents could be eliminated by using a *neutral resistor* only if *sequential switching* is implemented.

1.3 The Sequential Switching Mitigation Technique

In today's highly challenging power-system industry, many utilities have an urgent need to increase the availability and reliability of energy supplies in ageing electrical infrastructures. Adaptations are required to operate in a deregulated, competitive market where switching operations tend to be more frequent. Community opposition and environmental-impact considerations have limited the efforts to expand and re-enforce these networks.

Today, two recent developments in the power industry have re-ignited interest in finding better methods for controlling inrush currents. The deregulation of the electricity market is one of the main reasons for this interest, for more independent power producers and co-generators are taking advantage of this situation. Their proposed generators often need to have the generator transformers energized from the system side due to cost considerations.

Doing so results in the problem of large inrush currents being injected into the supply system. Another development is the increased awareness of power quality and the need to follow strict standard limits to avoid penalties. For these reasons, simpler and lower-cost schemes must be found to limit transformer inrush currents. Independent power producers are especially interested in such techniques.

This work investigates a novel sequential switching inrush-current mitigation technique that is a reliable, simple and cost-effective alternative to the currently available techniques, Figure 1.1. The sequential switching technique, as will be shown, was evaluated through experimental, simulation and analytical studies during the course of this work.

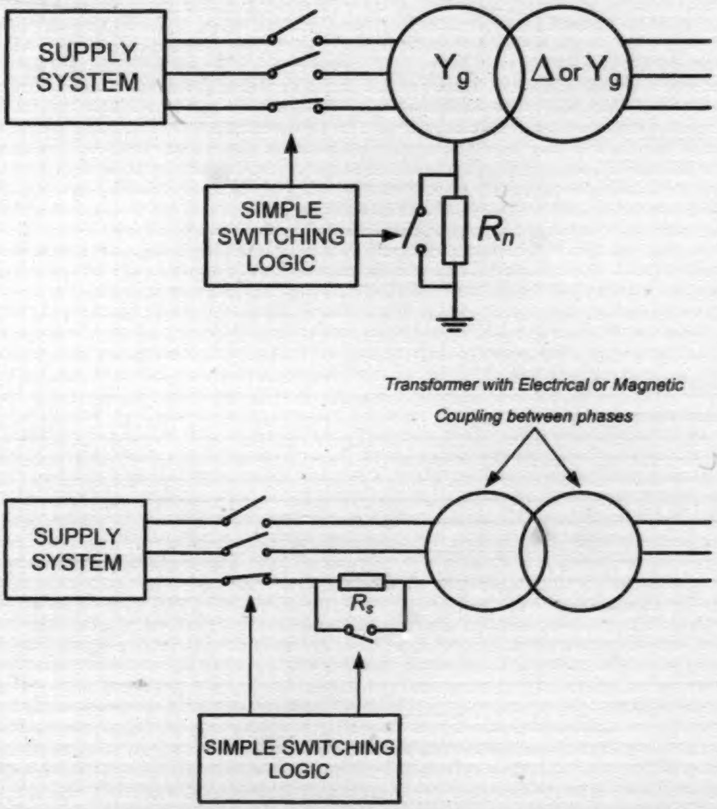
SUPPLY SYSTEM
Y_g
Δ or Y_g
SIMPLE SWITCHING LOGIC
R_n
Transformer with Electrical or Magnetic Coupling between phases
SUPPLY SYSTEM
R_s
SIMPLE SWITCHING LOGIC

Figure 1.1 The sequential phase energization scheme aided with an optimally-sized grounding resistor (top) and with a single pre-insertion resistor (bottom).

The sequential energization scheme was found to be capable of reducing the magnitude of inrush currents by 80% to 90%, depending on the transformer connection and the core structure type. Such an inrush-reduction rate makes the scheme as effective as the pre-insertion closing resistor and the controlled closing scheme, which were reported in literature. The scheme, as shown in Figure 1.1, involves the sequential energization of the three phases of the switched equipment, together with the insertion of a properly sized series/neutral resistor.

For the neutral resistor based scheme, during the sequential switching of phases, a neutral current will flow through the neutral grounding resistor, and a resulting neutral point voltage of the same shape as that of the neutral current scaled by the neutral resistor 'R_n' magnitude will be established. Generally, for the most severe cases in which the switched supply voltage has the same polarity as the residual 'or initial' flux in the switched transformer leg, the inrush current waveform will also have the same polarity as the supply system voltage, and, hence, the net voltage across the transformer terminals will be reduced. Accordingly, the voltage across the switched equipment phase can be controlled through proper sizing of the neutral resistor.

The type of voltage control achieved through the neutral resistor depends upon the scheme's desired application. For transformer inrush current mitigation, the neutral resistor has to minimize the voltage across the switched transformer phase and, accordingly, decrease the amount of induced flux. For the cases where the residual flux has the same polarity as the applied voltage, the transformer will reach saturation earlier, and, hence, the neutral voltage area will be greater, further decreasing the applied voltage across the windings.

Although applicable to all transformers with electrically and/or magnetically coupled transformers, the single series pre-insertion resistor scheme is more suitable for inrush current reduction in transformers with ungrounded primaries. The single pre-insertion resistor acts in series with the energized phase(s) during the first stage switching. For transformers with ungrounded primaries, the resistor acts in series with the next energized phase for a part of the power cycle. The resistor acts to eliminate the residual flux effect during second phase energization. After the second phase is energized, the third phase is closely in synchronism with the supply voltage and minimal transients are produced.

The sequential energization scheme has the main advantage of being simpler, more reliable, and more cost-effective than the synchronous switching and pre-insertion resistor schemes. The scheme has no requirements for the speed of the circuit breaker or the determination of the residual flux pattern in the transformer core. Sequential switching of the three phases can be implemented through either introducing a mechanical delay between each pole arm in case of three phase breakers or simply through adjusting the breaker trip-coil time delay for single pole breakers.

Numerous experimental and simulation results showed that only a mechanical delay might be sufficient to achieve the desired coordination between the energized phases, and, hence, sophisticated timing control circuitry for the circuit breaker pole tripping logic was not needed. Another advantage of the scheme is the reduced number of circuit switchers or breakers, which increases reliability and reduces both the initial and the maintenance costs. The pre-insertion scheme utilizes six breaker contacts. Three of them are for shorting the pre-insertion resistance after switching takes place.

1.4 Research Objectives

This research work focuses on the investigation and development of a new class of mitigation techniques for the reduction and mitigation of switching transients due to transformer and capacitor energization. The sequential energization techniques utilize a single resistor placed either in neutral or in series with one of the phases during energization and achieve an 80 to 90 percent reduction in inrush current magnitude. This research work was conducted to achieve the following objectives:

1. Investigate, analytically the transformer inrush current and core behaviour during sequential energization.
2. Develop stable and accurate modeling techniques for the modeling and simulation of transformers under inrush current conditions. Due to the nature of the problem under investigation, the modeling technique should successfully model transformers under sequential switching conditions with different winding connections and core structures.
3. Study the sequential switching scheme performance and its application to different transformer connections and core-structure types through simulation, and validate the modeling technique's accuracy against the experimental results.
4. Establish a solid design criterion for the sizing of the neutral resistor based on the analysis of the transformer core transient performance during energization.
5. Investigate the standard and practical application limitations of the sequential switching scheme.
6. Study additional potential applications for the sequential switching scheme for capacitor energization.

1.5 Thesis Contributions and Outline

In order to achieve the study objectives outlined in the previous section, the performance of transformers during sequential energization was investigated through transient simulation and analytically through the application of nonlinear circuits' analysis theory. It was found that transformers undergoing sequential switching developed the highest possible inrush current magnitude during the switching of the first phase. Based on this finding, the analytical study was directed towards deriving a relationship to relate the amount of inrush current reduction directly to the resistor size. This study was completed successfully [42] and [43].

Following the analysis of the dynamic flux behaviour in the transformer core during energization, it was found that if applied together with sequential switching, a single neutral or series resistor achieved a significant flux reduction and, consequently, inrush-current reduction similar to that of the classical series resistor schemes. A solid design guide was accordingly developed for both the neutral-resistor-based and the series-resistor-based sequential switching inrush mitigation schemes [42].

A transformer simulation and modeling technique for inrush current studies have been developed [45]. The technique was found to be numerically stable and time-efficient in capturing near-to-exact transformer nonlinear behaviour under inrush current conditions as compared to laboratory test results [45], [46] and [47]. The iron core's nonlinear characteristics can be modeled as either nonlinear functions of the respective flux or simply as piecewise linear approximations, which are imbedded in the formulation of the Jacobian matrix as a part of the Newton-Raphson solver algorithm. In all the simulation studies carried out in this research, this modeling technique proved to be extremely stable and processing-time-efficient [45].

Afterwards, a practical and easy-to-use algorithm had to be developed for estimating the transformer's nonlinear characteristics, especially for core-type transformers [44]. The work was extended in this area, leading to the development of a parameter-estimation scheme that utilizes the available captured terminal voltage and inrush current waveforms during normal transformer-energization procedures. One of the main advantages of the developed algorithm is that no special test equipment is required at the test location. This advantage is significant, especially for large in-service transformers. Moreover, the developed parameter estimation algorithm eliminates the need for a pre-defined residual flux pattern in the transformer core prior to energization. The requirement for delta winding current measurement during energization, which is rarely feasible, has also been eliminated.

The study was additionally extended to cover practical and standards limitations for the application of the proposed scheme, [42]. A review of the IEEE/ANSI standards was carried out together with the industrial recommended practice, and the neutral-resistor-based scheme was found to introduce a '*voltage rise at neutral*' limitation due to the common insulation grading practice for transformers with solidly grounded connections. Different solutions to the neutral voltage rise were investigated, and that the application of a nonlinear resistor (a resistor-arrester) arrangement was found to be a feasible solution, given the arrester's energy absorption capacity available today. The study also covered the impact of the sequential switching scheme on the development of ferroresonance conditions. Numerous simulation studies were carried out, and it was verified that the applied resistor provides sufficient damping to prevent ferroresonance from developing in the nonlinear circuit.

To date, the findings of this research have resulted in six journal publications in the fields of inrush-current mitigation, transformer modeling and parameter estimation techniques, and capacitor-switching transient mitigation [42], [46], [47], [45], [44] and [48] respectively. The sequential switching scheme can potentially be applied to generator and distributed generation unit transformers. In wind farm distributed generation applications, where a large number of relatively small transformer units need to be connected simultaneously to the grid during wind farm restoration processes, the scheme can provide a substantial cost reduction and allow a faster restoration and start-up process due to the large number of transformers that can be simultaneously energized.

This thesis is organized as follows:

- **Chapter 2** presents a brief description and the characteristics of inrush current behavior in single- and three-phase transformers.
- **Chapter 3** introduces the developed transformer modeling technique with the experimental model validation results.
- **Chapter 4** presents the developed transformer parameter estimation algorithm based on the captured voltage and current waveforms during transformer energization.
- **Chapter 5** presents the neutral-resistor-based sequential energization scheme for inrush-current mitigation. The performance of the scheme is evaluated through extensive experimental, simulation and sensitivity studies.
- **Chapter 6** presents a complete design guide for the neutral grounding resistor, NGR, for both the resistor value and its energy requirements. The scheme's performance and main limitations in practical implementations are also presented. The neutral point insulation level as specified by IEEE/ANSI standards are presented together with proposed solutions and evaluations.
- **Chapter 7** investigates the sequential switching scheme with a single pre-insertion resistor for inrush current limitation.

- **Chapter 8** presents the application of the sequential energization scheme for capacitor-energization applications.
- **Chapter 9** provides this project's conclusions and recommendations.

2. Transformer Inrush Current Phenomena and Its Analysis

This chapter presents in detail the characteristics and the development mechanisms of inrush current in different power transformers' core structures and connections. The chapter starts with a review of the analytical techniques available for the analysis of inrush current phenomena in power transformers. After defining the main factors affecting the development and severity of inrush currents, each factor's impact on the magnitude of the inrush current during energization is defined. Finally, the mechanisms of inrush current development in different transformer cores and connection types are thoroughly investigated and compared to those in single-phase transformer units. The analysis and discussion presented in this chapter focus on how to minimize each of the factors' influences on the inrush current's severity.

2.1 Introduction

Transformer inrush currents are transient electrical currents of high magnitude and a relatively long duration experienced in the transformer's energizing side windings during energization. Transformer iron cores are constructed using ferromagnetic materials, which have nonlinear magnetization characteristics including saturation and hysteresis. In general, due to cost and size limitations, power transformers are designed so that the maximum normal operating magnetic flux is slightly below the saturation region of their magnetization curve [1] and [2]. When the transformer is de-energized, a static residual flux remains in the transformer core. The amount of residual flux at the instant when the transformer is re-energized serves as the initial flux, above which, the transformer flux will build up during the next energization process. During the following transformer energization process, the induced flux might reach very high values beyond the normal operating maximum flux. Theoretically, depending on the amount of residual flux and the instant of switching on the applied voltage waveform, the core flux can reach values two or three times higher than the normal maximum operating value. As a result, the transformer core is driven into a deep saturation mode of operation. The magnetic flux transients are translated into magnetization inrush current transients, which are amplified by the nonlinear magnetization characteristics of the iron core, Figure 2.1.

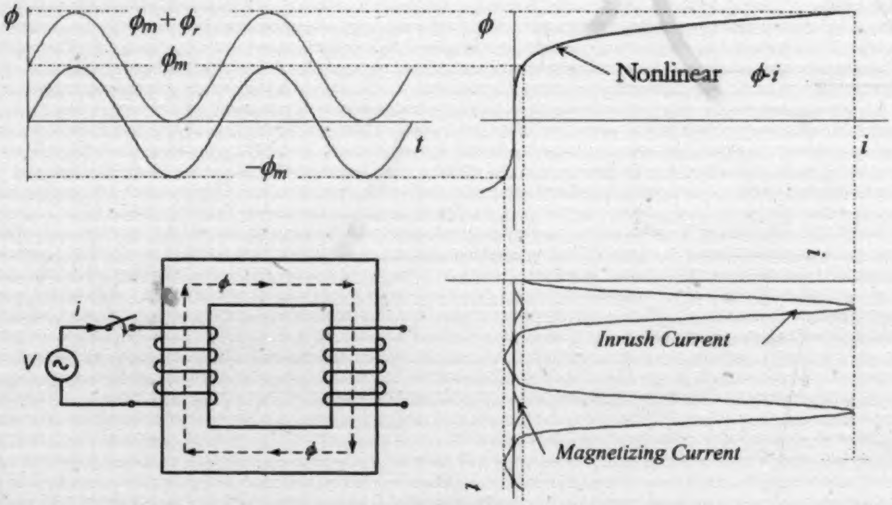

Figure 2.1 Nonlinear Flux-Current characteristics.

This chapter starts with a review of the available analytical work in the literature related to transformer inrush currents. This review is followed by a simplified analysis methodology, which its goal is deriving an accurate, non-iterative expression for the maximum '*peak*' inrush current. The inrush current waveform is first derived in order to investigate different parameters affecting the development of the inrush peak formula that follows. The analysis is afterwards extended to cover inrush phenomena in three-phase transformers during simultaneous pole closure. Different winding connections are investigated, and a comparison is carried out for the performance of each of the connection/core structure types studied against that of single-phase transformers.

2.2 Characteristics of the Saturable Inductor

When attempting to use an analytical modeling approach for saturable inductive circuits, the non-linear magnetizing characteristic curve 'saturation curve' must be accurately and adequately presented. One of the possible approaches is to model the saturation curve through a fitted expression which can take the form of a power series, a hyperbolic series, or even a trigonometric series. However, the problem will be very difficult to solve by using non-linear differential equations.

The work presented by Boyajian in [49] and [50] formed the basis of the analytical modeling for the study of nonlinear 'magnetic core' inductive circuits transients. The saturation curve is represented through a two-segment piecewise linear curve that splits the saturation curve into saturated and un-saturated regions, respectively, Figure 2.2. The analysis was carried out to develop expressions for the steady state current of a circuit that involves a saturable inductor with and without a constant series resistor, [49]. For starting transients '*magnetizing inrush currents*', it was mentioned that similar equations hold if the transition instants at which the saturable inductor goes into and out of saturation mode continuously change until the steady state is reached. It was also suggested that the residual flux could be accounted for by assuming a certain initial amount of current that corresponds to the assumed residual flux level.

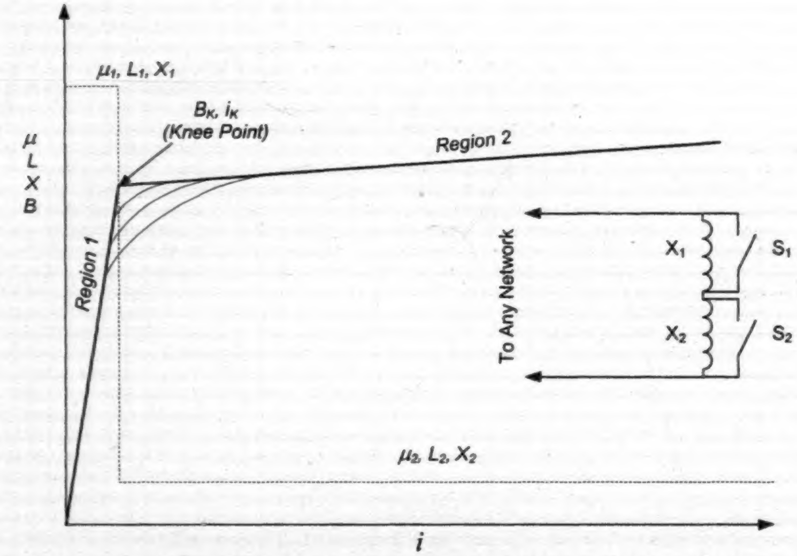

Figure 2.2 Saturation Curve of Iron, Showing "Regions" and the Corresponding Fictitious Equivalent of a Saturable Reactor, [49].

In [4] and [13], based on assuming a total flux build up during energization in single phase transformer units of $2\phi_{max}+\phi_{res}$ where ϕ_{max} and ϕ_{res} are the maximum steady state and the residual flux magnitudes respectively. Neglecting the voltage drop across the energizing system impedance 'both resistive and reactive', an approximate formula was given for the calculation of the inrush current peak value, (2.1) shown below, [4] and [13].

$$i_{max} = \frac{\phi_{res} + 2\phi_{max} - \phi_{sat}}{L_{air-core}} \tag{2.1}$$

The air-core reactance, $L_{air-core}$, where calculated based on transformer design data and structural dimensions. And since transformer with concentric windings have the high voltage winding on the outer side, a conclusion was drawn accordingly that, it is preferable to energize transformers with concentric windings from the high voltage side due to their higher percentage reactance since the high voltage is usually the outer solenoid.

In [52], using similar analysis procedure as presented earlier in [49], formulas and curves have been derived for approximately calculating the inrush current waveform for a single phase transformer over a number of cycles. The effect of energizing system resistance has been neglected and the magnetizing curve was assumed to have infinite slope in the unsaturated region. The expressions derived for the saturation angle θ_1, inrush current waveform i and the inrush peak i_M has been given respectively as follows;

$$\cos(\theta_1) = k_1 \frac{\phi_{sat} - \phi_{res} - \phi_{max}}{\phi_{max}} \qquad (2.2)$$

$$i = k_2 \cdot \frac{\sqrt{2} \cdot E}{X} \cdot (\cos(\omega \cdot t) - \cos(\theta_1)) \qquad (2.3)$$

$$i_M = k_2 \cdot \frac{\sqrt{2} \cdot E}{X} \cdot (1 - \cos(\theta_1)) \qquad (2.4)$$

The saturated reactance X has been adjusted so that the maximum inrush magnitude of the first cycle matches that given by [13], Eqn (2.1). Factors k_1 and k_1 were referred to as '*experience correction factors*' which have been suggested to equal 0.90 and 1.15 respectively based on experiments on seven transformer units ranging from 10 to 20,000 kVA. The work presented in [51] was further extended in [52] to include the effect of total energizing system resistance. The inrush waveform was derived similarly as done in [49] with the exception that the transformer is assumed to have zero magnetizing current in the un-saturated region.

Formula for the peak inrush current magnitude, I_p, was derived as function of the total resistance R, reactance X, the saturation θ and peak β angles respectively as flows, (2.5);

$$I_P = \left(\frac{\sqrt{2} \cdot E}{X}\right) \cdot \left(\frac{X}{R}\right) sin\, \beta \tag{2.5}$$

In order to evaluate (2.5), curves were given for the values of the peak angle β as function of the saturation angle θ and the R/X ratio, [52]. Expressions for the mean, RMS and decay rate of the inrush current waveform were also presented; however, no experimental work has been presented to validate the accuracy of the derived expressions.

In [27 and 28], based on an assumption of constant magnetizing inductance, an empirical formula has been given to predict circulating current between transformers. Another empirical formula was given in [17] for the peak inrush current before and after shorting a pre-insertion resistor. Very approximate formulas were given in [29] for the amount of DC component and time constant of inrush currents in single transformer banks.

2.3 Factors affecting inrush current magnitude

There are a number of factors that can contribute to the severity of inrush current development in transformers during energization. These factors could be defined as follows:

- Instant of switching on the supply voltage waveform.
- Amount of residual flux and saturation characteristics.
- Available series impedance in the energizing circuit.
- Transformer connection and core structure type.

In the following; the impact of each of the first three factors will be thoroughly discussed. The impact of each factor on the inrush waveform development as given by will be shown for and the impact on developed the inrush. The effect of transformer connection will be discussed separately in section 2.6.

2.3.1 Instant of Switching

The instant of switching on the supply voltage waveform plays a major role in the development of inrush current phenomena during transformer energization. In normal operating conditions, the flux lags the terminal voltage waveform by 90 degrees with amplitude of 1 p.u. which corresponds to half the integral of the voltage waveform in either polarity. Immediately after the transformer is energized, the flux starts to build up in the core as the integral of the supply voltage waveform. Theoretically, neglecting the effect of series impedance and residual flux, the maximum flux in the core can reach values up-to 2 p.u. The switching angle on the supply voltage waveform will contribute to how-far the transformer core will be driven into saturation, Figure 2.3.

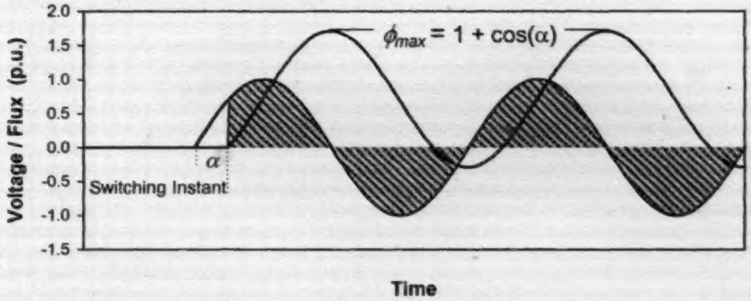

Figure 2.3 Influence of the switching angle α on the flux build up in the core.

Transformer performance during energization in unsaturated mode 'for each phase' will determine the time at which each phase will reach saturation, depending on the switching angle and the amount of initial flux linkages λ_o. Generally, the initial 'or residual' flux will be below the saturation flux level and accordingly, the apparent magnetizing impedance will be very high compared to other linear impedances in the series circuit. As a result, when the transformer is energized and λ_o is below λ_s and the total supply voltage is mainly distributed across the magnetizing branch until saturation is reached.

The saturation time 't_s' can be calculated as time required for the integral of the supply voltage added to the initial flux λ_o to reach the saturation flux λ_s. Hysteresis effect 'usually presented as a resistance in parallel with the magnetizing reactance' will not affect estimation of the saturation time t_s.

$$\lambda_{sj} = \int_{t=0}^{t_s} V_{mj} \sin(\omega t) dt + \lambda_o \tag{2.6}$$

$$t_{sj}(\lambda_{oj}) = \frac{1}{\omega} \cos^{-1} \left[1 - (\lambda_s - \lambda_{oj})\big|_{p.u.} \right] \tag{2.7}$$

Neglecting the effect of resistance and residual flux in the core, the maximum flux that can build up in the core as a function of the switching instant α, can be evaluated as follows;

$$\lambda_{max} = \int_{\alpha}^{2\pi} V_m \sin(\omega t) dt \tag{2.8}$$

$$\lambda_{max} = (1 + \cos \alpha) \tag{2.9}$$

The corresponding inrush current magnitude could be accordingly calculated as follows;

$$I_{max} = \frac{\Delta\lambda}{L_{sat}} = \frac{(\lambda_{max} - \lambda_s)}{L_{sat}} \tag{2.10}$$

The saturated inductance L_{sat} represents the total reactance in the series circuit including the transformer air-core inductance, leakage and the system inductance. The variation of the maximum theoretical flux ϕ_{max} and the corresponding maximum inrush current as function of the switching angle, α, is shown in Figure 2.5 for the case with no residual flux.

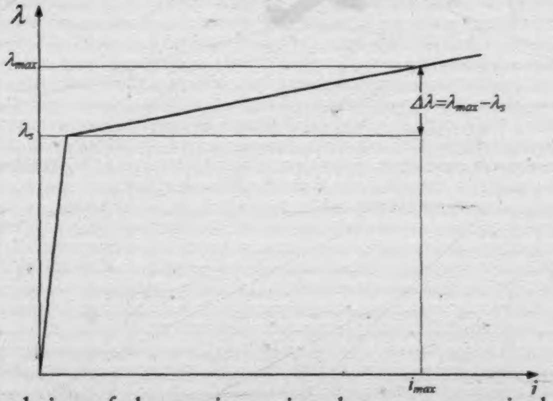

Figure 2.4 Calculation of the maximum inrush current magnitude using the maximum flux build-up and simplified saturation characteristics.

The saturable core will not experience any flux or current transients if the energizing instant was at $\pm\pi/2$ degrees which represents a steady state condition. However, the energizing instant could be slightly of nominal and still, there will be no inrush transients experienced. The reason is due to the fact that transformers have their saturation flux limit slightly above their maximum operating flux. Any flux disturbance that is higher than the maximum operating flux but below the saturation flux limit will not be reflected into inrush transients,

Figure 2.5. The optimal and critical switching angles can be calculated as follows, respectively;

$$\alpha_{opt} = \pm[\sin^{-1}(\lambda_r) + \pi/2] \tag{2.11}$$

$$\alpha_{cr1,2} = \cos^{-1}[\pm(\lambda_s - 1) - \lambda_r] \tag{2.12}$$

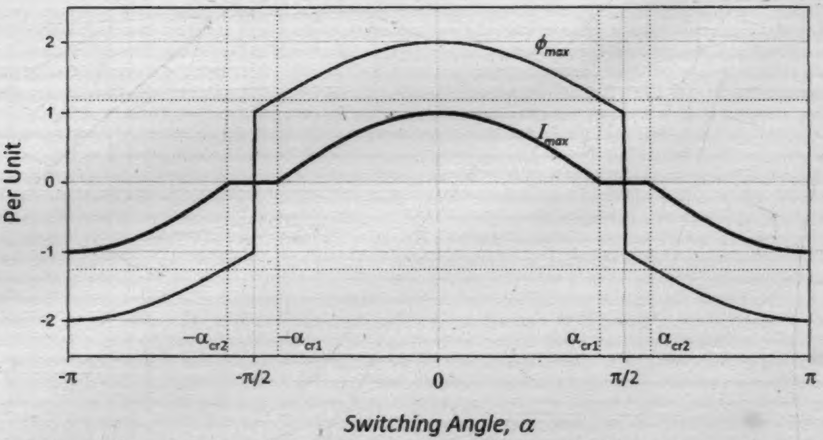

Figure 2.5 Theoretical maximum flux build-up limit and the corresponding peak inrush current as affected by the instant of switching, α. $\phi_s = 1.2(p.u.)$

The switching angle α will affect the voltage integral over the first half/cycle and accordingly affects the saturation angle $\omega \cdot t_s$ at-which the transformer core reaches saturation;

$$\lambda_{sj} = \int_{t=\alpha/\omega}^{t_s} V_{mj}\sin(\omega t)dt \tag{2.13}$$

$$t_{sj}(\alpha) = \frac{1}{\omega}\cos^{-1}\left[\cos\alpha - \lambda_s|_{p.u.}\right] \tag{2.14}$$

It is worth noting that, the saturation time as given by (2.14), defines the instant at which the saturation of the respective energized phase occurs. One could accordingly assume that inrush current won't exist until saturation time, t_s, is reached. However, this is only true for single phase transformers and Y-Y connected three-phase transformer banks. For other connection and/or core types, inrush current could be present in one phase due to the saturation of an external phase that is magnetically or electrically coupled. This behavior will be thoroughly explained in section 2.6.

2.3.2 Residual Flux and Saturation Characteristics

Residual flux represents the amount of magnetism present in the transformer core after being de-energized. The instantaneous value of the core flux during de-energization when the circuit is interrupted at zero-current is the residual flux. The magnitude of this residual magnetism of the iron core must be taken into account when studying inrush phenomena in transformers. With residual flux present in the transformer core, the flux build up process will start at the residual flux value during the following energization incident, Figure 2.6. This result in increasing the maximum theoretical flux limit that could be reached during the energization process to up-to $2\phi_{max} + \phi_r$ which will be reflected into higher inrush current magnitudes.

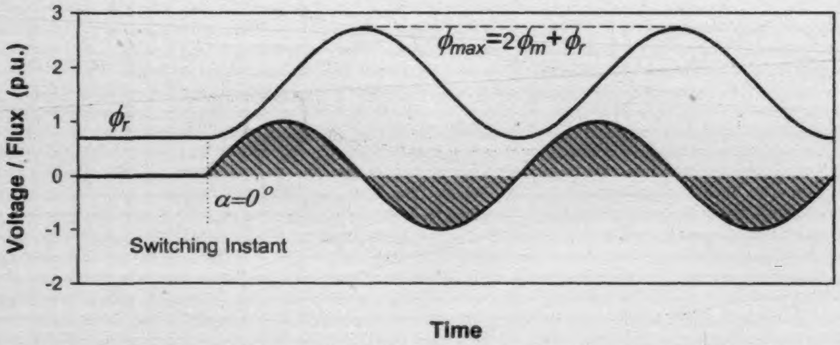

Figure 2.6 Influence of the residual flux ϕ_r on the flux build up in the core.

$$\lambda_{max} = \int_{\alpha}^{2\pi} V_m \sin(\omega t)dt + \lambda_o \tag{2.15}$$

$$\lambda_{max} = (1 + \cos\alpha) + \lambda_o \tag{2.16}$$

The maximum theoretical current I_{max} could be calculated similarly to as shown in (2.10).The variation of the maximum theoretical flux ϕ_{max} and the corresponding maximum inrush current is shown in Figure 2.7 for a residual flux of +0.7(p.u.) as function of the switching angle, α. It is clear that the maximum inrush nearly doubled in magnitude due to the presence of residual as compared to the case without residual. More interestingly, the switching angle band corresponding to near-optimal switching leading to a low inrush magnitude is significantly increased. The optimal and critical switching angles can be calculated as follows, respectively;

$$\alpha_{opt} = \pm[\sin^{-1}(\lambda_r) + \pi/2] \tag{2.17}$$

$$\alpha_{cr1,2} = \cos^{-1}[\pm(\lambda_s - 1) - \lambda_r] \tag{2.18}$$

Besides, with the presence of residual flux, the transformer will experience saturation in a shorter time leading to the existence of the inrush waveform for a longer duration over each cycle.

$$t_s(\lambda_o, \alpha) = \frac{1}{\omega}\cos^{-1}[\cos\alpha - (\lambda_s - \lambda_o)|_{p.u.}] \tag{2.19}$$

The worst 'fastest' saturation time t_s, depending on transformer saturation characteristics, could be evaluated through (2.19) assuming typical saturation and residual flux limits. Typical saturation and residual flux magnitudes for power transformers are in the range;

$$1.2[\text{p.u.}] \leq |\lambda_s| \leq 1.35[\text{p.u.}] \quad \text{and} \quad 0.7[\text{p.u.}] \leq |\lambda_o| \leq 0.9[\text{p.u.}] \tag{2.20}$$

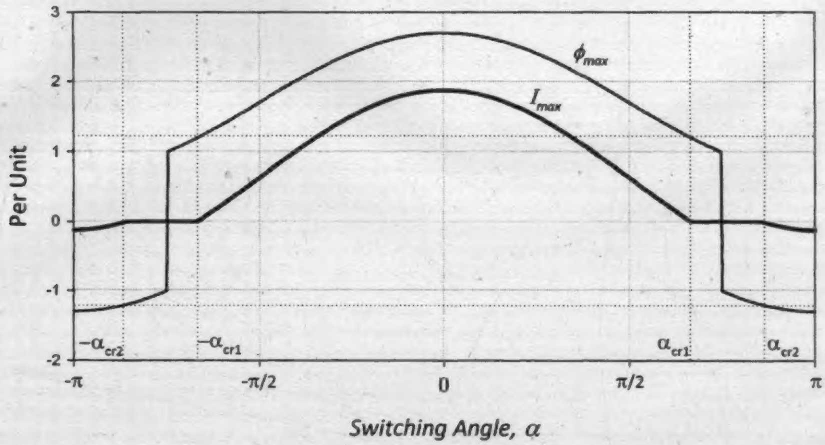

Figure 2.7 Theoretical maximum flux build-up limit and the corresponding peak in-rush current as affected by the residual flux $\phi_r = +0.7(p.u.)$ and the instant of switching, α. $\phi_s = 1.2(p.u.)$

This leads to typical upper and lower saturation angle limits of 45 and 70 electrical degrees respectively. As a conclusion, residual flux presence will affect the instant at which saturation is reached in the core. This is reflected into the amplitude of the DC component in the inrush waveform and consequently, increasing the maximum possible inrush current magnitude and duration.

Although the analysis carried out showed that inrush currents are strongly affected by residual flux, the residual flux itself has high sensitivity to core characteristics, load current and connected capacitance. Transformer with low-loss cores have higher residual flux limits as in the case with cold rolled laminations and higher silicon steel. In case of transformers with gap-type cores, the residual flux level is negligible, [4] and [15]. This clarifies the findings of [4] where inrush currents were more evident with, high quality, well-built transformers. The connected 'or available' capacitance has a strong influence on the residual flux in the core. After the current has been interrupted during de-energization, the magnetizing current continues to flow through the connected capacitance and accordingly lowering the residual flux level, [4], [7], [13] and [34].

2.3.3 Series Impedance

The available series impedance in the energizing circuit has a great influence on the severity of inrush currents during transformer energization process. Immediately after energization, the transformer phases are all unsaturated and accordingly, the series impedance will have no effect on inrush current before saturation is reached. However, the transformer apparent core reactance drops significantly during saturation. The available series impedance, even being relatively small as compared to the transformer unsaturated reactance, will carry a considerable voltage drop reducing the voltage imposed on the transformer terminals during saturation. This reduction in transformer terminal voltage translates into a reduction in the core-flux build up, and consequently, limiting the inrush current.

In its simplest form, the transformer saturable core inductance, leakage reactance, resistance together with the series impedance can all be considered as a single-series RL circuit. The inductive component of the series impedance acts to increase the slope 'apparent inductance' of the transformer core as seen by the ideal energizing supply source. Consequently this leads to a decreased inrush magnitude for the same amount of theoretical flux build-up in the core, ϕ_{max}. On the other hand, the developed voltage drop across the resistive component, acts to decrease the voltage applied across the equivalent inductance and consequently reducing the maximum flux-build up in the core.

It is worth noting that the series impedance has influence on reducing the inrush magnitude even before the energized phase reaches saturation. As has been shown in the previous section, depending on the residual and saturation flux levels of a transformer, the inrush waveform duration could be defined within a defined period in each cycle. However, during simultaneous or sequential switching, a high inrush current could flow in an unsaturated phase due to saturation of other phases in the magnetic circuit. Such behavior makes the small series impedance take a strong role in decreasing the voltage imposed on the transformer terminals on unsaturated phases. This leads to an increased saturation time and decreased maximum flux limit in the core.

2.4 Single Phase and Simultaneous Three Phase Energization Inrush Current

Inrush current due to simultaneous three-phase switching in three-phase transformers are generally quite different than in single-phase transformers. Both the magnitude and the inrush waveform shape will be affected by the transformer winding connection and core structure. This difference in performance between three-phase and single-phase transformers originates due to the presence of magnetic or electrical coupling between phases in three-phase transformers.

In single phase transformers, the line current on the energizing side during inrush condition mainly consists of the magnetizing inrush current of the energized phase. In three-phase transformers, the measured line current can contain additional current contributions from the delta 'secondary' winding or even inrush current component due to saturation of an external phase. If the transformer is energized from a delta connected winding, the line currents represent the summation of the inrush current flowing through two phase windings.

In the following, a brief discussion about the performance of single-phase banks and three-phase, core-type, transformers will be discussed with respect to transformer connection and core structure. The analysis compares the performance of three-phase transformers under simultaneous three-phase energization inrush conditions to that of single phase energization.

Case 1: Single-phase units in Yg-Y bank connection:

For this case, each phase will behave independently due to the absence of electrical or magnetic coupling between phases. Inrush current measured in each phase could be easily evaluated using similar procedure described earlier for single phase units. In other words, the maximum inrush current possible is in no-way different than that evaluated for single phase transformers.

Case 2: Single-phase units in Yg-Δ bank connection:

Although similar to case 1, this case has one difference which is the flow of a delta winding current due to the voltage unbalance in the secondary delta during energization. During normal operation conditions and with nearly identical transformer banks, the three-phase induced voltages on the delta side are balanced and no circulating delta-winding current will flow. However, during energization, not all phases reach saturation at the same time or at the same level. As the first phase reaches saturation, its apparent magnetizing reactance will drop resulting in the flow of a circulating current in the delta winding, i_Δ. With the other two phases unsaturated, the delta winding current will be reflected as a line current of the same magnitude, i_Δ. The flow of the delta winding current into un-saturated phases, even for a short time, will develop a voltage drop across the resistance that is available in the series circuit. Depending on the amount of resistance, the developed voltage drop reduces the applied voltage across un-saturated phases leading to lower inrush current magnitude than that experienced during single phase energization.

More importantly, the presence of the delta winding makes it possible for the other unsaturated phases to contribute to the required saturation current for the phase under saturation. In order to bring more understanding of the phenomena, Figure 2.8 represent the energizing voltage waveforms at the Yg side together with the instant of switching leading to the highest inrush magnitude in Phase A. In Figure 2.8, the flux waveforms are represented neglecting the effect of resistance in the circuit for the sake of simplicity and clarity.

It could be easily verified that the inrush flux waveform will exist in each phase at periods where the respective flux is exceeding saturation level. It is also shown that Phase A, will generate the highest inrush current magnitude since it represents the highest saturation level. Close to when phase A reaches the highest saturation level, both phases B and C are much less saturated and accordingly, a high delta winding current is excited on the delta side due to the voltage unbalance of each phase in the delta winding. Simulation studies carried out on this connection type verified the conclusion drawn earlier. It was found that simultaneous switching of Yg-Δ transformer banks leads to about 10% lower inrush current magnitude compared to that due to single phase switching. The reduction in inrush current magnitude is due to the delta winding current in the unsaturated and saturated modes of operation.

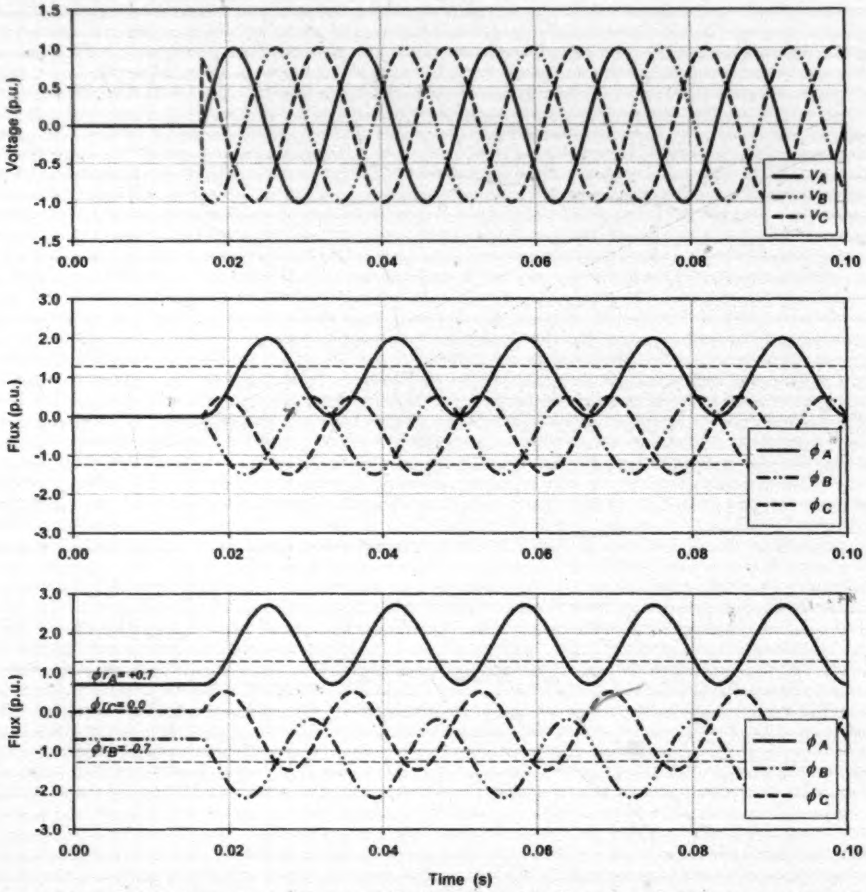

Figure 2.8 Supply voltage 'top' and the theoretical induced flux assuming zero-residual pattern 'middle' and with residual flux 'bottom' in the transformer cores during energization of Yg-Δ bank.

Case 3: Single-phase units in Y- Δ 'ungrounded' bank connection:

This case differs from the one presented earlier due to the absence of the ground return path in the primary transformer side. All line currents at the primary side must add-up to zero at any given time. Although the primary side winding connection is ungrounded, the presence of the delta connected secondary keeps the neutral point stable and close to zero, [4] and

[13]. This finding was verified through experimental and simulation studies on three-phase core type transformer and three single phase unit transformers where it was found that the maximum neutral voltage rise was below 20% of the nominal phase voltage.

Following a similar analogy to the one carried out in case 2, Figure 2.8 shows the developed flux waveforms assuming zero residual flux patterns and neglecting the effect of the primary side resistance. It is clearly shown that one phase 'A' will again represent the highest saturation condition while the two other phases 'B and C' are un-saturated. To allow the flow of inrush current in Phase A in such a condition, the two un-saturated Phases 'B and C' should each contribute to the saturation inrush current required by phase A by 1/3 of the total required magnetizing branch current I_s. In such a condition, a delta winding current that equals 1/3 of I_s will circulate on the delta side with 1/3 of I_s withdrawn from lines of Phases B and C and only 2/3 of I_s line-current is measured at terminals of Phase A, Figure 2.9.

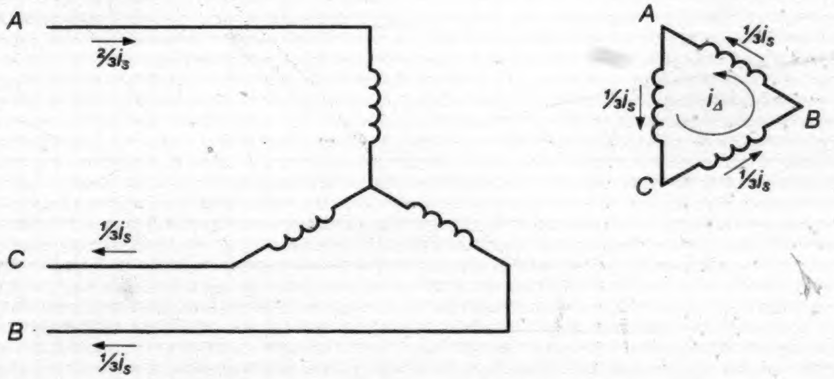

Figure 2.9 Distribution of current among 3-phase bank, Y-Δ windings due to saturation of Phase A with phases B and C unsaturated (low residual flux pattern).

From the above, it could be concluded that only 67% of the current measured due to single phase switching of individual banks will flow due to the simultaneous energization of a three-phase bank with Y-Δ connection. This finding although identical to that withdrawn in [4], [15] and [15] doesn't quite accurately hold since the neutral voltage point is not firmly held to zero potential. Additionally, the transformer is rarely switched in with any residual flux present in its bank cores.

Further investigation showed that with the consideration of residual flux presence in the core phases, the less saturated phases 'B and C' will experience a higher saturation condition while phase A is close to its peak saturation limit. Accordingly, inrush current can more freely return through phases B and C with all phases are saturated and with the delta side in more balanced 'lower-circulating current flow'. With the presence of residual flux in all phases, the maximum inrush current due to simultaneous switching was found not to exceed 80% of the maximum inrush due to single bank energization.

Case 4: Single-phase units in Y-Y 'ungrounded' bank connection:

For this case, inrush current will not flow unless at-least two phases saturate. The analysis of such condition is straight forward since the neutral point is totally floating and the two saturated phases are in series with the line-to-line voltage applied across their terminals. The unsaturated phase can be accurately assumed to be open-circuited due to its low saturation level.

As compared to single phase unit energization, the worst inrush current condition for this case could be modeled through an equivalent single phase unit representing the two in-series saturated phases. The equivalent single-phase bank will have a series resistance, leakage and saturated reactance of twice the magnitude of that of single phase bank with a source voltage that equals √3 the nominal phase voltage. The series-bank will also saturate in higher time, since only √3/2 or 85% of the nominal voltage is applied across the magnetizing branches before saturation. This leads to a maximum inrush magnitude of about 80% of the maximum single phase inrush current flowing through the two saturated phases in opposite directions with the third phase carrying a negligible inrush current.

Case 5: Three-phase core with grounded-Wye primary connection:

This case is similar to a three-phase bank with a grounded-wye primary and delta connected secondary, Case 2. The three-legged core type structure will have identical performance to a delta winding connected secondary regardless of its presence. Experimental and simulation results showed that with Yg primary, a three legged core will have a maximum inrush current that is 88% of that due to single phase switching. The presence of a delta connected primary resulted in lowering the inrush current by additional 2%, i.e. to 86%.

Case 6: Three-phase core with ungrounded-Wye primary connection:

Again, this case is similar to the case with three, single-phase transformers with Y/Δ connection. A reduction of 20% as compared to single phase switching is experienced with simultaneous three phase closing. Experimental and simulation results verified that the presence of a delta winding and/or a three-legged core will stabilize the neutral voltage close to zero during simultaneous switching. The maximum recorded inrush case is shown in Figure 2.10. The case represents the highest inrush in Phase C due to the switching close-to the voltage zero crossing of Phase C together with a matching negative residual flux polarity. The neutral voltage recorded was 19.5% of the nominal phase voltage with a delta connected secondary. The maximum inrush current is 1650 (A) representing 79% of the highest inrush current due to single phase switching. It could be verified that the delta winding current supplies partially the required magnetizing current of Phase C. Phase B doesn't reach saturation and carries only the delta winding current 'referred to the primary side'.

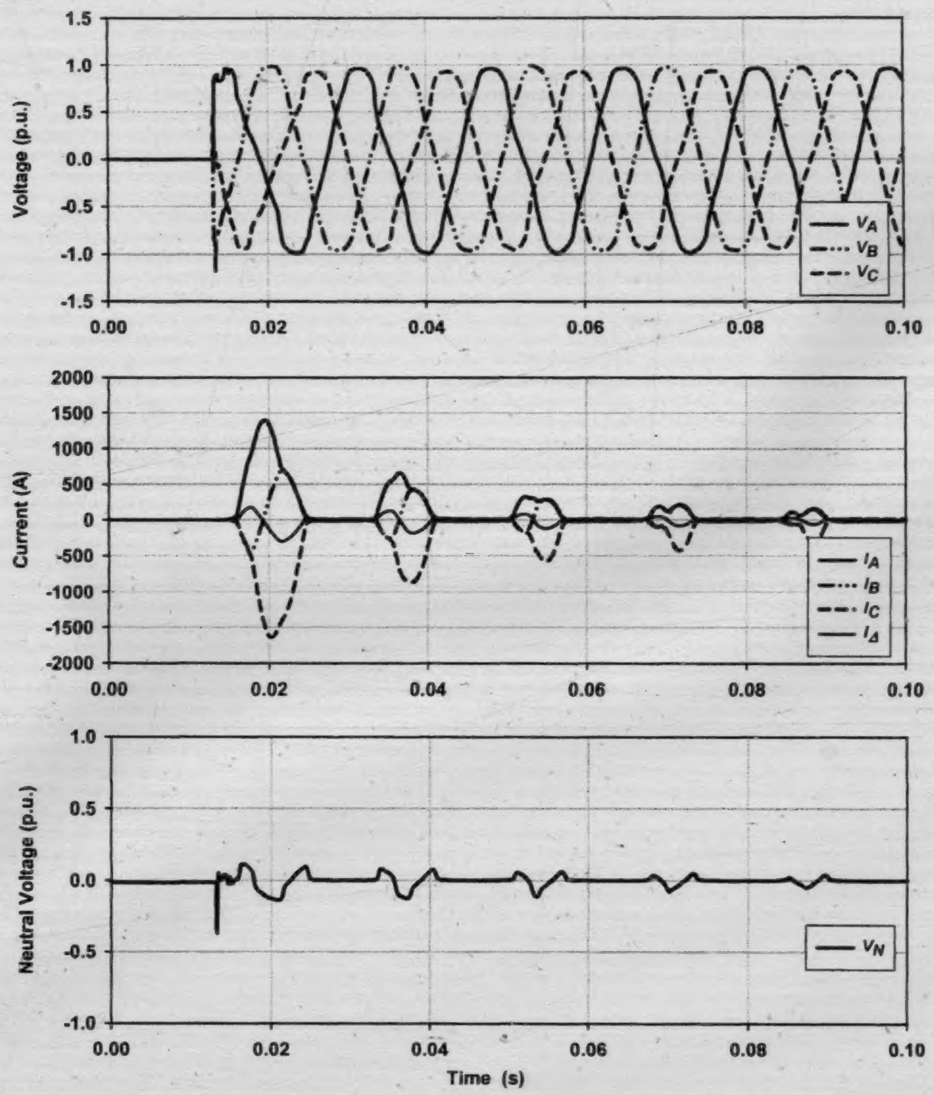

Figure 2.10 Maximum inrush condition, 3-Phase Transformer, Y-Δ connection. Terminal Phase voltage 'top', Inrush Currents 'middle' and Neutral Voltage 'bottom'.

Case 7: Transformers with Delta connected primary:

Transformers energized from a delta connected primary could be analyzed similarly to energizing single phase units as far as the phase currents are concerned. The voltage applied across each phase equals the energizing side line-to-line voltage. Accordingly, similar analysis procedure to that of preceding section could be carried out to evaluate the inrush current magnitude and waveform in each '*phase*' of the delta connected winding.

However, with a delta connected primary, the terminal inrush current as seen by the system side equals the difference of the two common phase currents at each terminal, Figure 2.11. Assuming the simplest condition with zero residual flux pattern in all three phases, and assuming worst energizing condition, only one phase is driven into saturation with the other two phases remain unsaturated, Figure 2.8, where the voltages in this case are line-voltages. In such a condition, both the line and phase currents of the saturated phase 'A' are equal, with phase B and C currents remain close to zero.

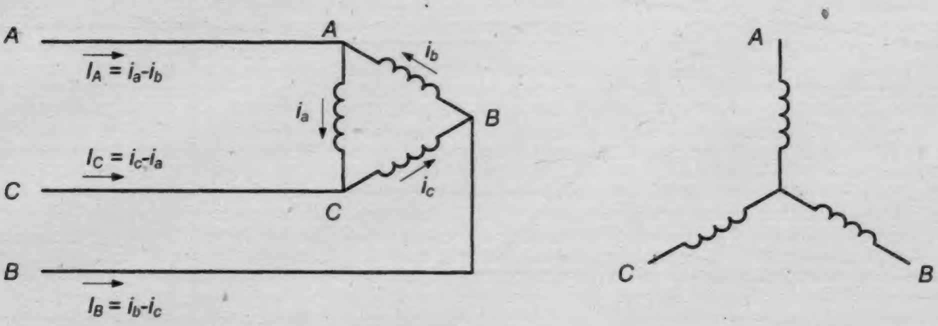

Figure 2.11 Distribution of current among 3-phase bank, Δ -Y windings due to saturation of Phase A with phases B and C unsaturated (zero residual flux pattern).

With consideration of residual flux, more than one phase can reach saturation, and consequently, line and phase currents are not anymore equal. Generally, if the worst energizing conditions are assumed together with a residual flux pattern leading to the highest flux build-up in the core, two phases will be saturated in opposite polarities with the third phase unsaturated, Figure 2.8c. The inrush current waveform measured at terminal A will mainly contain the inrush current of Phase A since phase C is unsaturated. On the other hand, Phase B terminal line current caries both current contributions from phases A and B which are in opposite polarities leading to a higher line current than the inrush current in Phase B or A. Figure 2.12 represents the highest recorded inrush condition for energizing the three-phase laboratory transformer from the delta side.

As could be shown from the phase currents, phase A is the unsaturated phase with phases B and C reaching saturation in opposite polarities. Phase B is the highest saturated phase with a maximum inrush current of 1030 (A) which represents 85% of that measured due to single pole switching at the primary grounded-wye side. As for phase C, the saturation level is lower due to the advanced point on wave switching instant. Since Phase A is unsaturated, line and phase currents are closely equal reaching a peak of 700 (A). The highest line current is that of Phase B which reaches 1350 (A) and accordingly, the maximum line and phase currents are not equal for this connection and off by 30%. This finding does not match with the findings reported in [13] which state that; "for Delta connected primaries, both phase and line currents are equal", which was not true if residual flux is present in the iron core during energization.

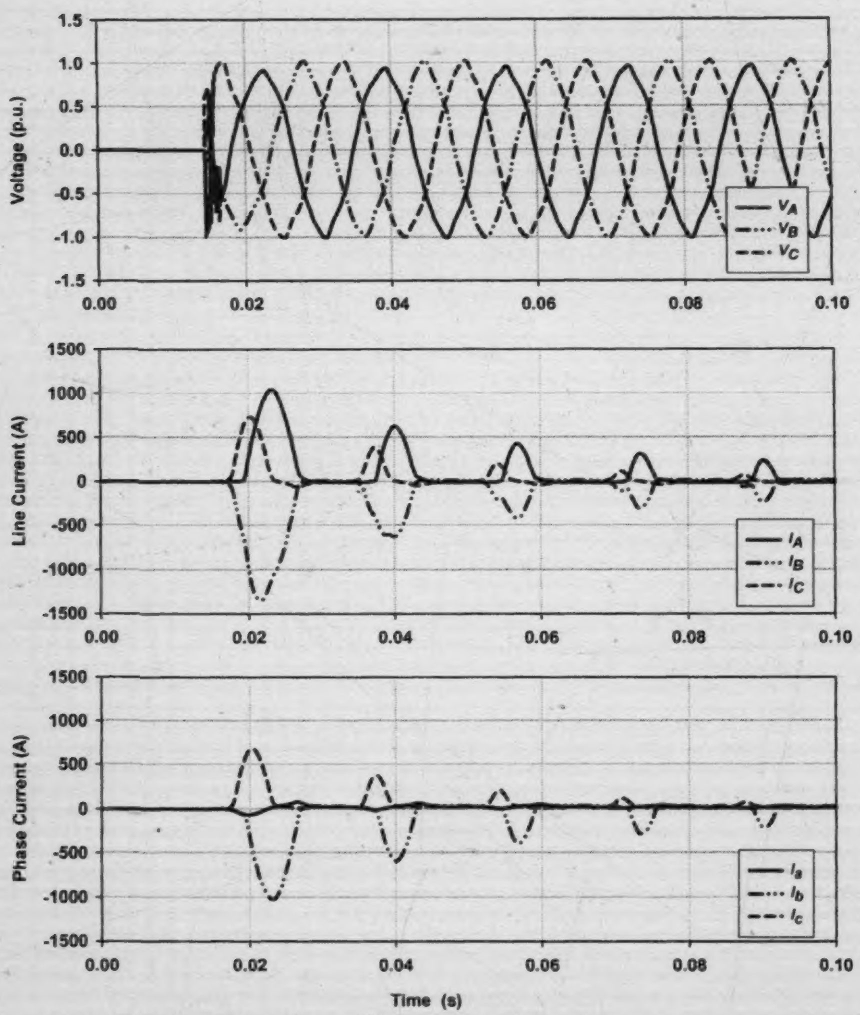

Figure 2.12 Maximum inrush condition, 3-Phase Transformer, Δ–Y connection. Terminal line voltage 'top', Line Inrush currents 'middle' and Phase Inrush currents 'bottom'.

Table 2.1: Relative magnetizing Inrush Currents for Various Transformer Connections (results published in [4] / values for lab transformer or simulation results 'banks')

Transformer Connection		Three Single-Phase Transformers		Three-Phase Transformers	
Primary	Secondary	Simultaneous Switching	Sequential Switching	Simultaneous Switching	Sequential Switching
Yg	OΔ or Y	26/27	26/27	13/24	14.5/27
Yg	Δ	26/24	29/27	13/23	14.5/27
Y	OΔ or Y	20/22	20/22	11/22	11/22
Y	Δ	20/22	20/22	11/22	11/22
Δ	OΔ or Y	20	30	15.5	15.5
Δ	Δ	20	30	15.5	15.5

2.5 Conclusions

This chapter presented an introduction to transformer inrush current phenomena and its analysis techniques. The different factors affecting the occurrence and severity of inrush phenomena were defined and thoroughly analyzed. The effect of each factor on the transformer's core behavior was studied, and the effect of the respective factors on the maximum inrush current's magnitude was shown.

The study was extended to cover inrush-current phenomena due to simultaneous switching. It was shown that modeling each phase in three-phase transformers independently during saturation, and accounting for the core structure and initial flux levels, could accurately explain the behavior of transformers under three-phase energization conditions. The study proved that the single pole switching of three phase transformers leads to the highest possible inrush current against simultaneous three-pole switching with all connections or core-structure types except for Delta Connected primaries.

3. Transformer Modeling and Simulation for Inrush Current Studies

This chapter presents a new, fast and stable approach for the simulation of transformer non-linearities during transient and unbalanced operating conditions. The proposed modeling technique implements separate magnetic and electric equivalent circuits for the transformer. The solution of the transformer non-linear mathematical model is carried out using the Newton-Raphson iterative method. Introducing the magnetic circuit non-linearities into the model as either continuous or piecewise functions eliminated the difficulty of the Jacobian formation. The parameter estimation technique was verified against the experimental and computed results. The application of the Jacobian iterative method increased the stability and convergence of the solution as compared to those of a predictor corrector scheme. The proposed method was able to accurately simulate the transformer's behaviour under switching and no-load conditions[1].

3.1 Introduction

The modeling and simulation of transformer and reactor nonlinearities is of special importance for studying inrush currents, ferroresonance, harmonics and sub harmonics. For the study of the sequential switching scheme, it was required to develop a transformer modeling technique capable of mimicking the transformer's behaviour under sequential switching procedure had to be developed. As an essential requirement, the modeling technique should be numerically stable with the inclusion of linear and non-linear elements at the neutral point. In addition, in order to evaluate the sequential switching scheme's performance with different transformer core structures and connection types, the implemented model should preferably use dual magnetic and electric circuits.

---

[1] A version of this chapter has been published: S.G. Abdulsalam, W. Xu and V. Dinavahi "Modelling and Simulation of Three Phase Transformers for Inrush Current Studies", *IEE Proceedings – Generation, Transmission and Distribution*, vol. 152, No. 3, pp. 328-333, May 2005.

Many nonlinear transformer models have been proposed in the literature [53], [57], [59], [60], [61] and [62]. The models implemented and reported for the study of slow transformer transients include two main modeling techniques. Some of the transformer models are based on the analysis of the electromagnetic field in the transformer [2], [53], [55], [56], [57] and [58]. Another approach is to model the transformer using lumped circuit models [59], [60] and [61]. The first approach tends to represent the transformer using two separate equivalent circuits, one for the magnetic circuit and the other for the transformer electric circuit. For the second approach, the magnetic behaviour and characteristics are modeled in a single electrical circuit with non-linear inductors, with the non-linear characteristics being a function of each non-linear inductor current.

From the implementation point of view, the main difficulties of using lumped circuit models are first, the equivalent circuit becomes quite complicated [61] and second, the resulting impedance matrices might become ill-conditioned for certain network connections. For the case of single-phase transformers, models have been proposed using the classical transformer equivalent circuit with a single non-linear inductor representing each phase of the three-phase transformers [59]. The approximation of the transformer model using three single-phase transformers can lead to serious errors, especially if the transformer's behaviour under transient and/or unbalanced conditions is to be studied [62].

Another problem associated with transformer transient simulation is related to the solution algorithm of the mathematical model. For example, the Electro Magnetic Transient Program, EMTP, uses the classical compensation method to obtain the system solution [63] and [64]. The system is first solved for Thevenin equivalents by ignoring the non-linear elements. Next, the intersection of the system solution curve with the non-linear element characteristic represents the current operating point. The problem with this method is that the Thevenin equivalent cannot be always determined due to possible floating network formations.

After evaluating a number of published models, it was found that a duo electric-magnetic circuit model proposed in [53], [54] and [56] offers a good balance between accuracy and complexity. The modeling technique is also general enough to simulate various transformer transient and/or nonlinear phenomena. In addition, the carried-out experimental work verified the validity of the model independently. A new mathematical modeling technique and a solution algorithm were developed and are presented based on the dual magnetic-electric circuit approach. Throughout this study, the proposed method was found to achieve accuracy, stability and computation-time efficiency. The method can use either piecewise or fitted non-linear characteristic curves to represent the transformer nonlinear magnetizing characteristics. Besides being topologically accurate in representing the transformer magnetic circuit, the proposed method has two more major advantages. First, since the model is linearized by using the trapezoidal integration rule, it can be easily implemented in EMTP-like programs. Second, the formation of the Jacobian is done only once using the continuous curve fitting technique or a maximum of two times if the piecewise characteristic curves are used, making the proposed approach faster than other simulation schemes.

3.2 Transformer Model Description

The implemented transformer model applies two separate equivalent circuits to model the transformer: the electric circuit model and the magnetic circuit model. For a three-limb transformer with a neutral wire, the general equivalent electric circuit for each phase is as shown in Figure 3.1. The transformer's magnetic circuit can be described by considering the transformer's fluxes and equivalent magnetic circuit shown in Figure 3.2.

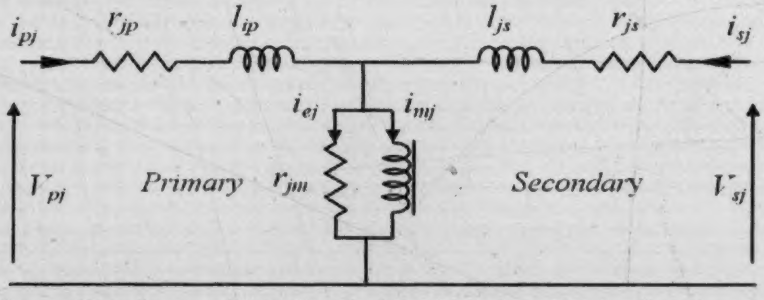
i_{pj}
r_{jp}
l_{ip}
l_{js}
r_{js}
i_{sj}
i_{ej}
i_{mj}
V_{pj}
Primary
r_{jm}
Secondary
V_{sj}

Figure 3.1 Transformer electrical equivalent circuit (per-phase) referred to the primary side.

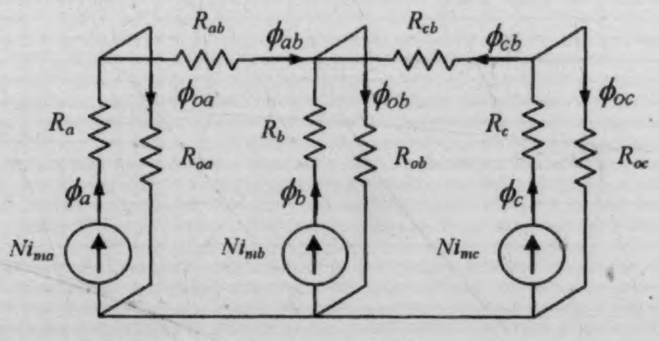
R_{ab}
ϕ_{ab}
R_{cb}
ϕ_{cb}
ϕ_{oa}
ϕ_{ob}
ϕ_{oc}
R_a
R_{oa}
R_b
R_{ob}
R_c
R_{oc}
ϕ_a
ϕ_b
ϕ_c
Ni_{ma}
Ni_{mb}
Ni_{mc}

Figure 3.2 Equivalent magnetic circuit and flux distribution for a three-limb, three-phase transformer.

In Figure 3.1, r_{ap}, r_{bp}, r_{cp} and l_{ap}, l_{bp}, l_{cp}represent the resistances and leakage inductances per each phase of transformer primary winding. These resistances and leakage inductances can be assumed to be linear. The shunt resistances r_{ma}, r_{mb}, r_{mc} represent the combined eddy and hysteresis losses (iron losses) of the respective phases. These magnetizing resistances are nonlinear and can be approximated with a constant value calculated at the fundamental frequency of the induced voltage [59] and [65]. The close agreement between measured and simulated inrush waveforms as will be shown throughout the results presented in this thesis verified this assumption. In fact, the magnetising branch resistance representing the transformer core losses varies with respect to saturation level and frequency. However the magnetising branch inductance changes by a much larger range with saturation level and in turn, overcomes the impact of the core loss resistance variation. The variable core-loss resistance influences the rate of decay of inrush current and can reflect more accurate prediction of the damping provided when studying ferroresonance.

The nonlinear magnetizing inductances are represented as an induced voltage depending on the respective limb flux ($N \cdot d\phi_j/dt$ where $j = a, b, c$). For the transformer secondary windings, only the winding resistances r_{as}, r_{bs}, r_{cs} and the leakage inductances l_{as}, l_{bs}, l_{cs} are represented. The system of equations describing the electric equivalent circuit can accordingly be written as follows for un-loaded secondary side operation;

$$v_j = r_{jp} \cdot i_{jp} + l_{jp} \cdot di_{jp}/dt + N \cdot d\phi_j/dt + v_n \tag{3.1}$$

$$v_n = r_n \cdot (i_a + i_b + i_c) \tag{3.2}$$

$$N \cdot \sum_{j=a,b,c} d\phi_j/dt = \sum_{j=a,b,c} r_{js} \cdot i_{js} + \sum_{j=a,b,c} l_{js} \cdot di_{js}/dt \tag{3.3}$$

$$i_{mj} = i_{jp} - \frac{N}{r_{mj}} \cdot d\phi_j/dt - i_{js} \tag{3.4}$$

$i_{as} = i_{bs} = i_{cs} = i_\Delta$ In case of unloaded secondary with delta connection.

From the flux distribution and the equivalent magnetic circuit shown in Figure 3.2, the system of equations describing the magnetic circuit behavior at any instant of time is given by equation sets (3.5) and (3.6).

$$\begin{gathered}
\mathcal{R}_{Lj} \cdot \phi_j + \mathcal{R}_{Oj} \cdot \phi_{Oj} = N \cdot i_{mj} \\
\mathcal{R}_{La} \cdot \phi_a + \mathcal{R}_{Ya} \cdot \phi_{ab} - \mathcal{R}_{Lb} \cdot \phi_b = N \cdot i_{ma} - N \cdot i_{mb} \\
\mathcal{R}_{Lc} \cdot \phi_c + \mathcal{R}_{Yc} \cdot \phi_{cb} - \mathcal{R}_{Lb} \cdot \phi_b = N \cdot i_{mc} - N \cdot i_{mb}
\end{gathered} \tag{3.5}$$

$$\begin{gathered}
\phi_a = \phi_{oa} + \phi_{ab} \\
\phi_b = \phi_{ob} - \phi_{ab} - \phi_{cb} \\
\phi_c = \phi_{oC} + \phi_{cb}
\end{gathered} \tag{3.6}$$

where,

N	The number of turns per phase.
i_{mj}	The primary side phase magnetizing currents (i_{ma}, i_{mb} and i_{mc}).
ϕ_j	The magnetic fluxes which link different phases and follow the magnetic circuit (ϕ_a, ϕ_b, ϕ_c, ϕ_{ab} and ϕ_{cb}).
ϕ_{oj}	The phase leakage fluxes PLF which link all the windings of one phase, and partially go through air.

$\mathcal{R}_{Lj,Yj}$ The nonlinear reluctances seen by the associated fluxes (ϕ_a, ϕ_b, ϕ_c, ϕ_{ab} and ϕ_{cb}).

$\mathcal{R}_{oj}$ The constant reluctances seen by the associated phase leakage fluxes PLF (ϕ_{oa}, ϕ_{ob} *and* ϕ_{oc}) in the case of three-limb, three phase transformer.

3.3 Transformer Model Implementation

3.3.1 Model Linearization

The previously described system of equations (3.5) and (3.6) modeling both the electric and magnetic transformer circuits consists of eight equations in eight unknowns. The system consists of five algebraic non-linear equations and three linear ordinary differential equations. In order to solve the complete set of equations at the same time, the differential equations need to be discretized and implemented as difference equations in the model. The resulting system will consist of eight discrete time equations, which are sufficient to solve for the unknown fluxes and currents at each instant of time t.

Due to its stability and proven accuracy, the trapezoidal rule of integration has been applied on the nonlinear system of equations. By applying the trapezoidal rule of integration on the non-linear ordinary differential equations (3.5) with an integration time step of $\Delta t = t - t_o$, the linearized difference equations (3.10) and (3.11) can be obtained for a numerical solution at any instant of time t:

$$v_j \cdot dt = r_{jp} \cdot i_{jp} \cdot dt + l_{jp} \cdot di_{jp} + N \cdot d\phi_j + v_n \cdot dt \tag{3.7}$$

$$\int_{t_o}^{t} v_j \cdot dt = \int_{t_o}^{t} r_{jp} \cdot i_{jp} \cdot dt + \int_{t_o}^{t} l_{jp} \cdot di_{jp} + \int_{t_o}^{t} N \cdot d\phi_j + \int_{t_o}^{t} v_n \cdot dt \tag{3.8}$$

$$\int_{t_o}^{t} v_j \cdot dt = r_{jp} \cdot \int_{t_o}^{t} i_{jp} \cdot dt + l_{jp} \cdot \int_{t_o}^{t} di_{jp} + N \cdot \int_{t_o}^{t} d\phi_j + \int_{t_o}^{t} v_n \cdot dt \tag{3.9}$$

$$\begin{aligned}[V_j(t) + V_j(t_o)]\frac{\Delta t}{2} = r_{jp}[i_j(t) + i_j(t_o)]\frac{\Delta t}{2} \\ + l_{jp}[i_j(t) - i_j(t_o)] + N[\phi_j(t) - \phi_j(t_o)] \\ + [v_n(t) + v_n(t_o)]\frac{\Delta t}{2}\end{aligned} \tag{3.10}$$

$$\begin{aligned}[i_{mj}(t) + i_{mj}(t_o)]\frac{\Delta t}{2} = [i_{jp}(t) + i_{jp}(t_o)]\frac{\Delta t}{2} - \frac{N}{r_{mj}}[\phi_j(t) - \phi_j(t_o)] \\ - [i_{js}(t) + i_{js}(t_o)]\frac{\Delta t}{2}\end{aligned} \tag{3.11}$$

$$v_n(t) = r_n \cdot (i_a(t) + i_b(t) + i_c(t)) \tag{3.12}$$

where;

j : *a, b and c.*

t : *present sampling step.*

t_o : *preceding sampling step.*

Δt : *sampling time step.*

Extending the above equations for three phases, the equations become a function in eight unknowns i.e., the magnetic fluxes (ϕ_a, ϕ_b, ϕ_c, ϕ_{ab} and ϕ_{cb}) and the phase currents (i_a,

i_b and i_c) and ten known quantities which are; the history values of fluxes $\phi_j(t_o)$,currents $i_j(t_o)$, present and history values of phase voltages $v_j(t)$ and $v_j(t_o)$ and present and history values of neutral point voltage $v_n(t)$ and $v_n(t_o)$.

At the start of the simulation, initial values for the fluxes and currents are required to be given. An initial value of zero for all fluxes and currents is typical for a relaxed initial condition state. In addition, remnant flux can be easily implemented by setting a proper initial value for the fluxes. The choice of Δt determines the accuracy and the computation time required by the simulation.

Rearranging equation (3.10) and (3.11) for the unknowns on the left hand side and the known quantities on the right hand side yields;

$$\begin{aligned}\left[r_{jp}\frac{\Delta t}{2}+l_{jp}\right]\cdot i_{jp}+N\cdot\phi_j+v_n\cdot\frac{\Delta t}{2}\\ =\left[V_{jp}(t)+V_{jp}(t_o)\right]\cdot\frac{\Delta t}{2}+N\cdot\phi_j(t_o)\\ -\left[r_{jp}\frac{\Delta t}{2}-l_{jp}\right]\cdot i_{jp}(t_o)+v_n(t_o)\cdot\frac{\Delta t}{2}\end{aligned} \tag{3.13}$$

$$\begin{aligned}i_{jp}\frac{\Delta t}{2}-i_{mj}\frac{\Delta t}{2}-\frac{N}{r_{mj}}\phi_j-i_{js}\frac{\Delta t}{2}\\ =-i_{jp}(t_o)\frac{\Delta t}{2}+i_{mj}(t_o)\frac{\Delta t}{2}+\frac{N}{r_{mj}}\phi_j(t_o)+i_{js(t_o)}\frac{\Delta t}{2}\end{aligned} \tag{3.14}$$

The system of equations can be described in matrix form as follows;

$$[\mathcal{R}, Z]_{8x8} \cdot [\phi, i]_{8x1} = [\phi_o, i_o, v, v_o]_{8x1} \tag{3.15}$$

where,

$[\mathcal{R}, Z]$ The Reluctance and Impedance matrix.

$[\phi, i]$ The vector of unknowns and is given by:

$$[\phi_a \quad \phi_b \quad \phi_c \quad \phi_{ab} \quad \phi_{cb} \quad i_{ap} \quad i_{bp} \quad i_{cp}]^T$$

$[\phi_o, i_o, v, v_o]$ The vector of history values and current voltage values and is given by:

$$[0 \quad 0 \quad 0 \quad 0 \quad 0 \quad v_{xa} \quad v_{xb} \quad v_{xc}]^T$$

$$v_{xj} = \left(v_{jp} + v_{jp}(t_o)\right) \cdot \frac{\Delta t}{2} - \left(\left(r_{jp} + r_n\right) - l_{jp}\right) \cdot i_{jp}(t_o)$$
$$+ N \cdot \phi_j(t_o) - v_n(t_o) \cdot \frac{\Delta t}{2}$$

3.3.2 Representation of Reluctance Curves

The non-linear reluctance-flux characteristics have been presented as a non-linear function of the respective flux. Leakage path reluctances $\mathcal{R}_{oj}$ are constant reluctances representing the reluctance seen by the leakage flux through air or through the combination of air and tank body. Limb and yoke reluctances ($\mathcal{R}_a, \mathcal{R}_b, \mathcal{R}_c, \mathcal{R}_{ab}$ and $\mathcal{R}_{cb}$) are non-linear in nature and can be computed knowing actual transformer design dimensions and material parameters from the manufacturer or through experimental tests [53] and [56]. A novel and efficient method for the determination of the nonlinear characteristics 'Reluctance-Flux curves' have been developed and will be presented thoroughly in detail in the following chapter. The $\mathcal{R} - \phi$

curve can then be fitted using a high order polynomial and hence the limb and yoke reluctance at any step can be easily calculated using the fitted curve.

$$\mathcal{R}_L(\phi) = 10^{\sum_{i=0}^{N} C_{L_i} \cdot \phi^i} \quad , \quad \mathcal{R}_Y(\phi) = 10^{\sum_{i=0}^{N} C_{Y_i} \cdot \phi^i} \tag{3.16}$$

C_{L_i} and C_{Y_i} are both the polynomial parameters of the fitting curves for the Limb '$\mathcal{R}_L(\phi)$' and Yoke '$\mathcal{R}_Y(\phi)$' reluctances respectively and N is the polynomial order. It was found that a suitable polynomial order for these curves is in the range from 9th to 20th degree. The more the detail required to be presented in the fitted curve, the higher is the polynomial order. For example, the fitted yoke reluctance-flux curve shown in Figure 3.3 was generated using a 12th order polynomial while for the limb due to the slowly varying nature of the curve for high saturation levels, the polynomial order was raised to 16th.

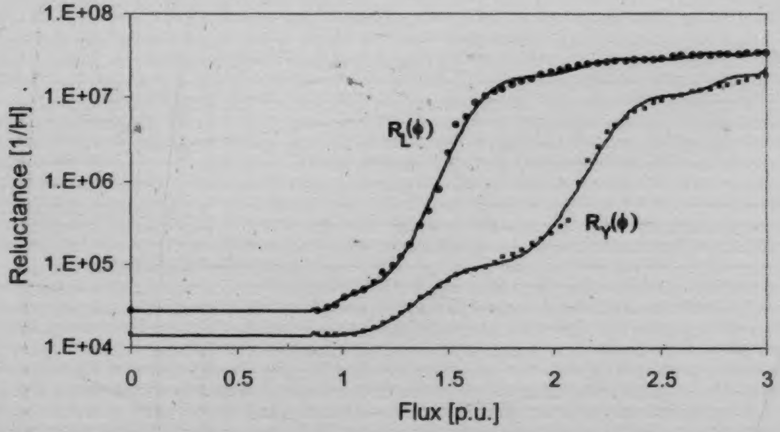

Figure 3.3 The fitted $\mathcal{R} - \phi$ curve for a typical three limb transformer.

For low and extreme values of flux the reluctance flux curve was assumed to be constant and the fitting was applied only to the nonlinear portion in-between. Using curve fitting techniques to represent the non-linear characteristics as shown in Fig. 3.3 might lead to some minor deviations in the fitted reluctance curve compared to the curve obtained experimentally. The slight differences between the fitted and experimental Reluctance-Flux data points lead to minor deformations in the Flux-Current characteristics. However, increasing the order of the fitting polynomial leads to a more precise representation of the fitted values. Another alternative is using a multi-segment piecewise representation of the saturation curve using directly the experimentally obtained data.

3.3.3 Solution Methodology

The objective of the simulation algorithm becomes the solution of equation (3.15) at each time step. The difficulty encountered is that the $[\mathcal{R}, Z]$ matrix is a nonlinear function of the solution results vector $[\phi, i]$. Accordingly, an iterative method has to be implemented to solve the equation. Three solution algorithms for solving the set of discrete time equations (3.15) were studied. Two of them are described here in detail, which are the Predictor-Corrector solution algorithm and the Newton-Raphson method. The choice of the Predictor-Corrector method and the Newton-Raphson method to be studied in detail was based on the fact that both methods can be described in matrix form and both can be easily implemented as an automated solution algorithm in EMTP type programs.

Predictor-Corrector method

Here, a predictor-Corrector scheme for solving the system of equations is described. Generally, the solution for the unknown flux and current values can be obtained using; (3.15). Since the matrix $[\mathcal{R}, Z]$ is non-linear and has elements depending on the 'present' solution of ϕ_j

and i_j, a predictor corrector method is used within each time step in order to calculate the correct $[\mathcal{R}, Z]$ matrix.

The predictor-corrector method can be applied as follows;

1. Matrix $[\mathcal{R}, Z]$ can be initially calculated from ϕ and i values at $(t - \Delta t)$ or from initial conditions at the first time step i.e. $t = 0$.
2. The calculated value of $[\phi, i]$ using the initial $[\mathcal{R}, Z]$ matrix calculated in (3.15) are used as a *Predictor* for the solution.
3. Since the exact solution of $[\phi, i]$ can only be found by using the matrix $[\mathcal{R}, Z]$ at the current solution of $[\phi, i]$ which is not yet available, the predictor found in (2) is again used to calculate a new matrix $[\mathcal{R}, Z]$.
4. New $[\mathcal{R}, Z]$ matrix calculated in (3) is used to calculate a *Corrector* value of $[\phi, i]$.
5. If the difference between the *predictor* and *corrector* values of the solution matrix $[\phi, i]$ calculated in steps 2 and 4 are within a pre-defined tolerance ε, proceed to the next time step.
6. If the error is larger than ε, go to step 2 again.

Newton-Raphson method

The predictor-corrector scheme described earlier was found unsuitable for the problem of transformer transient simulation. The reason is mainly due to the highly non-linear behavior of transformers especially during transient and saturation operating modes. The original system model described by the matrix equation (3.15), can be solved using the Newton-Raphson method through re-formulating the system solution algorithm. For a solution at any time step t and an iteration k, the solution can be obtained as given by equation (3.17).

$$[\phi, i]_k = [\phi_o, i_o] - J^{-1} \cdot ([\mathcal{R}, Z]_{k-1} \cdot [\phi, i]_{k-1} - [\phi_o, i_o, v, v_o]) \qquad (3.17)$$

Where;

J The Jacobian matrix for the system and is generated for each iteration *k*. The formulation of the Jacobian matrix is based on the total differential of function f at a solution x *using* Taylor expansion and hence, the solution of $f \approx f(x) + df(x)$, [66] and [67]. The $J_{m,n}$ element of the Jacobian matrix can be calculated using $J_{m,n} = \partial f_m / \partial x_n$ where f_m is the system equation representing row m in matrix $[\mathcal{R}, Z]$ and x_n is the variable represented in column n. Although, reluctances were not being considered as independent variables in the mathematical model, the partial derivatives of the reluctances were possible since they are dependent variables of respective flux variables and hence the terms $\mathcal{R}_i \cdot \phi_i$ can be mathematically expressed as two multiplied functions in one variable ϕ_i. The partial derivative of $\mathcal{R}_i$ will become a constant 'slope' if the reluctances are implemented using piecewise segments and will become a continuous variable in ϕ_i if the reluctances are represented as a continuous function of ϕ_i. The reluctance derivatives can be evaluated by differentiating the fitted reluctance flux function with respect to flux as given by (3.18).

$$\frac{\partial \mathcal{R}(\phi)}{\partial \phi} = 10^{\sum_{i=0}^{N} C_i \cdot \phi^i} . \sum_{j=1}^{N} j \cdot C_j \cdot \phi^{j-1} . ln(10) \qquad (3.18)$$

$[\phi, i]_k$ The solution vector of the system at iteration k.

$[\phi_o, i_o]$ The previous solution vector of the system at time $(t - \Delta t)$.

$[\mathcal{R}, Z]_{k-1}$ The reluctance-impedance matrix of the system *(described earlier)* at the previous iteration.

$[\phi_o, i_o, v, v_o]$ The vector of history variable values at $(t - \Delta t)$ and current voltage values at time t.

The developed Newton-Raphson solution scheme can be summarized as follows;

1. Calculate the vector of history variable values $[\phi_o, i_o, v, v_o]$ from the solution at the previous time step and the value of the current phase voltages. This is only done once in each time step.
2. Generate matrix $[\mathcal{R}, Z]$ using ϕ values at $(t - \Delta t)$ or from initial conditions at the first time step '$t = 0$'.
3. The Jacobian matrix J is generated using the values of fluxes ϕ at $(t - \Delta t)$ to calculate the reluctances and reluctances partial derivatives. For next iterations the newer values of ϕ will be used.
4. The mismatch solution vector is calculated;

$$[\Delta\phi, \Delta i] = J^{-1} \cdot ([\mathcal{R}, Z] \cdot [\phi, i] - [\phi_o, i_o, v, v_o])$$

5. New solution vector is calculated by: $[\phi_1, i_1] = [\phi_o, i_o] - [\Delta\phi, \Delta i]$
6. If the largest number in the modulus of the mismatch vector $[|\Delta\phi|, |\Delta i|]$ is greater than ε then; (1) set the initial values vector $[\phi_o, i_o] = [\phi_1, i_1]$. (2) Go back to step 2.
7. If the largest number in the modulus of the mismatch vector $[|\Delta\phi|, |\Delta i|]$ is less than or equal ε then; (1) set the solution vector $[\phi, i] = [\phi, i] = [\phi_1, i_1]$. (2) Proceed to the next time step.

3.4 Simulation Results

Predictor-Corrector scheme

The predictor corrector scheme was implemented to simulate the transformer described in [53] and [56]. The method was found to be suitable and converging for the simulation of single-phase switching. For three-phase switching, the method failed to converge and the solution contained heavy numerical oscillations regardless of how small is the time step, Figure 3.4.

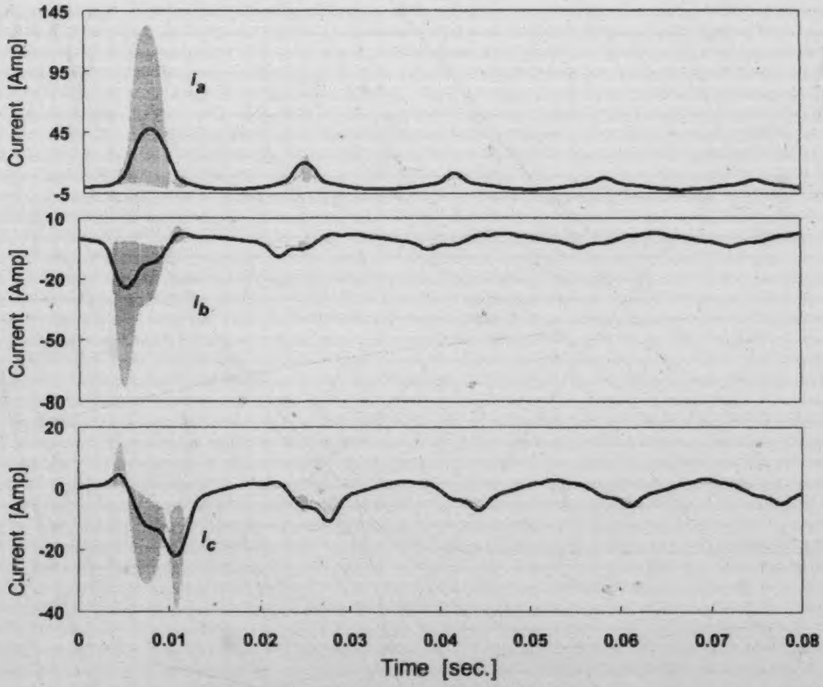

Figure 3.4 Phase inrush currents for instantaneous three phase switching using the predictor corrector scheme 'shadowed' and the Newton Raphson scheme 'solid' for the transformer given in [53] and [56].

The reason for the oscillations shown in Figure 3.4 is that, the transformer model is being driven more heavily into saturation mode among the three phases during instantaneous 3 phase switching and thus, increasing the non-linearity of the system 'operating on the non-linear portion of the reluctance curves'. The solution oscillates between two operating points for even number of iterations while for odd number of iteration, picks up only one part of the solution.

Instantaneous 3-phase switching using Newton-Raphson scheme

The proposed Newton-Raphson method was tested on single phase, instantaneous three phase and sequential 3 phase switching cases. In all simulated cases, the model was stable and converging with a time step of no less than 50 (μs). Figure 3.5 shows a comparison with the experimental results on the transformer described in the appendix for instantaneous three-phase switching using Yg-D connection.

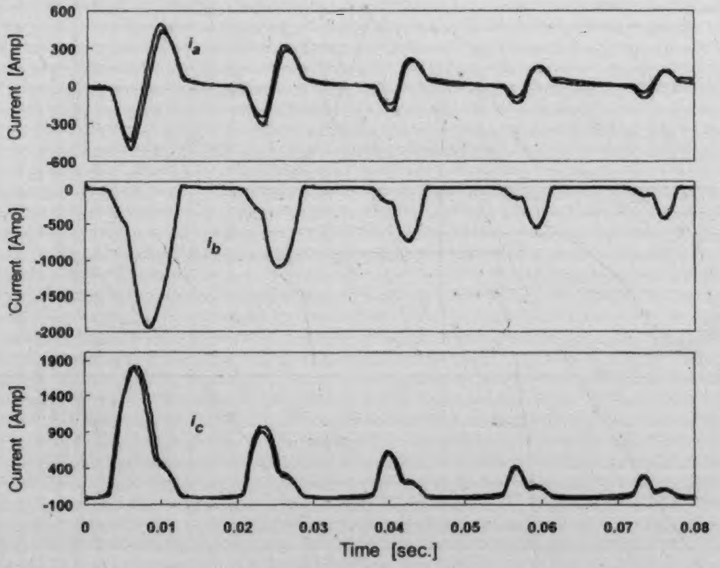

(a) Simulation 'solid' and measured 'dotted' inrush currents [Amps].

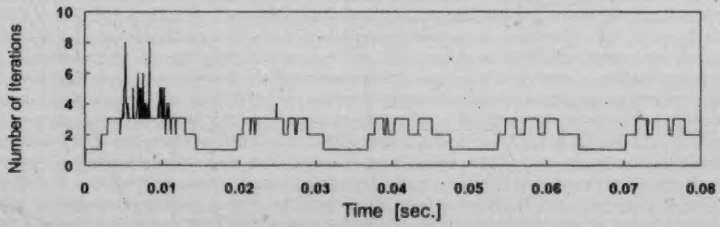

(b) Maximum number of iterations at each time step.

Figure 3.5 Instantaneous three phase switching of Yg-Δ transformer described in appendix.

It is clearly shown that the simulated and measured phase current values have close agreement. The simulation procedure requires three iterations for saturation region operation 'where the current experiences sharp magnitude rises' and a single iteration for low saturation levels. For extreme saturation operation conditions, the number of iterations rises to eight in order to achieve the required maximum converging tolerance of 10^{-6}.

The measured terminal voltage was fed into the simulation program with the recorded resolution. The sampling frequency was 256 samples/cycles, which dictates a simulation time step of about 65.1 (μsec). Such a relatively high simulation time step reflects the rigidity and the convergence nature of the developed algorithm. The time required for the simulation can be effectively reduced through the application of a variable time step in lower saturation levels which represent about 50% of the total simulation time. Due to the nature of the implemented discretization method, the variable time step can be easily implemented using dual multiplications of the original time step, i.e. $\Delta t' = 2n.(\Delta t_o)$.

Piecewise curve fitting technique

In order to verify the proposed method capability of handling the classical piecewise fitting technique for the transformer non-linear reluctances, simulation cases were carried out using different number of piecewise segments. Figure 3.6 shows the simulation results using a nonlinear reluctance curve with nine equal length segments. The results show that the proposed method also converges for the piecewise curve implementation. This is an important finding since it is in some cases neither simple nor possible to have a best-fitted curve for the non-linear characteristics. As can be shown in Figure 3.6, the piecewise technique results in a maximum error of 5% during first cycle and 30% as the transformer inrush current decays. Increasing the number of segments will enhance the simulation results. On the other hand, the number of iterations is increased due to the introduction of more segments which will introduce more breakpoints and hence require more iterations.

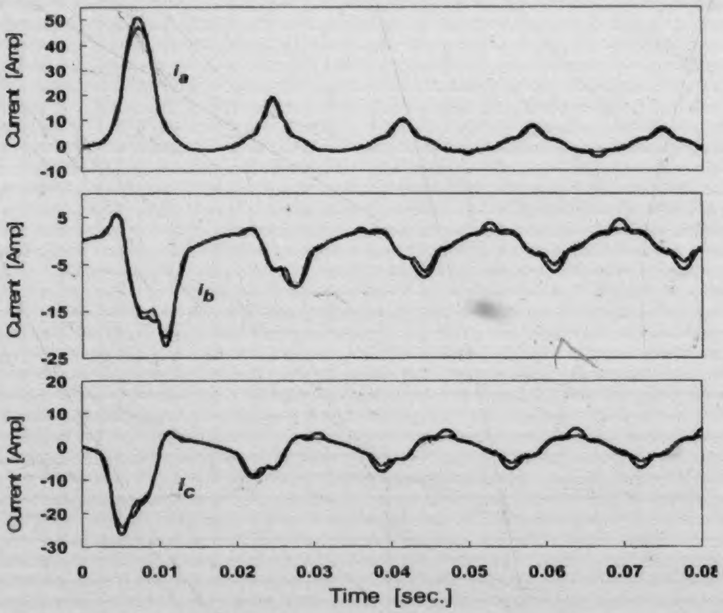

(a) Computed phase currents for piecewise 'doted' and continuous 'solid' reluctance curve representations.

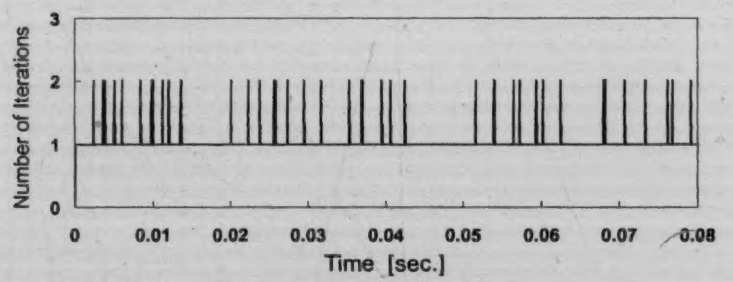

(b) Maximum number of iterations at each time step.

Figure 3.6 Instantaneous switching of the transformer described in 243 using 9-segment piecewise reluctance-flux curves.

3.5 Conclusions

In this chapter, a new application of the Newton-Raphson iterative method for solving three-phase non-linear transformer models has been developed and presented. The application of the Newton-Raphson method was based on the introduction of the non-linear reluctances as a function of system variables using either polynomial curve fitting techniques or piecewise segments.

A comparison of the proposed method against the predictor corrector method was carried out showing that the former method is not suitable for transformer inrush current modeling and simulation. The formulation of the Jacobian matrix using direct derivatives of the fitted reluctance curves or constant slopes of piecewise segments was shown to achieve a convergence error of less than 10^{-7} with a 10 μsec time step.

The simulation results using piecewise segments of equal length for the non-linear reluctances against the polynomial fitted method showed a tolerable difference between both the results. If a suitable fitted curve cannot be obtained, increasing the number of points of the piecewise curve will lead to the desired accuracy. The proposed simulation scheme can be easily applied for different applications, for example, other non-linear system components such as power electronic devices and variable speed drives.

4. Estimation of Transformer Saturation Characteristics from Inrush Waveforms

In this chapter, a novel method to estimate transformer saturation characteristics that extend to the 'deep' saturation region is presented. The basic idea of the method is to use the recorded inrush voltage and current waveforms to estimate the saturation characteristics. The recorded terminal voltage waveforms and phase currents directly available at the transformer terminals are used to estimate the transformer saturation characteristics. Accurate representation of a transformer's 'deep' saturation region is important for studying the impact of transformer energization and its inrush currents. The proposed parameter estimation technique does not require modification of the transformer terminals, measurement of transformers delta winding current nor special excitation sources at test location. The proposed method performance and accuracy have been verified by the close agreement between the simulation results and the recorded inrush waveforms.[2]

4.1 Introduction

As has been shown in preceding chapters, the proper and accurate representation of transformer saturation characteristics is essential for the analysis of transformer inrush behavior during saturation, either when using analytical or simulation analysis procedures. In addition, adequate modeling of transformer nonlinear characteristics is required for many electromagnetic transient studies where the study of overvoltages caused by ferroresonance is a representative example [68] and [69].

---

[2] A version of this chapter has been published: S.G. Abdulsalam, W. Xu, W. A. Neves and Xian Liu "Estimation of Transformer Saturation Characteristics from Inrush Current Waveforms", *IEEE Transactions on Power Delivery*, vol. 21, No. 1, pp. 170-177, Jan. 2006.

In this chapter, a novel, accurate and at the same time, practical method for determining transformer saturation characteristics will be presented. Moreover, the analysis carried out through the development of the parameter estimation technique reveals important characteristics of the transformer's core under saturation conditions. This analytical study was essential for obtaining an in-depth understanding of the sequential energization technique's effectiveness in reducing inrush currents.

It is well accepted that a straight line can approximate the flux-current curve for the deep saturation region: the so-called air core inductance. Unfortunately, standard tests usually do not drive transformer cores into deep saturation and may lead to large errors in the estimation of the air core inductance, affecting significantly the estimation of the transformer's inrush currents.

A number of methods for determining transformer saturation characteristics have been proposed in the literature. The most well-known procedure is the construction of the V_{rms}-I_{rms} open-circuit saturation curve by using a variable AC source. This method is feasible for laboratory set-ups using small and mid-range transformer sizes, but in many cases, the limited source capacity at the laboratory prevents this method from driving the transformer into deep saturation. Alternatively, the slope of the flux-current curve during saturation could be estimated from the physical dimensions of the transformer windings. Although this method is theoretically feasible, the transformer's detailed structural information is usually not available. Additionally, estimating the slope of the flux current curve during saturation is not sufficient for accurate representation of the flux-current curve since the point at which saturation occurs is not known.

A measurement method based on DC excitation was proposed in [70] and [71] to estimate transformer saturation curves. This method presents practical application difficulties for mid- and high-rating transformers due to the requirement for a large DC source at the test location. The algorithm presented in [38] to obtain the flux current relationship from inrush measurements strongly depends on the calculated residual flux values to determine the delta winding current. Reference [72] used finite element analysis to obtain saturation curves by accounting for the flux distribution in the iron core. The method requires the B-H characteristics supplied by the steel manufacturer. However, the butt joints and inevitable air gaps produced when assembling the transformer may lead to inaccuracies in the estimation of saturation curves.

An easy-to-use method for accurately estimating the transformer's non-linear characteristics is still lacking. The main goal of the work presented in this chapter is to develop such a method. As was shown in the previous chapter, an electric-magnetic circuit model represents the transformer, with the winding resistances, leakage inductances and the zero-sequence air reluctance assumed to be the known parameters from the classical short circuit, open circuit and zero sequence tests. In the developed method, all the remaining reluctances, which account for the effect of the limb and yoke fluxes, are calculated simultaneously from single-pole and three-pole switching inrush measurement data obtained from a three-limb three-phase transformer with Wye-Wye and Wye-Delta connections. The obtained reluctances account for the nonlinear magnetic coupling between the transformer limbs for a three-limb core topology and are very important in modeling transformers for transient or harmonic studies. The developed method does not have the pre-knowledge limitation of the residual flux level in the transformer and does not require the measurement of the delta winding current if present. The presented method could be applied for estimating the classical flux-current characteristics. After parameter identification, several inrush measurements were carried out and compared to the simulations for the corresponding situations. Very close agreement was found among them.

4.2 Parameter-Estimation Algorithm

The main focus of the parameter-estimation algorithm is to determine the nonlinear characteristics of the core limb and yoke reluctances for the transformer magnetic circuit shown in Figure 3.2 and described by the equation set (3.5). The algorithm utilizes the recorded voltage and current waveforms at the transformer primary winding produced during energization. The winding resistances, leakage inductances, exciting branch resistance and the air path reluctance are assumed to be known. The transformer's winding resistances and leakage inductances are linear parameters and can be determined through classical short circuit tests [73]-[76]. The open circuit tests can provide fairly accurate estimates of the magnetizing branch resistances representing losses in the transformer's iron core [77],[78],[79] and [80]. A zero sequence test as described in [71],[78], and [73] provides an accurate estimate of the air path reluctance $\Re_{oj}$ (assumed to be equal for each limb).

Fluxes and currents are the waveforms needed to find reluctances. The flux at each limb could be found easily through numerical integration of (4.1) solving for ϕ_j provided residual limb fluxes are known. Where the magnetizing current could be evaluated using (4.2) provided that the secondary winding current is known.

$$v_j = r_{jp} \cdot i_{jp} + l_{jp} \cdot di_{jp}/dt + N \cdot d\phi_j/dt \tag{4.1}$$

$$i_{mj} = i_{jp} - \frac{N}{r_{mj}} \cdot d\phi_j/dt - i_{js} \tag{4.2}$$

In other words, three fluxes and three current waveforms are all that are required to obtain the core reluctances. Unfortunately, using the detailed magnetic model described by in (3.5) there are five unknown fluxes ϕ_a, ϕ_b, ϕ_c, ϕ_{ab} and ϕ_{cb}. In order to find the limb and yoke reluctances; $\mathcal{R}_{La}$, $\mathcal{R}_{Lb}$, $\mathcal{R}_{Lc}$, $\mathcal{R}_{Ya}$ and $\mathcal{R}_{Yc}$ it is necessary to either add two additional equations or make assumptions to reduce the number of equations by two. In theory, the two new equations can be added by winding two new coils on both yokes to allow the measurement of magnetic fluxes from integration of induced voltage signals. This solution can only be implemented in research labs and it is not of practical application. The alternative used here is to assume that ϕ_{ab} and ϕ_{ab} are equal to the fluxes in the core outer limbs as shown in Figure 4.1.

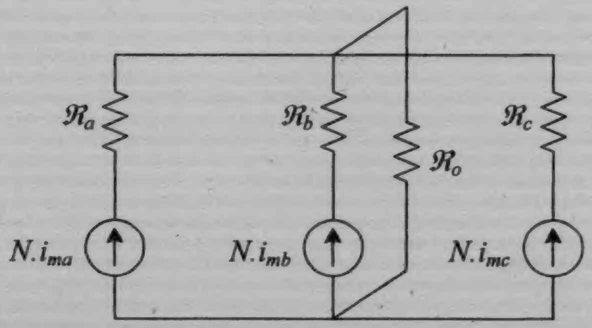

Figure 4.1 Approximate equivalent magnetic circuit for the three limb, E core, three-phase transformer.

The equivalent reluctances $\mathcal{R}_a$ and $\mathcal{R}_c$ represent the combined reluctance of limb and yoke reluctances $\mathcal{R}_{La} + \mathcal{R}_{Ya}$ and $\mathcal{R}_{Lc} + \mathcal{R}_{Yc}$ respectively. The combination of the air path reluctances $\mathcal{R}_{oa}$, $\mathcal{R}_{ob}$ and $\mathcal{R}_{oc}$ into a single central reluctance $\mathcal{R}_o$ will have a minor effect on the equivalent model accuracy [53], [54] and [77]. This is mainly due to the relatively high reluctance of air path as compared to the limb and yoke iron reluctances [71]. Here, $\mathcal{R}_o$ is assumed to be constant. It can be accurately calculated from zero sequence tests. It can be noted that the zero sequence flux from all limbs should strictly flow through the air path or a combined air gap-tank path in the presence of a tank. A comparison between the detailed and approximate magnetic circuit models represented in Figure 3.2 and Figure 4.1 has been done in [53] where the use of this model generated very good results regarding to both amplitude and shape of simulated waveforms compared to experimental results.

The approximate magnetic model shown in Figure 4.1 reduces the magnetic circuit model to 3 equations as follows,

$$\begin{gathered}
\mathcal{R}_a \cdot \phi_a - \mathcal{R}_b \cdot \phi_b = N \cdot i_{ma} - N \cdot i_{mb} \\
\mathcal{R}_b \cdot \phi_b - \mathcal{R}_c \cdot \phi_c = N \cdot i_{mc} - N \cdot i_{mb} \\
\mathcal{R}_b \cdot \phi_b + \mathcal{R}_o \cdot (\phi_a + \phi_b + \phi_c) = N \cdot i_{mb}
\end{gathered} \tag{4.3}$$

$$\begin{pmatrix} \mathcal{R}_a \\ \mathcal{R}_b \\ \mathcal{R}_c \end{pmatrix} = \begin{pmatrix} \phi_a & -\phi_b & 0 \\ 0 & \phi_b & -\phi_c \\ 0 & \phi_b & 0 \end{pmatrix}^{-1} \begin{pmatrix} N \cdot i_{ma} - N \cdot i_{mb} \\ N \cdot i_{mc} - N \cdot i_{mb} \\ N \cdot i_{mb} - \mathcal{R}_o \cdot \phi_o \end{pmatrix} \tag{4.4}$$

$$\phi_o = \phi_a + \phi_b + \phi_c \tag{4.5}$$

The general criterion to compute the core reluctances is as follows:

From measured current and voltage waveforms, use the trapezoidal rule of integration with appropriate time step Δt, calculate the magnetizing current in (4.2) taking into consideration the transformer connection and solve (4.1) for the flux ϕ_j in each core limb at each time step. The obtained tabulated values become as follows in series form:

$$i_{mj} = \{i_{mj}(t=0), i_{mj}(\Delta t), i_{mj}(2\Delta t), \dots\dots i_{mj}(N \cdot \Delta t)\} \tag{4.6}$$

$$\phi_j = \{\phi_j(t=0), \phi_j(\Delta t), \phi_j(2\Delta t), \dots\dots \phi_j(N \cdot \Delta t)\} \tag{4.7}$$

where N is the total number of samples.

Input magnetizing current and limb fluxes values into (4.3) and obtain all the core reluctances as a function of time for each time step:

$$\mathcal{R}_j = \{\mathcal{R}_j(t=0), \mathcal{R}_j(\Delta t), \mathcal{R}_j(2\Delta t), \dots\dots \mathcal{R}_j(N \cdot \Delta t)\} \tag{4.8}$$

The data series of ϕ_j and $\mathcal{R}_j$ defines the nonlinear reluctance characteristics of the transformer. Curve fitting techniques can be used to find equations most suitable to present the characteristic or simply through implementing a piece-wise representation as has been shown in earlier chapter.

In the following, more details of each step of the implemented algorithm is presented. Step 1 is accomplished through discretizing (4.1) and (4.2)

$$\begin{aligned}[V_j(t) + V_j(t_o)]\frac{\Delta t}{2} = r_{jp}[i_j(t) + i_j(t_o)]\frac{\Delta t}{2} + l_{jp}[i_j(t) - i_j(t_o)] \\ + N[\phi_j(t) - \phi_j(t_o)]\end{aligned} \tag{4.9}$$

$$\begin{aligned}[i_{mj}(t) + i_{mj}(t_o)]\frac{\Delta t}{2} = [i_{jp}(t) + i_{jp}(t_o)]\frac{\Delta t}{2} - \frac{N}{r_{mj}}[\phi_j(t) - \phi_j(t_o)] \\ - [i_{js}(t) + i_{js}(t_o)]\frac{\Delta t}{2}\end{aligned} \tag{4.10}$$

and solving for the flux at each limb;

$$\begin{aligned}\phi_j(t) = [V_j(t) + V_j(t_o)]\frac{\Delta t}{2N} - r_{jp}[i_j(t) + i_j(t_o)]\frac{\Delta t}{2N} \\ - \frac{l_{jp}}{N}[i_j(t) - i_j(t_o)] - [-\phi_j(t_o)]\end{aligned} \tag{4.11}$$

This equation implies that if the primary *voltage* and *current* waveforms together with the *initial fluxes* are known, corresponding to the first sample point of measured data, the waveform of the *fluxes* can be determined. It is worth noting that when calculating reluctances in step 2, the flux matrix shown in (4.4)(4.3) can, in theory, be ill conditioned. This case has never been encountered; however, if this happens in practice, the solution at that instant of time can be skipped. In the next two sections it will be shown how the magnetizing inrush current waveforms are computed considering transformer connections Wye-Wye and Wye-Delta, and how to estimate the residual flux needed to calculate the correct flux-current curve.

4.3 Calculation of Magnetizing Current

The magnetizing branch currents are essential in obtaining either the transformer Flux-Current or the Reluctance-Flux characteristics. According to the equivalent electric circuit shown in Figure 4.2, the measured primary current will contain the magnetizing current i_{mj} and the core loss current component, i_{cj}, in addition to the secondary winding current, i_{sj}.

For Wye-Wye connected transformers, each phase can be dealt with separately. Since there will be no current in the secondary winding, the magnetizing current waveform for each phase can be easily calculated subtracting the core loss current component from the measured primary current waveform as follows:

$$i_{mj} = i_{jp} - \frac{N}{r_{mj}} \cdot d\phi_j/dt \tag{4.12}$$

It should be noted here that the residual flux value is not required for the calculation of the magnetizing current. Only the induced voltage across the magnetizing branch is required which can be available directly from measurements on the secondary side. Another alternative is to calculate the induced voltage from the measured waveforms through direct substitution in equation (4.1) and calculating the induced voltage as:

$$N \cdot d\phi_j/dt = v_j - r_{jp} \cdot i_{jp} - l_{jp} \cdot di_{jp}/dt \tag{4.13}$$

For a Wye-Delta connected transformer the situation is quite different, Figure 4.2. During no-load steady state conditions, the induced voltages on the secondary side are nearly balanced and hence current in the delta winding can be neglected. However, during switching conditions, there might be an unbalance in the induced voltages due to the large voltage drops on the leakage reactance and resistance of the primary side winding. This unbalance is the main cause of the delta winding current during simultaneous three-pole switching.

According to Figure 4.2 and assuming the secondary side is connected in delta, the magnetizing current of each phase can be calculated by:

$$i_{mj} = i_{jp} - \frac{N}{r_{mj}} \cdot d\phi_j/dt - i_{delta} \tag{4.14}$$

The winding capacitance which is normally represented as a shunt capacitance in parallel with the magnetizing branch can be easily accounted for in (4.14). With a known winding capacitance, the capacitive charging current could be easily subtracted from the measured terminal current similar to the loss and delta current components in (4.14). The winding capacitance affects the shape of the saturation curve in the unsaturated region and results in an s-shpaed flux current curve if the capacitance charging current is not accounted for in the model and subtracted from the measured primary current, [77].

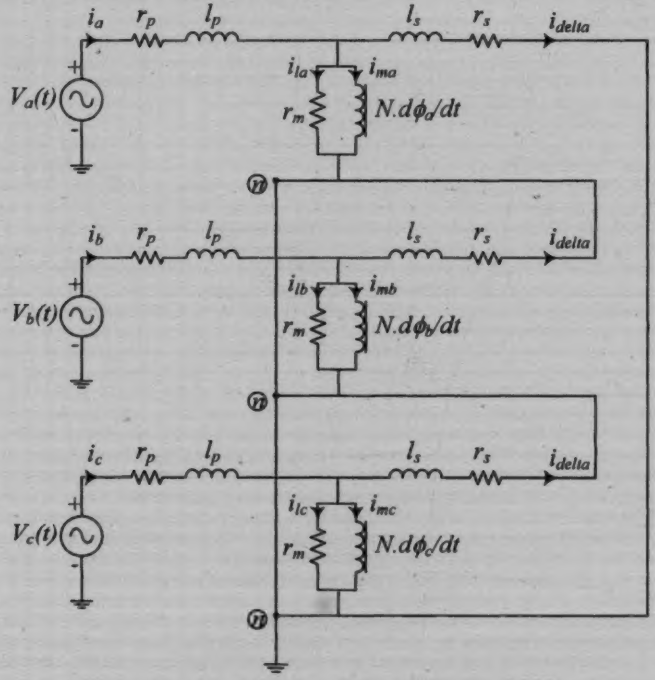

Figure 4.2 Equivalent electric circuit for a Wye-Delta transformer.

The circulating delta-winding current i_{delta} is calculated from the mesh equation for the closed delta at the transformer secondary according to:

$$N \cdot \sum_{j=a,b,c} d\phi_j/dt = 3 \cdot \left(r_{sj} \cdot i_{delta} + l_{sj} \cdot di_{delta}/dt\right) \tag{4.15}$$

The application of the numerical trapezoidal rule of integration to (4.15) leads to the following current at each time step.

$$i_{delta}(t) = \frac{N \cdot \sum_{j=a,b,c} \phi_j(t) - N \cdot \sum_{j=a,b,c} \phi_j(t_o) - 3 \cdot \left(r_s \cdot \frac{\Delta t}{2} + l_s\right) i_{delta}(t_o)}{3 \cdot \left(r_s \cdot \frac{\Delta t}{2} + l_s\right)} \tag{4.16}$$

The advantage of this method for calculating the delta winding current over the method described in [38] -regardless its simplicity- is that no assumption for residual flux values are needed. This is clear because when the transformer is switched off, there is no flux outside the core, and inside the core the residual limb fluxes always add up to zero. It can also be verified from (4.15) that the delta winding current depends only on the rate of change of flux 'induced voltages', which can be measured at the secondary side.

4.4 Residual Flux Estimation

When applying the previously described parameter estimation method, the values of initial fluxes in (4.11) must be known. If the recorded waveforms start at the instant of energization, the initial fluxes are essentially residual fluxes of the transformer limbs. Several methods have been proposed in literature to estimate or control the residual flux in transformer limbs [38],[81] and [74]. The most well known one is to record the de-energization voltage waveforms and to integrate them to estimate the residual flux [38].

Generally, it was found that the pre-estimate value of residual fluxes do not affect the shape of the flux-current curve in the saturation region. Figure 4.3 shows a family of saturation curves for different switching conditions, obtained assuming zero residual flux, for the laboratory transformer described in Appendix. The flux was obtained from numerical integration of the voltage waveform.

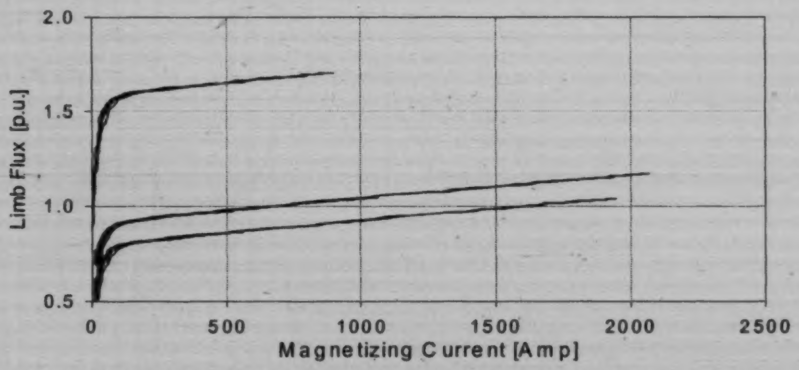

Figure 4.3 Flux-Current characteristics obtained for different cases assuming zero residual flux.

For all cases, when the current is greater than 2.0 [p.u], the slopes of the curves are the same constant value. Accordingly, the obtained constant slope can be used to extend the manufacturers or no-load test data. Usually, under no-load test conditions, such high current cannot be reached due to winding rated current limitations.

Alternatively to using de-energization data, a very simple method is proposed to estimate residual fluxes in order to find the correct flux inrush measurements. At least one point, corresponding to the tip of the no-load saturation curve (i_k, ϕ_k), needs to be known and taken as a reference. During transformer energization the current waveform is recorded and the flux is calculated numerically using (4.11) at each time step, assuming zero residual flux. For the magnetizing current i_k , two values of fluxes are calculated for the first cycle and averaged out to ϕ_{ave} The first flux value is calculated when the current reaches i_k and is increasing; the second when the current reaches i_k and is decreasing. The residual flux ϕ_r is equal to ϕ_k -ϕ_{ave}. Graphically, as shown in Figure 4.4, this corresponds to vertically shift the flux-current curve obtained numerically until it overlaps the no-load curve. If the estimated curve is above the no-load curve, the residual flux has negative polarity.

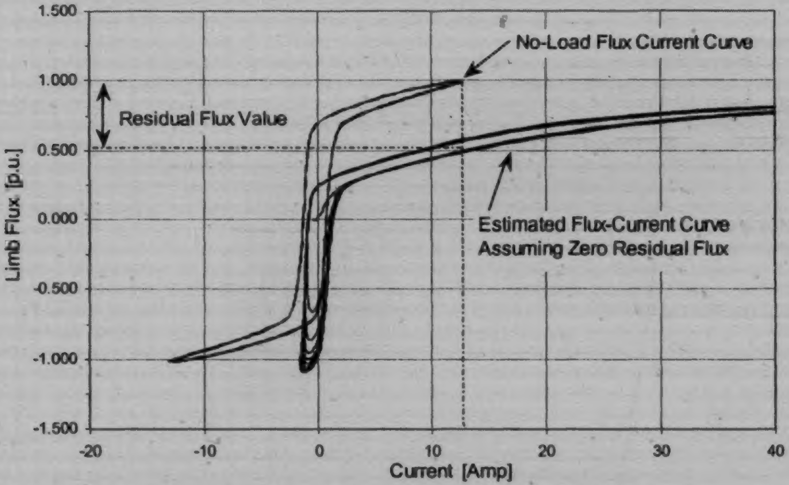

Figure 4.4 Estimating the residual flux value from No-Load Flux-Current curve and calculated flux-current curve during inrush conditions.

The method is repeated independently in each phase in case of using three-pole inrush energization data. First, the flux-current magnetizing curve in each phase is calculated assuming zero initial flux and taking into account the delta winding current if a delta connection exists. Second, the residual flux in each phase is adjusted independently in order to match the corresponding positive sequence hysteresis loop in that particular phase. The deeper the no-load curve gets into saturation, the higher the accuracy of the presented method and less sensitive to the accuracy of current measuring probes.

It is worth noting that only two residual fluxes need to be calculated since the residual fluxes in the three limbs add up to zero. Here, they were obtained from data of the two deepest saturated phases, corresponding to the transformer outer limbs. The approach described here is preferable than extending flux-current curves obtained from transformer manufacturer's data where the available data is off the deep saturation region, thus resulting in underestimation of inrush currents magnitude.

4.5 Model Verification and Simulation Results

The obtained transformer model non-linear characteristics were implemented to simulate the transformer response and compare the calculated current waveforms with those recorded during inrush. Three different operation conditions were simulated; no-load, single pole switching and three pole-switching conditions. The point-by-point recorded voltage waveforms at the transformer primary side together with the estimated initial residual flux values were used as inputs to the transient simulation program in order to simulate each case. In this condition no approximations or pre-estimates of the source impedance value or the switching angle were necessary.

4.5.1 Estimated Reluctance-Flux Curves

Transformer inrush currents can be three orders of magnitude higher than the no-load magnetizing current. As a practical limitation; measuring lab probes are usually not suitable for measurements in the two ranges simultaneously: the no-load magnetizing current range and the deep saturation range, for the same inrush measurements case. All the presented curves were obtained from primary voltages and currents waveforms sampled at 256 points per cycle. The parameter estimation algorithm here is implemented twice: first, for the unsaturated region; using data from no-load measurements and; for the saturated region, using data from single-pole and simultaneous three-pole switching inrush measurements for the transformer described in the Appendix with winding connections grounded Wye-Wye and grounded Wye-Delta. A sample result is shown in Figure 4.5 for the Flux-Current characteristics and in Figure 4.6 for the Reluctance-Flux curve obtained from the no-load waveforms.

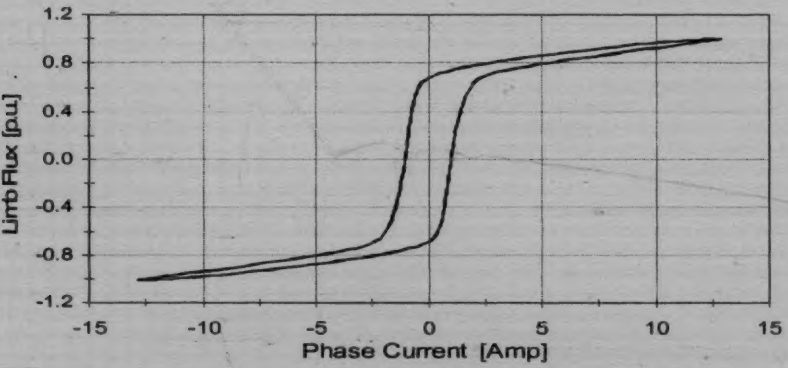

Figure 4.5 Calculated Hysteresis loop for the transformer under test.

In order to evaluate the nonlinear Reluctance-Flux characteristics up to the highest possible flux values, two switching procedures were implemented and compared: single-pole switching and simultaneous three-pole switching. For the first method, a number of single-pole switching cases have been carried out.

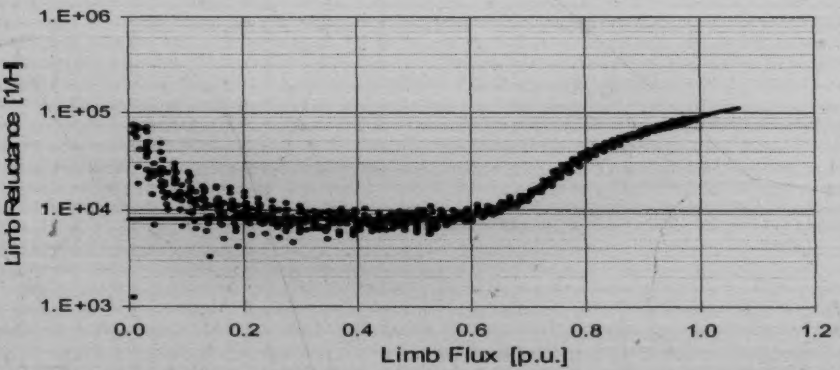

Figure 4.6 Reluctance-Flux characteristics obtained for the transformer under test using No-Load waveforms.

The highest recorded inrush current case is used to construct the higher part of the Reluctance-Flux curve. Figure 4.7 and Figure 4.8 are the calculated Flux-Current and Reluctance-Flux characteristics respectively obtained for the most severe inrush peak case. The calculated curve in Figure 4.8 was generated using the first ten cycles of the recorded maximum inrush current case due to single-pole switching.

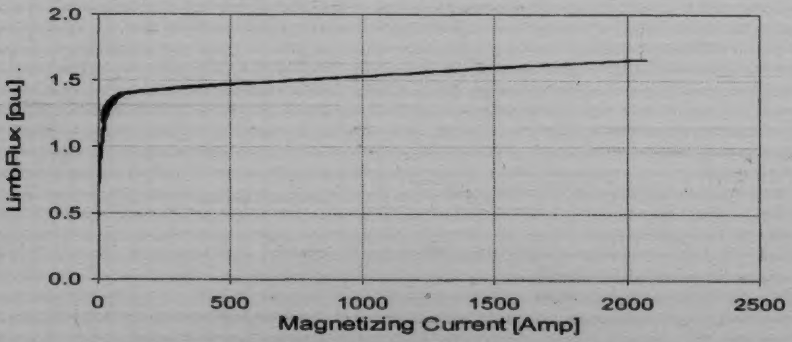

Figure 4.7 Flux-Current characteristics obtained for the highest recorded inrush peak considering the calculated residual fluxes.

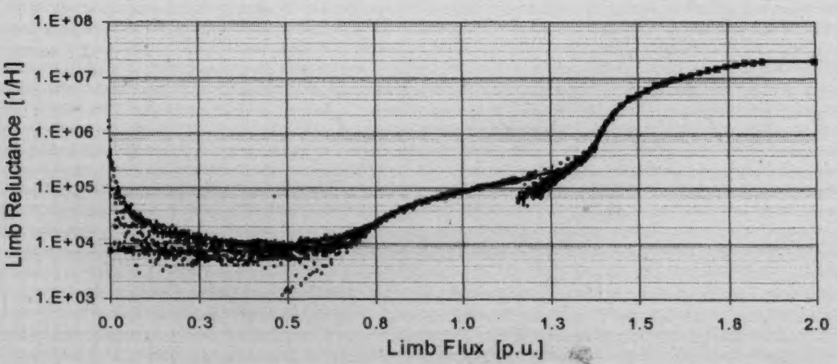

Figure 4.8 Reluctance-Flux characteristics obtained for the highest recorded inrush peak considering the calculated residual fluxes.

In order to measure current to a reasonable accuracy over a wide range, two simultaneous current measurements were taken at the same time using two different rating current clamps. The higher accuracy –Low Rating- clamp was used to record the current waveform up to 25 A, while higher current magnitudes were recorded from the high rating clamp. Generally, the accuracy of the estimated reluctance value depends on the accuracy of the current measurement. This describes the discontinuity and the noise experienced around a flux value of about 1.25 [p.u] in the reluctance curve shown in Figure 4.8. It is of value to note that the 25 Amps at which the measurements are been taken from the high-rating clamps only represent 1.0% of their rating and this clarifies the noise in the estimated value of reluctance. As the current picks up rapidly, in the saturation region, the accuracy of the current measurement will increase and hence the accuracy of the estimated reluctance value.

Flux-Current and Reluctance-Flux curves were obtained also using inrush waveforms from simultaneous three- pole switching. Here, more channels are required for recording signals of three-phase voltages and currents at the transformer primary side. The results are nearly the same as the ones obtained from single-pole switching. Figure 4.9 and Figure 4.10 show the calculated Flux-Current and Reluctance-Flux characteristics for the same transformer connected in Wye-Delta.

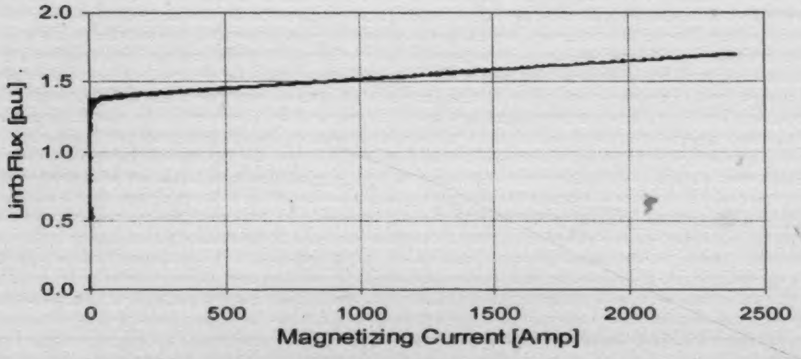

Figure 4.9 Flux-Current characteristics obtained for Wye-Delta connection and using simultaneous three-pole switching.

Only the saturated parts of the curves are shown in Figure 4.9 since only the higher rating clamps were used to limit the number of required recording channels. Using two different probes for measuring current simultaneously will require the use of 9 recording channels while the number of channels available was 8.

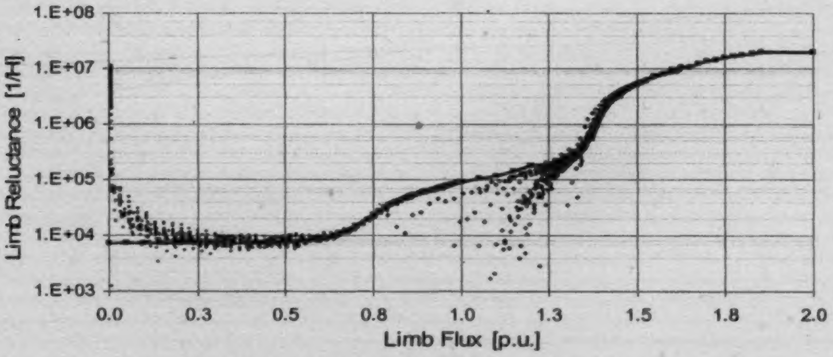

Figure 4.10 Reluctance-Flux characteristics obtained for Wye-Delta connection and using simultaneous three-pole switching.

Figure 4.10 verifies that using three phase switching waveforms will lead to the same transformer characteristics obtained from single phase switching. Finally, the non-linear portion of the Reluctance-Flux curve is fitted by a single polynomial function. The fitted non-linear portion of the Reluctance-Flux curve is shown in Figure 4.11.

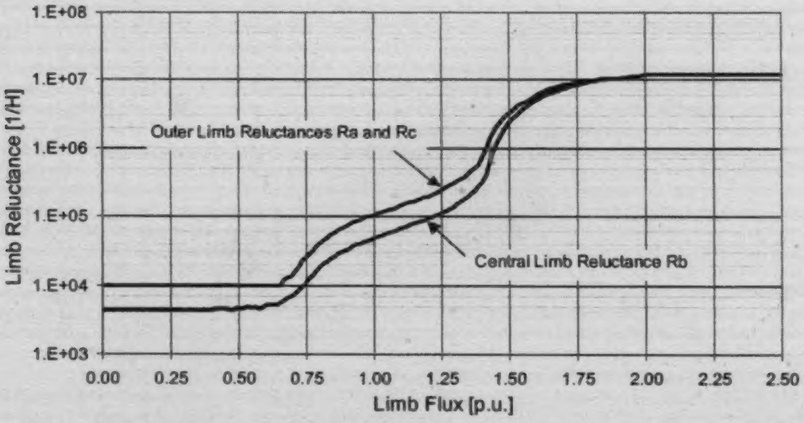

Figure 4.11 Reluctance-Flux characteristics obtained for central and outer limbs of the transformer given in Appendix.

For lower flux values, the curve is assumed to have a constant reluctance value while for higher flux; extrapolation might be used [53] and [54]. In this work, since a large number of experimental cases have been carried out, the highest reluctance value corresponding to the highest flux value obtained from experiments will be assumed to be the maximum reluctance.

The reluctance characteristics estimated from no load and inrush waveforms together will lead to the complete curve. Complete reluctance-flux curves are shown in Figure 4.11 for the outer 'phases A and C' and central 'phase B' limbs through combining the characteristic curves obtained through no-load and inrush conditions. It is clear from Figure 4.11 that the central limb will generally have a lower reluctance value for the same flux level as compared to the outer limb. This can be easily explained since the reluctances $\mathcal{R}_a$ and $\mathcal{R}_c$ combine both yoke and limb reluctances while the central limb consists only of the limb reluctance.

4.5.2 No-Load Operation

In order to verify the accuracy of the estimated reluctance at rated flux, no-load conditions were simulated and compared to measurements. Figure 4.12 shows measured and simulated waveforms for the current at one phase during no load test due to energizing phase A. The iron losses were modeled by a constant resistance with the value obtained at nominal no-load voltage.

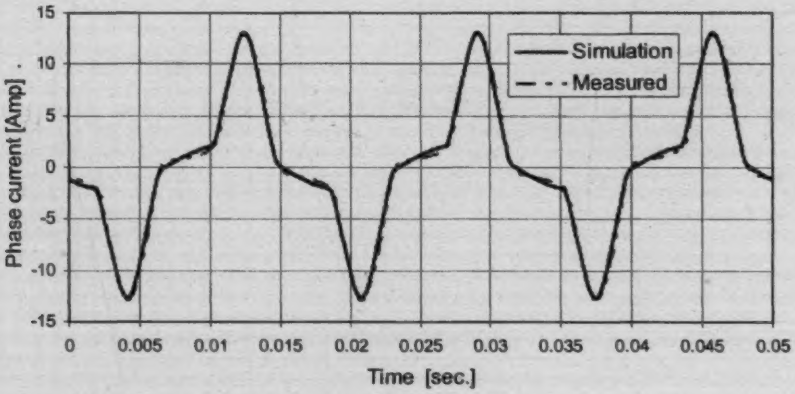

Figure 4.12 Measured and simulated No-Load current.

4.5.3 Single-Pole Switching

Here, a large number of single phase switching actions were carried out and the resulting inrush waveforms were recorded. Figure 4.13 shows the most severe inrush condition and both measured and simulated waveforms are presented. The first cycle of a less severe case is shown in Figure 4.15. The results show good agreement between simulated and measured waveforms from the magnitude and wave-shape point of view, which validates the accuracy of the estimated reluctance curve. A maximum error of no more than 5% in current magnitude was observed in all simulation cases.

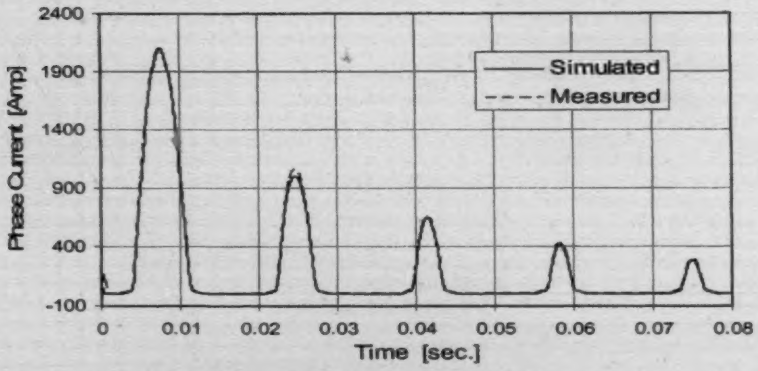

Figure 4.13 Simulated 'solid' and Measured 'dotted' highest inrush waveforms using the obtained Reluctance-Flux characteristics.

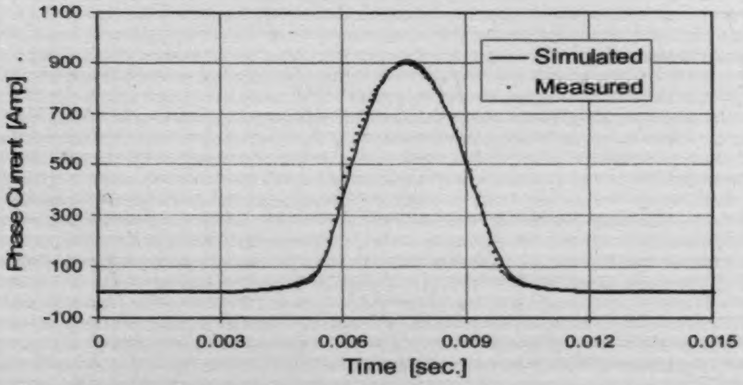

Figure 4.14 The first cycle of the simulated 'solid' and recorded 'dotted' mid-range inrush using single phase switching.

4.5.4 Simultaneous three-pole switching

Two cases for simultaneous three-pole switching on the transformer described in Appendix, with Wye-Delta and Wye-Wye connection, are presented. Figure 4.15 shows the measured and simulated inrush currents for Wye-Delta connection and Figure 4.16 for Wye-Wye connection. The estimated reluctance flux curve can accurately describe the nonlinear behaviour of the transformer during switching and normal operating conditions.

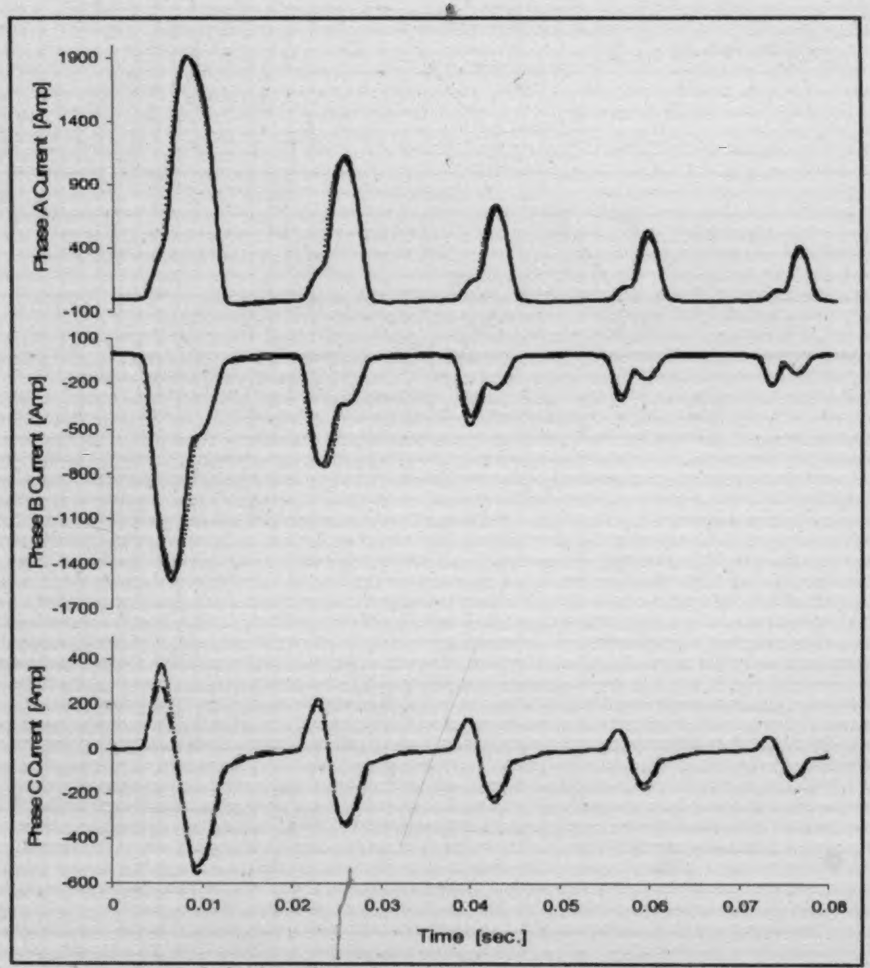

Figure 4.15 Recorded 'dotted' and simulated 'solid' energizing inrush currents for Wye-Delta connection.

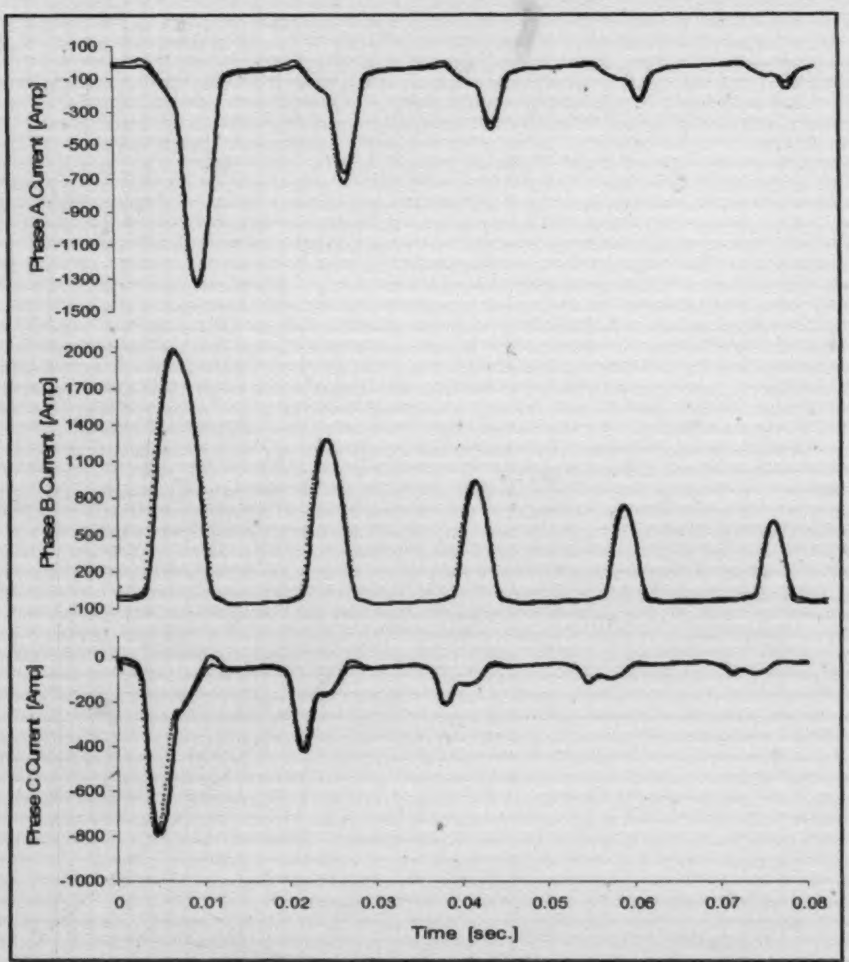

Figure 4.16 Recorded 'dotted' and simulated 'solid' energizing inrush currents for Wye-Wye connection.

4.6 Conclusions

In this chapter, a practical method for the estimation of nonlinear core reluctances of three-phase three-limb power transformers from inrush waveform data has been developed and was presented. The method could also be implemented for the estimation of the classical Flux-current saturation curve. In addition, it was shown that residual fluxes at each transformer limb could be estimated as well provided at least one point of the no-load curve, in the flux-current plane, is known. The use of inrush waveforms will ensure the estimation of the nonlinear characteristics up to high saturation levels. The developed method provides an accurate, easily implemented means for the estimation of transformer saturation characteristics. The estimated core nonlinear characteristics were used for the simulation of energization of a three-phase transformer with Wye-Wye and with Wye-Delta connections. Simulations and measurements were performed for single-pole and simultaneous three-pole switching operations and had shown to be in close agreement. The close matching brings confidence in the applicability of the method for practical purposes.

5. Performance of the Sequential Energization Scheme

In this chapter, the performance of the sequential energization scheme performance as applied to different transformer ratings and core-structure types will be investigated. The experimental investigation of the sequential energization scheme's effectiveness was carried out and presented on a laboratory, core-type, 30 kVA transformer. However, carrying out an experimental investigation on higher-rating transformers was not feasible. After developing the transformer modeling technique and validating its accuracy, it became possible to apply and study the sequential energization scheme's performance through simulation with different cases. A sensitivity study was carried out on the effect of the saturation parameters' deviation from the general performance characteristics of the sequential switching scheme.

5.1 Introduction

The sequential energization technique presents a novel inrush-reduction scheme due to transformer energization with possible application to capacitor switching. As was briefly explained in Chapter 1, the scheme involves the sequential energizing of the transformer's three phases together with the insertion of a properly sized resistor at the neutral point of the transformer's energizing side.

The neutral-resistor based scheme acts to minimize the induced voltage across the energized windings during sequential switching of each phase and, hence, minimizes the integral of the applied voltage across the windings. This neutral voltage will reduce the net voltage applied across the energized winding if this voltage has the same polarity as the applied supply voltage.

The scheme has the main advantage of being a simpler, more reliable, and more cost-effective than the synchronous switching and pre-insertion resistor schemes. The scheme has no requirements for the speed of the circuit breaker or the determination of the residual flux. Sequential switching of the three phases can be implemented through either introducing a mechanical delay between each pole arm in the case of three phase breakers or simply through adjusting the breaker trip-coil time delay for single pole breakers.

As will be explained in this chapter, experimental and simulation studies verified that the sequential energization scheme with a properly sized neutral resistor is as effective as the pre-insertion scheme. However, a much smaller resistor size is required with a sufficient insertion time. Both the experimental and simulation results showed that only a mechanical delay might be sufficient to achieve the desired coordination between the energized phases, and, hence, a sophisticated timing control circuitry for the circuit breaker pole tripping logic is not needed. More importantly, the neutral resistor's impact on the inrush current magnitude was found to be similar to that of the series resistors with first-phase energization leading to the highest inrush current magnitude.

The neutral-resistor-based scheme was further investigated by using higher-rating single-core type and three-limb core-type transformers with different secondary winding arrangements. All transformers with electrically or magnetically coupled circuits showed similar inrush-current-reduction behaviour as a function of the neutral resistor's size.

The scheme's performance was further tested through a sensitivity analysis study to show the impact of different saturation parameters on the performance and the optimum neutral resistor size.

5.2 Scheme Performance

In this section, the scheme's performance will be thoroughly presented through extensive experimental and simulation methodologies. First, the experimental results of the work conducted on the 30kVA laboratory transformer are presented to show the general performance characteristics of the sequential energization scheme. The transformer's behaviour during each energization stage was also studied, and inrush current waveforms were observed during all stages for different neutral resistor values. The performance of the scheme with both positive and negative switching sequences was also investigated and will be presented. The investigation was extended to other higher transformer ratings and to different transformer connection types and core-type structures.

5.2.1 Experimental Results

The sequential switching scheme was investigated through extensive laboratory experiments conducted on a 30-kVA, 208/208 Y-Delta, three-limb transformer (see Appendix). The main goal of the experimental work was to investigate the influence of the neutral grounding resistor on the resulting magnitude of the inrush current during sequential phase switching. The experiments were conducted by scanning different neutral resistor sizes for each energizing step. The main difficulties encountered in the experiments were as follows:

1. The switching instant could not be controlled.
2. An unknown amount of residual flux was present when the first phase is energized.
3. The supply system had impedance.

In order to overcome the first difficulty, for each switching stage, the switching event was repeated more than 100 times per each neutral resistor size. The results were then grouped according to the recorded phase angles of the supply voltage just prior to the instant of switching. The highest 'maximum' inrush current magnitude was extracted from the results accordingly for each resistor size. To overcome the second difficulty, the large number of switching events recorded was assumed to cover most conditions of the possible residual flux pattern in the core. The presence of the supply system impedance led to a higher inrush current estimate during the simulation study verification process. However, the impact of the series supply system's impedance was minimized using single core-type cable of sufficiently high gauge. Figure 5.1 demonstrates the impact of the system impedance on the distortion of the recorded phase-to-ground voltages at the transformer terminals during simultaneous three-phase energization with a Yg-Y connection. The corresponding three-phase inrush currents are shown in Figure 5.2.

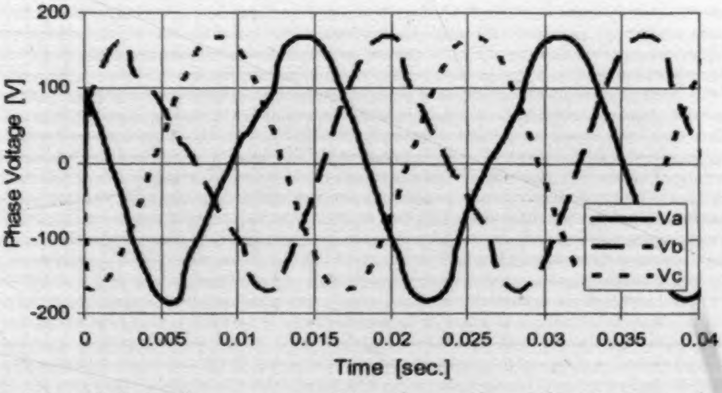

Figure 5.1 Recorded simultaneous energizing phase voltages for Yg-Y transformer.

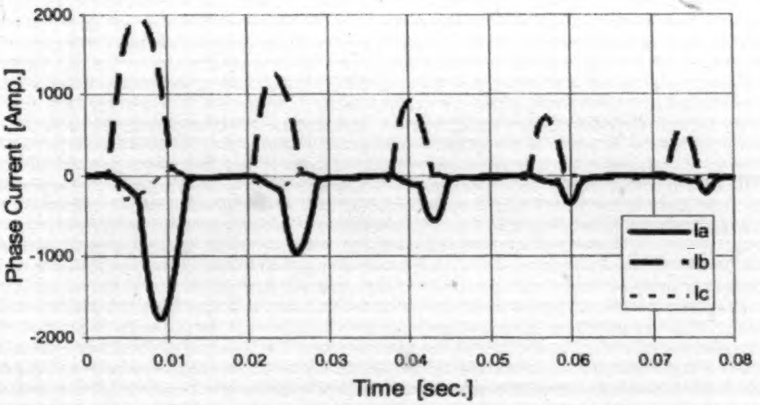

Figure 5.2 Recorded simultaneous energizing phase currents for Yg-Y transformer

- Impact of the neutral resistor size on inrush current:

The neutral resistor impact on the inrush current magnitude during sequential phase energization, $I_{max}(R_n)$, is shown for each energizing stage for the 30kVA transformer in Figure 5.3 below. The three curves have been produced independently as explained earlier through scanning different values of neutral resistor size and energizing from steady state conditions of the preceding stage.

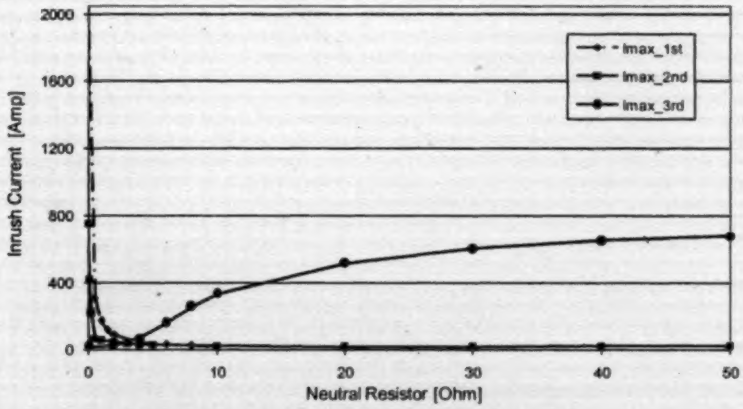

Figure 5.3 Magnitude of inrush current as affected by the neutral resistor, for Yg-Δ connection, positive sequence switching order.

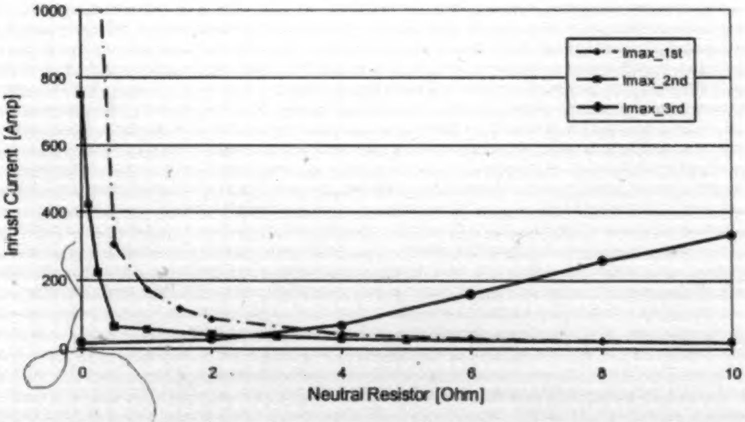

Figure 5.4 Magnitude of inrush current as affected by the neutral resistor, for Yg-Δ connection, positive sequence switching order. (Enlarged Portion)

The general characteristics of the sequential energization scheme could be obtained from the $I_{max}(R_n)$ curves shown in Figure 5.3 and Figure 5.4 as follows;

- The sequential energization technique could effectively reduce the inrush current magnitude through the application of a properly-sized neutral resistor.
- There is no requirement for a precise selection of the neutral resistor size. For the transformer under investigation, a neutral resistor size between 2 and 4Ω is sufficient to reduce the inrush current magnitude to below the transformer's rated current.
- The inrush current reduces rapidly for the first energized stage as the neutral resistor size; R_n.as the neutral resistor size is increased. This finding is obvious since the neutral resistor acts in series with the energized phase.
- Similar behaviour exists for the second energized phase. However, after a knee-point is reached, the inrush current continues to reduce at a much slower rate

before it starts to increase after a relatively large resistor value is reached, Figure 5.5.

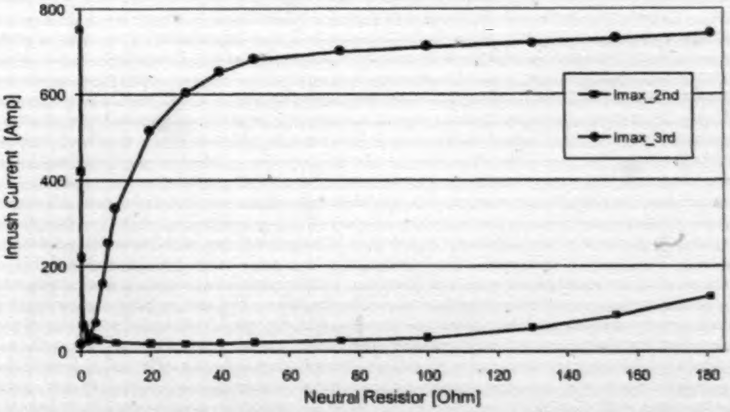

Figure 5.5 Extended 2nd and 3rd $I_{max}(R_n)$ curves, for Yg-Δ connection, positive sequence switching order.

- The third energized phase produces the lowest inrush current magnitude as compared to the first and second phases. This is true for the region at which the inrush current is effectively reduced by the neutral resistor. The inrush current magnitude increases sharply as the neutral resistor size is increased beyond the knee point of the $I_{max}(R_n)$ curves.

- For the region where the neutral resistor is highly effective in reducing the inrush current among the three phases, i.e. close to and slightly beyond the knee point of the $I_{max}(R_n)$ curves, the first switching stage leads the highest inrush current magnitude. The third phase $I_{max}(R_n)$ curve reflects the highest inrush current magnitude after it intersects with that of the first phase.

- It is not desirable to have the neutral resistor in the circuit when the 3rd phase is energized. It can easily be verified that for a magnetically or electrically coupled three phase transformer (3-leg Core or single phase units), the flux induced in the third winding core must be (neglecting leakage flux);

$$\phi_c = -(\phi_a + \phi_b)$$

- And hence for a zero neutral resistor value, the core flux of the third energized winding will be automatically synchronized with the voltage of the third switched phase regardless the switching instant, Figure 5.6.

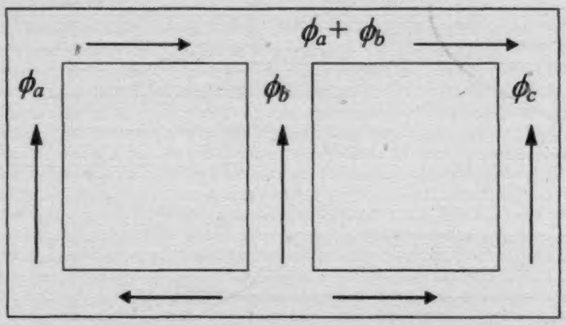

Figure 5.6 Flux distribution after energizing phases A and B.

Although the general characteristics listed above are derived directly from a study conducted on a single transformer unit, other transformer types/connections share similar general characteristics as will be shown in detail in the following sections through simulation studies.

- Impact of the sequential switching order on inrush current:

Similar experimental procedures have been carried out on the 30kVA transformer using a negative sequence switching order. The transformer terminals are energized with the following order Phase A followed by Phase C and finally Phase B completes the energization process. Figure 5.7 and Figure 5.8 present the $I_{max}(R_n)$ performance curves during each switching stage.

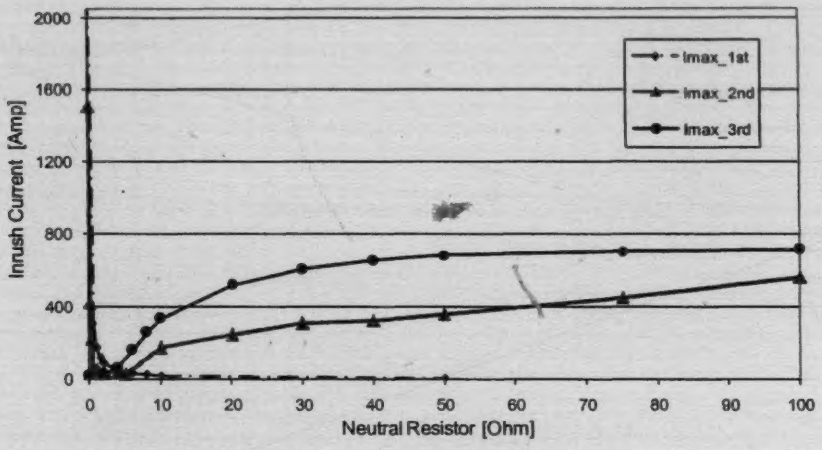

Figure 5.7 Magnitude of inrush current as affected by the neutral resistor, for Yg-Δ connection, negative sequence switching order.

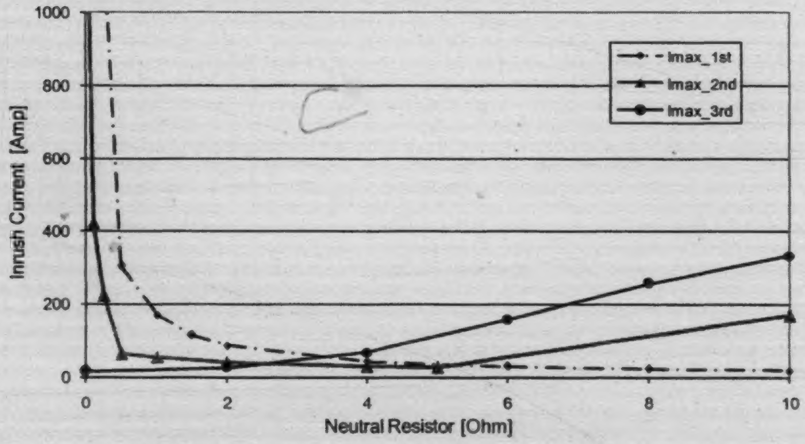

Figure 5.8 Magnitude of inrush current as affected by the neutral resistor, for Yg-Δ connection, negative sequence switching order. (Enlarged Portion)

Both the first and third switching stages share quite-similar performance characteristics as that for a positive energization procedure. However, the second stage energization has different behavior as the neutral resistor value increases beyond the knee point of the $I_{max}(R_n)$ curve. For small neutral resistor values, the 2nd stage $I_{max}(R_n)$ curve behaves similarly to that of the 1st stage and the inrush current reduces sharply as the neutral resistor size increases. However, after reaching the knee point, the current starts rising again as the neutral resistor size is increased further. Although, this behavior is one way or another, similar to that using a positive energization sequence, the inrush current magnitude doesn't remain close-to the no-load current for a large neutral resistor range beyond the knee point, Figure 5.11.

- Inrush Current Waveforms:

Figure 5.9 through Figure 5.11 show the inrush current waveforms during the energization of the first 'A', second 'B' and third 'C' phase respectively for a 2.0Ω neutral resistor that is slightly beyond the knee point of the $I_{max}(R_n)$ performance curves. From Figure 5.9, it is clear that for the first energized phase, Phase A, inrush current settles within few cycles to the normal no-load magnetizing current level. This finding is straightforward as the neutral resistor acts in series with the energized phase. As compared to the highest simultaneous inrush current level of 2100 A, the 2.0 W neutral resistors achieves more than 95% percent reduction of inrush current 'to 74 A' during first phase energization.

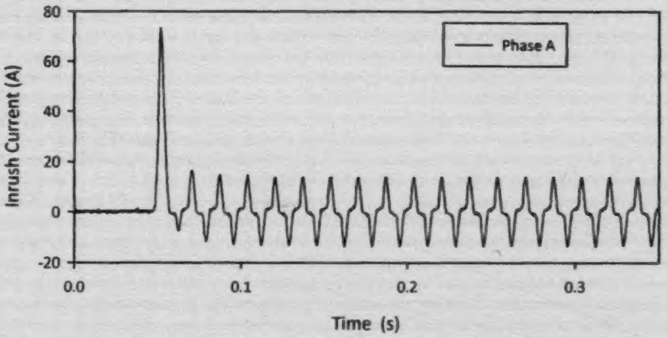

Figure 5.9 Typical inrush current waveform during 1st phase energization, R_n =2.0Ω.

For the second energization stage, Figure 5.10 shows the phase and neutral current waveforms for the highest recorded inrush current condition. It is clear through the inrush current decay rate, as compared to first phase energization, that the neutral resistor doesn't act fully in series with the energized phase(s). However, the neutral resistor reduced the inrush current during this stage to slightly below 40 A. More importantly, the energized phase B inrush current, doesn't correspond to the highest inrush current level. Alternatively, phase A yields the highest inrush level of 39A as compared to 17A for phase B.

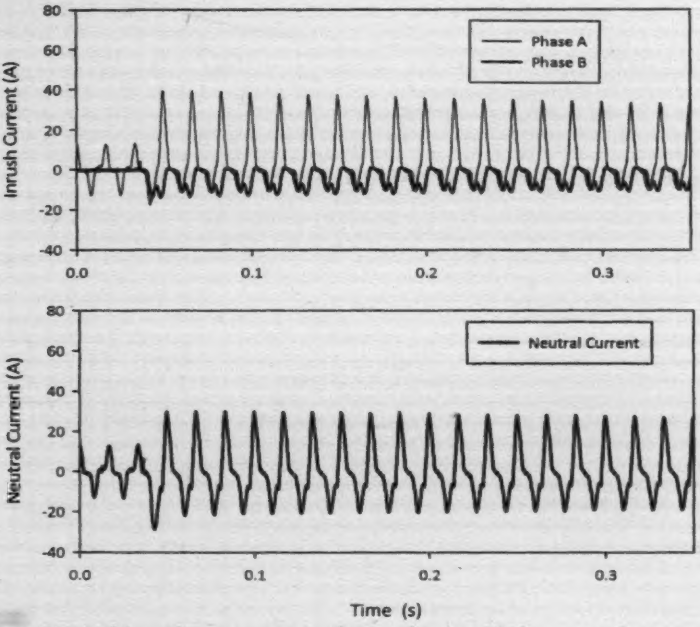

Figure 5.10 Typical inrush current waveforms (top) and the neutral current (bottom) during 2nd phase energization, $R_n = 2.0\ \Omega$.

At lower neutral resistor values ahead of the $I_{max}(R_n)$ curve knee point, the switched phase 'B' inrush current becomes higher than that of the earlier energized phase 'A'. Figure 5.11 shows the inrush current waveforms for this case with $R_n = 0.25\Omega$ which is slightly lower than the knee-point resistance. Closer to the knee point, Figure 5.12 shows the inrush waveforms for the case with $R_n = 0.5\Omega$. From the presented cases, it could be concluded that the maximum inrush current magnitude during the second energization stage could either exist in phase A or B depending on the neutral resistor value.

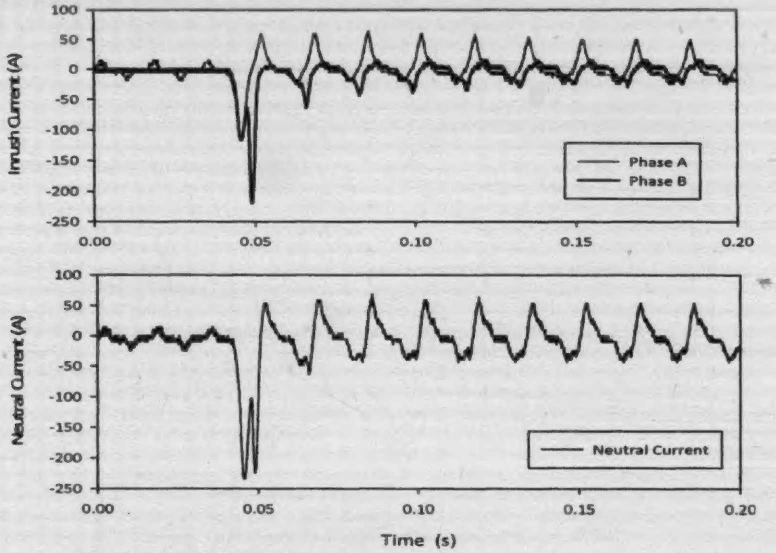

Figure 5.11 Inrush current waveforms (top) and the neutral current (bottom) during 2nd phase energization, $R_n = 0.25\Omega$.

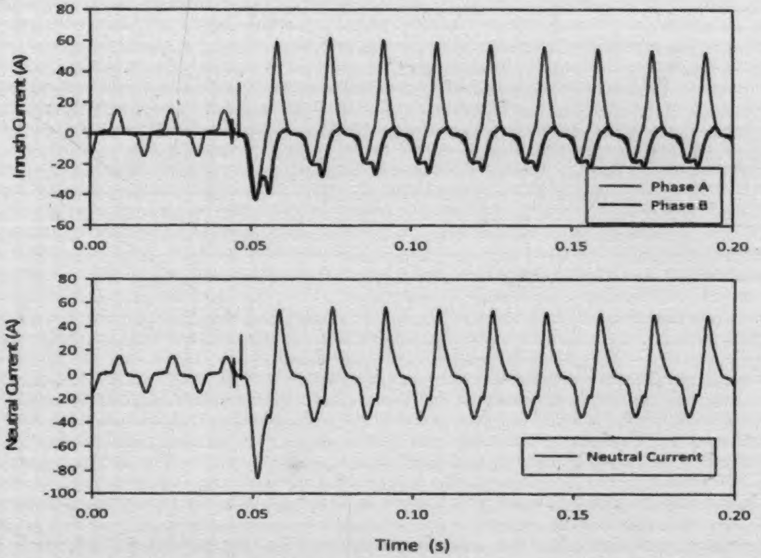

Figure 5.12 Inrush current waveforms (top) and the neutral current (bottom) during 2nd phase energization, $R_n = 0.5\Omega$.

As the neutral resistor size is increased further beyond the $I_{max}(R_n)$ curve knee point, the neutral resistor size becomes sufficiently large to pass the inrush current and both phases have nearly the same inrush current in opposite polarities. Figure 5.13 shows inrush waveforms for the case with R_n =50Ω. It is clear that a small neutral current magnitude is passing through the neutral resistor and both phases behave as if they are connected in series.

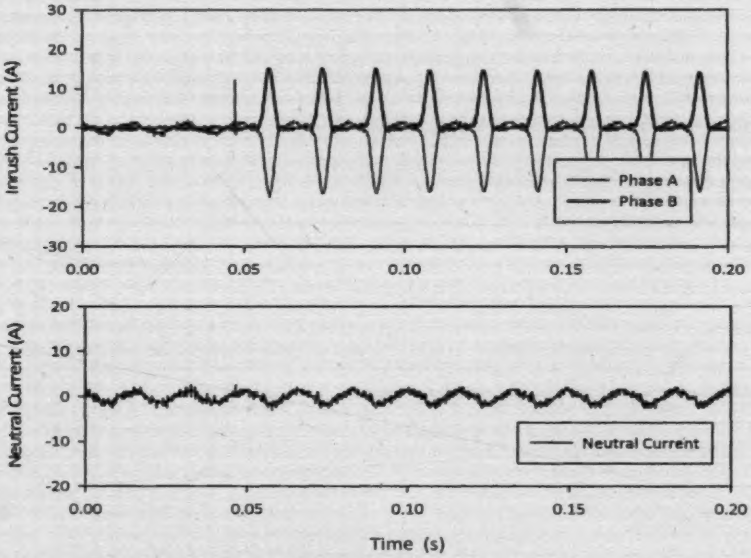

Figure 5.13 Inrush current waveforms (top) and the neutral current (bottom) during 2nd phase energization, R_n =50Ω.

Figure 5.14 shows the inrush currents in all three phases when the last phase, C, is energized with R_n =2.0Ω. Minimal transients are experienced in all three phases and a close to completely synchronous closing condition is established. More interestingly, the neutral current reduces almost instantaneously to zero when the third phase is energized. Accordingly, the transformer although with a resistor connected to the neutral point, behaves as a solidly grounded transformer in this case. This behaviour justifies why simultaneous energization of the three-phases with a neutral resistor doesn't work as an inrush mitigation technique.

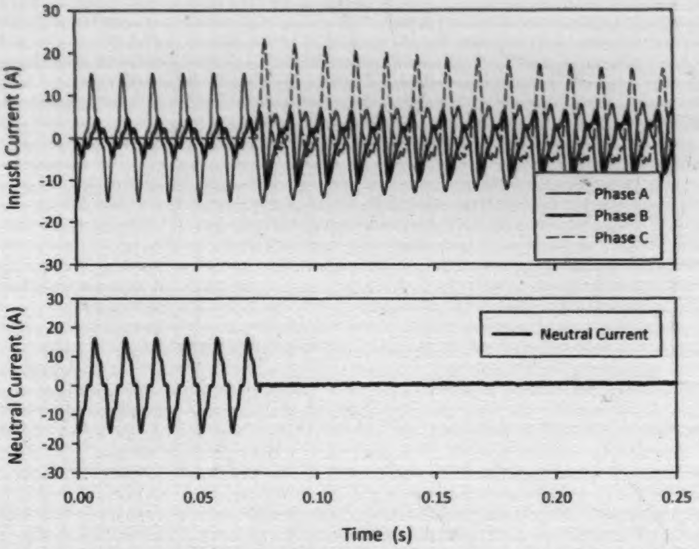

Figure 5.14 Inrush current waveforms (top) and the neutral current (bottom) during 3rd phase energization, $R_n = 2.0\ \Omega$.

A closer look at the neutral current waveforms during the second and third energization stages shows that most of the energy dissipated through the neutral resistor will be essentially during the second stage energization. The neutral current drops to zero immediately as the third phase is energized. For the first energization stage, although a neutral current exists that is equal to phase A current, immediately after the first few cycles, the inrush current drops significantly close to the no-load current level. Accordingly, the voltage across the resistor will be minimal as the knee-point neutral resistor value corresponds to a fraction of the transformer unsaturated reactance. More detailed analysis of the scheme performance and the neutral resistor sizing criteria will be discussed in detail in the following chapter.

5.2.2 Simulation Results

The sequential switching inrush mitigation scheme was further investigated through computer simulations. The simulation study provides means for applying the scheme to different transformer core-types, ratings, residual flux patterns and winding connections. Additionally, once the developed simulation model has been verified against the already measured experimental results, the scheme could be further investigated beyond the experimental facility capabilities. The simulation program was further enhanced with the capability of scanning through all possible voltage switching phase angles and outputting the resulting maximum inrush current. All simulation results presented here are for three transformers covering the major type of transformers available in the power system. The first transformer is the 30kVA, E-Core laboratory transformer described earlier. A real utility transformer that is 138MVA, 72/13.8kV, E-Core type transformer has also been modeled and extensively investigated. The third transformer model presents a 3X300MVA, 199.2/13.8 kV single phase bank units. All model parameters and data are given in the appendix for the three tested transformers. For each transformer under investigation, three sets of simulations were conducted on the transformer model derived earlier. The first set involves the closing of the first phase. The second set simulates the closing of the 2nd phase after the first phase has reached steady state. The third set is the energization of the 3rd phase with the second phase switching has reached steady state. Typical inrush current waveforms are shown in Figure 5.15 for the 30 kVA laboratory transformer with R_n =2.0Ω while different phases are energized. It is clear that the developed simulation technique replicate closely the sequential scheme performance as compared to the experimental results shown earlier. In terms of inrush current magnitude, simulation results yield 81, 45 and 24(A) for the first, second and third switching stages respectively which are in close agreement with experimental results.

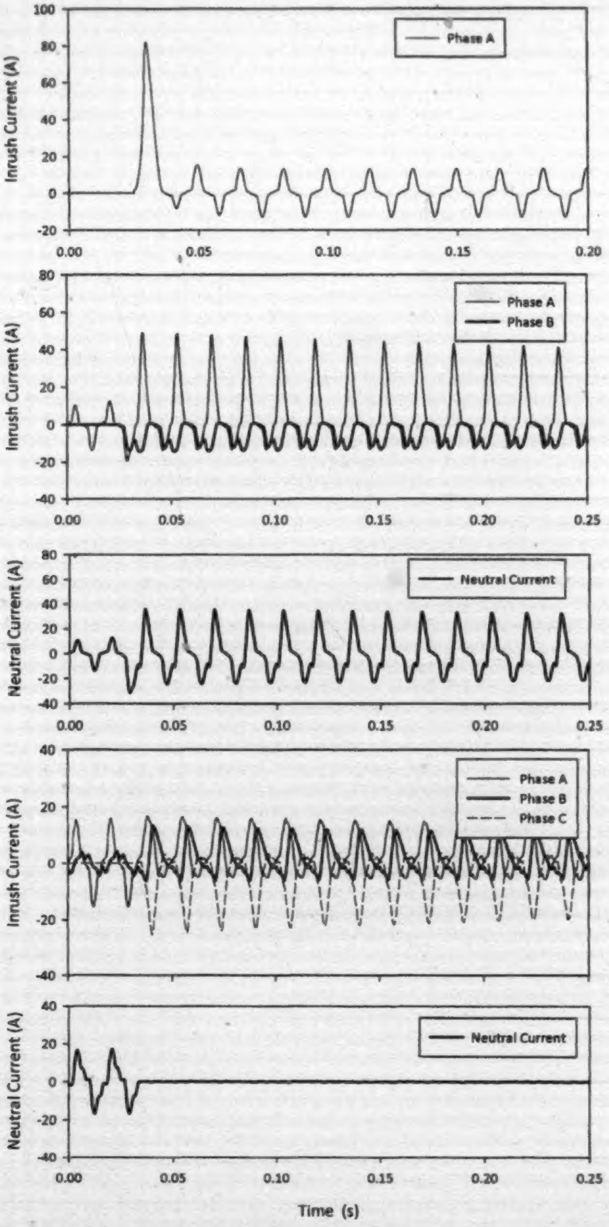

Figure 5.15 Sequential energization scheme performance through simulation for; First (Top), Second (Center) and Third (Bottom) energizing stages, R_n =2.0Ω.

- **Impact of the neutral resistor size on inrush current:**

The most important parameter for the proposed scheme is the neutral resistor value, R_n. In order to cover all possible energizing conditions, the voltage phase angles at the breaker closing instants are scanned through a complete cycle to obtain the maximum inrush current occurring in the energized phases after each energizing incident. The energizing angle was changed at steps of 4 electrical degrees on the supply voltage waveform. The $I_{max}(R_n)$ performance curves generated from simulation results are shown in Figure 5.16 and Figure 5.17 for the 30kVA laboratory transformer.

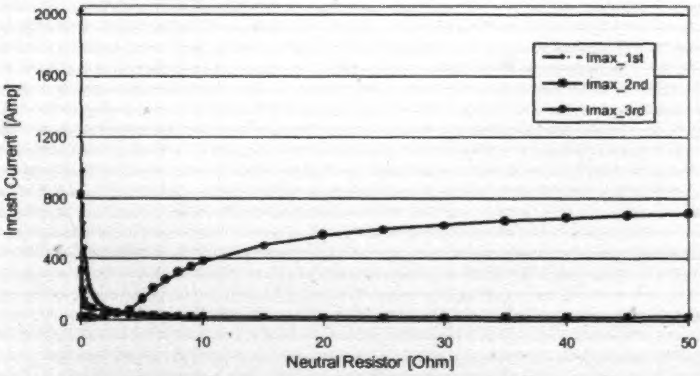

Figure 5.16 Magnitude of inrush current as affected by the neutral resistor, for Yg-Δ connection, positive sequence switching order.

d, simulation results lead to slightly higher inrush current estimate as compared to those of experimental results. Figure 5.18, shows the $I_{max}(R_n)$ curves extended to a neutral resistor value of 400Ω. Maximum deviation is in the order of 5-14% higher than those obtained through experimental work. With a positive-sequence energizing order, the second phase energization has a much lower inrush current magnitude and is much less sensitive to the change in R_n value compared to a negative switching sequence, Figure 5.19.

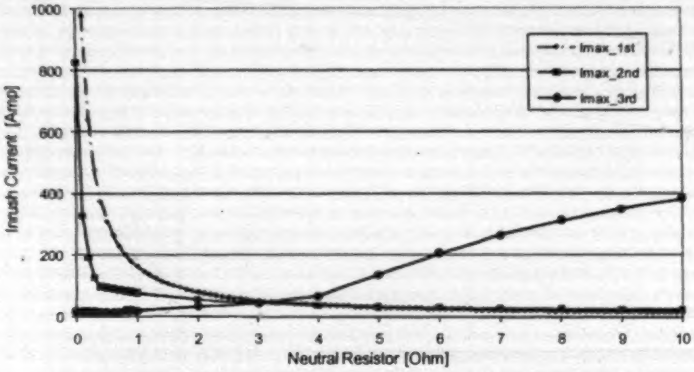

Figure 5.17 Magnitude of inrush current as affected by the neutral resistor, for Yg-Δ connection, positive-sequence switching order. (Enlarged Portion)

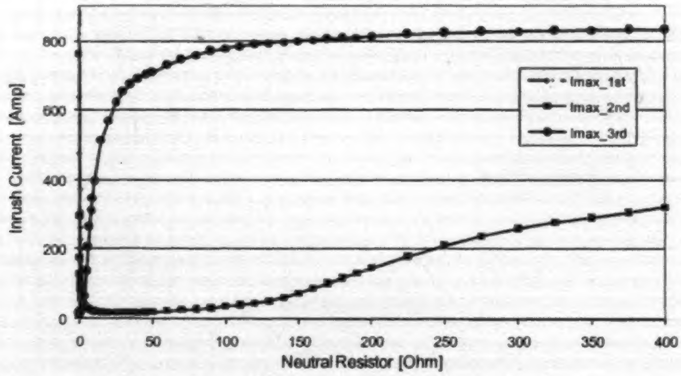

Figure 5.18 Extended $I_{max}(R_n)$ performance curves for a positive-sequence switching order.

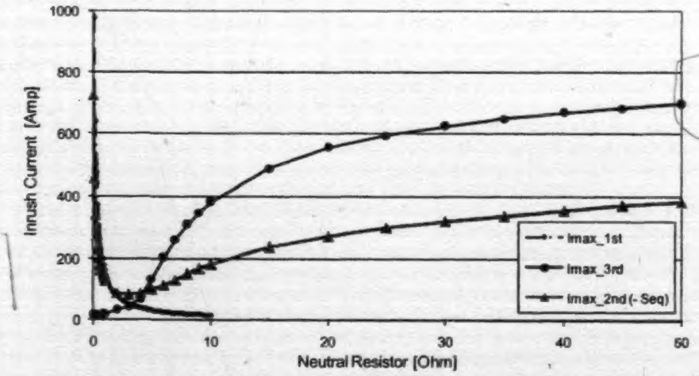

Figure 5.19 Magnitude of inrush current as affected by the neutral resistor, for Yg-Δ connection, negative-sequence switching order. (Enlarged Portion)

Same study was adopted on the 138MVA, 72/13.8 kV, Yg/Δ transformer,; the results are shown in Figure 5.20 and Figure 5.21. It is clear that this case follows the general performance characteristics as those concluded for the 30kVA transformer. However, inrush current magnitude and corresponding effective neutral resistor values are quite different due to the ratings of both transformer.

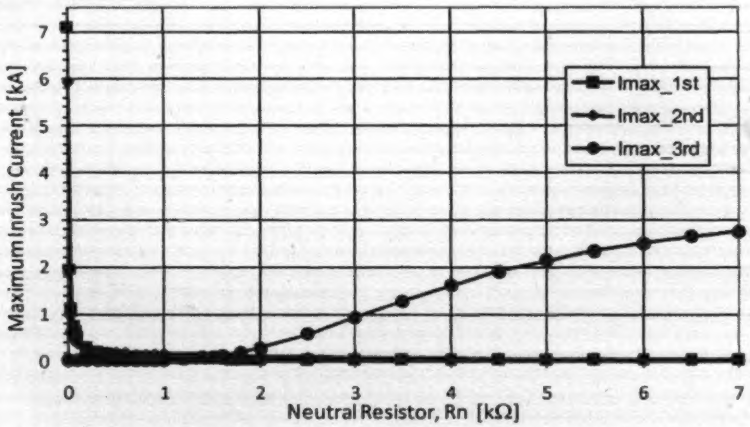

Figure 5.20 $I_{max}(R_n)$ performance curves for the 138MVA, 72/13.8 kV, Yg-Δ transformer with a positive –sequence switching order.

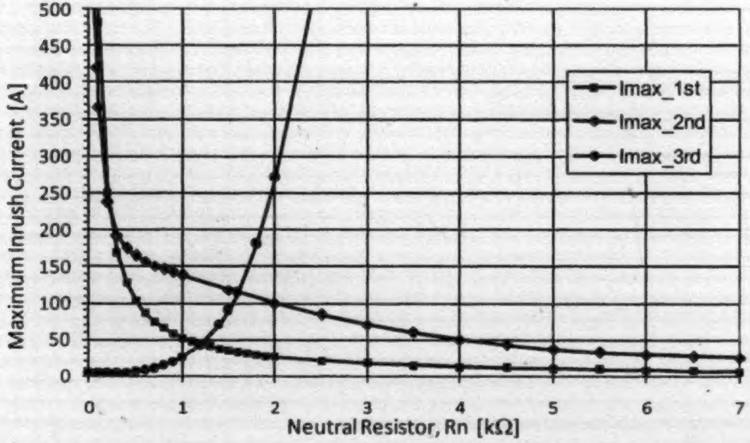

Figure 5.21 $I_{max}(R_n)$ performance curves for the 138MVA, 72/13.8 kV, Yg-Δ transformer with a positive –sequence switching order. (Enlarged Portion)

More importantly, the 2nd phase energization $I_{max}(R_n)$ shown in Figure 5.21 and Figure 5.17 for the 138MVA and the 30kVA transformer respectively shows that the 138MVA transformer has a slightly higher inrush current magnitude than that of the 30kVA one. In fact, the difference between both 1st and 2nd $I_{max}(R_n)$ curves is negligible with respect to the current rating of the transformer. The selection of the neutral resistor value close to the knee point of the $I_{max}(R_n)$ is sufficiently effective. The sensitivity analysis that will follow in the following section brings more understanding of the scheme performance as affected by different saturation characteristics.

For transformers consisting of three single-phase units, the case of 3x300 MVA, 199.2/13.8kV transformer units described in reference [26] was simulated. Figure 5.22 and Figure 5.23 show the results for Yg-Δ and Yg-Y connections respectively. For both cases only the second and third switching $I_{max}(R_n)$ curves are shown.

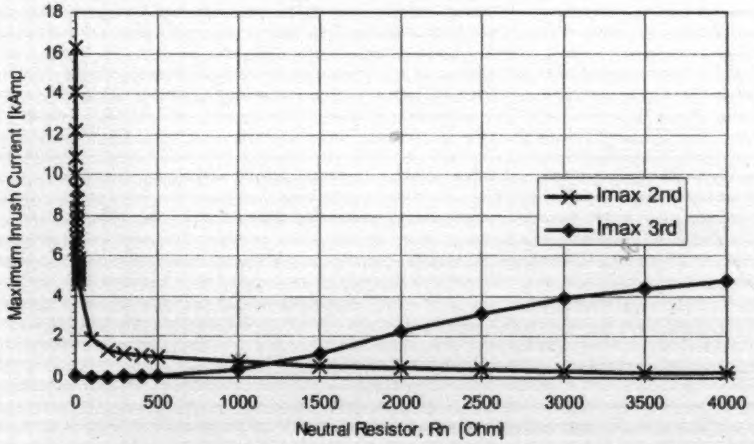

Figure 5.22 Maximum inrush current as affected by the neutral resistor, for 3x300MVA, 199.2/13.8kV, Yg-Δ connection, positive-sequence switching order.

It is clear that with a coupled electric circuit through the delta connection, a similar performance to transformers with E-Core structure exists. More interestingly, for a Yg-Y connection, the scheme could provide 85% reduction of inrush current among the three phases. Both second and third phase energization experience a sharp decrease of inrush current magnitude similarly to the achievable reduction of that for the first phase. Again, if an optimum neutral resistor is selected, it should be close to the knee-point of any of the three $I_{max}(R_n)$ curves.

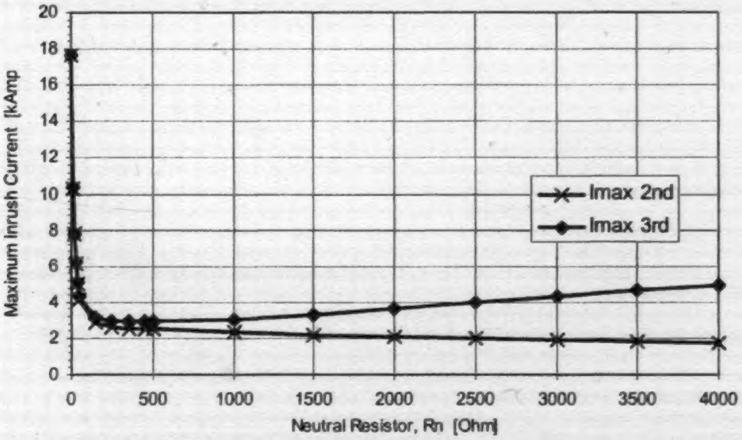

Figure 5.23 Maximum inrush current as affected by the neutral resistor, for 3x300MVA, 199.2/13.8kV, Yg-Y connection, positive-sequence switching order.

5.3 Sensitivity Analysis

In order to evaluate the effect of transformer saturation curve parameters on the $I_{max}(R_n)$ performance curves, sensitivity studies need to be performed assuming different saturation parameters. The study gives a general idea on how different saturation parameters affect the selection of an optimum neutral resistor size. Sample sensitivity studies are presented for the

72/13.8kV, Yg-Δ, 138 MVA, E-Core transformer, [26]. Two main saturation parameters have been varied:

1. The saturation curve slope L_s :

First a reference value has to be chosen which is the value shown for Ls=100%. This value has been set to results in a maximum inrush of 10 times the nominal full load current at the high voltage side (72 kV) with no residual flux. The value of Ls=175% results in approximately 10 times rated full load current with the assumption of 70% residual flux in Phase A.

2. Saturation Flux level:

Two typical saturation flux levels are presented. One is for saturation flux level of 1.25 [p.u.] and the other point is chosen at 1.35 [p.u.]. The choice of these two saturation levels based on the complete saturation curves measured and published in [32] and on transformer parameter estimation work presented in [25]. Figure 5.24 shows the complete measured saturation curve for 1MVA, Yg-Δ 3-Limb transformer published in [32].

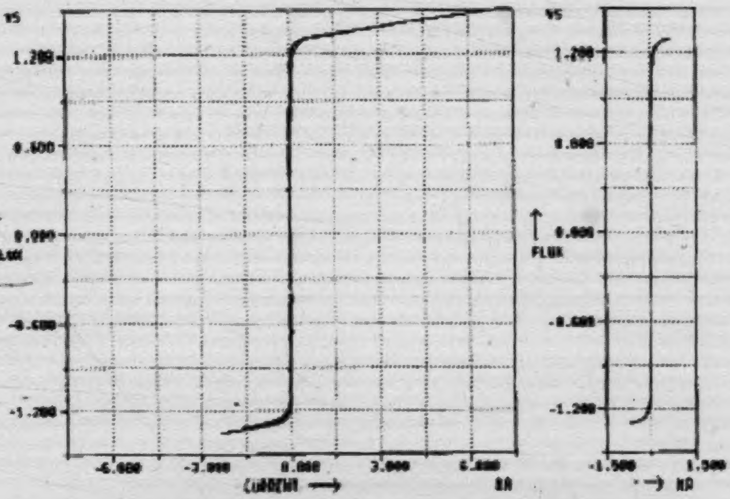

Figure 5.24 Measured saturation curve for 1 MVA, Yg-Δ 3-Limb transformer, [32].

Figure 5.25 shows the maximum inrush current performance curves, $I_{max}(R_n)$, for the first and second stage energization. A saturation level of 1.25 (p.u.) is assumed and the saturation slope has been varied from 75% to 125% of the rated saturation slope 100% as described earlier.

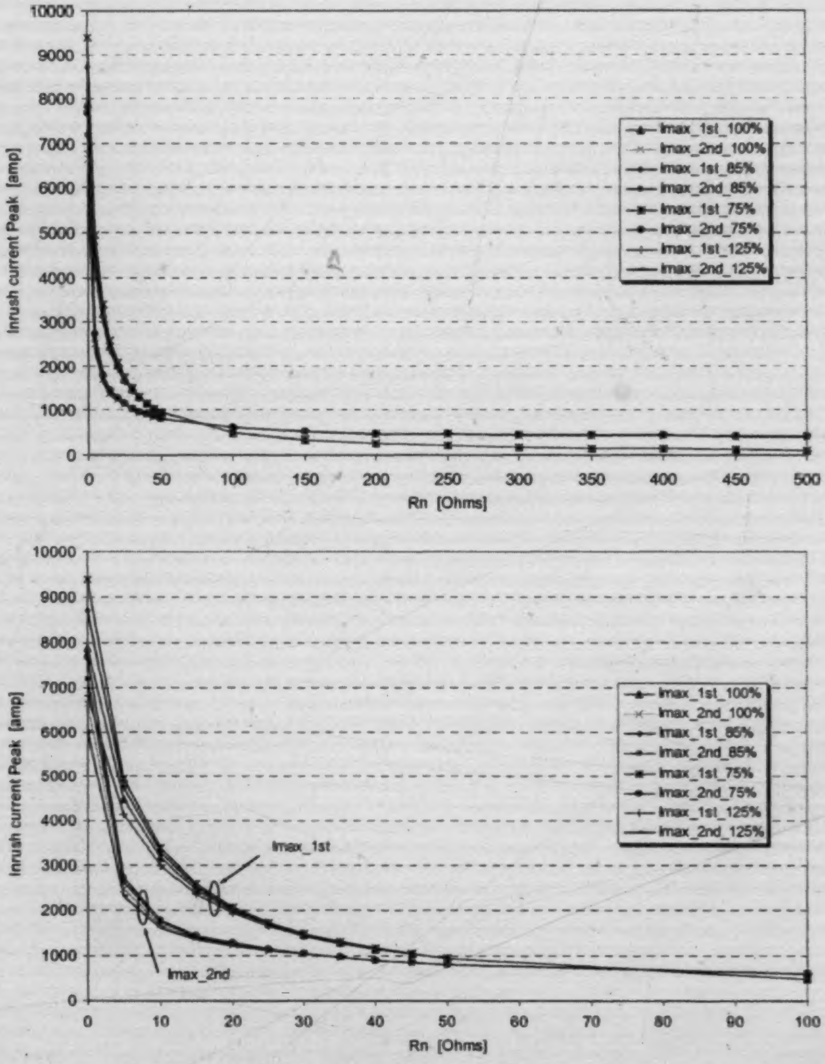

Figure 5.25 First and Second phase switching $I_{max}(R_n)$ curves for saturation starting at 1.35 p.u (Top). Enlarged portion (Bottom) showing the intersection points of the curves (around 80 Ohms)

It is clear from Figure 5.25 that the change of saturation slope 'air-core inductance', affects significantly the maximum inrush current for small neutral resistor values during both first and second stage energization. The higher the saturation slope 'L_s', the lower is the maximum inrush current magnitude for a given value of R_n. For $R_n = 0$, varying the saturation slope from 75% to 125% leads to inrush current level of 9400 and 6800 respectively for the first energization. For second phase energization, the maximum inrush current is 7800 and 6000 (A) respectively. However, as R_n increases, the effect of the saturation slope L_s becomes minimal and the inrush current magnitude is more dominantly related to the neutral resistor, R_n.

More importantly, the second phase switching $I_{max}(R_n)$ curve experiences a similar sharp decrease rate to that of the first phase switching as R_n increases. Additionally, the second switching $I_{max}(R_n)$ curve is below that of the first switching up to the knee point of either curve. In other words, the neutral resistor acts similarly to a series pre-inserted resistor during second phase energization. After passing the knee point, both first and second switching stage maximum inrush current decreases at a much slower rate as R_n is increased further. Beyond the knee point of the $I_{max}(R_n)$, increasing the neutral resistor size won't have a significant effect of reducing the inrush current magnitude during either switching stages.

For a lower saturation flux level at 1.25 p.u., Figure 5.26 and Figure 5.27 show the $I_{max}(R_n)$ performance curves for the first and second switching stages respectively. As expected, with a lower saturation flux level, inrush current magnitudes are higher for the same value of R_n as compared to a saturation level of 1.35 p.u.. For $R_n = 0$, varying the saturation slope from 75% to 125% leads to inrush current level of 11200 and 7100 respectively for the first phase energization. For second phase energization, the maximum inrush current is 8500 and 6500 (A) respectively.

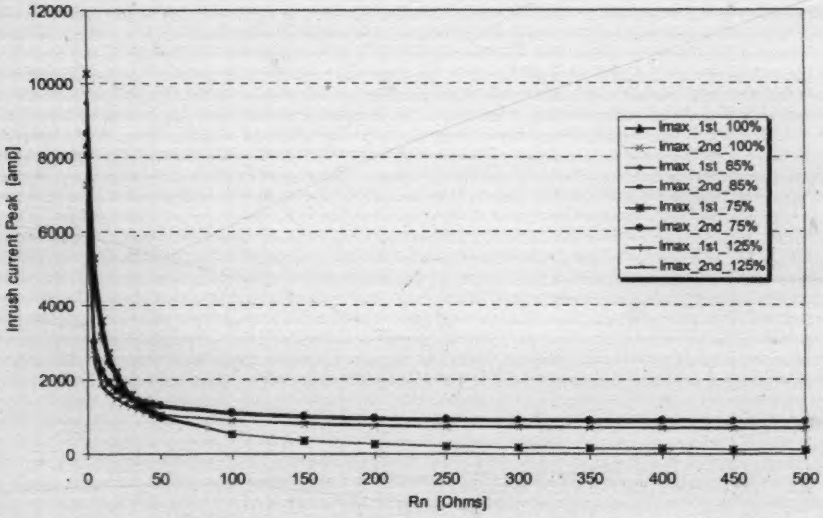

Figure 5.26 First and Second phase switching $I_{max}(R_n)$ curves for saturation starting at 1.25 p.u.

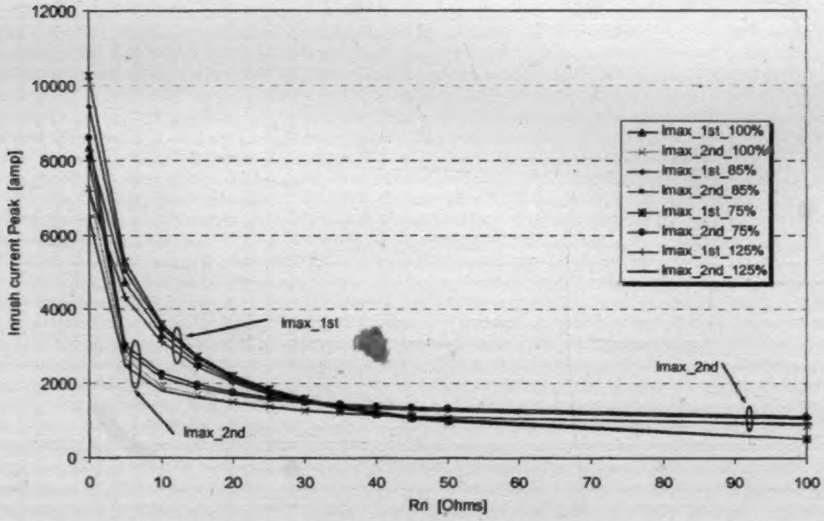

Figure 5.27 First and Second phase switching $I_{max}(R_n)$ curves for saturation starting at 1.25 p.u (Top). Enlarged portion (Bottom) showing the intersection points of the curves (around 30-40 Ohms).

Following the knee point of both first and second phase energization, the inrush current decreases at a slower rate but however, around a higher magnitude as compared to that of the former case with 1.35 p.u. saturation level. Moreover, the knee point of both $I_{max}(R_n)$ curves occurs at a lower neutral resistor value of 30-40Ω as compared to 80Ω in the former case. The effect of the saturation slope L_s becomes more evident with lower saturation flux levels for the second phase energization stage. Although the $I_{max}(R_n)$ of the second phase energization stage follow the same slowly-decreasing pattern following the knee point, the inrush current magnitudes settle at different values for each respective saturation slope. The steeper 'loser slope' saturation characteristics leads to a higher inrush magnitude and vice versa. However, all curves, share a common knee-point around 30-40Ω of R_n.

Figure 5.28 and Figure 5.29 show the individual first and second phase energization $I_{max}(R_n)$ curves for both saturation levels respectively. The results show that with a lower saturation flux level, more deviation in the performance curves are pronounced for either stage.

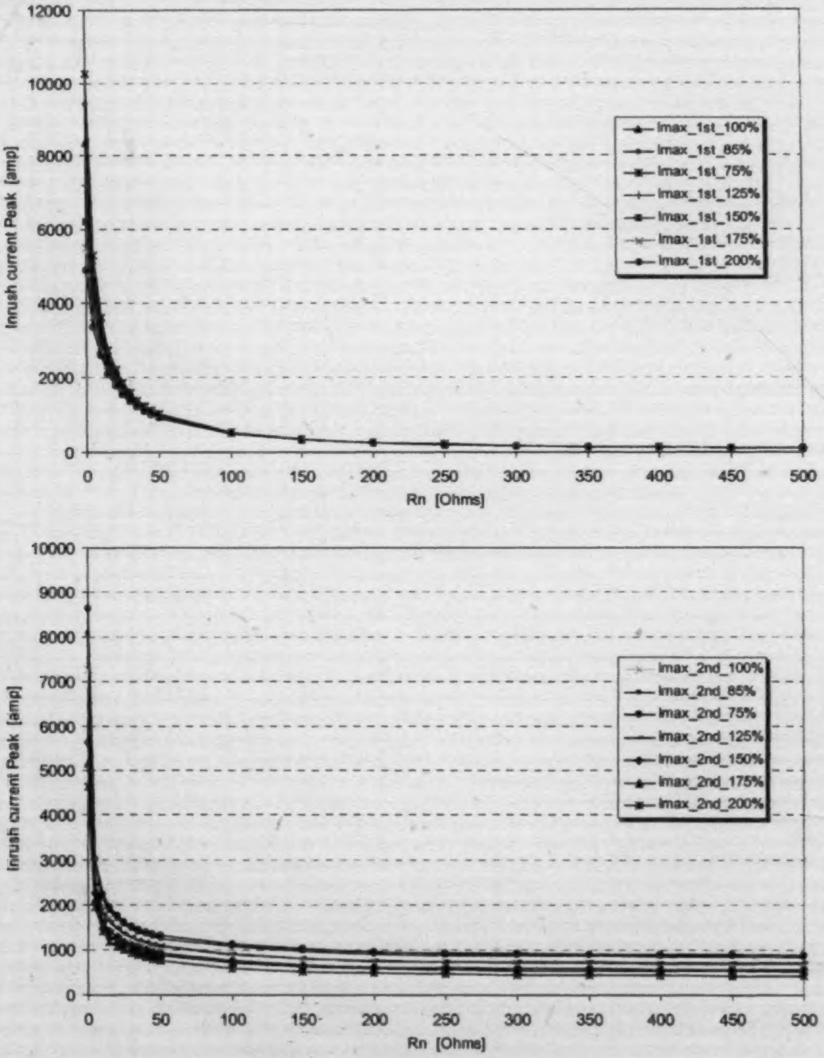

Figure 5.28 $I_{max}(R_n)$ curves for saturation starting at 1.25 p.u. First phase energization (Top) and second phase (Bottom).

The impact on the second energization is more evidently shown from comparing the 2nd phase energization $I_{max}(R_n)$ curves shown in Figure 5.28 and Figure 5.29. It is clear that the neutral resistor will have a lower ability to reduce the inrush current magnitude with higher saturation levels combined with a lower saturation slope.

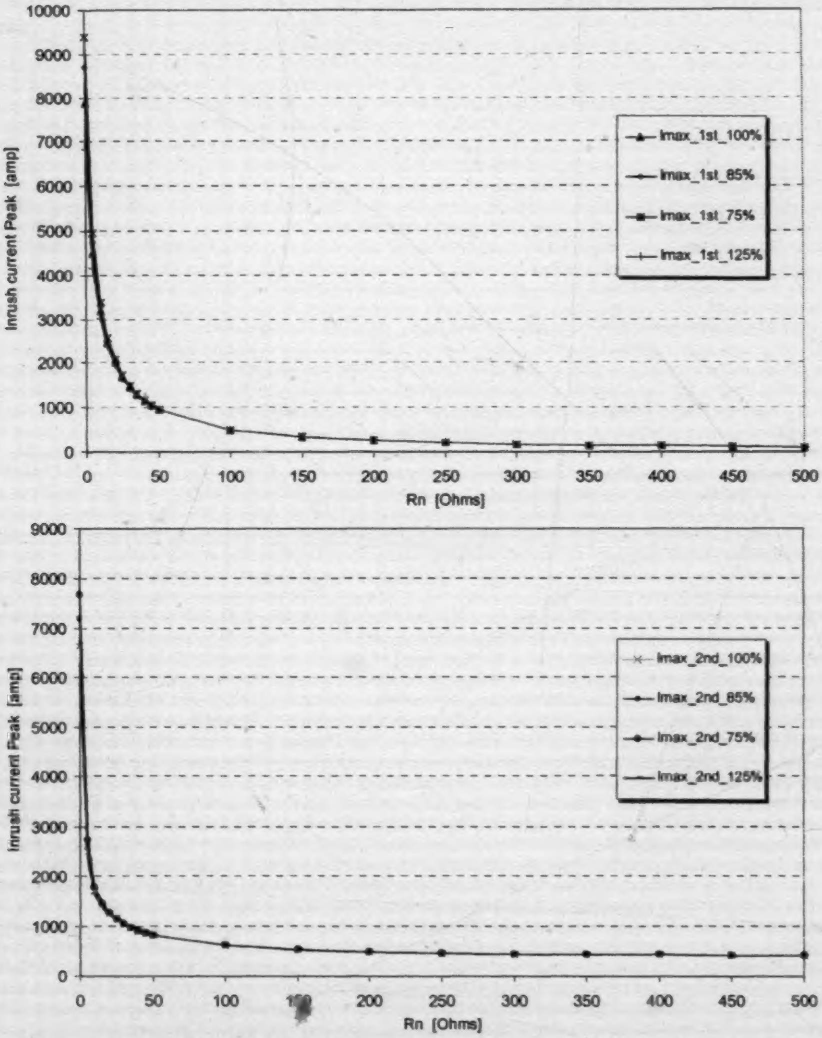

Figure 5.29 $I_{max}(R_n)$ curves for saturation starting at 1.35 p.u. First phase energization (Top) and second phase (Bottom).

5.4 Conclusions

After the investigation of extensive experimental, simulation and sensitivity analysis results for different transformer types and/or connections, the following performance characteristics of the sequential energization technique can be listed as follows;

- ☐ The sequential energization technique is effective in reducing the inrush current level to more than 90% for all transformer types energized from the Yg side.
- ☐ A sufficiently reasonable range of neutral resistor values is capable of achieving an optimized inrush current reduction among all-three phases.
- ☐ Inrush current occurs in all the electrically energized phases. For example, all three phases experience inrush currents when the third phase is switched in. The highest inrush current does not necessarily occur in the switched phase.
- ☐ During first-phase switching for any kind of transformer connection or core type, the neutral resistor will act directly in series with the switched phase. Due to the high damping of the inrush current during first-phase energization, second-phase switching can take place after about 2 cycles from the instant at which the first phase has been energized.
- ☐ For the second-phase energization, the inrush current magnitude is always lower than that for first-phase energization for the same neutral resistor value. Moreover, for an electrically 'through a delta winding connection' or magnetically-coupled 'through multi-limb cores', the second-phase inrush current level is always below that of the first phase.

- After the second phase has been switched in, the induced inrush currents will take a longer time to reach the steady sate. However, with a properly sized neutral resistor, the very low peak current (about 3 times the no-load peak) reveals that the transformer is operating close to the nominal flux limit and below saturation. This result means that the third phase switching can take place immediately after 5-30 cycles after the switching of the second phase.

- Both the first and second energization stage $I_{max}(R_n)$ performance curves experience a sharp inrush current reduction for small values of R_n before reaching a knee point. Beyond the knee point, the inrush current continues to decrease at a much slower rate as R_n is further increased. Both the first- and second-phase $I_{max}(R_n)$ curves have knee points occurring at approximately the same neutral resistor value.

- With high neutral resistor values, the second energized phase acts in series with the first energized phase, leading to a high inrush current of similar magnitude in both phases with opposite polarity.

- A positive energization sequence was found to be much less sensitive to the variation of the neutral resistor size. This result led to a wider range of effective neutral resistor values that could reduce the inrush current during both the first and second switching stages.

- For electrically or magnetically coupled transformers, the third-phase energization inrush current is directly proportional to the neutral resistor size. Within the effective region the neutral resistor, the third phase led to the lowest inrush current level. Small neutral resistor values led to a close-to synchronous closing condition with minimal transients.

- For transformer banks with Y-Y connection, the third energized phase behaved similarly to that of the second energized phase behaviour with an opposite sequence.
- The first-phase switching curve is much less sensitive (almost the same curve) for a variation of either the slope or the starting point of saturation, especially for values of R_n that prevent the transformer from operating in the saturation mode and, hence, make the saturation parameters ineffective.
- The second switching $I_{max}(R_n)$ curve is more sensitive to variations in the saturation parameters. The steeper (lower) the slope is, the higher the almost constant slope of the $I_{max}(R_n)$ curve is.
- For transformers with a lower saturation flux-level, the effect of various saturation inductances becomes clearer. However, according to the shown curves, changing the slope of the saturation curve from 75% to 200% will insure a reduction in the inrush current for the second switching stage of 75-90%, respectively. The reduction in the first phase inrush will be lower.
- For the intersection point between the first and second $I_{max}(R_n)$ curves, steeper (lower) saturation slopes will result in intersection points at higher current values, whereas higher saturation slopes will cause the intersection point to exist at lower current values. In other words, for higher saturation slopes (those with

higher saturation inductance) the second-phase $I_{max}(R_n)$ curve will be lower than the first-phase $I_{max}(R_n)$ curve for higher neutral resistor values.

- Lower saturation flux-levels result in lower knee-point neutral resistor values than those with higher saturation 'less-severe' flux levels. However, the difference in reduction within that range is negligible, even for lower values of R_n.

6. Transient Analysis of the Sequential Energization Scheme and Design Guide

This chapter presents the analysis of the sequential switching scheme from a transient performance perspective. An improved design method for the neutral-resistor-based scheme is also presented. As was shown in the previous chapter, the experimental and simulation results demonstrated the scheme's effectiveness. In this chapter, an analytical method based on nonlinear circuit transient analysis is developed to solve the resistor-sizing problem. The method models transformer nonlinearity by using two linear circuits and derives a set of analytical equations for the waveform of the inrush current. In addition to establishing a set of formulas for optimal resistor determination, the results also reveal useful information regarding the inrush behaviour of a transformer and the characteristics of the sequential energization scheme. This chapter also addresses the main limitation of the sequential phase energization scheme: the rise of neutral voltage. The application of surge arresters was investigated as a solution for the neutral voltage rise limitation. The performance of the improved scheme is discussed, and the thermal-energy requirements for the neutral resistor arrangement are evaluated.[3]

---

[3] The work presented in this chapter have been published: S.G. Abdulsalam and W. Xu "A Sequential Phase Energization Method for Transformer Inrush Current Reduction-Transient Performance and Practical Considerations", *IEEE Transactions on Power Delivery*, vol. 22, No. 1, pp. 208-216, Jan. 2007.

6.1 Introduction

This chapter presents a thorough transient analysis of the sequential energization scheme's performance. This analysis leads to a solid design guide for the associated neutral resistor. When the sequential energization technique was first presented in [46] and [47], it was found that a neutral resistor which is 8.5% of the un-saturated magnetizing reactance would reduce the inrush current by 80% to 90%. However, the resistor-sizing issue was not investigated from the transient performance perspective due to the difficulties in conducting a transient analysis of nonlinear circuits.

A further study of the scheme was presented in the previous chapter through experimental and simulation studies, revealing that a much lower resistor size is equally effective. The steady-state theory developed for neutral resistor sizing [46] is unable to explain the effectiveness of the neutral resistor in reducing the inrush current with small neutral resistor values. Extensive investigation showed that the phenomenon must be understood by using transient analysis. The key point of the presented neutral-resistor-sizing criteria depends on selecting the appropriate neutral resistor to minimize the peak of the actual inrush current directly, and, accordingly, a much lower resistor value can be obtained. As was shown earlier, the first-phase energization leads to the highest inrush current among the three phases and, as a result, the resistor can be sized according to its effect on the first-phase energization. With the help of nonlinear circuit theory [48]-[49], it was possible to derive an analytical relationship between the peak of the inrush current and the size of the resistor, and to develop a transient-analysis-based theory for the resistor selection. The derived analytical expression was compared against the experimental and simulation results and was verified to be accurate for a wide range of neutral resistor values.

In addition, this chapter also addresses the main limitation of the proposed scheme – the rise of neutral voltage. Two methods to control the neutral voltage rise have been proposed: the use of surge arrestors and saturable reactors connected at the neutral point of the energized transformer. The use of surge arresters was found to be more effective in overcoming the neutral voltage rise limitation. The performance of the improved scheme is presented.

The results reveal a great deal of information about the inrush behaviour of transformers and the characteristics of the sequential energization scheme. In addition, the developed analytical method made it possible to accurately estimate energy requirements for the grounding resistor and the voltage limiting surge arrester. A literature review of the neutral grounding resistors and voltage limiting arresters was conducted in order to assess if the proposed scheme energy requirements fall within acceptable industry standards.

Since the scheme adopts sequential switching, each switching stage can be investigated separately. For first-phase switching, the scheme's performance is straightforward. The neutral resistor is in series with the energized phase and this resistor's effect is similar to that of a pre-insertion resistor. When the third phase is energized, the voltage across the breaker contacts to be closed is close to zero due to the existence of a delta secondary or a three-legged core, so minimal switching transients will occur when the third phase is energized [46] and [47].

The second- phase energization is the one most difficult to analyze. Fortunately, from numerous experimental and simulation studies, it was found that the inrush current due to second-phase energization is lower than that due to first-phase energization for the same value of R_n. This result is true for the region where the inrush current of the first-phase is decreasing rapidly as R_n increases. As a result, when developing a neutral-resistor-sizing criterion, the focus should be directed towards the analysis of the first-phase energization.

6.2 Analysis of First-Phase Energization

The following analysis focuses on deriving an inrush current waveform expression covering both the unsaturated and saturated modes of operation respectively. The presented analysis is based on a single saturable core element, but is suitable for analytically modeling single-phase transformers and for the single-phase switching of three-phase or multi-limb transformers. As shown in Figure 6.1(a), the transformer's energized phase was modeled as a two-segmented saturable magnetizing inductance in series with the transformer's winding resistance, leakage inductance and neutral resistance.

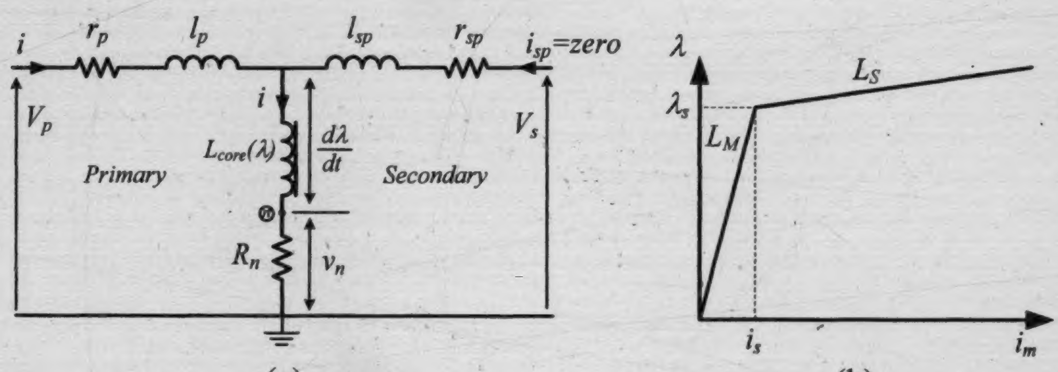

(a) (b)

Figure 6.1 Simplified equivalent circuit for the energization of the first phase and the corresponding characteristics.

For the first-phase switching stage, the equivalent circuit represented in Figure 6.1 can accurately represent the transformer's behaviour for any connection or core type by using only the positive sequence Flux-Current characteristics. Based on the transformer connection and core structure type, the phases are coupled either through the electrical circuit (3 single phase units in Yg-Δ connection) or through the Magnetic circuit (Core type transformers with Yg-Y connection) or through both, (the condition of Yg-Δ connection in an E-Core or a multi limb transformer). The coupling introduced between the windings will result in flux flowing through the limbs or magnetic circuits of un-energized phases. For the sequential switching application, the magnetic coupling will result in an increased reluctance (decreased reactance) for zero sequence flux path if present.

The equivalent electric and magnetic circuits for 3-Limb core transformers connected in Yg-Δ during the first phase switching can be represented as shown in Figure 6.2 and Figure 6.3 respectively. It is shown in Figure 6.2 that the current drawn from the first switched Phase (A) is equal to the magnetizing current in Phase (A), i_{ma} and the Delta winding Current, i_{Δ}.

During first phase switching and for the case of E-Core type transformers, both Limbs B and C combined will carry the total flux flowing through phase A (approximately). This means that phases B and C combined will act as a very low reluctance return path for the flux of phase A. Consequently, the zero sequence flux, ϕ_O, will be close to zero. As a result; the summation of the induced voltages in the secondary Delta windings of phases B and C will be equal to the induced voltage in phase A. As a result no current will flow through the Delta winding during the first phase energization. The current drawn from Phase A (inrush current during switching) will be only consisting of the magnetizing current of Phase A, i_{ma}.

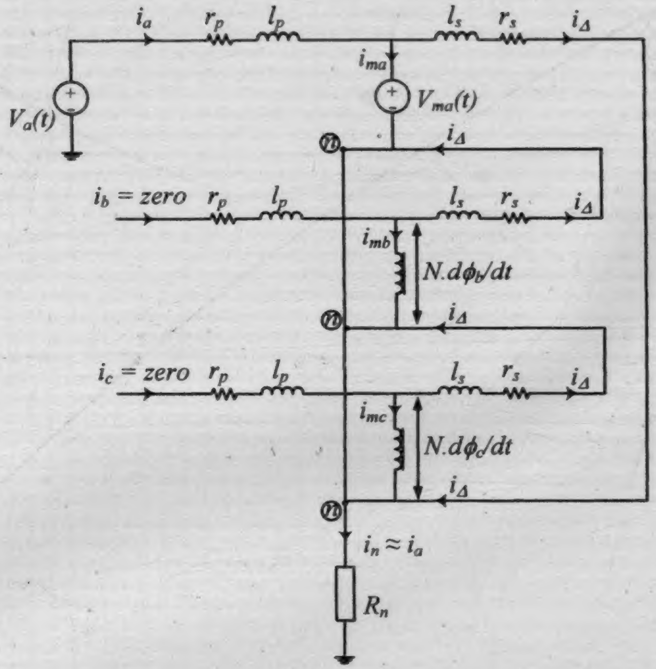
i_a
r_p
l_p
l_s
r_s
i_Δ
i_{ma}
$V_{ma}(t)$
$V_a(t)$
$i_b = zero$
i_{mb}
$N.d\phi_b/dt$
$i_c = zero$
i_{mc}
$N.d\phi_c/dt$
$i_n \approx i_a$
R_n

Figure 6.2 Simplified equivalent circuit for the energization of the first phase

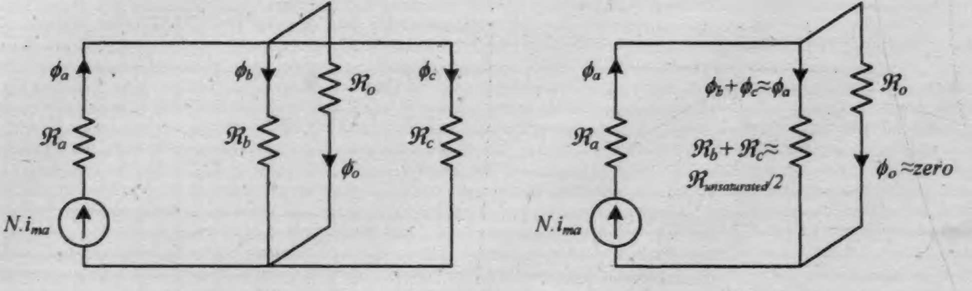
ϕ_a
ϕ_b
$\Re_o$
ϕ_c
$\Re_a$
$\Re_b$
$\Re_c$
ϕ_o
$N.i_{ma}$
(a)
ϕ_a
$\phi_b+\phi_c\approx\phi_a$
$\Re_o$
$\Re_a$
$\Re_b+\Re_c\approx$
$\Re_{unsaturated}/2$
$\phi_o\approx zero$
$N.i_{ma}$
(b)

Figure 6.3 (a) Magnetic circuit with flux distribution during first-phase switching and (b) Simplified equivalent magnetic circuit.

From the above, the transformer behaviour during the first phase switching can be modeled accurately -regardless of the connection or core type- using only one single-phase saturable reactor representing the saturation characteristics of Phase (A). Phases B and C will always have a very low reluctance value and as a result, will not change the total reluctance of the flux path as compared to the increased reluctance of the switched phase due to saturation. This explains the accuracy of the 1st phase energization expression using one single saturable core reactor.

For single-phase transformer energization, the differential equation describing the behavior of the saturable iron core transformer can be written as follows;

$$V_{pj} = (r_p + R_s) \cdot i_{pj} + l_p \cdot \frac{di_{pj}}{dt} + \frac{d\lambda_j}{dt} \tag{6.1}$$

$$V_{pj} = (r_p + R_s) \cdot i_{pj} + l_p \cdot \frac{di_{pj}}{dt} + \frac{d\lambda_j}{di_{pj}} \cdot \frac{di_{pj}}{dt} \tag{6.2}$$

As the rate of change of the flux linkages with magnetizing current $d\lambda/di$ can be represented as an inductance equal to the slope of the λ-i curve, (6.2) can be re-written as follows;

$$V_{pj} = (r_p + R_s) \cdot i_{pj} + l_{core}(\lambda_j) \cdot \frac{di_{pj}}{dt} \tag{6.3}$$

$$l_{core}(\lambda_j) = \begin{cases} L_m + l_p & \lambda_j \le \lambda_s \\ L_s + l_p & \lambda_j > \lambda_s \end{cases}$$

$$L_m = \frac{d\lambda}{di} \quad \lambda < \lambda_s \qquad and \qquad L_s = \frac{d\lambda}{di} \quad \lambda \ge \lambda_s$$

The general solution of the differential equation (6.3) has the following form;

$$i(t) = \begin{cases} A_1 \cdot e^{-t/\tau_1} + B_1 \cdot \sin(\omega \cdot t - \theta_1) & \lambda \le \lambda_s \\ (A_2 + i_s) \cdot e^{-(t-t_s)/\tau_2} + B_2 \cdot \sin(\omega \cdot t - \theta_2) & \lambda > \lambda_s \end{cases} \tag{6.4}$$

Subscripts 1 and 2 denote un-saturated and saturated operation respectively. The parameters given in the above equation for *i(t)* are given by;

$$B_1 = \frac{V_m}{\sqrt{(r_p + R_n)^2 + \left(\omega \cdot (L_m + l_p)\right)^2}} \qquad B_2 = \frac{V_m}{\sqrt{(r_p + R_n)^2 + \left(\omega \cdot (L_s + l_p)\right)^2}}$$

$$\theta_1 = \tan^{-1}\left(\frac{\omega \cdot (L_m + l_p)}{r_p + R_n}\right) \qquad \theta_2 = \tan^{-1}\left(\frac{\omega \cdot (L_s + l_p)}{r_p + R_n}\right)$$

$$A_1 = B_1 \sin(\theta_1) \qquad A_2 = B_2 \sin(\theta_2 - \omega t_s)$$

According to (6.4), the required inrush waveform assuming two-part segmented $\lambda - i$ curve can be calculated for two separate un-saturated and saturated regions. For the first un-saturated mode, the current can be directly calculated from the first equation for all flux linkage values below the saturation level. After saturation is reached, the current waveform will follow the second given expression for flux linkage values above the saturation level. For any given value of R_n, the saturation time t_s by which the core reaches saturation can be found at the same time the current reaches the saturation current level i_s.

6.3 Expression for Inrush Current Peak

As has been shown from extensive simulation and experimental results, the first phase energization leads the highest inrush current magnitude among the three energized phases. This is true for the region where the neutral resistor can effectively reduce the inrush current magnitude. Since the neutral resistor should be sized close to this effective region, an inrush current peak expression that relates the amount of inrush reduction directly to the neutral resistor during first phase energization is sufficient to achieve the desired sizing criteria. The inrush current waveform peak will essentially exist during saturation mode of operation; the focus should be concentrated on the second current waveform equation describing saturated operation mode, equation (6.5).

$$i(t) = (i_s + A_2)e^{-(t-t_s)/\tau_2} + B_2 \sin(\omega \cdot t - \theta_2) \qquad t \geq t_s \tag{6.5}$$

The expression of inrush current peak could be directly evaluated from (6.6) given that both saturation t_s and peak t_{peak} times of the inrush current waveform are known;

$$I_{Peak} = (i_s + A_2)e^{-\left(t_{peak}-t_s\right)/\tau_2} + B_2 \sin\left(\omega \cdot t_{peak} - \theta_2\right) \tag{6.6}$$

Mathematically, as shown by (6.4), the inrush waveform consists of exponentially decaying 'DC' term and a sinusoidal 'AC' term. Both DC and AC amplitudes are significantly reduced with the increase of the available series impedance. The inrush waveform, neglecting the relatively small saturating current i_s, could be normalized with respect to the amplitude of the sinusoidal term as follows;

$$i(t) = B_2 \cdot \left[\frac{A_2}{B_2} . e^{-(t-t_s)/\tau_2} + \sin(\omega \cdot t - \theta_2)\right] \tag{6.7}$$

$$i(t) = B_2 \cdot \left[\sin(\theta_2 - \omega \cdot t_s) . e^{-(t-t_s)/\tau_2} + \sin(\omega \cdot t - \theta_2)\right] \tag{6.8}$$

$$i_{Norm}(t) = \sin(\theta_2 - \omega \cdot t_s) . e^{-(t-t_s)/\tau_2} + \sin(\omega \cdot t - \theta_2) \tag{6.9}$$

The exponential term of the inrush waveform is fractional compared to the sinusoidal term. Moreover, it could be easily verified that with increased damping 'resistance' in the circuit, where the circuit phase angle θ_2 has lower values than the saturation angle $\omega \cdot t_s$, the exponential term is negative resulting in an inrush magnitude that is lower than the sinusoidal term amplitude. The normalized exponential and complete inrush waveforms for different R/X ratios are shown in Figure 6.4 and Figure 6.5 for saturation angles of 45 and 70 electrical degrees respectively.

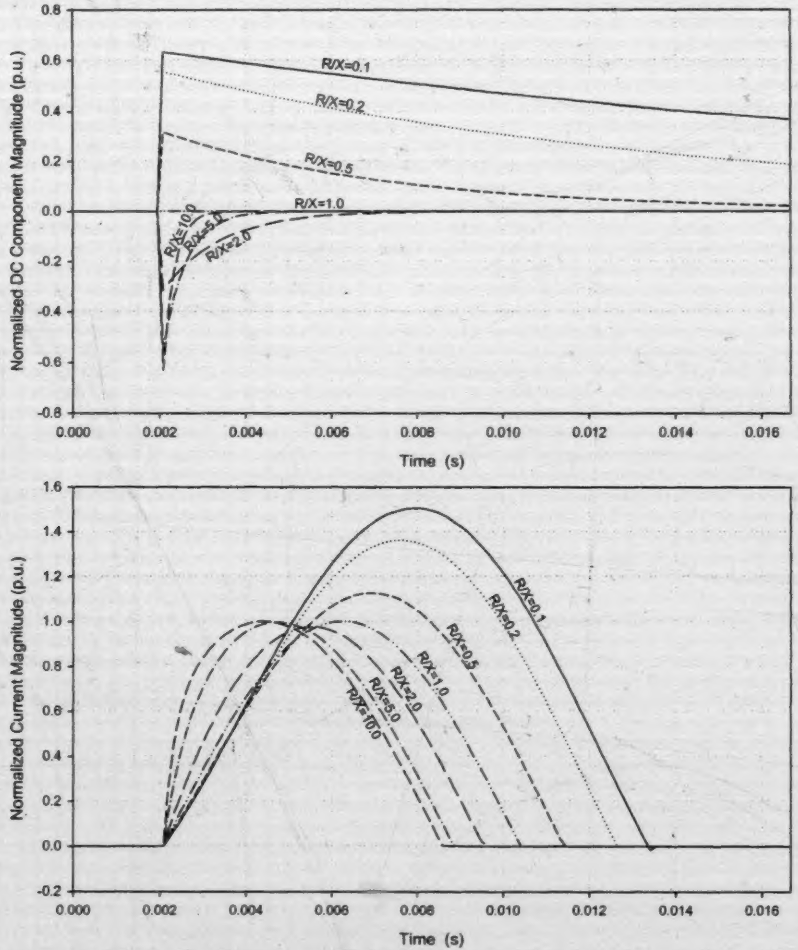

Figure 6.4 Normalized exponential (top) and complete inrush waveforms for a saturation angle of 45 electrical degrees.

It becomes clear that with more severe saturation characteristics 'higher residual flux and lower saturation flux level' the DC component reaches high values close to 60% of the inrush waveform sinusoidal term amplitude. On the other hand, less severe saturation characteristics 'lower saturation flux and higher saturation flux level' leads to a lower DC component and higher inrush waveform deformation, especially with high R/X ratios, Figure 6.5(b) and Figure 6.6(b).

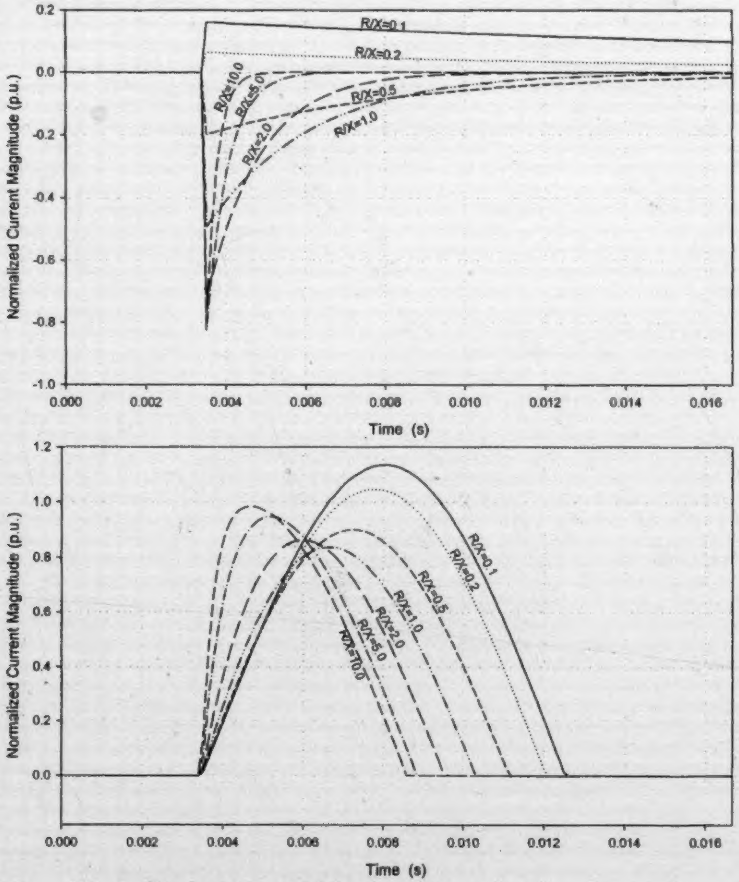

Figure 6.5 Normalized exponential (top) and complete inrush waveforms for a saturation angle of 70 electrical degrees.

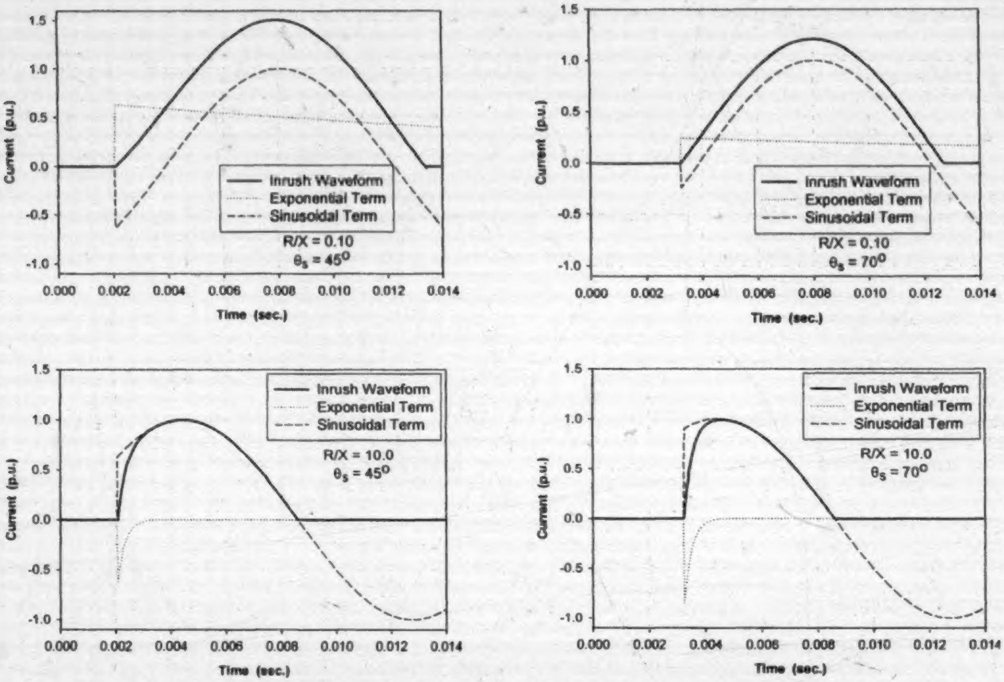

Figure 6.6 Normalized inrush current waveforms showing exponential and sinusoidal components for saturation angles of 70 and 45 electrical degrees.

The saturation time t_s, could be evaluated directly through (2.19) for any given switching instant; α, residual flux ϕ_r and saturation flux limit ϕ_s. The peak time t_{peak} at which the inrush current will reach its peak can be numerically found through setting the derivative of equation (6.5) with respect to time equal to zero at $t = t_{peak}$.

$$0 = -\frac{(i_s + A_2)}{\tau_2} e^{-(t_{peak}-t_s)/\tau_2} + B_2 \cdot \omega \cdot \sin(\omega \cdot t_{peak} - \theta_2) \qquad (6.10)$$

However, the process described earlier is iterative and doesn't provide a direct expression for the inrush current peak as function of the series resistor in the circuit. Alternatively; the inrush current peak could be fairly-accurately evaluated close to the peak of inrush current waveform at the time which the sinusoidal term of the inrush waveform (6.5) reaches its peak. As could be shown from Figure 6.6, the inrush current waveform reaches its peak at an instant slightly before the sinusoidal term peak. This could be more evident for cases with higher saturation angles. However, the derivative 'variation' of the inrush waveform close to the peak is relatively small. Accordingly, estimating the inrush current peak value in the neighbourhood of the sinusoidal term peak instant will not result in a noticeable error. The inrush current peak I_{Peak} could be evaluated at the sinusoidal term peak, t_{pk} as follows;

$$\omega \cdot t_{pk} = \frac{\pi}{2} + \theta_2 \tag{6.11}$$

$$I_{Pk}(R_s) \approx A_2 \cdot e^{-(t_{pk}-t_s)/\tau_2} + B_2 \sin(\omega \cdot t_{pk} - \theta_2) \tag{6.12}$$

The inrush current peak Equation (6.12) was found to be very accurate as compared to both experimental and simulation results. The $I_{Pk}(R_s)$ 'analytical' and the $I_{\max\_R}$ curves for the experimental 30kVA laboratory transformer are shown in Figure 6.7. It is clear that the $I_{Pk}(R_s)$ equation can accurately determine the maximum inrush peak current for a given residual level and using only the simplified two slope saturation curve.

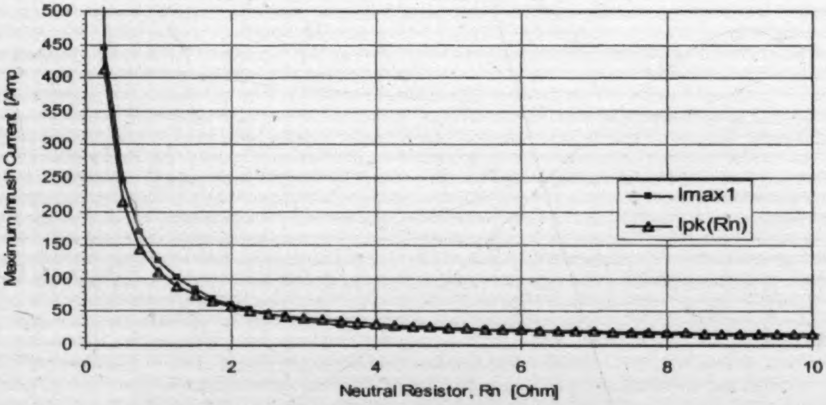

Figure 6.7 $I_{Pk}(R)$ compared to the experimental inrush peak current for the 30 kVA, 208/208 Yg-Δ, three limb transformer.

6.4 Investigation of Second Phase Switching Inrush Current

Due to the sequential nature of the inrush mitigation technique, it was possible to analyze the transformer behaviour during second phase switching with a similar analysis procedure as explained in the preceding section. However, due to the transformer highly nonlinear behaviour, it is obvious that the analysis of the electric and magnetic circuit behavior during second phase switching will be sufficiently more complex than that for first phase switching. As been shown in the previous section, the severity of inrush current condition will depend on many factors that include; amount of residual or 'initial' flux present at the instant of switching, the instant of switching itself and the available damping in the circuit which results in reducing the flux build-up process in the core.

Generally, transformer behaviour during second phase switching varies with respect to the connection and core structure type. Transformers with delta connected secondary or having a multi-limb core structure have different behaviour during the second phase switching from those of single phase units without a delta winding. However, a general behaviour trend exists during the second switching stage for all transformer connections and core types for low neutral resistor values, where the neutral resistor sufficiently reduces the inrush current magnitude by 80%.

The target of the analysis being presented in this section is to investigate the behavior of the transformer core under sequential switching procedure and to highlight the neutral resistor influence on inrush current magnitude. The study will be focused on understanding the mechanism behind the inrush current reduction that is achieved through the neutral resistor coupled with sequential switching. Quantitative and qualitative analysis of the neutral resistor effect on the core saturation level and accordingly, inrush current magnitude, have been carried out and will be presented.

It will be shown through analytical evaluation that the scheme will lead to significant reduction in inrush current magnitude during the second phase energization. Additionally, it will be proven that for small values of neutral resistance R_n, the in inrush current magnitude during second phase energization is less-than or close-to the inrush magnitude during first phase energization. This will form the basis of the neutral resistor sizing criteria that will follow.

First, the application of the scheme to three phase transformers with three single units connected in Yg-Y will be discussed. Second, the performance of the scheme as applied to transformers with coupling between primary and secondary windings through either a magnetic (Multi Limb Cores), electric (Delta Winding) or both (Multi Limb and Delta Winding connection) coupling types will be briefly investigated.

6.4.1 Three Single Phase Units Connected in Yg-Y

For this condition and with no delta secondary or tertiary winding(s), the transformer behaviour can be modeled using separate saturable inductor circuits representing each energized phase. The only coupling between the two switched phases is introduced through the neutral resistor itself. Depending on the neutral resistor ohmic value and the corresponding inrush current level, the voltage developed across the neutral resistor will control the voltage across the magnetizing branches of the energized phases, Figure 6.8.

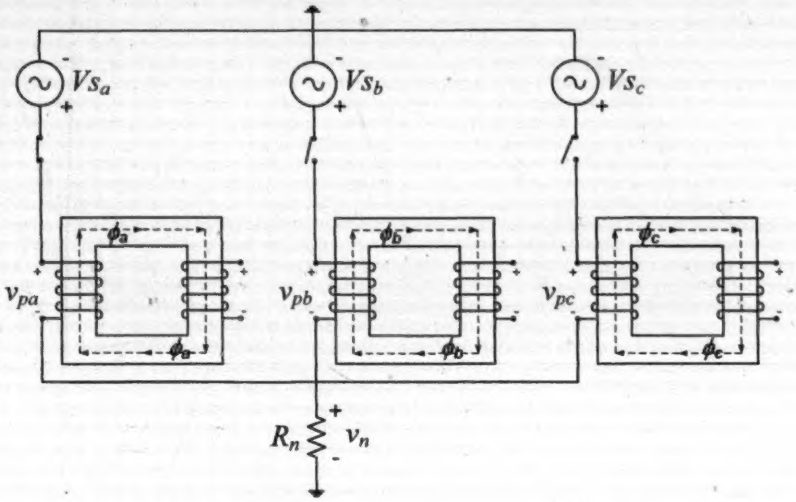

Figure 6.8 Sequential energization of a 3-phase transformer consisting of three Single-Phase units with a neutral grounding resistor.

For any energized phase j, the flux linkages λ_j as function of the primary phase voltage v_{pj} and the neutral voltage v_n can be given by;

$$\lambda_j = \int v_{pj}(t)dt - \int v_n(t)dt + \lambda_j\big|_{t=zero} \tag{6.13}$$

$$v_n(t) = i_n \cdot R_n = (i_a + i_b) \cdot R_n \tag{6.14}$$

For a 'solidly' grounded, three single-phase units with Yg-Y connection, energizing the second phase will not influence the already energized phase (A) and the second energized phase will have the same performance as for first phase energization. For small values of R_n where the neutral voltage rise won't have much effect on changing the voltage across the magnetizing branch of previously energized phase (A), the energized phase (B) need to first reach saturation in order to have a significant neutral voltage rise due to the large current drawn during saturation condition. With phase (A) in steady state, a disturbance in the terminal voltage leading to approximately 120% of the rated flux value is required to result in a high current flow.

After Phase B reaches saturation, the current drawn from phase B increases, raising the neutral voltage, v_n, Phase A might saturate as well, depending on the instant of switching. Consequently, the transformer behavior during 2nd phase energization can be modeled in three different stages; first, the stage where both phases are not yet saturated (immediately after energizing phase B), stage where only Phase B reaches saturation and a final stage where both phases are saturated. The most severe inrush current condition will exist due to an energizing instant that leads to a maximum value of the applied voltage integral on the switched phase. Accordingly, a switching instant at the zero crossing of the voltage waveform will result in the maximum inrush current. Switching at zero voltage crossing and rising together with a positive residual flux value leads to the maximum positive inrush current.

At a switching angle of zero on the applied voltage waveform of phase B:

$$v_b(t) = V_m \cdot sin(\omega \cdot t) \qquad (6.15)$$

$$v_a(t) = V_m \cdot sin(\omega \cdot t + 120^o) \qquad (6.16)$$

Accordingly, with the first energized phase in steady state, the current and flux flowing in phase A can be given by:

$$i_a(t) = i_m \cdot sin(\omega \cdot t + 30^o) \qquad (6.17)$$

$$\phi_a(t) = \phi_m \cdot sin(\omega \cdot t + 30^o) \qquad (6.18)$$

Based on (6.17) and (6.18), both currents and fluxes of phase A and B are positive immediately after the energizing instant leading to maximum inrush current condition (The neutral resistor value is small and the neutral voltage change will be relatively small prior to saturation). As a result, the flux in phase B can be calculated as follows;

$$\frac{d\lambda_b}{dt} = v_b(t) - r_p \cdot i_b - l_p \cdot \frac{di_b}{dt} - R_n \cdot i_n \tag{6.19}$$

$$\frac{d\lambda_b}{dt} = v_b(t) - r_p \cdot i_b - l_p \cdot \frac{di_b}{dt} - R_n \cdot (i_a + i_b) \tag{6.20}$$

$$\lambda_b = \int \left(v_b(t) - r_p \cdot i_b - l_p \cdot \frac{di_b}{dt} \right) - \int R_n \cdot (i_a + i_b) + \lambda_{bo} \tag{6.21}$$

During second phase energization, Phase B will reach saturation in slightly more time than the case of first phase energization. Which is due to the presence of phase A positive current in-feed into the neutral resistor, leading to a small positive voltage drop across the neutral resistor. As an approximation with the worst possible condition (neglecting the effect of the neutral resistor before saturation), the saturation time of phase B, t_{sb} can be approximately calculated by:

$$\lambda_b = \int_{t=0}^{t=t_{sb}} \left(v_b(t) - r_p \cdot i_b - l_p \cdot \frac{di_b}{dt} \right) - \int_{t=0}^{t=t_{sb}} R_n \cdot (i_a + i_b) + \lambda_{bo} \tag{6.22}$$

$$R_n <<<$$

$$\lambda_m \approx \int_{t=0}^{t=t_{sb}} v_b(t) + \lambda_{b0} \tag{6.23}$$

$$t_{sb} = \frac{1}{\omega} \cdot \cos^{-1}\left(1 - (\lambda_s - \lambda_{b0})|_{p.u.}\right) \tag{6.24}$$

After Phase B reaches saturation, the current from phase B considerably increases leading to a high current flow through the neutral resistor. With phase A in steady state, drawing normal magnetizing current, the neutral current mainly contains the contribution of Phase B inrush current. Accordingly, the neutral resistor acts in series with the energized phase B;

$$v_b(t) = r_p \cdot i_b - l_p \cdot \frac{di_b}{dt} - \frac{d\lambda_b}{dt} - R_n \cdot (i_a + i_b) \tag{6.25}$$

$$v_b(t) \approx r_p \cdot i_b - l_p \cdot \frac{di_b}{dt} - \frac{d\lambda_b}{dt} - R_n \cdot i_b \tag{6.26}$$

Depending on the size of the neutral resistor R_n, inrush current reduction could be achieved through the neutral resistor for the second phase energizing stage, similar to that of pre-insertion resistor scheme. From (6.26), the induced flux linkages in phase B could be accordingly calculated by;

$$\lambda_b \approx \int \left(v_b(t) - r_p \cdot i_b - l_p \cdot \frac{di_b}{dt}\right) - \Delta\lambda \tag{6.27}$$

$$\Delta\lambda = \int R_n \cdot i_b \tag{6.28}$$

Similarly, for phase A, the flux linkages during energizing of phase B could be calculated by;

$$\lambda_a \approx \int \left(v_a(t) - r_p \cdot i_a - l_p \cdot \frac{di_a}{dt}\right) - \Delta\lambda \tag{6.29}$$

$$\lambda_a \approx \int \left(v_a(t) - r_p \cdot i_a - l_p \cdot \frac{di_a}{dt} \right) - \Delta\lambda \qquad (6.30)$$

$$\lambda_a \approx \int v_a(t) - \Delta\lambda \qquad (6.31)$$

$$\lambda_a \approx \lambda_{a-ss} - \Delta\lambda \qquad (6.32)$$

It becomes clear from (6.26) and (6.27) that the neutral resistor acts in series with phase B immediately after phase B reaches saturation. The saturation of phase B will significantly raise the phase B current and consequently the neutral current through the neutral resistor R_n. For this stage, phase A current is close to the normal magnetizing current until phase A itself saturates due to the rise of the neutral voltage as a result of the inrush current of phase B leading to the disturbance in flux $\Delta\lambda$ affecting both phases B and A as shown in (6.27) and (6.30) respectively. Referring to equation (6.24), phase B will saturate after $\omega \cdot t_{sb}$ radian degrees following phase B energizing instant. To this point, it is obvious that for Yg-Yg , 3 bank transformers; the second phase energization could drive phase A into saturation depending on the amount of disturbance in flux $\Delta\lambda$. With the assumption of worst switching and residual flux conditions, the amount of disturbance in flux $\Delta\lambda$ is directly proportional to the size of neutral resistor R_n.

In summary, the transformer during second phase energization undergoes three different saturation stages;

Both Phases Un-Saturated: Immediately after energization of second phase; both phases are unsaturated. The first energized phase is already near steady-state condition and the second energized phase starts operation with its independent residual flux.

Second Energized Phase Saturated: The second energized phase reaches saturation first. The time at which second phase reaches saturation could be found assuming negligible neutral voltage before saturation, (6.24).

Both phases Saturated: With the second energized phase saturated and drawing large inrush current, a neutral voltage is established across the small neutral resistor which might drive the first switched phase into saturation.

An analytical expression for the inrush current waveform during second stage energization could be evaluated for the three different stages of operation. This could be achieved through implementing a similar derivation procedure carried out for first stage energization. The magnetizing branches of phases A and B could be modeled by their un-saturated and saturated magnetizing inductances respectively. However, the only difference will be in the number of stages the inrush waveform is evaluated. While the first phase switching inrush waveform was fully derived using two saturation stages 'un-saturated and saturated', the second stage inrush waveform will describe three saturation stages as explained earlier.

The effort of evaluating such an analytical expression becomes a task of deriving the analytical expression describing the two-phase circuit with three consecutive switching incidents. Moving from one saturation stage into the next one just requires proper determination of the instant at which the respective saturation point is reached. However, the target of the analysis presented here is not the derivation of the analytical expression itself but rather; bring more understanding on how the transformer bank behaves during the sequential switching process.

Considering the extreme condition of a solidly grounded bank, no neutral voltage is established during the switching process, and the second energized phase behaves exactly the same as the first switching condition. The first energized phase is not disturbed since there will be 'ideally' no change in the voltage imposed on its terminals. With phase A already in steady state, as the neutral resistor is slightly increased, reduction in the induced flux in the second energized phase could be achieved without driving the first phase into saturation. Accordingly assuming that the reduction of flux achieved for the second energized phase leads to the same amount of increase in the flux of the first energized phase, it is possible to increase R_n until a reduction that equals the difference between the saturation and rated flux levels. In other words, the neutral resistor will behave in series with the second switched phase for values that do not lead to driving the first energized phase into saturation. Accordingly, the $I_{max}(R_n)$ curve of the second phase switching will closely follow that of the first phase switching for small values of R_n. using typical saturation flux levels of 1.25 to 1.35 p.u., it will be possible to reduce the saturation level of the second energized phase by 0.25-0.35 p.u. even without disturbing the first energized phase.

As the neutral resistor is increased further, the neutral voltage will increase and consequently it's integral which represents the amount of differential flux $\Delta\lambda$ as given by (6.28). Due to the 120° phase shift of three phase power systems, this differential flux $\Delta\lambda$, will act to reduce the induced flux in the second energized phase and increase that of the previously energized phase.

6.4.2 Three single Phase Units Connected in Yg-Δ or 3 Limb, Yg-Y or Yg-Δ

The performance during sequential switching for this type will be quite different than for single phase, Yg-Y, banks transformers due to the following reasons:

- Dynamic Flux will exist in un-energized phases.
- Inrush current can exist in one phase due to external saturation in un-energized phase (return path of the flux).

For the second phase switching, the equivalent electric circuit can be represented as shown in Figure 6.9. It is clear that during second phase energization for transformers connected in Yg-Δ or with Multi-limb core types, there will be a flux induced in the third (un-switched) phase. This flux will be introduced due to the magnetizing branch voltages of the first switched phases either electrically through the delta winding circuit or magnetically due to the magnetic coupling in multi limb transformers.

For transformers with delta connections and, with all phases un saturated ($i_{\Delta} = zero$), the voltage across the magnetizing branch of phase C can be calculated as follows;

$$v_{mc}(t) = v_{ma}(t) + v_{mb}(t) \qquad (6.33)$$

Same conditions apply for E-Core type transformers without delta connections. The leakage path reluctance through air 'or tank-oil combination' is high and accordingly, both energized phase fluxes will add up in the low reluctance path of the un-energized phase. Accordingly, for low values of R_n and before saturation occurs in either phases, the neutral voltage will be negligible and the magnetizing branch voltage can be assumed to equal the applied voltage for each of the energized phases and hence;

$$v_{mc}(t) \approx v_a(t) + v_b(t) \tag{6.34}$$

$$v_{mc}(t) \approx -v_c(t) \tag{6.35}$$

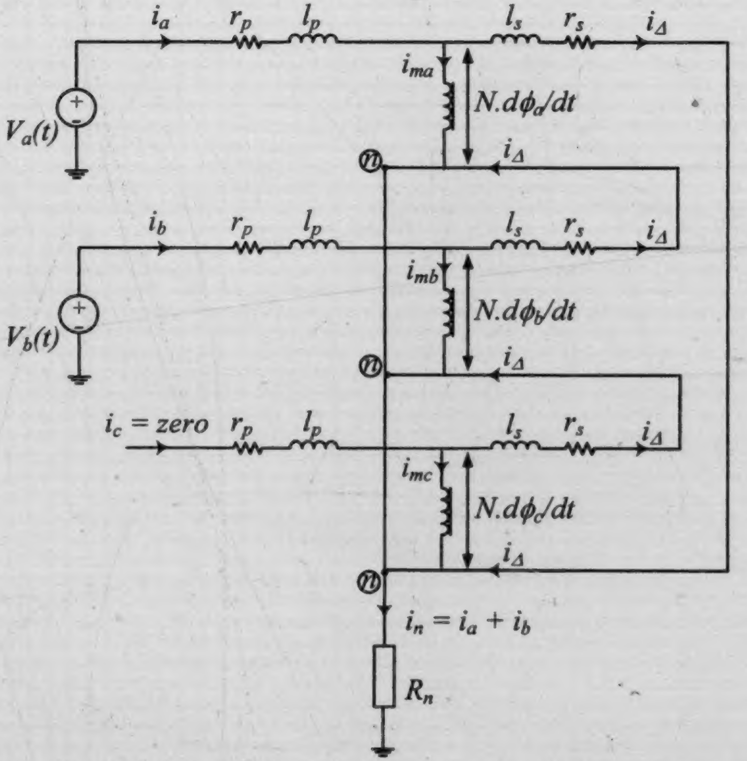
i_a
r_p
l_p
l_s
r_s
i_Δ
i_{ma}
$N.d\phi_a/dt$
$V_a(t)$
i_b
i_{mb}
$N.d\phi_b/dt$
$V_b(t)$
i_c = zero
i_{mc}
$N.d\phi_c/dt$
n
$i_n = i_a + i_b$
R_n

Figure 6.9 Equivalent electric circuit for three phase transformers, Yg-Δ connection.

The steady state voltages and fluxes in each phase can be given through referring all vectors to phase B voltage;

$$v_b(t) = V_m \cdot \sin(\omega \cdot t) \tag{6.36}$$

$$v_a(t) = V_m \cdot \sin(\omega \cdot t + 120^o) \tag{6.37}$$

$$\phi_a(t) = \phi_m \cdot \sin(\omega \cdot t + 30^o) \qquad t \leq t_{sb} \tag{6.38}$$

$$\phi_b(t) = -\frac{\phi_m}{2} \cdot \sin(\omega \cdot t + 30^o) \qquad t \leq t_{sb} \tag{6.39}$$

$$\phi_c(t) = -\frac{\phi_m}{2} \cdot \sin(\omega \cdot t + 30^o) \qquad t \leq t_{sb} \tag{6.40}$$

- Instant of switching leading to maximum inrush current:

In order to maximize the flux of the switched phase and consequently represent the condition of highest inrush current, the critical switching angle on phase B voltage waveform θ_b should be found. The induced flux in phase B after switching can be calculated as follows;

$$v_b(t) = V_m \cdot \sin(\omega \cdot t + \theta_b) \tag{6.41}$$

$$v_a(t) = V_m \cdot \sin(\omega \cdot t + \theta_b + 120^o) \tag{6.42}$$

$$\phi_a(t) = \phi_m \cdot \sin(\omega \cdot t + \theta_b + 30^o) \tag{6.43}$$

$$\phi_b|_{t=0} = -\frac{\phi_m}{2} \cdot \sin(\theta_b + 30^o) \tag{6.44}$$

The maximum flux induced in phase B could be evaluated as follows;

$$\hat{\phi}_b(\theta_b) = \phi_b(0) + \frac{1}{N} \int_{t=0}^{t=\frac{\pi-\theta_b}{\omega}} V_m \cdot \sin(\omega \cdot t + \theta_b)\, dt \qquad t > zero \tag{6.45}$$

$$\hat{\phi}_b(\theta_b) = -\frac{\phi_m}{2} \cdot \sin(\theta_b + 30^o) + \phi_m \cdot (1 + \cos(\theta_b)) \tag{6.46}$$

In order to find the critical switching angle leading to maximum flux build-up in the core;

$$\partial \hat{\phi}_b(\theta_b)/\partial \theta_b = 0 \tag{6.47}$$

$$-\frac{\phi_m}{2} \cdot \cos(\theta_b + 30^o) - \phi_m \cdot \sin(\theta_b) = 0 \tag{6.48}$$

$$\therefore \quad \theta_b = -\frac{\pi}{6} = -30^o \tag{6.49}$$

Accordingly, a switching angle of $\theta_b = -30^o$ leads to the maximum flux and inrush current condition. This accurately matches with both simulation and experimental results. In order to evaluate how will the increase of R_n value affect the value of maximum inrush during second phase switching; the condition with small R_n values need to be compared to the case with solidly grounded neutral. Two conditions need to be proved;

I. $I_{max-2nd} < I_{max-1st}$ for a solidly grounded condition ($R_n = 0$).

II. $I_{max-2nd} \leq I_{max-1st}$ for small values of R_n.

For the first condition;

It can be easily seen from the expression for the maximum flux that could be reached theoretically during second phase energization, with solid ground ($R_n = 0$); that the flux can have a maximum value of 1.866 p.u. neglecting any damping 'resistance in the circuit';

$$\hat{\phi}_b(\theta_b) = -\frac{\phi_m}{2} \cdot \sin(\theta_b + 30^o) + \phi_m \cdot (1 + \cos(\theta_b)) \tag{6.50}$$

$$\hat{\phi}_b = 1.866 \cdot \phi_m \tag{6.51}$$

Where for first phase energization, the flux can theoretically reach a value of twice the nominal flux, $2\phi_m$ even with no residual flux present in the core. It should also be noted that the maximum condition of inrush current for the first phase will be also influenced by the value of residual flux, and accordingly, the maximum inrush can easily reach higher values than $2\phi_m$ for any residual flux polarity in phase with the switched voltage.

For the second condition;

Phase B will start operating in the unsaturated region with its own residual flux. As a result, both phase currents will be low and the neutral voltage remains close to zero, $R_n << X_m$. As soon as Phase B reaches saturation, its current will increase and the neutral voltage will start to build up. The neutral current will be mainly due to the contribution of phase B. Hence, the neutral resistor can be assumed to be in series with phase B and a similar inrush reduction performance, to that of first phase switching, will hold. The process will continue until the neutral voltage integral 'amount of ϕ_b reduction' becomes sufficient to drive Phase A into saturation. With phase A originally in steady state, a disturbance in flux equal to the difference between the rated and saturation flux values is required for phase A to reach saturation. Conservatively assuming that the reduction in flux in Phase B results in an increase of the same amount in phase A, it will be possible to increase R_n to achieve at least 20 to 35% reduction in its flux before disturbing phase A, Figure 6.10.

As R_n is increased further, more inrush current reduction can be achieved in phase B until both phases reach the same saturation level for a specific value of R_n. As the difference between saturation and rated flux values increases, more reduction in phase B current can be achieved. The same conditions apply during third switching stage.

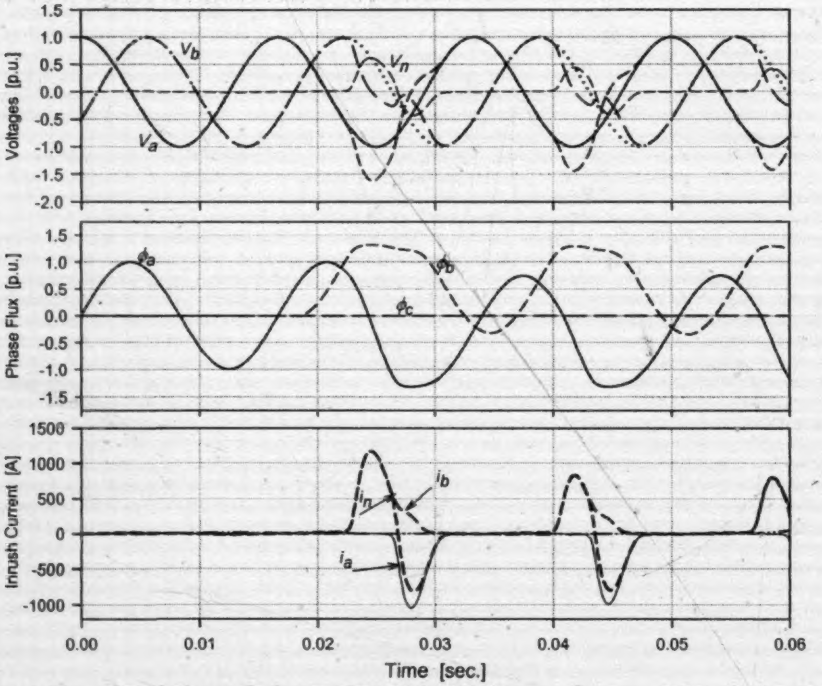

Figure 6.10 Simulation of the 3x300MVA, Yg-Y transformer, [10], during second phase switching for $R_n = 150\ [\Omega]$.

6.4.3 Effect of Delta Winding Connection

For the first phase energization, it was earlier shown that delta winding connection will have no influence on the inrush current. However, for second phase energization, and either with delta winding connection or three limb transformers; the transformer can be modeled as shown in Figure 6.11.

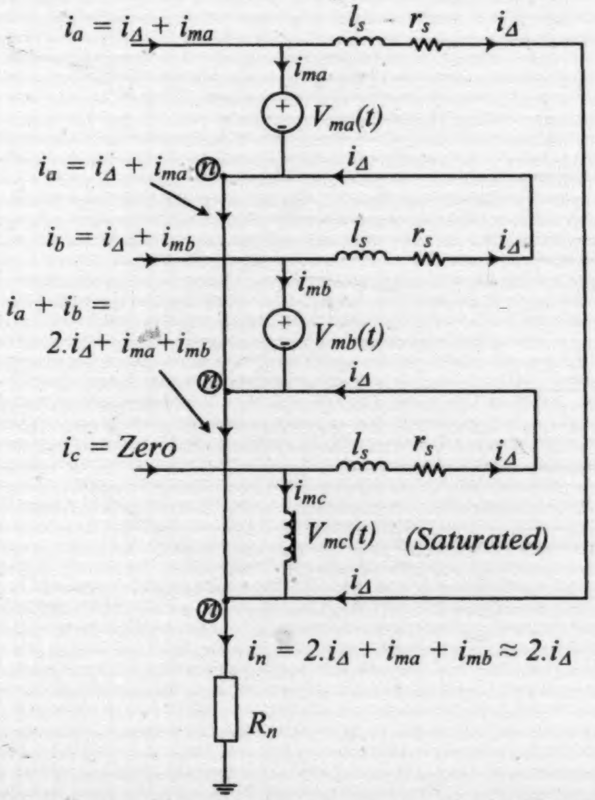
$i_a = i_\Delta + i_{ma}$
l_s
r_s
i_Δ
i_{ma}
$V_{ma}(t)$
$i_a = i_\Delta + i_{ma}$
n
i_Δ
$i_b = i_\Delta + i_{mb}$
l_s
r_s
i_Δ
i_{mb}
$i_a + i_b =$
$2.i_\Delta + i_{ma} + i_{mb}$
$V_{mb}(t)$
n
i_Δ
$i_c = Zero$
l_s
r_s
i_Δ
i_{mc}
$V_{mc}(t)$
(Saturated)
i_Δ
n
$i_n = 2.i_\Delta + i_{ma} + i_{mb} \approx 2.i_\Delta$
R_n

Figure 6.11 Electrical equivalent circuit for the transformer during second phase switching and under saturation condition of un-energized phase C

Immediately after *30°* of the switching instant leading to the highest inrush current, the fluxes in phases A and B are both positive and determined by the terminal voltage integral of both phases. This will lead phase C which represents the return path of both fluxes to saturate first. As shown in Figure 6.11, the saturation of phase C will drive a delta winding current equal to the magnetizing current of phase C under saturation. The induced delta winding current will be reflected as zero sequence current of the same magnitude flowing through phases A and B and a neutral current equal to twice the delta current.

In order to evaluate the impact of the return flux path (Phase C) saturation on the inrush magnitude drawn from both energized phases, the time at which phase C saturates, t_{sC}, need to be evaluated first. With t_{SW-B} denoting the switching instant of phase B;

$$\phi_b(t_{SW-B}) = \phi_c(t_{SW-B}) = \frac{-\phi_a(t_{SW-B})}{2} = zero \tag{6.52}$$

$$\phi_b(t) = \frac{1}{N}\int_{t=0}^{t_{sC}} V_m \cdot sin(\omega \cdot t - 30^o)dt \qquad t > t_{SW-B} \tag{6.53}$$

$$\phi_c(t) = \frac{1}{N}\int_{t=0}^{t_{sC}} V_m \cdot sin(\omega \cdot t - 150^o)dt \qquad t > t_{SW-B} \tag{6.54}$$

Before saturation is reached at t_{sC}, the magnetizing branch voltage across phase C could be evaluated as follows;

$$v_{mc}(t) = v_{ma}(t) + v_{mb}(t) \tag{6.55}$$

$$v_{ma}(t) = v_a(t) - i_n \cdot R_n \tag{6.56}$$

$$v_{mb}(t) = v_b(t) - i_n \cdot R_n \tag{6.57}$$

After phase C saturates and with phases A and B unsaturated, the current through the neutral resistor mainly consist of twice the delta winding current since both phases A and B are unsaturated and hence their '*magnetizing current*' is negligible;

$$i_n = 2 \cdot i_\Delta + i_{ma} + i_{mb} \tag{6.58}$$

$$i_n \approx 2 \cdot i_\Delta \tag{6.59}$$

$$v_{mc}(t) = v_a(t) + v_b(t) - 2 \cdot i_\Delta \cdot R_n \tag{6.60}$$

$$v_{mc}(t) = -v_c(t) - 2 \cdot i_\Delta \cdot R_n \tag{6.61}$$

$$v_{mc}(t) = V_m \cdot cos(\omega \cdot t + 7.6^0) - 2 \cdot i_\Delta \cdot R_n \tag{6.62}$$

$$v_{mc}(t) = 3 \cdot i_\Delta \cdot R_n + (3 \cdot l_s + L_{Sc}) \cdot \frac{di_\Delta}{dt} \tag{6.63}$$

Accordingly the delta winding current could be evaluated from (6.62) and (6.63) as follows;

$$V_m \cdot cos(\omega \cdot t + 7.6^0) = 3 \cdot i_\Delta \cdot R_n + (3 \cdot l_s + L_{Sc}) \cdot \frac{di_\Delta}{dt} + 2 \cdot i_\Delta \cdot R_n \tag{6.64}$$

Equation (6.64) could be represented alternatively as shown in Figure 6.12 which reveals that the delta winding current will see twice the magnitude of the neutral resistor value and three times the magnitude of the total series impedance of the energizing side. This means that the delta winding current will be effectively and quickly damped after the energization of the second phase.

The saturation time of phase C, t_{sC}, can be calculated by;

$$\phi_c(t) = -\phi_m = \frac{1}{N}\int_{t=0}^{t_{sC}} V_m \cdot sin(\omega \cdot t - 150^o)dt \tag{6.65}$$

$$t_{sC} = \frac{67.6^o}{\omega} \tag{6.66}$$

This means that the saturation of phase C will occur after 67.6° after phase B is energized. The saturation time calculated above is accurate for all values of R_n close to zero that will not cause a significant rise of neutral voltage before saturation occurs.

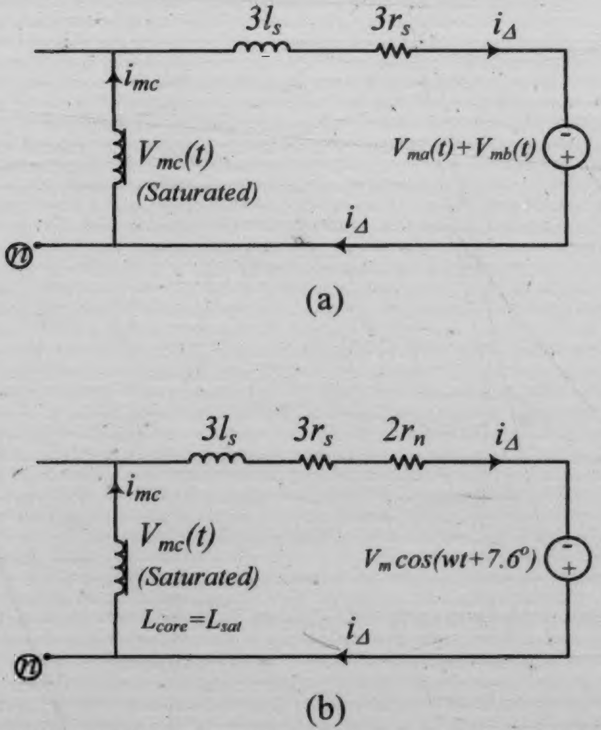
$3l_s$
$3r_s$
i_Δ
i_{mc}
$V_{mc}(t)$
(Saturated)
$V_{ma}(t)+V_{mb}(t)$
i_Δ
n
(a)
$3l_s$
$3r_s$
$2r_n$
i_Δ
i_{mc}
$V_{mc}(t)$
(Saturated)
$L_{core}=L_{sat}$
$V_m\cos(wt+7.6^\circ)$
i_Δ
n
(b)

Figure 6.12 Modeling of the Delta winding during saturation condition of Phase C.

More importantly, as could be easily verified from Figure 6.11, the neutral current will mainly consist of twice the zero sequence 'delta' current value which flows in the two energized phases equally. In other words, the delta winding will result in making the neutral resistor acting in series with both phases A and B at the same time even before they reach saturation which results in a significant reduction of their terminal voltages and consequently limiting the inrush current magnitude.

Due to the saturation of the phase C (even though not yet connected), a Delta winding current will be excited through the induced voltage across phases A and B. The delta winding current will circulate in the delta winding through impedance three times larger than the phase leakage impedance with addition to the saturable inductance of phase C. This condition will ensure that the delta winding current will not exceed the phase inrush current.

The peak value of the delta winding current can be easily found using the previously derived expression for the maximum peak inrush current of one phase. This is true since Phase B would not get saturated before phase C. and since the total resistance and inductance in the delta winding circuit is much larger than that of single phase switching, this current will be much lower than that of single phase switching. It can also be noted that for this condition, the inrush current reduction capability of the neutral resistor will be doubled for the same resistor value as compared to that during first phase energization. According to the last derived equation, the polarity of the delta winding current will be positive and hence, the same amount of current will be drawn from phases A and B, Figure 6.13. As a result, a reduction of twice of that introduced from single phase switching will be introduced on the switched phase Voltage of Phase A (same positive polarity), and hence reducing the saturation level below the case with $R_n = zero$.

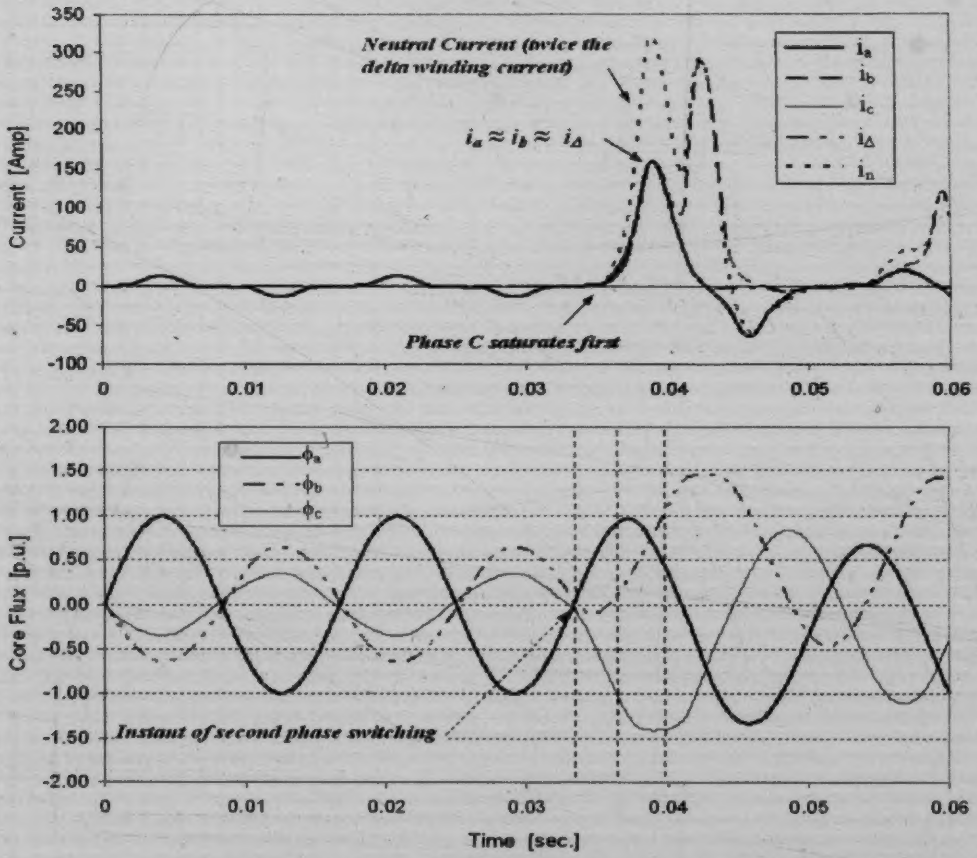

Figure 6.13 Simulation of the 30kVA, 208/208V, E-Core transformer for the second phase switching condition showing the effect of Delta winding current for $R_n = 0.1\ (\Omega)$.

In conclusion, the delta winding current will have two main effects that will result in reducing the inrush current level during second phase switching as compared to the first phase switching condition. First, due to the early saturation of phase C 'un-energized', a relatively large current will be drawn equally from both energized phases. As a result, the neutral current will carry twice the magnitude of currents in the phases and hence having a large voltage drop across the neutral resistor even before saturation is reached for phase B. Second, the saturation of phase B will be delayed, since the voltage drop caused due to the drawn delta winding current will lead to lowering the voltage across the magnetizing branch of the energized phases. For phase A, the effect will be reversed (due to the negative polarity of the voltage), and phase A current will start to increase as R_n increase, this clarifies why phase B (the switched phase) current is larger than Phase A during the second switching stage for low values of R_n. This condition reverses as R_n is increased and phase A current will start to rise until it exceeds that of phase B.

6.5 Neutral Resistor Sizing

As has been shown from the sequential energization scheme performance, the neutral resistor size plays the significant role in the scheme effectiveness. Earlier work based on steady state analysis [46] and [47], proposed a neutral resistor that is 8.5% of the un-saturated magnetizing reactance in order to achieve 80% to 90% inrush currents reduction.

However, the extended study of the scheme as presented in this work revealed that a much lower resistor size is equally effective. The steady-state theory developed for neutral resistor sizing [46] is unable to explain the effectiveness of small neutral resistor values in reducing the inrush current magnitude among the three phases. If the neutral resistor size is directly selected to minimize the peak of the actual inrush current directly, a much lower resistor value could be found.

The performance of the sequential energization scheme as presented earlier showed that the first phase energization leads to the highest inrush current among the three phases and, as a result, the resistor can be sized according to its effect on the first phase energization. Based on the derived inrush current peak expression (6.12), it is now possible to select a neutral resistor size that can achieve a specific inrush current reduction ratio $\alpha(R_n)$ given by:

$$\alpha(R_n) = I_{peak}(R_n)/I_{peak}(R_n = 0) \qquad (6.67)$$

The inrush peak expression (6.12) can be re-written as follows;

$$I_{peak}(R_n) = B_2(R_n) \cdot \left[K(R_n) \cdot e^{-t_{peak}/\tau_2} + 1\right] \qquad (6.68)$$

The factor; $K(R_n)$, in (6.68) is a dimensionless factor which depends on transformer saturation characteristics ($|\lambda_s|$ and $|\lambda_r|$) as well as the total X/R ratio during saturation;

$$K(R_n) = sin(\theta_2 - \omega \cdot t_s) \qquad (6.69)$$

For the maximum inrush current condition ($R_n = 0$), the total energized phase X/R ratio including system impedance is high and accordingly, the damping of the exponential term in (6.68) during the first cycle can be neglected;

$$I_{peak}(R_n = 0) = \frac{V_m}{\sqrt{r^2 + X_s^2}} \cdot [K(0) + 1] \qquad (6.70)$$

Typical saturation and residual flux magnitudes for power transformers are in the range;

$$1.2(p.u.) < |\lambda_s| < 1.35(p.u.) \qquad and \qquad 0.7(p.u.) < |\lambda_r| < 0.9(p.u.)$$

Accordingly, switching at voltage zero instant with a polarity that matches the maximum possible residual flux, the saturation angle '$\omega \cdot t_s$' w.r.t. instant of switching and $K(0)$ are within the following ranges respectively;

$$45^o < \omega \cdot t_s < 70^o \tag{6.71}$$

$$0.7 > K(0) > 0.35 \tag{6.72}$$

High R_n values leading to considerable inrush reduction will result in low X/R ratios. It is clear from (6.69) and (6.71) that X/R ratios equal to or less than 1 ensure negative DC component factor '$K(R_n)$' and hence the exponential term shown in (6.68) can be conservatively neglected. Accordingly, (6.68) can be re-written as follows;

$$I_{peak}(R_n) \approx B_2(R_n) = \frac{V_m}{\sqrt{(r + R_n)^2 + X_s^2}} \tag{6.73}$$

Using (6.70) and (6.73) to evaluate (6.67), the neutral resistor size which corresponds to a specific reduction ratio α can be given by;

$$R_n(\alpha) = \frac{1}{\alpha \cdot [K(0) + 1]} \cdot \sqrt{r^2 + X_s^2} \tag{6.74}$$

Equations (6.72) and (6.71) reveal that transformers with less severe saturation characteristics 'high saturation flux and low maximum residual flux values' require higher neutral resistor value to achieve the desired inrush current reduction rate. Based on (6.71) and (6.72), inrush current reduction of 90% can be achieved within the range of R_n;

$$5.9 \cdot X_{series} \leq R_{n\_Optimum} \leq 7.4 \cdot X_{series} \tag{6.75}$$

Based on (6.75), a small resistor 'less than 10 times the saturation series reactance' can achieve more than 90% reduction in inrush current. The amount of reduction in flux during the first cycle can be found as follows;

$$\Delta\lambda(R_n) = \int_{t_s}^{t_o} i(t) \cdot R_n \, dt \qquad (6.76)$$

$$t_o = (\pi + \theta_2)/\omega$$

$$\Delta\lambda(R_n) = \lambda_m \left(sin(\theta_2) \cdot sin(\theta_2 - \omega t_s) \cdot e^{-\left(\frac{t_s - t_o}{\tau_2}\right)} + cos(\omega t_s) - cos(\theta_2) \right) \qquad (6.77)$$

Within the optimum neutral resistor value defined by (6.75), the total flux reduction during first phase switching is within;

$$\Delta\lambda\left(R_{n\_Optimum}\right) \approx 1.5\ (p.u.) \qquad (6.78)$$

As the second cycle starts, an initial flux level of $\left(\lambda_r - \Delta\lambda\left(R_{n\_Optimum}\right)\right)$ will exist. This results in the absence of inrush current after the first cycle since the maximum flux $(2\lambda_m - 0.75 \approx 1.25(p.u.))$ is close to -or below- the saturation flux.

6.6 Neutral Voltage Rise

From simulation studies carried out on various transformer types and connections, it was found that the peak neutral voltage will reach values up to 1 [p.u.] rapidly as the neutral resistor value is increased. Typical neutral voltage peak profile against neutral resistor size is shown in Figure 6.14 for the 132.8MVA transformer during 1st and 2nd phase energization.

The effectiveness of the inrush mitigation scheme depends on introducing a voltage drop across the grounding resistor and hence reducing the applied voltage across the magnetizing branch of the energized phase(s). As a result of reducing the magnetizing branch voltage, the induced flux, which is the integral of the applied voltage, can be controlled and hence reduced preventing the transformer from operating into heavy saturation modes.

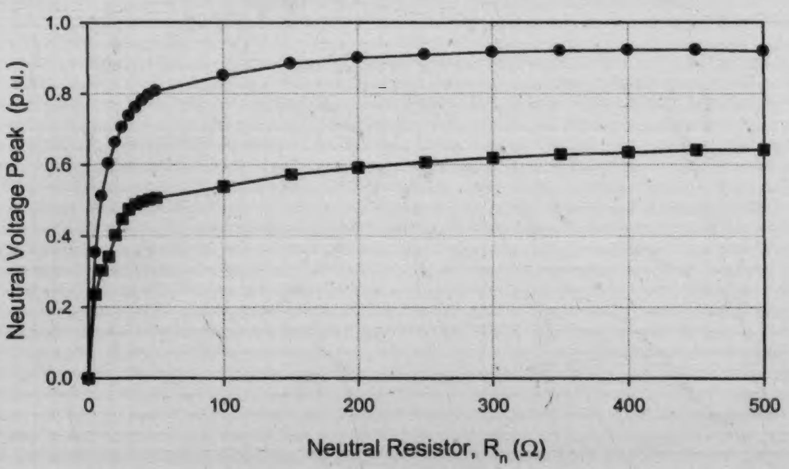

Figure 6.14 Neutral voltage peak as function of R_n during the first and second switching stages for the 132.8 MVA transformer.

Increasing the integral (area) of the neutral voltage drop will generally result in reducing the overall inrush current due to the reduction in the induced flux, which is the integral of the applied terminal voltage across the transformer windings. For the first phase energization, the waveform shape of the neutral voltage will be the same as that of the inrush current waveform scaled by the value of the neutral resistor value R_n.

The scheme performance during complete switching sequence is shown in Figure 6.15 with optimum neutral resistor of 50Ω. A delay of one second between each switching stage is required to allow phase fluxes to lose most of the DC component. The neutral voltage during the first cycle will reach 85% of the rated phase voltage. Quickly after the first cycle, the transformer is unsaturated and the neutral voltage is negligible since $R_{n\_Opt} \ll X_m$.

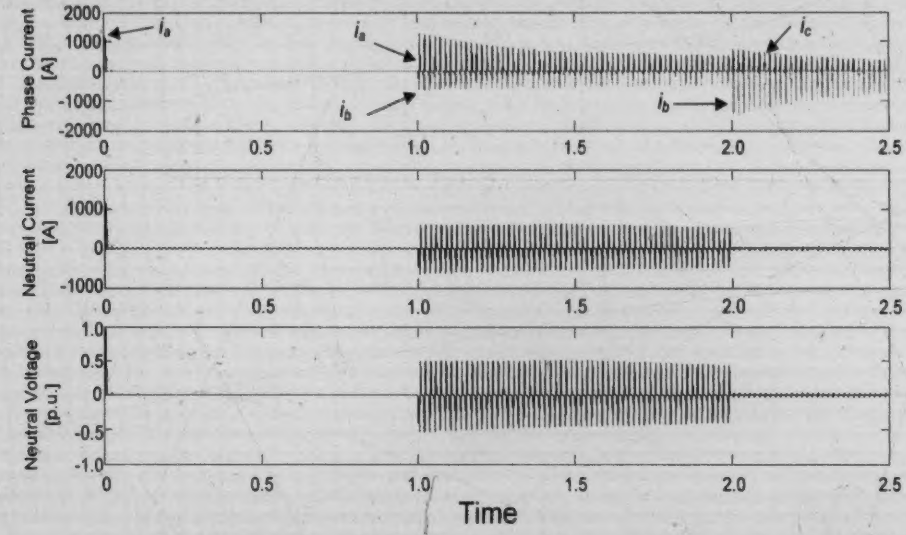

Figure 6.15 Phase currents, neutral current and neutral voltage during complete switching sequence for the 132.8, Yg-Δ transformer, $R_n = 50\Omega$.

The un-saturated magnetizing reactance is about 900 times the saturation reactance of a transformer, [7]. Accordingly, with the transformer operating in un-saturated mode, the neutral resistor voltage is negligible. Within the optimum resistor value, the neutral voltage peak is less than or close to 0.5 [p.u.] during second phase energization. As soon as the third phase is switched in, the neutral voltage will remain close to zero.The residual flux will have effect only during first phase switching for Yg-Δ and multi limb core type transformers. The effect of the residual flux on the neutral voltage rise and on the $I_{max}(R_n)$ curves for the first phase switching are shown in Figure 6.16 and Figure 6.17 respectively for the Hyundai 138 MVA transformer. The curves are evaluated for residual flux values varying from 70% to zero in the switched phase with same polarity as the energizing voltage.

It is a common industry practice to grade the insulation over the Yg winding for solidly grounded transformers [7], [82], [83] and [84]. This can introduce limitations to the applicability of the proposed scheme at high voltage levels. The following section addresses the standard requirements and limitations for the application of the proposed scheme to both dry-type and liquid immersed transformers.

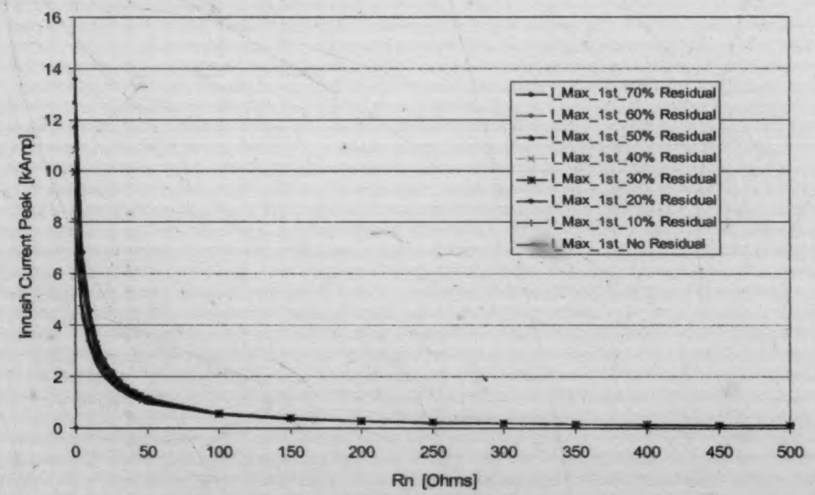

Figure 6.16 First phase energization $I_{max}(R_n)$ performance curves with different residual flux levels for the Hyundai, 72/13.8 kV, 132.8 MVA transformer.

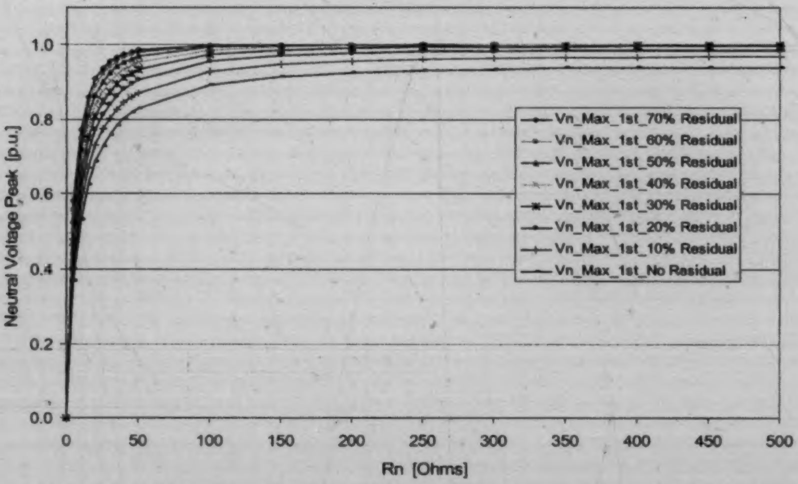

Figure 6.17 Neutral voltage rise curves for the first switching stage with different residual flux levels for the Hyundai, 72/13.8 kV, 132.8 MVA Transformer.

6.6.1 IEEE/ANSI Standards for the Neutral Terminal Insulation

A review of the IEEE standards, [82], [83] and [84], which specifies the recommended specifications of the insulation level at the neutral point of three phase transformers have revealed the following findings:

IEEE std C57.12.00-2000: "IEEE Standard General Requirements for Liquid-Immersed Distribution, Power and Regulating Transformers", [82]:

For solidly grounded transformers or transformers with CT's at the neutral point or grounded through regulating transformer: The neutral voltage insulation level for Nominal system voltages up to 25kV; the insulation level is at least 10kV, but significantly higher or matching (at 25 kV level) the nominal system line terminal voltage. For higher system voltages over 69 kV, the insulation level shall in no case be less than 34 kV. In other words, for solidly grounded transformers, the insulation level at the neutral should not be less than 50% of the line terminal system voltage.

For transformers grounded through a ground-fault neutralizer or isolated but impulse protected, the neutral insulation level should be not less than 10kV or approximately 140-150% of the rated system terminal voltage whatever is higher.

Table 6.1: IEEE std C57.12.00-2000, Minimum low frequency test levels at neutral for class I 'Power transformers having high voltage winding of 69kV and below', [82].

Minimum low-frequency insulation level (kV rms)			
Application	Nominal System voltage (kV)[a]	Grounded solidly or through a current transformer or through a regulating transformer	Grounded through a ground-fault neutralizer, or isolated but impulse protected
Distribution or Power	1.2	10	10
	2.5	15	15
	5.0	19	19
	8.7	26	26
	15.0	26	26
	25.0	26	34
	34.5	26	50
	46.0	34	70
	69.0	34	95

[a] For higher line terminal system voltages than shown above, the low frequency insulation level at the neutral shall be specified column with service requirements, but in no case shall e less than 34kV.

IEEE std C57.12.01-1989: "IEEE Standard General Requirements for Dry-Type Distribution and Power Transformers", [83]:

Generally, the neutral terminal of a winding, which is designed for grounded Yg connection, only may have insulation level lower than that for the line terminal. Windings of transformers and auto transformers designed for Y connection only with the neutral brought out and solidly grounded directly or through a current transformer shall have neutral insulation as described below:

- Windings with line-to-line voltages of 1.2 kV or less shall have the neutral insulated for a 4 kV low frequency applied voltage test.
- Windings with line-to-line voltages higher than 1.2 kV shall have the neutral insulated for a 10 kV low frequency applied voltage test.
- When specified, the neutral shall be designed for higher insulation levels.

ANSI/IEEE std 32-1972: "IEEE Standard Requirements, Terminology, and test procedure for Neutral Grounding Devices", [84]:

For transformers with neutral grounding devices, this standard specifies the insulation classes for the neutral grounding device "which shall be coordinated with the transformer neutral terminal". Generally, the Neutral insulation is determined by the maximum neutral voltage rise across the neutral device during fault conditions. However, the minimum Insulation level shall not be less than that shown in column 4 in Table 6.2. For neutral voltage rise levels during fault conditions higher than that specified in Column 3, the system insulation class shall be used 'column 1'.

As a conclusion, the neutral terminal insulation of Yg transformer windings shall not have less than 50% of the rated line terminal voltage in case the transformer is grounded through a grounding device. The neutral insulation level is higher for lower system voltages. Depending on the calculated neutral voltage rise during short circuits, this insulation level can be raised to the rated line terminal insulation level.

Accordingly, a lower neutral voltage rise is generally desirable when applying the proposed inrush current mitigation scheme. This is especially when applying the scheme to transformers that are originally solidly grounded and/or having lower neutral insulation levels. For transformers, which are already grounded through neutral grounding device, there might be no limitation on the neutral voltage rise.

Table 6.2: IEEE Std 32-1972, Insulation Classes for Neutral Grounding Devices, [84].

Insulation Class			
System Insulation Class, kV (Note 1)		Fault Voltage Criteria (Note 2)	
Column 1	Column 2	Column 3	Column 4
Class	BIL	kV	kV
1.2	45	1.2	1.2
2.5	60	2.5	2.5
5.0	75	5.0	5.0
8.7	95	8.7	8.7
15.0	110	8.7	8.7
23.0	150	15.0	8.7
34.5	200	25.0	8.7
46.0	250	34.5	15.0
69.0	350	46.0	15.0
92.0	450	69.0	15.0
115.0	550	69.0	15.0
138.0	650	92.0	15.0
161.0	750	92.0	15.0
180.0	825	115.0	15.0
196.0	900	115.0	15.0
230.0	1050	138.0	15.0

6.6.2 Surge Arrester Application to limit Neutral Voltage Rise

In order to achieve some control 'reduction' over the neutral-voltage rise level using the proposed inrush mitigation scheme; a number of solutions have been tested. The first and most effective solution is the use of a surge arrester in parallel with the neutral grounding resistor. A surge arrester with a saturation voltage 50% of the nominal phase voltage can insure the limitation of the neutral voltage rise. However, since the surge arrester will clip the neutral voltage waveform at the rated saturation voltage '0.5 [p.u.]' there will be some reduction in the effectiveness of the mitigation scheme. Clipping the neutral voltage waveform will reduce the integral area of the neutral voltage waveform and hence reducing the capability to control the induced flux in the energized phase. The impact of the arrester for the first switching stage can be analytically derived and proven easily through assuming that the arrester will act as a fixed DC source after being driven into saturation, Figure 6.18.

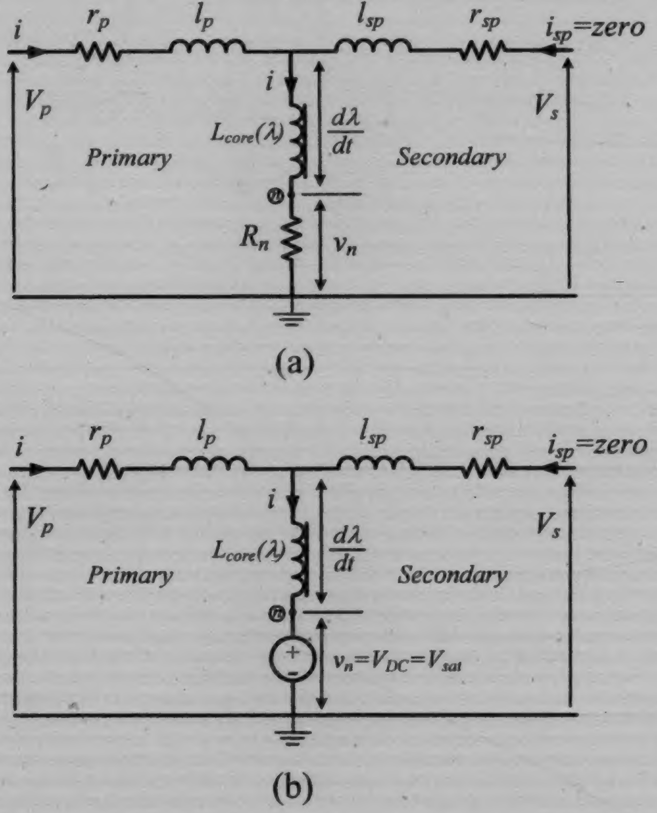
i
r_p
l_p
l_{sp}
r_{sp}
i_{sp}=zero
V_p
i
$L_{core}(\lambda)$
$\frac{d\lambda}{dt}$
Primary
Secondary
V_s
R_n
v_n
(a)
i
r_p
l_p
l_{sp}
r_{sp}
i_{sp}=zero
V_p
i
$L_{core}(\lambda)$
$\frac{d\lambda}{dt}$
Primary
Secondary
V_s
+
-
$v_n=V_{DC}=V_{sat}$
(b)

Figure 6.18 Modeling of surge arresters before and after saturation.

This means that after the arrester saturates, the applied voltage across the transformer coil cannot be further controlled through the neutral resistor. Instead, the voltage across the transformer coil in this stage can be assumed to be equal to $v_s - v_{sat}$. From this assumption, it is possible to easily obtain an analytical expression for the $I_{max}(R_n)$.

Figure 6.19 shows the $I_{max}(R_n)$ curves during first phase switching at different arrester saturation voltages with respect to the nominal phase terminal voltage. It is clear that limiting the neutral voltage rise will reduce the capability of the proposed inrush mitigation scheme. However a reduction of 60% to 70% of inrush current can still be achieved for a maximum allowable neutral voltage rise of 50%. Figure 6.20 shows the $I_{max}(R_n)$ curves for the first and second switching stages for different arrester saturation voltage levels. It can be clearly shown that the 2^{nd} stage switching will not be strongly affected by the application of the surge arrester since the neutral voltage rise is almost close to 0.5 [p.u.] without the arrester application.

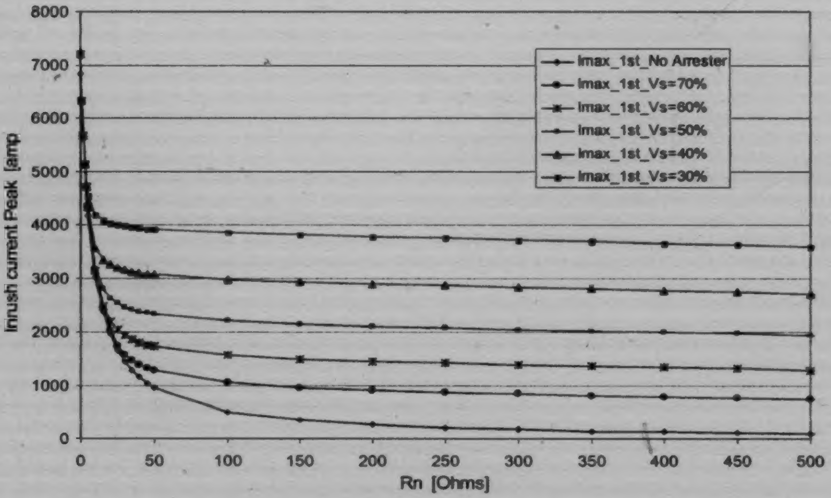

Figure 6.19 First phase energization $I_{max}(R_n)$ curves with different arrester saturation voltages for the 132.8, Yg-Δ transformer.

Similar condition exists for the second phase switching. The arrester will have two effects; first it will prevent the neutral point to be floating (open circuit) for higher neutral resistance values. And hence prevents the formation of a series phase-to-phase energization. As a result, this will limit the inrush current for higher resistance values as compared to the case with no arrester. The second effect is that with the arrester saturation voltage selected at low values, the neutral point voltage will be set to closer values to the ground and hence limiting the amount of current flowing into the neutral resistor. In other words, the lower the saturation voltage of the arrester, the characteristic curve of the second phase switching will become closer to a solid grounding energization case.

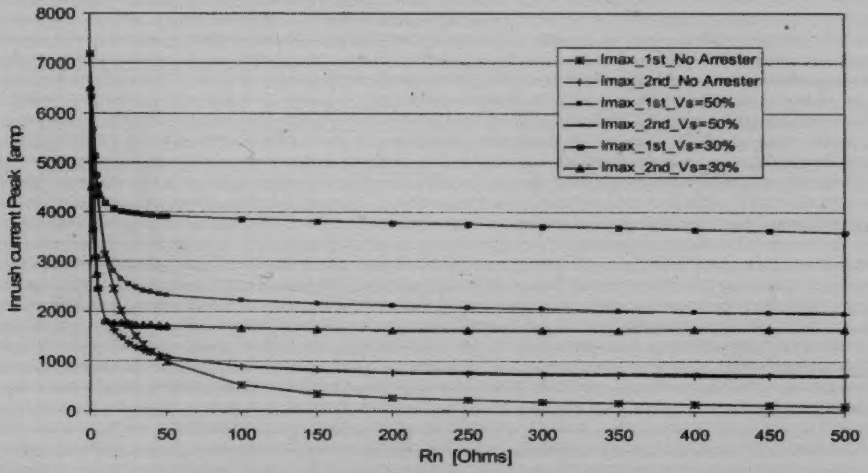

Figure 6.20 First and second phase energization $I_{max}(R_n)$ curves with different arrester saturation voltages for the 132.8, Yg-Δ transformer.

Similar deduction procedure to the one presented in Section 6.4, leads to the following inrush expression;

$$i(t) = B_2 \cdot \left[\left(sin\left(\theta_2(0) - \omega \cdot t_{s\_AR}\right)\right) \cdot e^{-(t-t_{s\_AR})/\tau_2(0)} + 1\right] \tag{6.79}$$

Accordingly the peak inrush current during arrester operation can be expressed as;

$$\begin{aligned} I_{pk-Ar}(R_n) = B_2(0) \cdot \left[\left(sin\left(\theta_2(0) - \omega \cdot t_{s\_AR}\right)\right) \cdot e^{-(t_{pk-Ar}-t_{s\_Ar})/\tau_2(0)} + 1\right] \\ - \frac{V_{S\_Ar}}{r}\left[1 - e^{-(t_{pk-Ar}-t_{s\_Ar})/\tau_2(0)}\right] \end{aligned} \tag{6.80}$$

From (6.80), the amount of reduction in current will depend on how fast the arrester will become saturated, t_{s_AR}. However, since the neutral voltage will start rising after the transformer saturates at t_s, the neutral voltage integral will have a maximum limit as the arrester saturation time t_{s_AR} approaches t_s. This clarifies the 'almost' steady profile of the inrush current as R_n increases shown in Figure 6.19. The resistor-arrester arrangement performance during complete switching sequence is shown in Figure 6.21. The results shown in Figure 6.15 and Figure 6.21 were obtained assuming an infinite system bus.

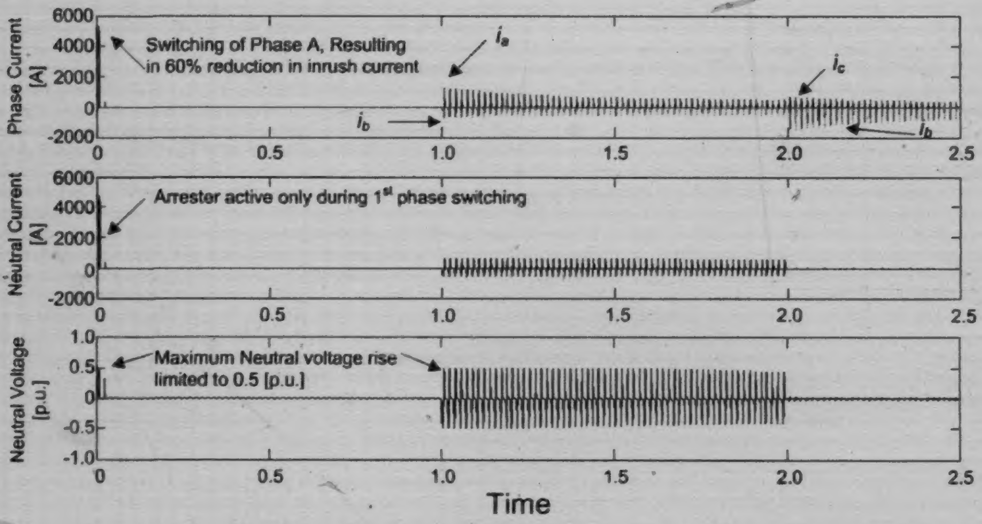

Figure 6.21 Phase currents, neutral current, and neutral voltage during complete switching sequence $R_n = 50\Omega$. Arrester saturation voltage is 0.5 (p.u.) for the 132.8MVA, Yg-Δ transformer.

From Figure 6.10 and 6.21, it is shown that after energizing the second phase, the neutral voltage remains close to 0.5 p.u. and consequently leading the un-energized phase C terminal voltage close to 1.5 p.u.. However, the phase voltage across the un-energized phase is close to the normal phase voltage and consequently there is no over voltage imposed across its windings. In terms of the transformer bushings overvoltage withstand capability, such overvoltage condition should be avoided and the energization of the third phase should take place after few cycles from energizing phase B. As could be shown from Figure 6.10 and 6.21, the amount of reduction in the flux waveform DC content is minimal after few cycles and accordingly allowing a long settling time between 2nd and 2rd energization events is not essential for the scheme effectiveness.

The combined effect of the residual flux together with the application of surge arrester was also studied. Figure 6.22 shows the $I_{max}(R_n)$ curves during first phase switching with arrester saturation voltage set to 0.5 [p.u.] and with different saturation levels. Although the application of the surge arrester will reduce the capability of the mitigation scheme, it can be observed that the scheme can still achieve a minimum of 60% reduction in inrush current even with the worst residual flux conditions. Table 6.3 summarizes the performance of the mitigation scheme for the Hyundai transformer evaluated at a neutral resistor value of R_n = 50 [Ohms] and at different residual flux levels. The arrester saturation level was set to 50%.

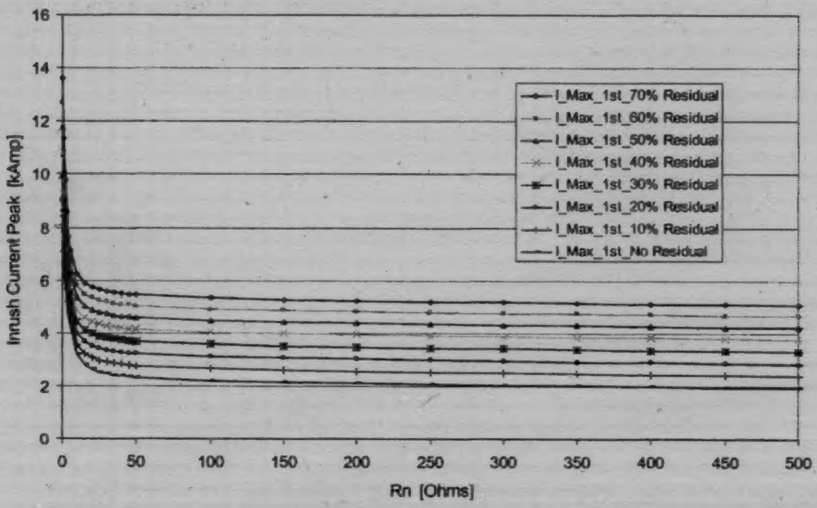

Figure 6.22 First phase energization $I_{max}(R_n)$ curves showing the effect of arrester 50%saturation voltage with different residual flux levels for the 132.8, Yg-Δ transformer.

Table 6.3: Performance of the Inrush mitigation scheme with and without arrester application for the Hyundai 138MVA transformer Evaluated at different residual flux levels.

Residual Flux (%)	No Arrester				Arrester with 50% Saturation Voltage		
	$I_{max-1st}$ ($R_n = 0$)	$I_{max-1st}$ ($R_n = 50$)	V_{n-max} ($R_n = 50$)	% Reduction	$I_{max-1st}$ ($R_n = 50$)	V_{n-max} ($R_n = 50$)	% Reduction
70%	13612	1150	0.986	91.55	5455	0.5	59.93
60%	12690	1152	0.980	90.92	5034	0.5	60.33
50%	11776	1140	0.970	90.32	4596	0.5	60.97
40%	10860	1122	0.954	89.67	4143	0.5	61.85
30%	9944	1097	0.933	88.97	3686	0.5	62.93
20%	9026	1065	0.905	88.20	3228	0.5	64.24
10%	8110	1026	0.871	87.35	2770	0.5	65.84
0%	7194	977	0.830	86.42	2326	0.5	67.67

6.6.3 Saturable-Inductor Grounding Application to limit Neutral Voltage Rise

The application of a grounding saturable 'Iron Core' reactor has also been studied. The performance of the saturable reactor will be to increase the total inductance in the energized circuit and consequently reducing the inrush current. Before the grounding reactor saturates, the applied energizing voltage will be shared between the two magnetizing reactances of the main and grounding reactor and hence reducing the applied voltage across the terminals of the main transformer. During saturation, the saturable reactor will have a very low $d\phi/dt$ and hence voltages drop of zero across its magnetizing branch. In the other hand, the neutral voltage waveform will make the control of the neutral voltage through an additional surge arrestor much easier. The reason is that most of the over voltage exist during the first cycle only, and for a short period of time. For the second phase switching, the transient overvoltage occurs for a relatively small period of time.

The $I_{max}(R_n)$ performance curves are shown in Figure 6.23 for a grounding reactor designed to have a saturation flux of 10% of the main transformer and with a series resistor that will result in a maximum of 0.55 [p.u.] neutral voltage rise during first phase switching, Figure 6.24. It is clear that a reduction of 75% can be achieved in the inrush current of the first phase together with a neutral voltage rise limiting to 55%.

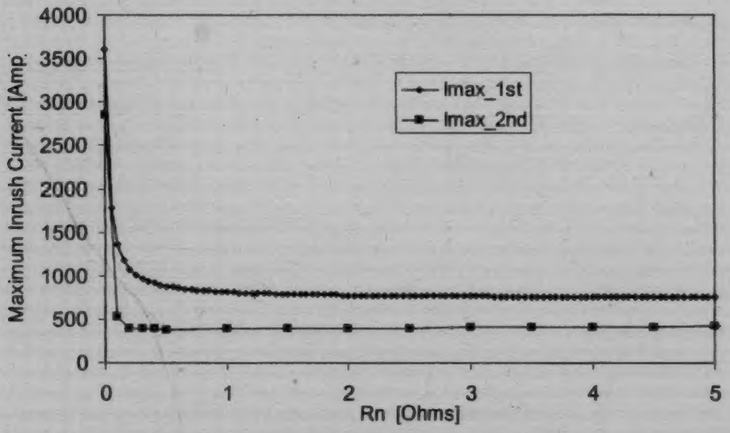

Figure 6.23 Inrush currents $I_{max}(R_n)$ performance curves during 1st and 2nd switching phases. Reactor series resistor designed of ~0.55pu rise during first switching for the 30kVA, laboratory transformer.

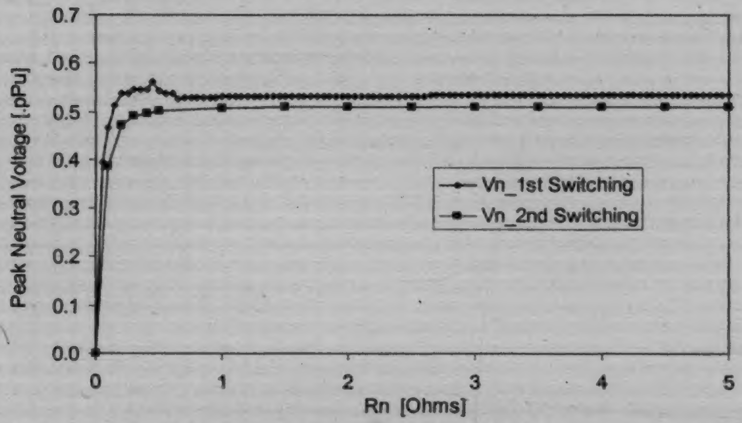

Figure 6.24 Neutral voltage magnitudes during 1st and 2nd switching phases. Reactor series resistor designed for ~0.55pu rise during first switching phase Inrush currents for the 30kVA, laboratory transformer.

As a conclusion, the neutral resistor with a surge arrester application is the best combination in means of controlling the neutral voltage rise and the reduction of inrush current. However, the saturable rector will solve the problem of the neutral voltage rise (together with a small arrester). If an arrester that can tolerate the high power during switching exist, or can be easily manufactured, the resistor-arrestor combination will be the best choice.

The performance of the sequential energization scheme during the first and second switching is shown in Figure 6.25 and Figure 6.26 respectively. It is clear that although the saturable reactor can provide some means of controlling the neutral voltage rise, a significant loss of effectiveness can be observed.

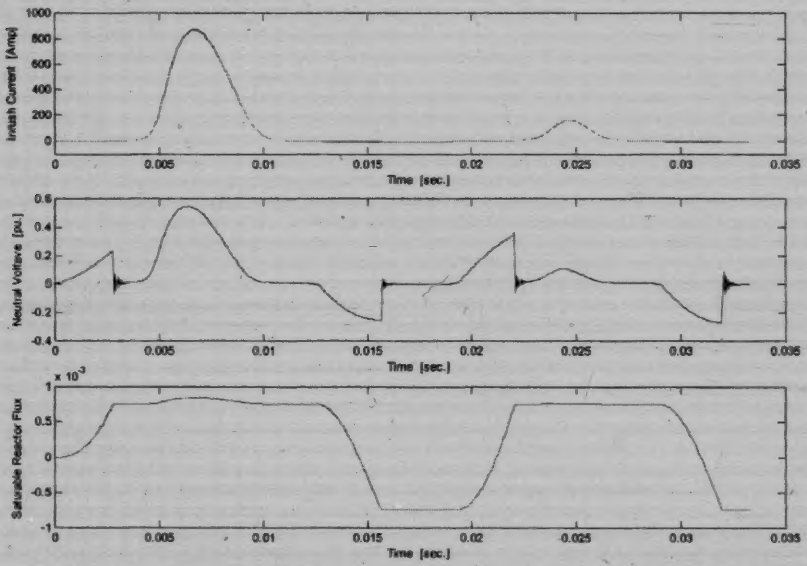

Figure 6.25 Saturable Reactor performance during the first phase switching. (please note the magnitude of the neutral voltage after the first cycle and the duration of the overvoltage).

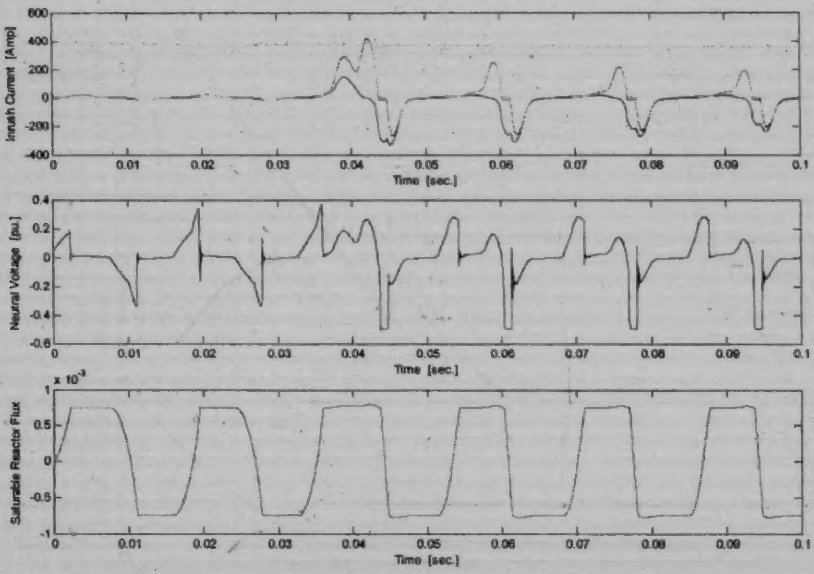

Figure 6.26 Saturable Reactor performance during the second phase switching. (please note the magnitude of the neutral voltage before switching phase 2 and after switching 2nd phase.

6.7 Energy Requirements for the Neutral Grounding Resistor/ Arrester Scheme

Simulation studies can provide accurate calculation of energy requirement level for the scheme. In this section, approximate formulas will be given for a quick -but accurate- estimate of the energy withstand capability for both the resistor and the resistor-arrester arrangements.

6.7.1 Literature Review and Industry Practice

Neutral Grounding Resistor, NGR:

A review of the IEEE/ANSI standards [82]-[84] has been carried out in order to evaluate the acceptable neutral voltage rise limit on different power transformer types. The main application of the proposed scheme is the generator's step up transformers for Independent Power Producers, IPP, which are interconnected to the system at the distribution or sub transmission levels. The interconnection transformer is preferably Wye-grounded on the system side and Delta connected on the generator side [85]-[86]. A literature review has been conducted for the published work regarding the main design guidelines (from energy perspective) for NGRs or any power resistor in general. No numerical evaluation of the resistor energy requirements based on the actual performance of the resistor during transient conditions has been found either in research or industry 'manufacturing' literature. However, all of the design guidelines for the NGRs were based on the recommended requirements by the IEEE std 32-1972, [83], which deals with the standard requirements of grounding devices. All manufacturers strictly follow the requirements of this standard. The ratings for the grounding devices in general (IEEE std 32-1972) are based on standard operating conditions including:

Rated Current: The basis for this rating shall be the thermal current. This will be the current through the neutral device during a ground-fault condition at the device location. (Maximum ground fault current through the neutral resistor). For the case of the neutral resistor under study, this current would be the maximum current through the neutral resistor either during energization or during a ground fault condition.

Rated Voltage: Generally, the rated voltage shall be taken as the product of the rated thermal current (maximum allowable current through resistor) and the impedance of the grounding device (resistor) at rated frequency and at 25°C. If the product of the neutral resistor and the maximum thermal current exceeds 80% of the rated L-G voltage, the resistor shall be rated to continuous voltage and rated voltage shall be equal to the rated of L-G system voltage. Most of the manufactures rate there resistors to a full L-G voltage and some other require L-L voltage in the US.

Frequency: The rated frequency shall be the fundamental.

Basic Impulse Insulation Level (BIL) and Insulation Class: Follow the insulation levels stated in IEEE std 32-1972.

Rated Time: Rated time shall be 10 seconds, 1 minute, 10 minutes and extended time (based on design requirements). Extended time operation shall not exceed an an average of 90 days per year. According to manufacturers, two main key design factors are used;

The maximum temperature rise: This is the resulting effect from both the "Thermal current Limit" and the "Rated-Time of operation". These two factors decide how much energy will be produced and need to be dissipated during energization.

As stated in the standards, [84], the temperature rise (for resistors) is based on the application of the rated voltage for the rated time duration and the (hot-spot) temperature shall not exceed the given ratings.

The allowable terminal voltage 'insulation': This shall strictly follow the IEEE std 32-1972 and mainly based on the rated system voltage.

As a conclusion, the available NGR by the industry (in order to comply with the standards) will exceed the general requirements for the proposed NGR-based inrush mitigation scheme. If the supplier has a resistor capable of operating at the rated voltage and current, the NGR supplied should be able to handle the maximum inrush current-waveform (or the maximum fault current whichever is greater) for at least 10 continuous seconds (rated time).

Several manufacturers can provide (already has installed) NGR resistors that can handle 1000-1500 amps RMS continuous current for 10 seconds at voltage levels of 33kV or more. Other examples are 400amps for 15 sec at 77kV level.

Voltage limiting arrester:

Based on the information found in literature; arresters can handle less energy dissipation (absorption) than resistors. This is due to the fact that they are originally designed for short period operation duration. However, a way of stacking a number of arresters in parallel together with a small series resistor (designed not to alter the voltage clipping characteristics of the arrester) in order to handle a higher energy rating was suggested in [87]. The resistor is added in series with each arrester element in the stack to prevent one arrester to activate before the others. In [7], Maximum energy capability (specific energy kJ/kV) of GE MOV arresters is given as shown in Table 6.4.

For the NGR inrush mitigation scheme, it should be noted that the Arrester rating kV will be a percentage of the rated voltage, i.e. for a 72 kV system, the arrester rated voltage will be 36kV if the maximum allowable neutral voltage rise is 50%.

Table 6.4: Maximum energy capability (specific energy kJ/kV) of GE, MOV arresters, [7].

Arrester Class Rating kV	Energy Capability	
	kJ / kV of Rating	kJ / kV of MCOV (Maximum continuous over voltage)
2.7 – 48	4.0	4.9
54 – 360	7.2	8.9

In [87] and [88], the probability of withstand an energy stress is given as function of specific energy kJ/kV for Metal Oxide Surge Arrester for different rated voltage levels. It was shown that the withstand capability can reach 99.999% for kJ/kV of 1.0 and can drop to between 50 and 95% depending on the voltage level for kJ/kV of 2.5, [88]. As the kJ/kV factor increases, the probability of energy-withstand decreases rapidly (The probability of failure increases).

Generally, according to [11], [87], [88] and [89] the desired energy capability can be achieved for the application of a surge arrester for limiting the neutral voltage rise during transformer switching either using single or multiple stacked arresters. In the other hand, as will be shown from the coming results, that if the neutral grounding resistor is correctly designed 'close to the knee point of the first switching stage, the neutral voltage rise during second energization stage will be very close to 0.5 which will result in a limited or no energy absorption for the arrester during the second and thirds phase switching. The arrester will be active only during the first phase switching for one cycle and will not operate during the next phase switching for allowable neutral voltage rise of 0.5 p.u. lower neutral voltage rise, will result in activating the arrester during second stage switching for longer periods as the allowable neutral voltage rise goes lower.

6.7.2 Energy Requirements for Neutral Grounding Resistor

As has been shown earlier, there will be negligible neutral voltage across the resistor after energizing the third phase. Accordingly, the focus will be directed on the assessment of energy requirements during first and second phase switching stages. Figure 6.27 shows the accumulated energy absorbed by the neutral resistor during the complete switching sequence for the 132.8MVA transformer for the case shown in Figure 6.21.

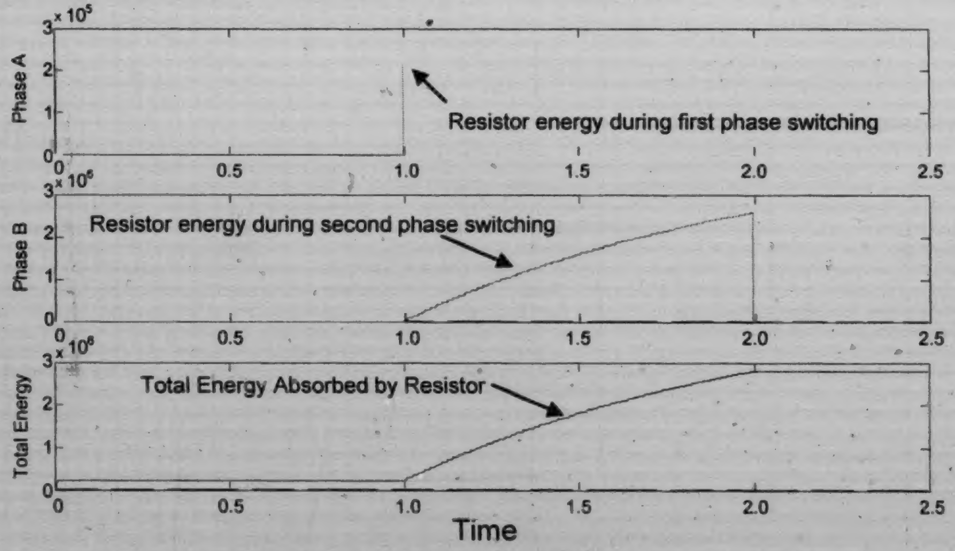

Figure 6.27 Accumulated energy during different switching stages. Results are for the 132.8 MVA transformer with infinite system.

It is clear from Figure 6.27 and Figure 6.21 that negligible neutral voltage will exist after the first cycle of the 1st phase energization and the energy dissipated through the resistor can accordingly be calculated as follows;

$$E_{1-Cycle} = \int_{t=\frac{0}{\omega}}^{t=\frac{\pi}{\omega}} R_n \cdot I_{max}(R_n)^2 \cdot sin(\omega \cdot t)^2 dt \tag{6.81}$$

$$E_{1-Cycle} = \frac{1}{240} \cdot R_n \cdot I_{max}(R_n)^2 \tag{6.82}$$

For the second phase, as can be seen from Figure 6.10 and Figure 6.13, the neutral current can be presented using two sinusoidal half-waves of twice the frequency. Since the neutral voltage rise during second phase is around 0.5 [p.u.] with the same neutral resistor, the energy during 60-cycle period of the second phase switching can be calculated as follows;

$$E_{2-60-Cycle} = 60 \cdot \int_{t=\frac{0}{\omega}}^{t=\frac{\pi}{\omega}} R_n \cdot \left[\frac{I_{max}(R_n)}{2}\right]^2 \cdot sin(\omega \cdot t)^2 dt \tag{6.83}$$

$$E_{2-60-Cycle} = 15. E_{1-Cycle} \tag{6.84}$$

As can be seen from (6.84), most of the energy absorbed by the grounding resistor will be during second phase switching. After the third phase is switched in, the neutral current will be very close to zero and energy dissipation through the resistor can be neglected.

For the resistor-arrester arrangement, the arrester will be active only during the first cycle of the first switching stage. As shown in (6.79) the total current through the switched phase will be composed of a DC component through the resistor and an AC component through the arrester. Accordingly, the energy dissipated through the resistor and the arrestor can be calculated respectively as follows;

$$E_{1-Cycle-R_n} = 60 \cdot \int_{t=\frac{0}{\omega}}^{t=\frac{\pi}{\omega}} \frac{V_{s-Ar}}{R_n} \cdot V_{s-Ar}\, dt = \frac{1}{120} \cdot \frac{V_{s-Ar}^2}{R_n} \tag{6.85}$$

$$E_{1-Cycle-Ar} = \int_{t=\frac{0}{\omega}}^{t=\frac{\pi}{\omega}} V_{s-Ar} \cdot \left(I_{pk-Ar}(R_n) - \frac{V_{s-Ar}}{R_n}\right) \cdot sin(\omega \cdot t)\, dt \tag{6.86}$$

$$E_{1-Cycle-Ar} = \frac{V_{s-Ar}}{\pi \cdot 60} \cdot \left(I_{pk-Ar}(R_n) - \frac{V_{s-Ar}}{R_n}\right) \tag{6.87}$$

The arrester will not be active for saturation voltages of 0.5 [p.u.] or higher within the optimal neutral resistor value. The neutral resistor energy is the same as that of the original scheme during second switching stage for the same R_n. As shown in Figure 6.28 below, the total energy absorbed by the resistor during all switching stages is about 1.30MJ, and 250kJ for the surge arrester(s).

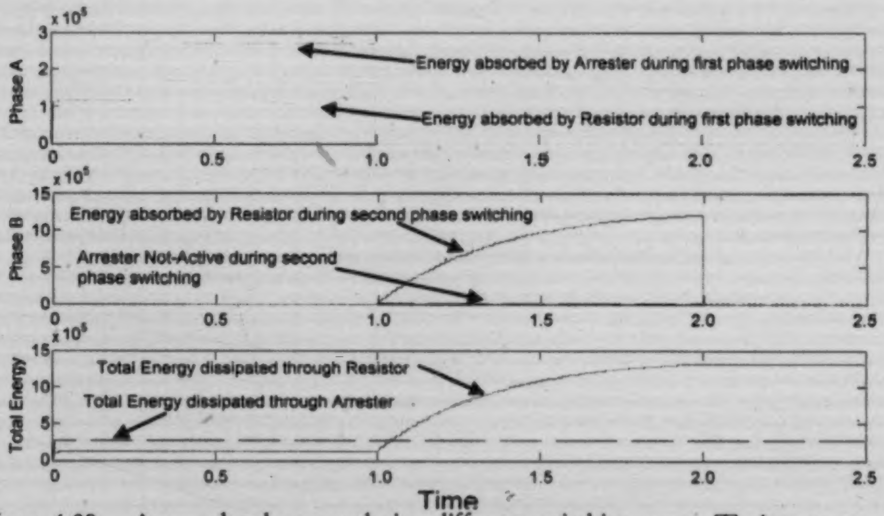

Figure 6.28 Accumulated energy during different switching stages [J]. Arrester set at 0.5 [p.u.] saturation voltage with 1000MVAsc system.

6.8 Considerations on Ferroresonance

The proposed sequential energization scheme could expose a transformer to ferroresonance. Fortunately, the neutral resistor is in series of the resonant circuit and will provide sufficient damping to prevent ferroresonance from happening. In fact, reference [90] proposed the idea of using a neutral resistor to mitigate ferroresonance. Based on numerous TNA studies, reference [90] found that a neutral resistor less than $0.05X_m$ is sufficient to prevent the occurrence of ferroresonance in Yg-Δ transformer banks. Based on the finding, we can conclude that the proposed scheme will not experience ferroresonance problem. Our simulation studies on 22/0.48kV, 4.5%, 160kVA, Y-Δ transformer, also confirmed this conclusion. Figure 6.29 shows the voltage waveforms at the energizing side of the transformer due to energizing phase A. It is clear that using the optimal resistor successfully damped the overvoltage at un-energized phases B and C within one cycle.

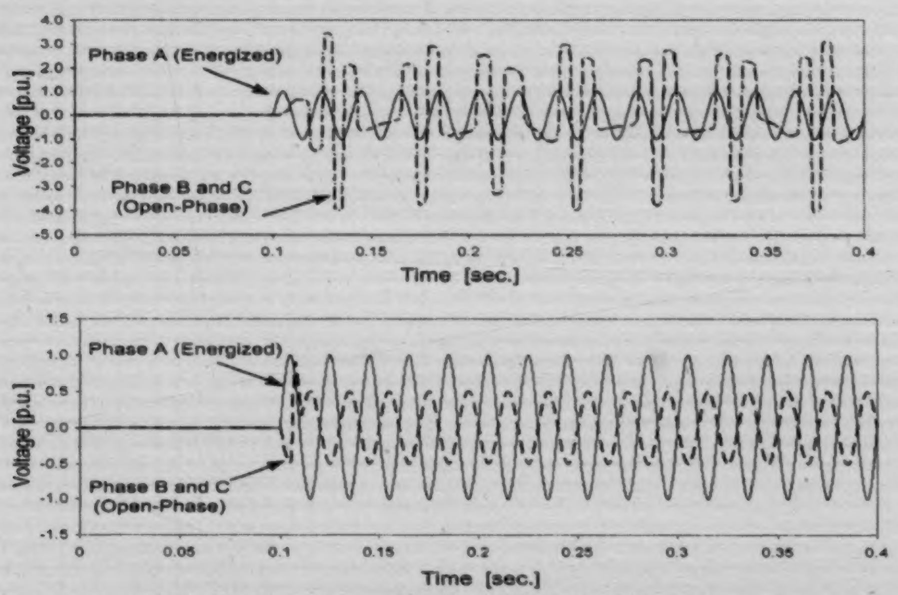

Figure 6.29 Voltage at the primary side of a 22/0.48, 160kVa, Y-Δ transformer due to energizing Phase A. Top: Isolated neutral. Bottom: Neutral grounding.

It should be noted that the neutral resistor will effectively damp ferroresonance conditions where the possible ferroresonance circuit involves the grounding resistor in series with the circuit. In conditions where phase-to-phase capacitance is significant, the neutral resistor might not have the similar damping capability. However, most cable installations use per-phase shielding and accordingly, the main capacitance involved is the self, phase to ground, capacitance.

6.9 Conclusions

In this chapter, the transient performance of the sequential energization scheme was thoroughly investigated, and an improved, more complete design criterion for the transformer sequential energization scheme was presented. It was shown that a small neutral resistor size of less than 10 times the transformer series saturation reactance can achieve an 80-90% reduction in the inrush currents among the three phases.

The scheme's transient performance was presented, and a detailed analysis demonstrated that the first-phase switching leads to the highest inrush current level. Moreover, it was shown that during the second energization with small neutral resistor values, the neutral resistor acts in series with the energized phase and leads to a significant reduction of the inrush current's magnitude. The study of the scheme's performance with different connection types was also investigated. It was shown that with a delta winding or an E-core structure, the zero sequence current makes the neutral resistor two times as effective in reducing the inrush current's magnitude during second-phase energization.

The work presented in this chapter also addressed the scheme's main practical limitation: the permissible rise of neutral voltage. Through the conducted literature review on insulation requirements at the neutral of the grounded and ungrounded transformers, a feasible application range for both dry-type and liquid-immersed transformers was proposed. The use of surge arresters to extend the scheme's application range was also presented. Formulas were also derived to estimate the amount of energy that both the neutral resistor and the arrestor (if applicable) must be able to withstand.

7.Single Pre-Insertion Resistor with Sequential Switching

This chapter presents an innovative, easy-to-implement and effective scheme for reducing transformer energization inrush currents and the voltage sag associated with them. As was shown in previous chapters, the neutral resistor-based sequential energization scheme has limitations due to the allowable neutral voltage rise limit of transformers at high voltage levels. In this chapter, a scheme based on using a single series pre-insertion resistor in one of the transformer phases with rapid sequential energization is presented to overcome that limitation. The proposed method, although originally designed for use with ungrounded primary connections, is also applicable to solidly grounded primaries and can achieve up to a 75% reduction of the inrush current. By using the analysis methodology described in earlier chapters, the scheme performance is thoroughly analyzed from a transient performance perspective. Resistor-sizing criteria and formulas were derived and are presented. Finally, a brief study of the chances of ferroresonance development with the sequential energization scheme is also presented.

7.1 Introduction

A neutral-resistor-based sequential energizing scheme for the reduction of inrush current was earlier introduced in Chapters 5 and 6. However, the scheme is applicable only to transformers with a grounded primary connection and has the limitation of increased transformer insulation cost at high-voltage levels. In this chapter, the application of a sequential switching scheme utilizing a *single series pre-insertion resistor* is presented to overcome both limitations, Figure 7.1. Simulation and experimental studies showed that the scheme could achieve an inrush current reduction of 85%, 70% and 50% when applied to transformers with *Y-ungrounded*, *Y-grounded* or *Delta* primary side, respectively. Although the scheme could reduce inrush currents by only 50% for delta connected primaries, such a reduction might be sufficient for meeting the allowable voltage sag level at the point of common coupling. Due to the increased application of highly sensitive loads, utilities are restricting the allowable voltage sag level at the point of common coupling (PCC) to values as low as 3%.

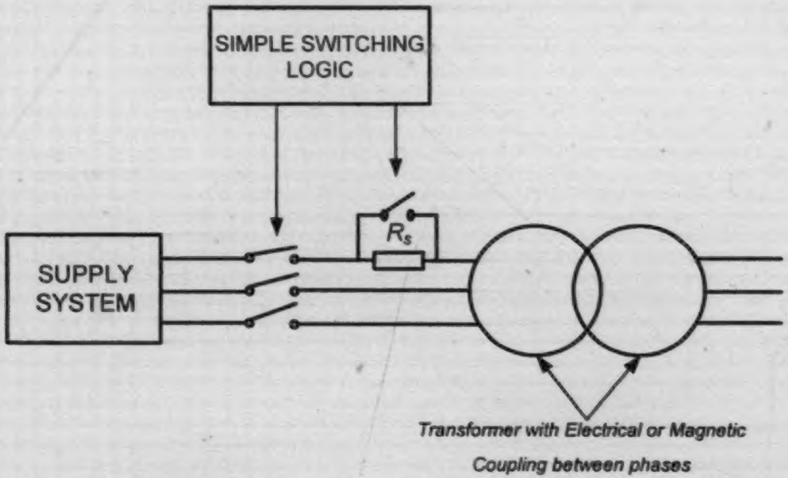
SIMPLE SWITCHING LOGIC
R_s
SUPPLY SYSTEM
Transformer with Electrical or Magnetic Coupling between phases

Figure 7.1 Single pre-insertion resistor sequential energization technique for inrush current reduction.

For transformers with ungrounded primaries (*Y-ungrounded or Delta*), the energization process is completed in two stages, Phases A and B followed by Phase C. For a Y-grounded primary, the three phases are switched in sequence. For both applications, the single pre-insertion resistor is placed in series with the first energized phase. The delay between the switching stages can be placed in the order of 5 cycles. The series pre-insertion resistor could be shunted out of the circuit after all the phases have been energized.

The scheme's performance could be further enhanced through the application of a simple closing instant control after switching the first phase. This scheme has a major cost reduction advantage as compared to the synchronous switching scheme, especially when applied to wind farm applications requiring the inrush current to be controlled for a large number of transformers where each unit needs its own residual-flux estimating device. Another advantage is that the scheme's effectiveness will not be influenced by tripping conditions caused by protection interaction, which is a frequent event with IPP anti-islanding protections.

The scheme's performance was investigated and will be presented through experimental and computer-simulation studies. Simple and straightforward sizing criteria for the series' pre-insertion resistor were developed and will be presented.

7.2 Experimental and Simulation Results

The proposed scheme has been tested through extensive experimental and simulation studies to assess the effectiveness of the scheme as applied to different transformer connections and the amount of inrush reduction corresponding to the size of the single pre-insertion resistor. The experimental work has been carried out on the 30kVA laboratory transformer. For each switching stage, the process is repeated sufficiently 'around 100 times' in order to capture a close to maximum inrush current condition for each resistor size tested. In the following sections, the impact of the pre-insertion resistor on the maximum inrush current during the complete switching sequence is being presented for all possible primary connections.

7.2.1 Y-Δ Connection (energizing from Y side)

For this connection, the series pre-insertion resistor can be placed on either of the first two phases to be energized. Phases A and B are switched first with the series pre-insertion resistor connected as shown in Figure 7.1. Switching phase C completes the transformer energization process. The series pre-insertion resistor is shunted-out after switching of phases A and B or simply after the third phase is energized. Figure 7.2, shows the resultant maximum inrush current magnitude as function of the applied series pre-insertion resistor (I_{max}-R, curves) for both experimental and simulation results.

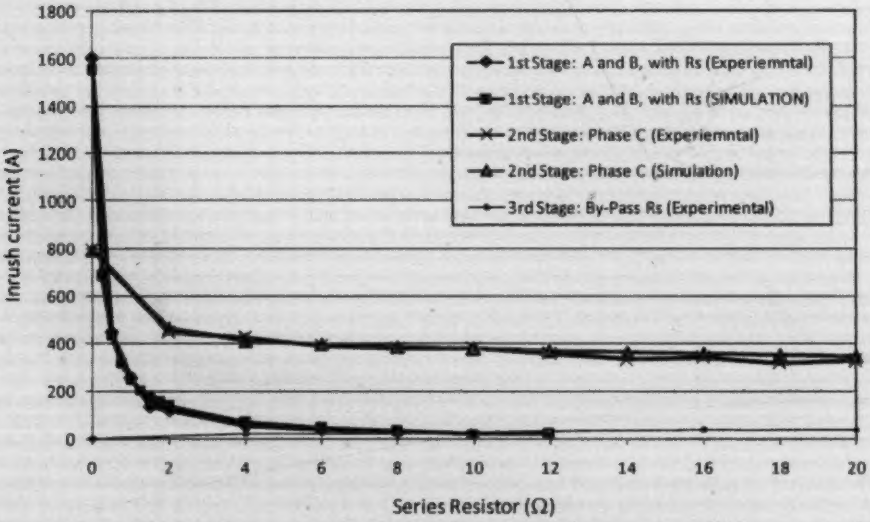

Figure 7.2 The performance of the pre-insertion scheme as applied to a 208/208, 30kVA, E-core,Y/Δ transformer. (Energizing from Y side).

As can be shown from Figure 7.2, the series pre-insertion resistor can effectively reduce the inrush current magnitude for the first switching stage. For the switching of the last phase C, the scheme can still reduce the inrush current magnitude to 400 amps compared to 800 amps. The overall reduction in inrush current for this scheme is at least 85% since simultaneous energization will lead to a current close to the 1600 Amps maximum inrush current during first phase switching.

It is clear from Figure 7.2 that by-passing the series pre-insertion resistor results in minimal disturbance that can be ignored. Due to the high core reactance, X_m, during steady state, the voltage drop established across the resistor is small. Shunting 'by-passing' the resistor will therefore reflect the differential voltage across the resistor on the core flux. However, the small differential voltage magnitude is no sufficient to drive the core into saturation. From the above, the series pre-insertion resistor can be sized based directly on its effect on the first switching stage.

7.2.2 Δ-Y Connection (energizing from Δ side)

Usually this connection is applied for interconnections at the sub-transmission and distribution levels since it provides ground fault isolation. This practice makes the protection coordination easier at the transmission side, provides isolation for generator produced harmonics from being transferred to the system side [90]. The scheme is applicable to transformers with delta connection. Phases A and B are switched first with R_s in series with one of the terminals and the third phase switching (Phase C) follows. The series pre-insertion resistor could be shunted out 'by-passed' either after switching phases A and B or after switching phase C. The $I_{max}(R_s)$ curves for this application are shown in Figure 7.3.

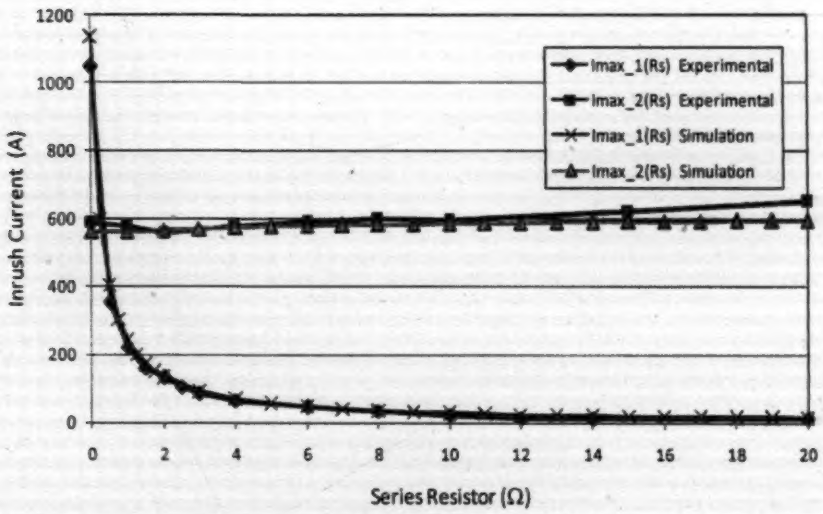

Figure 7.3 The performance of the pre-insertion scheme as applied to a 208/208, 30kVA, E-core, Δ/Yg transformer.

From Figure 7.3, it is clear that the scheme can successfully reduce the inrush current magnitude during the first switching stage. However the series pre-insertion resistor has no effect on reducing inrush current during switching of last phase C. This limits the overall achievable inrush reduction to about 50%. From Experimental and simulation results, it was found that due to the delta electrical interconnection between phase, the fluxes and current settle rapidly to steady state values in the transformer core. This finding makes the application of a simple point on wave closing for the final phase an attractive solution for completely eliminating inrush currents during energization.

7.2.3 Yg-Δ Connection (energizing from Yg side)

This transformer connection is the most popular interconnection arrangement for generation units, [91]. One of its major advantages is the reduction in insulation cost due to using phase voltage winding on the high voltage side coupled with insulation grading. The main disadvantage is that the arrangement will provide in-feed current to the utility side for an upstream ground fault [92].

For this transformer connection, the phases are sequentially energized one at a time with the series resistor connected to the first energized phase. The resistor could be bypassed either after complete phase energization or alternatively after switching of phase A. The $I_{max}(R_s)$ curves for this application are shown in Figure 7.4, below.

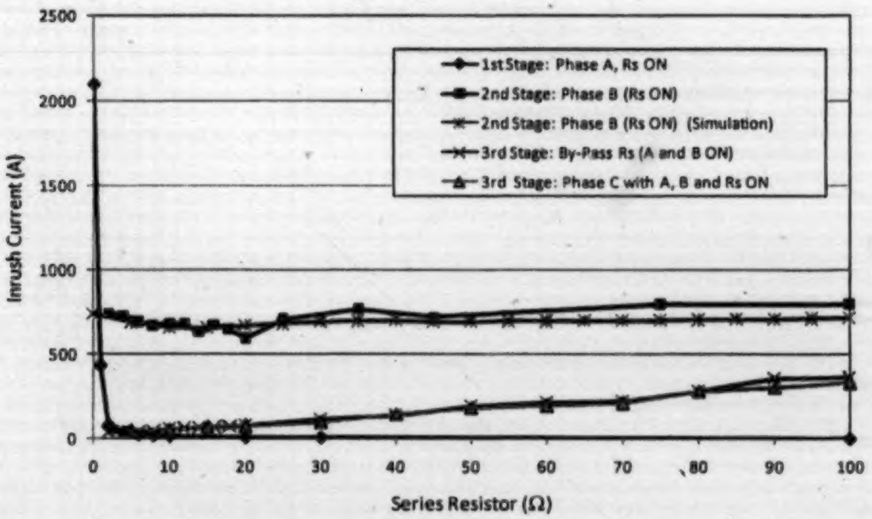

Figure 7.4 The performance of the pre-insertion scheme as applied to a 208/208, 30kVA, E-core, Yg/Δtransformer.

As shown in Figure 7.4, the scheme has a strong impact reducing the inrush current for phase A. For phase C, due to the presence of the delta winding and/or the 3 legged core, the flux is closely synchronized with the third phase voltage when the third phase is energized, [46] and [47]. This is true when the series resistor is shunted out before switching phase C, shunting the resistor after complete energization will result in a slight imbalance, linearly proportional to the resistor magnitude. The limiting factor here is the second phase switching, the series resistor in phase A has negligible impact on reducing the inrush current when phase B is energized. The scheme as shown in Figure 7.4 is capable of limiting the inrush magnitude to 700 Amps which represents an overall reduction of up to 70% in inrush current.

From the results presented so far, the scheme characteristics could be summarized as follows:

- The scheme can successfully reduce inrush level by 50% for Delta connections, 70% for Wye-Grounded Connections and 80% for Wye-ungrounded primaries respectively.
- The resistor could be sized based on its effect on the first switching stage. This is because the resistor effect during second switching stage is of much less impact on the resulting inrush current.
- When coupled with simple synchronous closing mechanism, only for the second stage, the scheme can completely eliminate inrush current during energization without the residual flux estimation or controlled de-energization.

7.3 Theoretical Analysis and Resistor Sizing

In this section the scheme performance will be analytically studied and investigated for the previously described connection arrangements. The presented analysis models each phase winding of the transformer by a two-sloped saturable inductance to model transformer saturation. The analysis is further extended to develop sizing criteria for the series resistor value.

7.3.1 Y-Δ Connection (energizing from Y side)

The scheme performance during the first switching stage could be analyzed through the equivalent circuit shown in Figure 7.5 below.

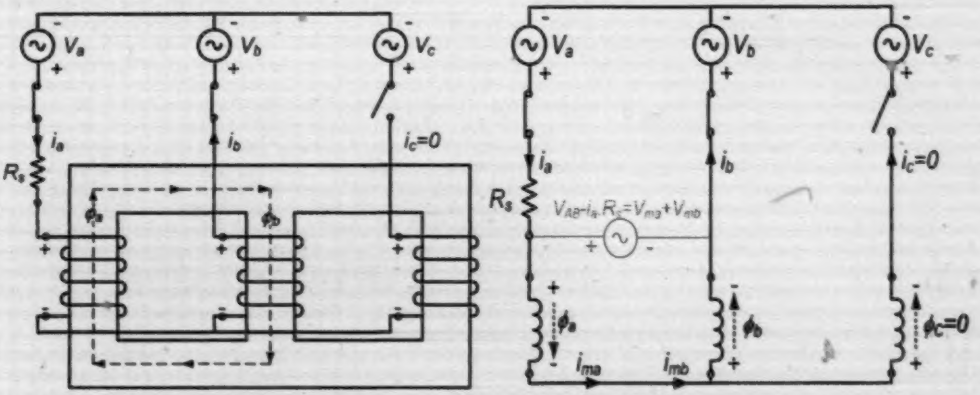

Figure 7.5 Equivalent circuit for the analysis of the pre-insertion resistor scheme during first stage switching. (Energizing from Y side).

The voltage applied across phases A and B is the line voltage; $V_{ab} = \sqrt{3} \cdot \hat{V}_{pk} \cdot sin(\omega t + \alpha)$. With a switching angle of; $(\alpha = 0)$, the maximum inrush current condition exists for a maximum residual flux in phase A of $+\phi_{r-max}$ *and* $-\phi_{r-max}$ in phase B. Both phases will start operating in unsaturated mode since; $\phi_{r-max} < \phi_{sat}$. Assuming that both phases will have approximately similar magnetizing characteristics, the applied terminal voltage will be distributed equally between phases before saturation. Before saturation is reached, the voltage drop across the series resistor is negligible due to the large apparent reactance of the core before saturation. For inrush current to flow through the series path A-B, both phases need to reach saturation. Since both phases (A and B) are electrically in series as shown in Fig. 3, the flux will build up in opposite polarities.

$$\lambda_a(t) = \lambda_{ao} + \int \frac{V_{ab}(t)}{2} dt \qquad \text{and} \qquad \lambda_b(t) = \lambda_{bo} - \int \frac{V_{ab}(t)}{2} dt \tag{7.1}$$

In order to find an expression for inrush current through the series A-B circuit shown in Figure 7.5, the saturation time needs to be evaluated first. From (1), the saturation time t_{sA} and t_{sB} can be evaluated as follows;

$$\lambda_s = \lambda_o + \int_{t=0}^{t=t_{sA}} \frac{V_{ab}(t)}{2} dt \tag{7.2}$$

$$\omega \cdot t_{sA}(\lambda_o) = \cos^{-1}\left(1 - \frac{2 \cdot (\lambda_s - \lambda_o)_{p.u.}}{\sqrt{3}}\right) \tag{7.3}$$

After saturation is reached in phases A and B at; $t_s = t_{sA} = t_{sB}$, the saturation curve for the combination can be modeled with an equivalent saturated reactance of $2l_p + 2L_s$, where l_p and L_{sat} are the primary winding leakage and saturated inductance respectively. Te excitation voltage across both phases in this case is the total line to line voltage, V_{ab}. Accordingly the inrush current waveform can be expressed similarly to the derived earlier for first-phase energization with Yg connection as follows;

$$i(t) = A_2 \cdot e^{-(t-t_s)/\tau_2} + B_2 \cdot sin(\omega \cdot t - \theta_s) \qquad t > t_s \tag{7.4}$$

Parameters A_2 and B_2, are magnitude of the DC and AC magnitudes of the inrush current waveform. The parameters could be evaluated similarly to those of single-phase energization with twice the single phase resistance and inductance and the line voltage. The maximum peak inrush current with the application of the series resistor can be given by;

$$I_{peak}(0) = A_2 \cdot e^{-(t_{pk}-t_s)/\tau_2} + B_2 \tag{7.5}$$

$$I_{peak}(R_s) \approx B_2(R_s) = \frac{V_m}{\sqrt{(2r_p + R_s)^2 + (2x_{sys} + 2x_p + 2x_{sat})^2}} \tag{7.6}$$

The series resistor that can achieve the maximum possible reduction can be sized to be close to the knee of the $I_{peak}(R_s)$ performance curve during first phase energization which represents a ratio of $I_{peak}(R_s)/I_{peak}(0)$ leading to about 90-95% reduction in inrush current. Similarly to the derivation carried out earlier for the neutral resistor sizing;

$$\alpha_Y(R_s) = I_{peak}(R_s)/I_{peak}(0) \tag{7.7}$$

$$I_{peak}(R_s) = B_2(R_s) \cdot [K_Y(R_s) \cdot e^{-t_{peak}/\tau_2} + 1] \tag{7.8}$$

The factor; $K(R_n)$, could be evaluated as follows;

$$K_Y(R_s) = sin(\theta_2 - \omega \cdot t_s) \tag{7.9}$$

For the maximum inrush current condition $(R_s = 0)$, the total energized phase X/R ratio including system impedance is high and accordingly, the damping of the exponential term in (6.68) during the first cycle can be neglected;

$$I_{peak}(R_s = 0) = \frac{V_m\sqrt{3}}{\sqrt{(2r)^2 + (2X_s)^2}} \cdot [K_Y(0) + 1] \tag{7.10}$$

Using typical saturation and residual flux magnitudes as been explained earlier;

$$1.2(p.u.) < |\lambda_s| < 1.35(p.u.) \qquad and \qquad 0.7(p.u.) < |\lambda_r| < 0.9(p.u.)$$

Accordingly, the saturation angle '$\omega \cdot t_s$' w.r.t. instant of switching and $K_Y(0)$ are within the following ranges respectively;

$$50^o < \omega \cdot t_s < 75^o \tag{7.11}$$

$$0.65 > K_Y(0) > 0.26 \tag{7.12}$$

From (7.11) and (7.12) it is clear both the saturation angle and the $K_Y(0)$ factor did not significantly change compared to the single phase factors derived earlier, (6.71) and (6.72). Although for this case, the line voltage is applied across both phases, and consequently the voltage imposed on each phase represents $\sqrt{3}/2$ of the phase voltage which equals 87% of the rated phase voltage. This slight reduction in the applied voltage across each phase resulted in increasing the saturation angle and decreasing the DC component factor as given by x and y respectively. Accordingly, (7.10) can be re-written as follows;

$$I_{peak}(R_s) \approx B_2(R_s) = \frac{V_m\sqrt{3}}{\sqrt{(2r + R_s)^2 + (2X_s)^2}} \tag{7.13}$$

Using (7.13) (7.12) and (7.10) to evaluate (7.7), the series resistor size which corresponds to a specific reduction ratio α can be given by;

$$R_s(\alpha_Y) = \frac{2}{\alpha_Y \cdot [K_Y(0) + 1]} \cdot \sqrt{r^2 + X_s^2} \tag{7.14}$$

Based on (7.14) and (7.12), inrush current reduction of 90% can be achieved within approximately twice the range evaluated earlier for neutral resistors as follows;

$$12.1 \cdot X_{series} \leq R_{sY\_Optimum} \leq 15.9 \cdot X_{series} \tag{7.15}$$

When phase C is energized to complete the transformer energization process. There is no initial flux in the core limb of phase C winding. Moreover, due to the absence of the neutral ground wire, phase currents at the neutral point should add up to zero. This means that Phase C will be in series with one of the phases alternatively for part of the cycle depending on the flux polarity. The coupling between phases in a 3-limb core or with a delta connected secondary makes one of the limbs serve as a return flux path for the other two limb fluxes. As a result, phase C winding will be in series with phase A winding 'and the series resistor' for a part of the power cycle. This explains the 50% reduction in inrush current of phase C as shown in Figure 7.2.

7.3.2 Δ-Y Connection (energizing from Delta side)

Figure 7.6 shows the magnetic flux paths and the electric equivalent circuit for the analysis of the first switching stage. For this connection, energizing phase A with the line voltage v_{AB} as shown in Figure 7.6, will impose the full rated voltage across the winding of phase A and half of this voltage across phase B and C. Phases B and C serve as the return path of the flux excited by the energized winding of phase A.

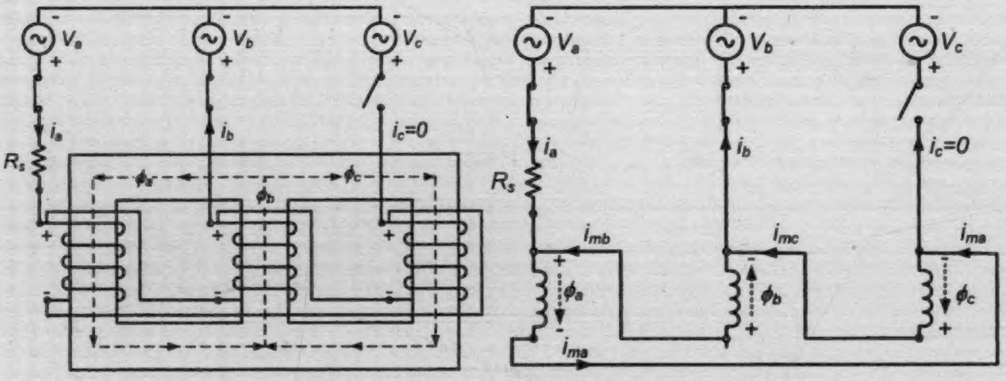

Figure 7.6 Equivalent circuit for the analysis of the pre-insertion resistor scheme during first stage switching. (Energizing from Δ side).

As shown in Figure 7.6, the windings of phases B and C are in series with the reverse of the voltage applied on phase A. As half of the rated voltage is applied on phase B and C, only the rated flux will be generated in each winding through the integral of the applied sinusoidal voltage during a full half cycle. The worst inrush current condition exists with the maximum residual flux present in phase A, $+\phi_{r\_max}$. Accordingly, phase B and C will have their total residual flux level of $\phi_{r\_B} + \phi_{r\_C} = -\phi_{r\_max}$ in order to keep the summation of residual flux in the three limbs equal to zero. Immediately after energization phase A, the flux equalizes rapidly in Phase B and C to half of that of phase A with an opposite polarity. This makes phase B and C much less likely to reach saturation during first stage switching and accordingly, the line currents in terminals A and B will be mainly composed of the contribution of the phase B current;

$$V_{ab} = R_s \cdot i_a + r_p \cdot i_{ma} + l_p \cdot di_{ma}/dt + N\, d\phi_a/dt \tag{7.16}$$

$$i_a = i_{ma} + i_{mc} \tag{7.17}$$

$$i_{mc} = i_{mb} \ll i_{ma} \tag{7.18}$$

$$V_{ab} \approx R_s \cdot i_{ma} + r_p \cdot i_{ma} + l_p \cdot di_{ma}/dt + N\, d\phi_a/dt \tag{7.19}$$

Based on (7.19), it could be concluded that the Resistor R_s acts in series with the energized phase A. The maximum inrush condition during first phase energization can accordingly be modeled similarly to the case of first phase switching with Yg connection. Since the energizing voltage across the energized phase A is the rated voltage 'phase-phase', and that the series resistor will act in series with the energized phase, the series pre-insertion resistor can be sized similarly to the neutral resistor case.

$$5.9 \cdot X_{series} \leq R_{s\Delta\_Optimum} \leq 7.4 \cdot X_{series} \tag{7.20}$$

The series resistor has a negligible impact on the magnitude of inrush current during third phase energization. However the maximum inrush magnitude tends to increase slightly as the series resistor is increased beyond the knee of the first-stage $I_{max}(R_s)$ curve.

7.3.3 Yg -Δ Connection (energizing from Yg side)

With the implementation of the resistor in series with the first energized phase, this application is essentially the same as that of first phase energization with a neutral resistor. The scheme will have the same $I_{max}(R_s)$ performance curve as that of $I_{max}(R_n)$ during first phase energization. However, for second phase energization, sequential energization insures that the condition for maximum inrush level exists with a zero initial flux. Compared to the neutral resistor application, this scheme arrangement will accordingly not benefit from the significant reduction in inrush current due to the zero sequence current flowing through the neutral resistor. Although there will be minimal impact on the inrush magnitude during second phase energization, the overall reduction due to the existence of a zero-initial flux, is significant and reaches to about 70%, Figure 7.4.

For third phase energization, the terminals will be in synchronism with small series resistor values. As the series resistor size increases, the inrush current level increases linearly with the resistor size. Accordingly shunting the series resistor immediately after the first phase is energized minimizes the energy dissipated through the resistor and ensures a synchronous energization state when the third phase is energized. Accordingly the sizing of the series resistor for this application could be based on its impact on first phase energization as follows;

$$5.9 \cdot X_{series} \leq R_{sYg\_Optimum} \leq 7.4 \cdot X_{series} \tag{7.21}$$

7.4 Considerations on Ferroresonance

The problem of ferroresonance triggered by sequential switching originates from the interaction between the L-C circuit formed by the un-energized transformer phase(s) inductance and the capacitance of the connecting cable, structre, winding self-capacitance...etc. For a ferroresonance condition to occur, the un-energized phase needs to have 'voltage induced' on it to trigger the ferroresonance condition. The open-phase condition could be developed through 'blown fuse(s)' or an open conductor feeding the 'cable-transformer' arrangement as well as sequential switching.

From the above basic conditions, it can be concluded that Yg-Y or Yg-Yg transformer with 3 single phase units are not affected by ferroresonance. Moreover, the problem could be eliminated from the source by limiting the value of capacitance connected to the un-energized phase(s). This can be achieved through placing the energizing Circuit Breaker as close as possible to the transformer. This solution reduces the cable length and accordingly reduces the amount of capacitance connected at the un-energized terminals of the transformer during sequential energization. Transformers with higher no-load losses are much less prone to ferroresonance [62] and [93]-[96]. Basically, the core loss resistance R_C acts in parallel with the cable capacitance which provides damping especially when the magnetizing reactance is high during un-saturated operation. Older transformers which have higher no load losses were less prone to ferroresonance compared with higher efficiency transformers available today [93]-[95].

From the above, it can be concluded that very little damping could greatly reduce chances of ferroresonance occurrence. Most references have recommended loading the transformer through light loads (1-10% of rating) prior to energization to eliminate ferroresonance problem, [62] and [93]. Some of the reported research work recommends the use of dummy loading resistors during energization if no other mitigation means are available, [62] and [96].

As for sequential switching with a single series-resistor, the problem could be analyzed separately for each winding connection. Starting with the un-grounded Wye connection, both phases A and B are energized simultaneously during the first stage and accordingly only phase C has the chance of developing a ferroresonance condition. However, for this case ferroresonance has much less chances of occurrence due to the fact that no voltage is induced across the un-energized phase C. In other words, the flux in the un-energized phase remains constant and close to the residual flux value. As shown in Figure 7.5, energizing the terminals of phases A and B with the series resistor in the circuit, forces the flux to circulate strictly through phase A and B with negligible flux flowing through phase C. Accordingly, the excitation voltage on phase C will be weak enough to develop a ferroresonance condition for this case. More importantly, the series resistor will act in series alternatively with phases B and C in parts of each cycle as explained earlier since for a Wye-ungrounded connection, the currents in all phases must add-up to zero. Moreover, with an adequately sized series resistor, rapid energization of phase C could follow after energizing phases A and B to eliminate any chance of ferroresonance development.

For transformers with delta primaries, the voltage developed is half of the nominal voltage at the terminal of the un-energized phase; C, immediately after energizing the first two terminals; A and B. In addition the terminal that doesn't have the resistor in series with it provides a low damped path for ferroresonance to be established, Figure 7.7. However, taking into account that the common phases at terminal C act as a return path for the flux developed in phase A, the voltage of terminal C will be to some extent tied to half of the nominal phase voltage. With the large number of experimental studies carried out n this connection, a ferroresonance condition was not observed.

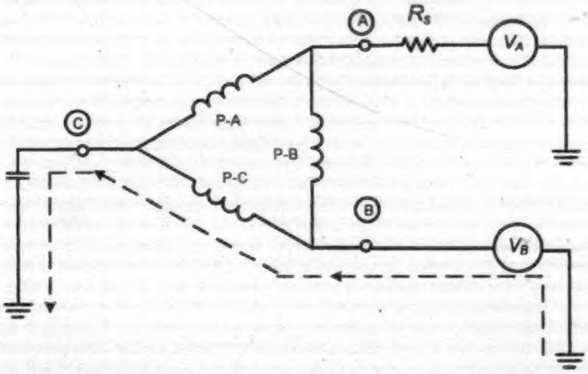

Figure 7.7 Development of ferroresonance in delta connected winding. (Energizing from Δ side).

The case was also studied through computer simulation with different capacitor sizes connected at the transformer terminals with scanning different energizing instants. A damped-fundamental ferroresonance condition was established finally with a relatively high capacitance of 100uF directly connected at the transformer primary, Figure 7.8. Again, rapid energization of phase C following phases A and B by 5 cycles will reduce significantly the chances of ferroresonance development.

The grounded-Wye connection is the one most prone to ferroresonance if coupled with sequential phase energization in absence of adequate damping. In contrary with the neutral-resistor based scheme, the series resistor doesn't act in series with the ferroresonant circuit in this case. In fact, during experimental evaluation of the $I_{max}(R_s)$ performance curves of during second phase energization, a chaotic behaviour has been observed, Figure 7.9. The resulting maximum current was never the same for each set of experiments up to a resistor size of 50Ω which is a clear sign of ferroresonance development. This is the only case where ferroresonance has been observed during the experimental evaluation of the sequential energizing scheme on the 30kVA laboratory transformer.

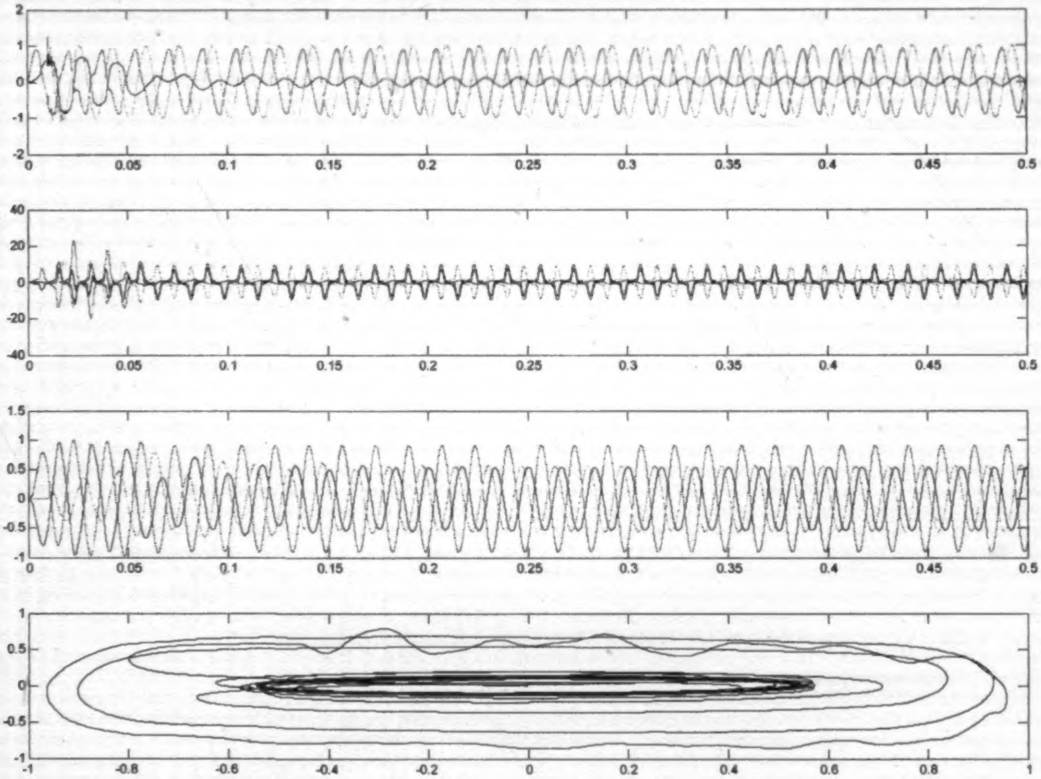

Figure 7.8 Damped fundamental Ferroresonance condition during sequential energization and a series resistor of 4.0 (Ω). From top to bottom; terminal voltage, inrush current, core flux and the V-ϕ loops.

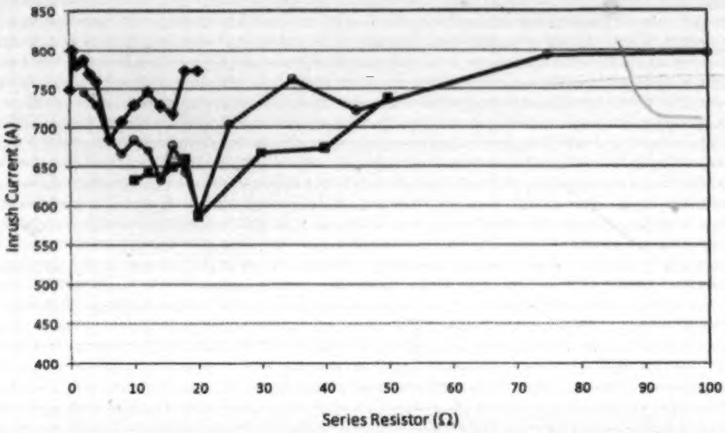

Figure 7.9 Experimental $I_{max}(R_s)$ performance curve trials during second phase energization with a single series resistor. (Energizing from Yg side).

Figure 7.10, shows the development of sub-harmonic ferroresonance condition during sequential energization through simulation with a shunt capacitance of 100uF and a 4Ω series resistor. Table 7.1 summarizes the performance, effectiveness and limitations of the single series-resistor based sequential energizing scheme.

Table 7.1 Summary of the single-series resistor scheme performance.

Switching Stage	Maximum Inrush Current Reduction Corresponding to Switching Stage		
	Energizing from Y side		Energizing from Δ side
	Y/Δ	Yg/Δ	
Phase A	100%	+90%	100%
Phase B	+90%	70%	+90%
By-Pass Rs	N/A	N/A	N/A
Phase C	80%	+90%	55%
By-Pass Rs (after phase C)	+95%	+90%	N/A
Overall Reduction	80% (due to Phase C)	70% (due to Phase B)	55% (due to Phase C)
Ferroressonance Occurrence	Low No dynamic Flux in the un-energized phase C after energizing terminals A and B	High Only after switching phase B, ferroresonance circuit could be excited through the phase without the resistor (phase B)	Moderate

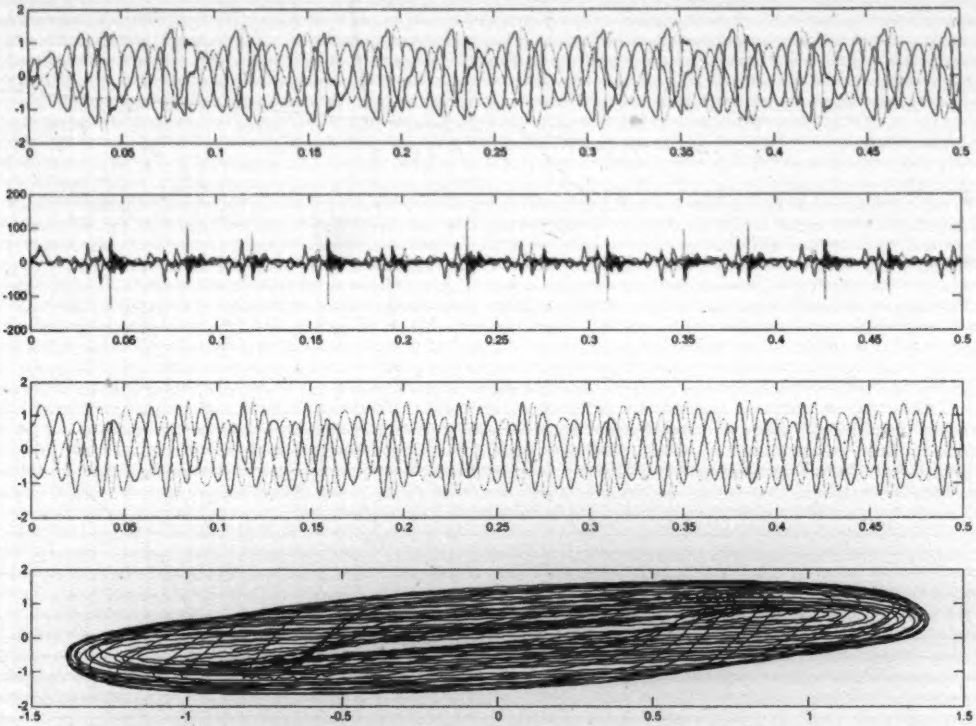

Figure 7.10 Sub-harmonic ferroresonance condition during sequential energization and a series resistor of 4.0 (Ω). From top to bottom; terminal voltage, in-rush current, core flux and the V-ϕ loops.

7.5 Conclusions

This chapter presented the application of a single series-resistor scheme as an inrush-current-mitigation technique. By using the presented experimental, simulation and analytical studies, it was shown that the scheme is most applicable to transformers with un-grounded primaries. The presented scheme provides an effective solution to the problem of high inrush current magnitudes and, accordingly, provides a simple solution for independent power producers wishing to meet or exceed the requirements of the allowable maximum voltage sag level the point of common coupling.

The scheme was shown to be capable of achieving an 80% and 55% reduction in inrush current magnitude for transformers energized from ungrounded-Wye and Delta-connected primaries, respectively. For transformers energized from Wye-grounded primaries, the scheme is capable of reducing the inrush magnitude by 70% by using a single series resistor. For ungrounded primaries, a rapid energizing strategy of 5 cycles can be applied, which reduces the chances of developing the ferroresonance condition without compromising the scheme's efficiency. The analytical sizing procedures carried out towards the sizing of the series resistor showed that a relatively small resistor size of 16 to 10 times the total series reactance in the energizing circuit was capable of achieving or exceeding the scheme's required performance.

However, for transformers with grounded primaries, a rapid closing strategy could not be implemented with a small resistor size. Alternatively, the scheme could be applied for this connection with a simple point-on-wave closing after energizing the first phase with a small series resistor.

8. Application for Capacitor Switching Transients Mitigation

This chapter presents the application of the sequential switching scheme for the mitigation of capacitor-switching transients. The scheme utilizes neutral grounding impedance connected at the neutral point of the switched capacitor bank together with sequential pole switching. The neutral impedance is sized to minimize the open circuit contact voltage of the capacitor breaker phases. A theoretical analysis of the proposed scheme was carried out together with computer simulation. In addition, a neutral-impedance-sizing criterion is presented in order to achieve the minimal transient over-voltage caused by capacitor switching. The proposed application was found capable of reducing the transient over-voltage at the utility's switched capacitor location to 1.07 p.u. and to 1.12 p.u. at the customer load bus.[4]

8.1 Introduction

The increased awareness of power-quality problems due to the application of modern and sensitive load equipment has motivated both utilities and customers to find more efficient methods for controlling and limiting power systems' switching transients [97]-[101]. Due to the frequency of capacitor-switching incidents and the high switching over-voltages involved, capacitor-switching transients are of special concern. High-frequency and high-magnitude transients produce excessive electrical and mechanical stresses. Moreover, transient over voltages due to utility capacitor switching typically reaching 1.8 [p.u.] might be magnified at the customer load bus to magnitudes of up to 2.6 p.u., [98] and [101]. Voltage magnification due to capacitor switching occurs when the transients oscillating frequency is close to the natural frequency of the L-C circuit at the load bus formed by the system impedance and the power factor correction capacitors. Short duration over voltages that do not damage equipment may still cause sensitive loads such as variable speed drives, VSD, protective devices to unexpectedly disrupt a critical load from the system.

---

[4] A version of this chapter has been published: S.G. Abdulsalam and Wilsun Xu "A Sequential Phase Energization Technique for Capacitor Switching Transient Reduction", *IET Proceedings – Generation, Transmission and Distribution*, vol. 1, No. 4, p.p. 596-602, July 2007.

To-date, various methods of controlling capacitor energization transients have been implemented by the industry, [97]-[100]. These methods include the use of pre-insertion resistors and inductors and synchronous closing. Each has different advantages and disadvantages in term of cost, reliability, and effectiveness [97] and [98].

As will be shown in this chapter, the neutral resistor-based scheme is not effective as a transient over voltages mitigation technique when applied to capacitor switching applications. A modified technique is being introduced using two different neutral grounding arrangements. The first arrangement implements a single-stage *R-L* neutral impedance and the second utilizes a dual stage *R-L* impedance. The performance and characteristics of the proposed application have been investigated using theoretical analysis and computer simulations. The theoretical analysis leads to the establishment of a design guide for the optimum neutral impedance. Simulation studies have shown that the scheme can successfully reduce the transient over voltages at the switched capacitor location to 1.27 and 1.07 p.u. using arrangements 1 and 2 respectively. This chapter will present the proposed idea and the scheme performance characteristics.

8.2 Scheme Arrangement and Theoretical Analysis

The presented transient mitigation scheme is shown in Figure 8.1, which utilizes optimally-sized neutral (or grounding) impedance together with sequential phase energization. The capacitors are energized one phase at a time in the sequence of *ACB*. The delay between two energization events is a simple 'mechanical' delay of 4 to 15 cycles and there is no need to precisely time the instant of closing. A general rule is that a switching act can proceed as long as the transients associated with the previous switching act have almost died out. The entire switching procedure lasts less than 30 cycles. After complete energization of the capacitor phases, the neutral voltage is close to zero and the neutral impedance can be shunted through an optional bypass switch.

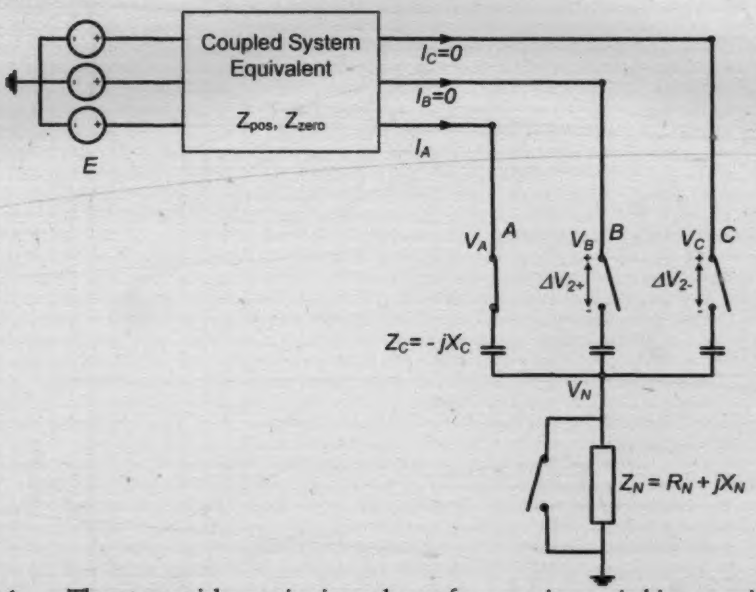

Figure 8.1 The sequential energization scheme for capacitor switching transients mitigation.

The principle of the proposed scheme is the following: Before a switch is closed, there is a steady-state fundamental frequency voltage across the switch (which is called switch open circuit voltage here). If the magnitude of this sinusoidal voltage is zero, closing the switch will not result in any switching transients regardless of the instant of switching. If we can reduce this voltage, the corresponding transients will also be reduced. In fact, it can be proven that, for a linear circuit, the magnitudes of switching transients (voltage or current) are in proportion to the magnitude of the open circuit voltage. The goal of the proposed scheme is therefore to minimize the open circuit voltages through an optimally-sized neutral impedance.

Performance of the scheme during first phase energization is similar to that of the pre-insertion scheme. The neutral impedance serves as a series impedance and it will effectively dampen the switching transients, [97]-[98]. For the energization of the second and third phases, the open circuit voltages across the switch contacts will be determined and then minimized with the help of the neutral impedance. Referring to Figure 8.1, the open circuit voltage corresponding to the second phase closing is shown as ΔV_{2+} and $\Delta V_{2-}$for positive ABC and negative sequence ACB, respectively. Representing the equivalent system by its short circuit positive and zero sequence equivalent reactance's, the terminal voltages at the capacitor location after switching the first phase can be calculated as follows;

$$\begin{bmatrix} V_A \\ V_B \\ V_C \end{bmatrix} = \begin{bmatrix} E_A \\ E_B \\ E_C \end{bmatrix} - \begin{bmatrix} jX_s & jX_m & jX_m \\ jX_m & jX_s & jX_m \\ jX_{\text{[illegible]}} & jX_m & jX_s \end{bmatrix} \cdot \begin{bmatrix} I_A \\ I_B = 0 \\ I_C = 0 \end{bmatrix} \tag{8.1}$$

$$I_A = I_N = \frac{E_A}{Z_s + Z_N + Z_c} \tag{8.2}$$

The self and mutual reactance's for the equivalent system are represented as function of the positive and zero sequence short circuit reactance's, X_{pos} and X_{zero} respectively;

$$X_s = \frac{X_{zero} + 2X_{pos}}{3} \qquad and \qquad X_m = \frac{X_{zero} - X_{pos}}{3} \tag{8.3}$$

For both switching sequences, the neutral voltage, V_{N1}, established after switching of the first phase can be given by;

$$V_{N1} = E \cdot \frac{jZ_N}{jX_s - jX_c + Z_N} \tag{8.4}$$

The second phase open circuit voltage can accordingly be evaluated as follows;

$$\Delta V_2 = V_2 - V_{N1} \tag{8.5}$$

$$V_2 = E_2 - I_1 \cdot jX_m = E\left(\frac{E_2}{E_1} - \frac{jX_m}{jX_s - jX_c + Z_N}\right) \tag{8.6}$$

E_1 and E_2 are respectively the equivalent system source voltage phasors of the first and second switched phases. Based on (8.6) and depending on the switching sequence represented by the complex ratio E_2/E_1, the second phase switching open circuit voltage ΔV_2 can be given by;

$$\Delta V_{2\pm} = E \cdot \left(1\angle \mp 120^o - \frac{jX_m + Z_N}{jX_s - jX_c + Z_N}\right) \tag{8.7}$$

Equation (8.7) can be further evaluated as follows for positive sequence switching;

$$\Delta V_{2+} = E \cdot \left(1\angle - 120^o - \frac{R_N + jX_N + jX_m}{jX_s - jX_c + R_N + jX_N}\right) \tag{8.8}$$

$$\Delta V_{2+} = E \cdot \left(\left(\frac{-1}{2} - j\frac{\sqrt{3}}{2} \right) - \frac{R_N + j(X_N + X_m)}{R_N + j(X_N - X_{cs})} \right) \tag{8.9}$$

$$\Delta V_{2+} = E \cdot \left(\frac{\left(-3R_N + \sqrt{3}(X_N - X_{cs})\right) + j\left(X_{cs} - 2X_m + \sqrt{3}R_N - 3X_m\right)}{2R_N + j2(X_N - X_{cs})} \right) \tag{8.10}$$

With similar procedure for negative sequence switching, the magnitude of the open circuit voltage can be calculated accordingly as follows;

$$|\Delta V_{2+}| = E \cdot \sqrt{\frac{\left(-3R_N + \sqrt{3}(X_N - X_{cs})\right)^2 + \left(X_{cs} - 2X_m + \sqrt{3}R_N - 3X_m\right)^2}{4R_N^2 + 4(X_{cs} - X_N)^2}} \tag{8.11}$$

$$|\Delta V_{2-}| = E \cdot \sqrt{\frac{\left(-3R_N - \sqrt{3}(X_N - X_{cs})\right)^2 + \left(X_{cs} - 2X_m - \sqrt{3}R_N - 3X_m\right)^2}{4R_N^2 + 4(X_{cs} - X_N)^2}} \tag{8.12}$$

Accordingly, it becomes clear from (8.11) and (8.12) that negative switching sequence ACB results in a lower open circuit contact voltage as compared to positive switching sequence ABC for the same neutral impedance. Additionally, it could be easily verified from (8.11) and (8.12) that the impact of the mutual coupling reactance could be neglected since the capacitor bank reactance, X_c, is sufficiently higher than the mutual coupling reactance, X_m. The second phase open circuit voltage could be evaluated as follows;

$$|\Delta V_{2+}| = E \cdot \sqrt{\frac{\left(X_{cs} + 2\sqrt{3}R_N\right)^2 + 3(X_{cs} - 2X_N)^2}{4R_N^2 + 4(X_{cs} - X_N)^2}} \tag{8.13}$$

$$|\Delta V_{2-}| = E \cdot \sqrt{\frac{\left(X_{cs} - 2\sqrt{3}R_N\right)^2 + 3(X_{cs} - 2X_N)^2}{4R_N^2 + 4(X_{cs} - X_N)^2}} \tag{8.14}$$

The resulting open circuit voltage during second phase switching as a function of the neutral impedance magnitude $Z_N = \sqrt{R_N^2 + X_N^2}$ and phase angle $\phi_N = atan(X_N/R_N)$ is shown in Figure 8.2(a) and (b) for positive and negative switching sequences respectively.

Similarly to second phase switching, the open circuit voltage during the third phase switching ΔV_3 can be evaluated as follows;

$$V_{N2} = (E_1 + E_2) \cdot \frac{-Z_N}{(Z_c + Z_s + Z_m) + (Z_m + Z_N)} \tag{8.15}$$

$$\Delta V_3 = V_3 - V_{N2} \tag{8.16}$$

$$V_3 = E_3 - (E_1 + E_2) \cdot \frac{Z_m}{(Z_c + Z_s + Z_m) + (Z_m + Z_N)} \tag{8.17}$$

V_{N2} represents the neutral voltage phasor established after second phase switching. For a balanced system, the summation of all three source phase voltages equal zero $\left(\sum E_{1,2,3} = 0\right)$, accordingly, the open circuit voltage ΔV_3 can now be given as follows;

$$\Delta V_3 = E_3 \left[1 + \frac{(Z_m + Z_N)}{(Z_c + Z_s + Z_m) + (Z_m + Z_N)}\right] \tag{8.18}$$

$$\Delta V_3 = E_3 \left[\frac{3R_N - j(X_{cs} - 2X_m - 3X_N)}{2R_N - j(X_{cs} - X_m - 2X_N)}\right] \tag{8.19}$$

And neglecting the effect of the mutual reactance X_m as compared to the capacitor bank reactance X_c leads to the following expression;

$$|\Delta V_3| = E\sqrt{\frac{(3R_N)^2 + (X_{cs} - 3X_N)^2}{(2R_N)^2 + (X_{cs} - 2X_N)^2}} \tag{8.20}$$

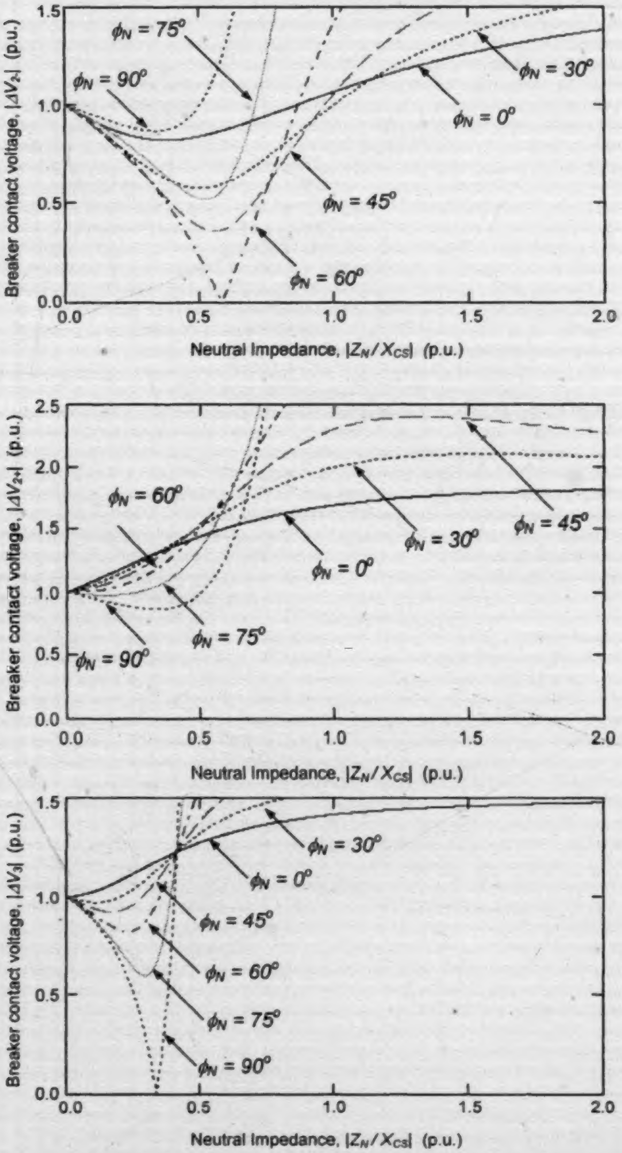

Figure 8.2 Open circuit voltage as affected by the neutral impedance for (top) second phase switching $|\Delta V_{2-}|$, (middle) second phase switching $|\Delta V_{2+}|$ and (bottom) Third phase switching $|\Delta V_3|$.

It becomes clear from (8.20) that the third phase switching open circuit voltage ΔV_3 is not dependent on the switching sequence. Additionally, the third phase open circuit voltage ΔV_3 can be effectively reduced through the neutral impedance inductive component X_N. Figure 8.2(c) illustrates the third phase open circuit voltage as affected by the neutral impedance magnitude and phase angle.

8.3 Neutral Impedance Sizing

The design criterion is to achieve minimal open circuit voltages for the 2nd and 3rd switching stages. Two different neutral impedance arrangements, one involves single stage *R-L* neutral impedance and the other utilizes dual stage *R-L* neutral impedance, are proposed to achieve this goal. The characteristics of the schemes and the corresponding equations to size the neutral impedance are presented in the following sections.

8.3.1 Single-stage R-L neutral impedance

For the presented application, a single-stage '*R-L*' neutral impedance is used to minimize 2nd and 3rd phase energization open circuit contact voltages. As can be shown from Figure 8.2, using a single neutral impedance value might result in different open circuit voltage levels before the 2nd and 3rd phases are energized. Accordingly, our objective is to minimize the highest contact voltage of either $|\Delta V_{2-}|$ or $|\Delta V_3|$ due to a specific neutral impedance value. Mathematically, the objective function to be minimized f_{Voc} can be expressed as follows;

$$f_{Voc}(R_N, X_N) = maximum(|\Delta V_{2-}(R_N, X_N)|, |\Delta V_3(R_N, X_N)|) \tag{8.21}$$

$$f_{Voc}(R_N, X_N) = \begin{cases} |\Delta V_{2-}(R_N, X_N)| & |\Delta V_{2-}| \geq |\Delta V_3| \\ |\Delta V_3(R_N, X_N)| & |\Delta V_3| > |\Delta V_{2-}| \end{cases} \tag{8.22}$$

The objective function f_{Voc} as defined by (8.21) is generally discontinuous and accordingly, the analytical evaluation of the minimum contact voltage becomes a complex problem. However, transferring open circuit contact voltage expressions (8.14) and (8.20), into per-unit values of the equivalent reactance X_{cs}, (8.23) and (8.24), will simplify the problem and a numerical solution could be obtained.

$$|\Delta V_{2-}| = E \cdot \sqrt{\frac{\left(1 - 2\sqrt{3}R_N\right)^2 + 3(1 - 2X_N)^2}{4R_N^2 + 4(1 - X_N)^2}} \tag{8.23}$$

$$|\Delta V_3| = E\sqrt{\frac{(3R_N)^2 + (1 - 3X_N)^2}{(2R_N)^2 + (1 - 2X_N)^2}} \tag{8.24}$$

Minimizing (8.22), using (8.23) and (8.24) leads to a minimum open circuit voltage and corresponding optimum R_N and X_N values as follows;

$$f_{Voc\_Min} = 0.678\ (p.u.) \tag{8.25}$$

$$R_{N\_Optimum} = 0.089 \times X_{cs} \qquad and \qquad X_{N\_Optimum} = 0.322 \times X_{cs} \tag{8.26}$$

Figure 8.3, shows the open circuit contact voltages $|\Delta V_{2-}|$, $|\Delta V_3|$ and the maximum contact voltage function f_{Voc} for the optimum neutral impedance angle, $\phi_{N\_Optimum} = 74.0^o$. The optimum neutral impedance angle is the angle resulting in the lowest open circuit voltage as defined by the function f_{Voc}.

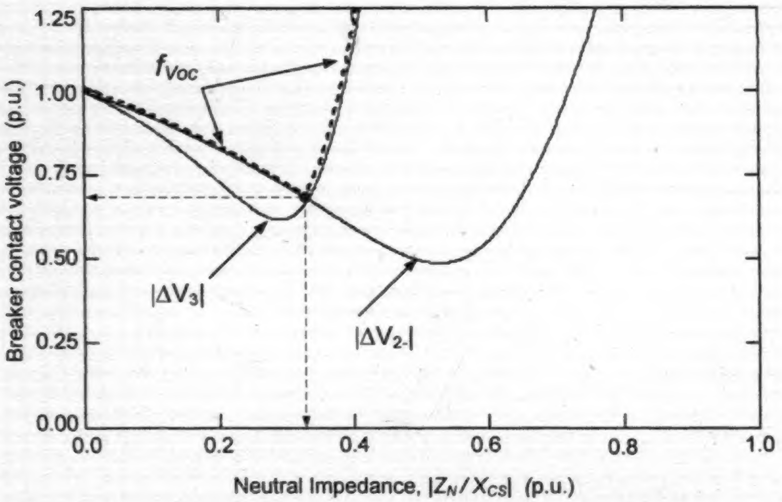

Figure 8.3 Open circuit voltages $|\Delta V_{2-}|$, $|\Delta V_3|$, and the objective function $f_{V_{oc}}$.

8.3.2 Dual-stage R-L neutral impedance

As has been shown in the previous section, the single-stage *R-L* neutral impedance was optimized to achieve the lowest open circuit voltage for both 2nd and 3rd switching stages. However, as can be seen from Figure 8.2, using two different neutral impedance values can lead to a zero switching open circuit contact voltage for both stages independently.

A closer look at the 2nd and 3rd switching contact voltages as given by (8.14) and (8.20) reveals that; *'theoretically'* zero open circuit voltage can be achieved if the numerator of both expressions is brought to zero. For the second switching stage as given by (8.14), both terms in the numerator should be brought to zero to achieve the condition $|\Delta V_{2-}| = zero$ as follows;

$$R_{N2} = \frac{X_{cs}}{2\sqrt{3}} \qquad and \qquad X_{N2} = \frac{X_{cs}}{3} \tag{8.27}$$

Similarly for the third switching stage;

$$R_{N3} = zero \qquad and \qquad X_{N3} = \frac{X_{cs}}{3} \tag{8.28}$$

These results strictly agree with the characteristic curves of the 2nd and 3rd switching stages shown in Figure 8.2. Per-unit neutral impedance of the 2nd and 3rd switching $\big(Z_{N2} =$ $13,\phi N2=60o$ and $ZN3=13,\phi N2=90o$ respectively will result in a zero switching voltage in both stages. Based on (8.27) and (7.21), the neutral impedance arrangement can be constructed as shown in Figure 8.4.

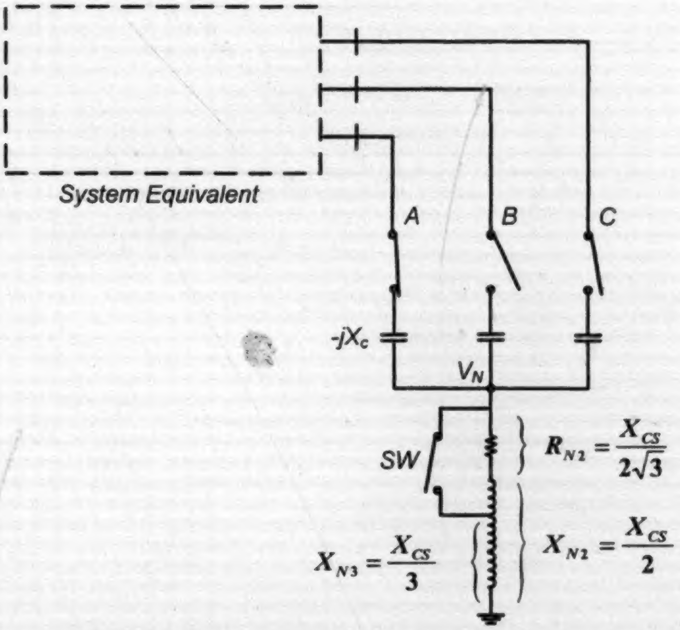
System Equivalent
A
B
C
$-jX_c$
V_N
SW
$R_{N2} = \frac{X_{cs}}{2\sqrt{3}}$
$X_{N3} = \frac{X_{cs}}{3}$
$X_{N2} = \frac{X_{cs}}{2}$

Figure 8.4 Scheme 2 for mitigating capacitor switching transients using dual stage neutral impedance.

The arrangement shown in Figure 8.4 consists of a single resistor and two inductors all of which are in series. The two inductors could be replaced by a single inductor with a tap dividing the inductance by a ratio of 1:2 and a total inductance of $X_{cs}/2$ as required by the second switching stage. The resistive element will be connected to the smaller ratio inductance with an additional switch to short the branch in preparation for third switching stage.

Although steady state analysis showed that an optimum third phase neutral impedance should –theoretically- be totally inductive, a resistive component needs to be added to the inductive element in order to account for the inductor resistance and provide adequate damping. It was found that the third phase impedance of the same magnitude and with an 85^0 angle has a much more favorable performance as compared to a pure inductor.

8.4 Scheme Performance and Transient Simulation Study

The effectiveness of the proposed transient mitigation technique was studied for the single and dual stage *R-L* neutral grounding arrangements through simulation. Both applications of the grounding technique were compared against each other and against instantaneous switching as well. In order to classify the severity of the resulting voltage transients due to each switching condition, an equivalent damped oscillatory waveform technique is implemented [102]. The transient disturbance is classified by the transient component amplitude V_d and the disturbance duration time, τ_d, which is the time required for the transient oscillatory component to reach half of its maximum amplitude. The IEEE 13-Bus Industrial test system, [103], Figure 8.5, was used to evaluate the effectiveness of the proposed mitigation technique through transient simulation study using PSCAD, EMTDC software package. All presented capacitor switching simulation cases were implemented at the 6 MVAR, 13.8kV utility capacitor bank located at Bus 3:MILL-1.

For each simulated switching scheme, the switching instant has been changed over a complete cycle at 0.2 ms intervals for each switching stage. The resulting phase voltage transients due to each switching condition were then analyzed and ranked using the transient classification procedure described earlier. One of the study objectives is to assess the effect of system damping on the capacitor switching transients. Although steady state analysis using a Thevenin equivalent at the capacitor location gives an accurate estimate of the established open circuit contact voltage during each switching stage, the actual transient performance will be strongly influenced by how the load is being represented, [101].

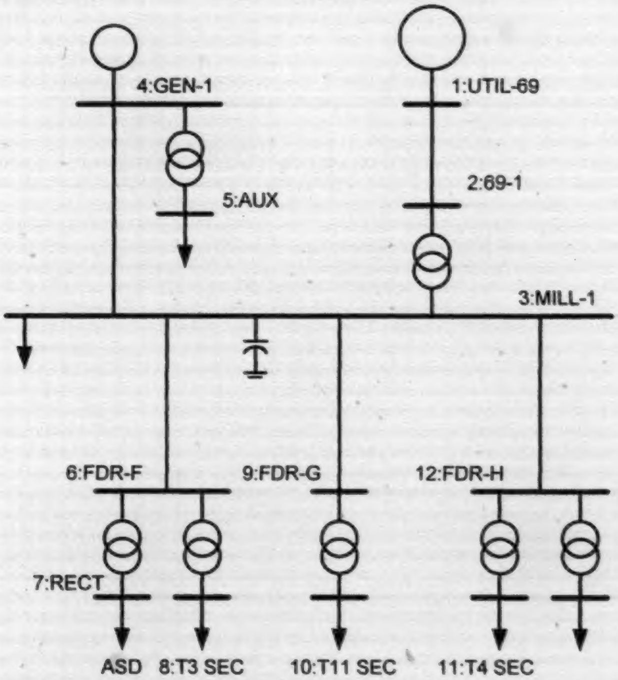
4:GEN-1
1:UTIL-69
5:AUX
2:69-1
3:MILL-1
6:FDR-F
9:FDR-G
12:FDR-H
7:RECT
ASD
8:T3 SEC
10:T11 SEC
11:T4 SEC

Figure 8.5 IEEE 13-Bus industrial test system.

8.4.1 Instantaneous Switching with solid ground:

For this case, instantaneous switching of the capacitor bank phases will take place. The worst case switching condition is shown in Figure 8.6(a). The phase voltages collapse to 0 p.u. suddenly after energization followed by a high-frequency transient recovery voltage oscillating at the natural frequency of the system-capacitor bank arrangement, $f_s = 1/2\pi\sqrt{L_s C}$ which equals 453 Hz.

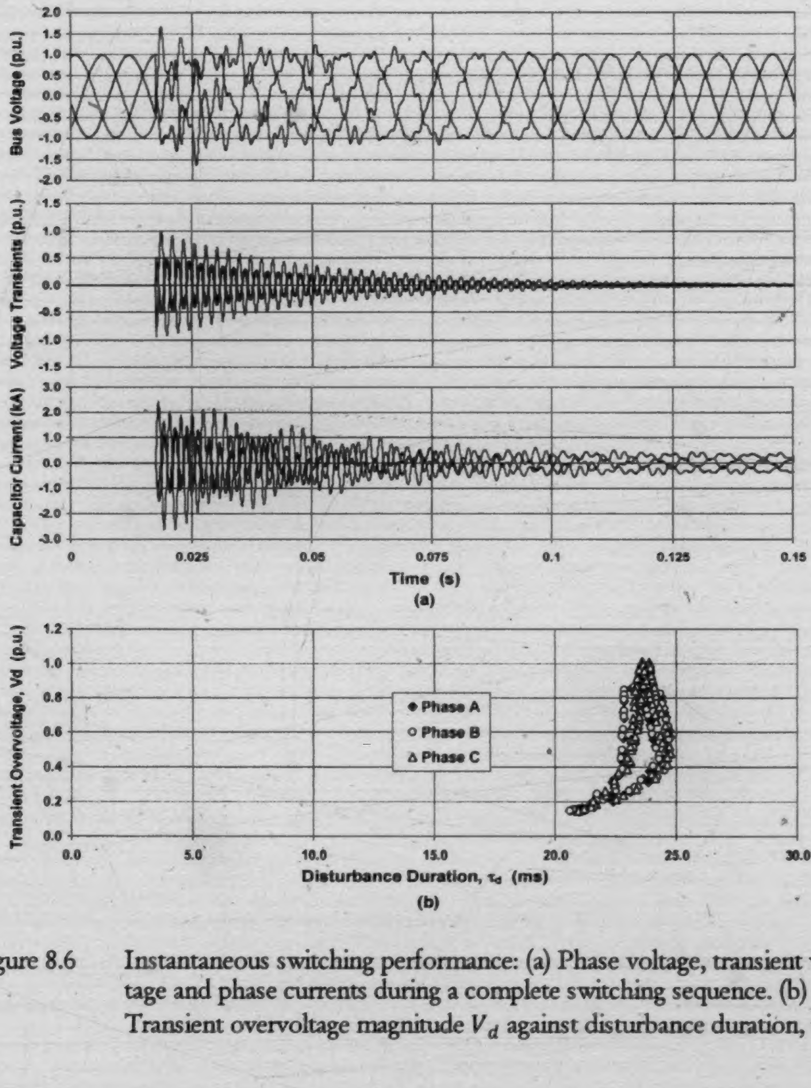

Figure 8.6 Instantaneous switching performance: (a) Phase voltage, transient voltage and phase currents during a complete switching sequence. (b) Transient overvoltage magnitude V_d against disturbance duration, τ_d.

The voltage of phase A reaches a peak of 1.91 p.u. which might be magnified at remote capacitor locations. Figure 8.6(b) shows a quantitative summary of the disturbance transient over voltage peak V_d against the equivalent disturbance duration τ_a due to changing the instant of switching in steps of 0.2 ms for a complete cycle. It is clear that the disturbance duration is almost constant at around 23.0 ms and that lower magnitude transients have a lower disturbance duration. For the capacitor energizing inrush current, the maximum inrush current peak reaches a magnitude of up to 2.7 kA but not less than 2.4 kA during instantaneous switching condition regardless of the switching instant.

8.4.2 Sequential switching with single-stage neutral impedance:

Here, the single stage R-L neutral impedance arrangement sequential switching is applied. The three phases are switched one after another using a negative sequence order ACB with a delay of approximately 4 cycles as compared to the typical 7-12 cycles delay required for pre-insertion arrangements [98]. Figure 8.7(a) presents the worst switching condition in which, the switching instants of phases A, C and B are selected to lead to the highest over voltage magnitude in each stage.

As can be seen from Figure 8.7(a), the maximum over voltage transient occurring from this arrangement is about 1.27 p.u. of the nominal operating voltage due to the switching of the last phase, B. The switching of the first phase 'A' leads to minimal transients as it represents an over-damped switching condition since the neutral impedance is in series with the switched phase.

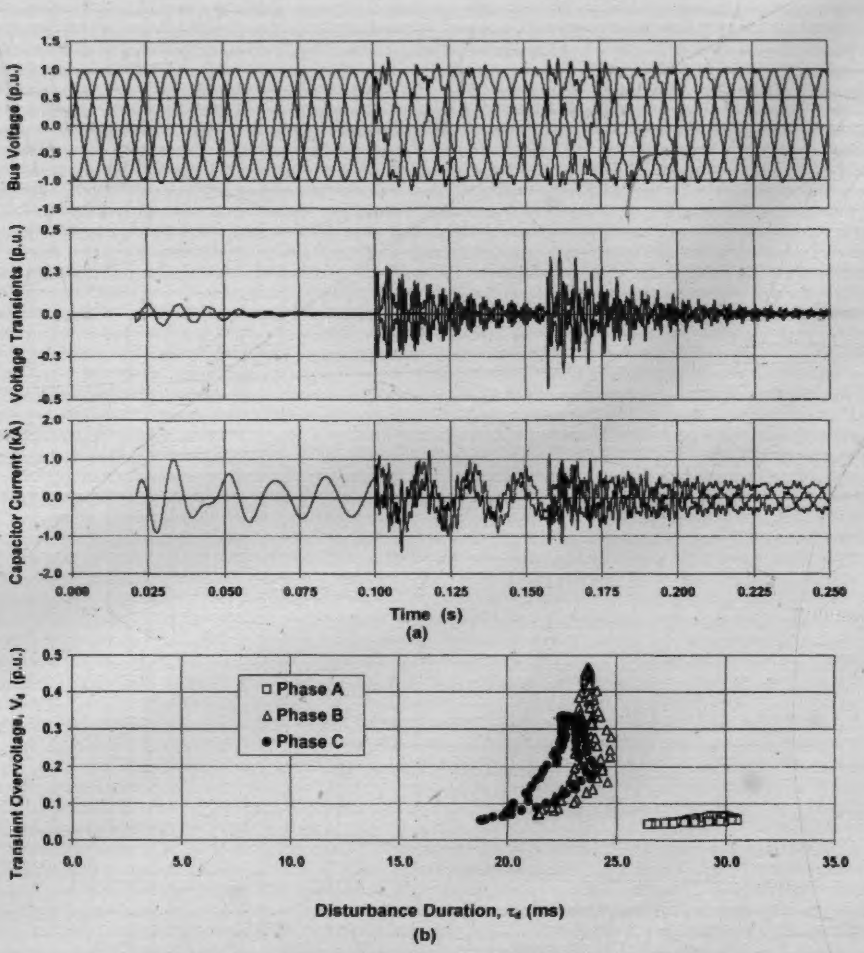

Figure 8.7 Single-stage neutral impedance mitigation technique: (a) Phase voltage, transient voltage and phase currents during a complete switching sequence. (b) Transient overvoltage magnitude V_d against disturbance duration, τ_d.

Additionally, it can be noted that the phase voltage did not instantaneously collapse to zero immediately after switching. This is due to the presence of the neutral impedance which allows the neutral point voltage to rise instantaneously to nearly the phase voltage magnitude at instant of switching. Figure 8.7(b) shows that the single-stage neutral impedance arrangement limits the disturbance transient magnitude to about 0.46 p.u.. Additionally, the disturbance duration stays almost the same at 25 ms as compared to simultaneous switching conditions.

The maximum phase voltage at the capacitor location reached 1.4 p.u. which corresponds to a 60% reduction. The maximum inrush current is lowered from 2.7 kA to 1.4 kA which corresponds to about 50% reduction.

8.4.3 Sequential switching with dual-stage neutral impedance:

In this case, the three phases are switched sequentially with the dual stage R-L neutral impedance. The performance of the scheme during a complete switching sequence is shown in Figure 8.8(a). Only the switching of the last phase 'B' voltage waveform is shown since as can be seen from the transient voltage response, the transients due to the switching of phases A and C and the closure of the shunting switch will lead to minimal switching transient 'below 0.035 p.u.' that won't appear in the voltage waveform of those phases.

The maximum disturbance over voltage is shown in Figure 8.8(b) for switching stages of Phases A, B and C and the closure of the neutral impedance shunting switch. For Phase C and the closure of the shunting switch, the transient over voltage is very small and lower than 0.02 p.u.. It is clear from Figure 8.8(b) that the dual stage R-L arrangement leads to the lowest over voltage transient level with a maximum of 0.19 p.u. and maximum disturbance duration of 26.0 ms.

It should be noted that although, the disturbance duration due to switching phase C and the closure of the switch is relatively high, the extremely low over voltage magnitude and energy content makes these transient of insignificant value and can be totally neglected. This arrangement leads to the lowest possible inrush current level in the switched capacitor bank. A reduction to about 1.9 kA is achievable which represents an 80% reduction.

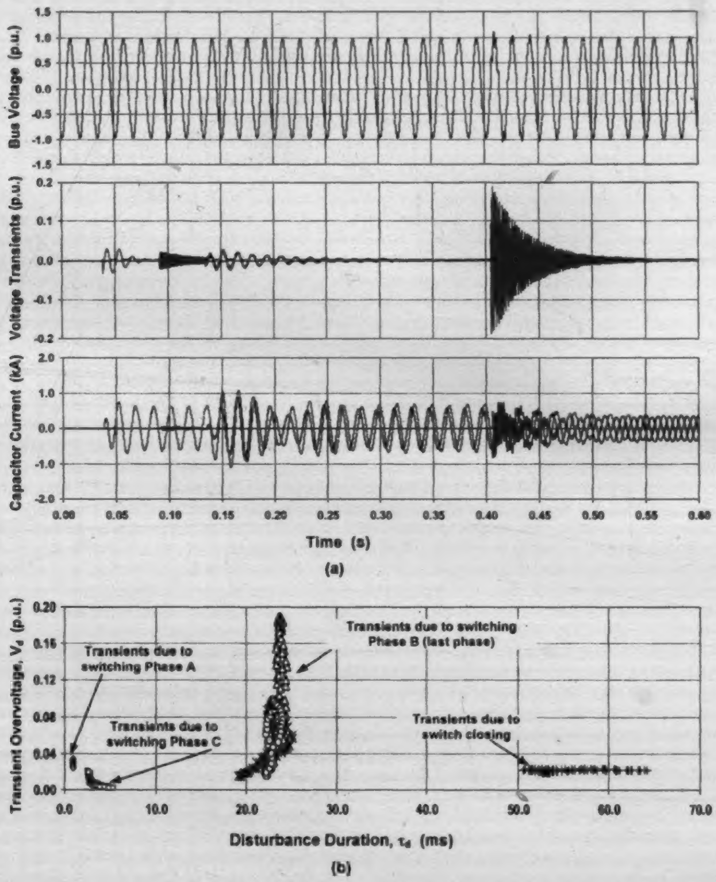

Figure 8.8 Dual-stage neutral impedance mitigation technique: (a) Phase voltage, transient voltage and phase currents during a complete switching sequence. (b) Transient overvoltage magnitude V_d against disturbance duration, τ_d.

8.5 Impact on Voltage Magnification

Transient overvoltages due to utility capacitor switching can get magnified at remote customer load bus in presence of power factor correction capacitors. The phenomenon has been documented in [97]-[101]. In the case of customer facilities having sensitive loads especially VSDs, nuisance tripping can occur due to the low overvoltage protection setting of these drives which is typically in the range of 1.2 to 1.3 p.u. of the rated voltage, [98]. The effectiveness of the proposed transient mitigation technique in presence of voltage magnification was studied through applying a 1 MVAR power factor correction, PFC, capacitor at the local load bus 13 which raises the p.f. at the bus to 0.9. Figure 8.9, shows the voltage at the switched utility capacitor bus and the load bus due to voltage magnification for instantaneous, single-stage and dual stage neutral impedance arrangements.

As can be shown from Figure 8.9(a), the Power Factor Correction (PFC) capacitors magnified the transient over voltage at the load bus to 2.2 p.u.. Without PFC capacitors, the voltage at the load bus will be equal to or less than the transient level at the switched utility capacitor. The application of the proposed mitigation technique using a single-stage R-L neutral impedance reduces the magnified voltage at the customer bus to 1.6 p.u. during the third switching stage which represents the highest transient level, Figure 8.9(b). Using dual stage neutral impedance, the magnified transients reaches a maximum of 1.12 p.u. at the load bus, Figure 8.9(c). Due to the dominance of induction motor loads at industrial load buses, all the results presented so far were evaluated modeling the load at all distribution level by lumped R-L series equivalent impedance. This resulted in obtaining the highest possible transient level due to the limited damping provided.

The response of Variable Speed Drives (VSDs) at remote busses where voltage magnification occurs will vary depending on their over voltage trip setting and the type and/or rating of the choke coil used. Limiting the transient over voltage at the remote bus to 1.2 p.u. will most probably prevent overvoltage tripping of VSDs. With higher over voltage magnitudes, the drive tripping will depend on the type and rating of the AC or DC choke coil rating used.

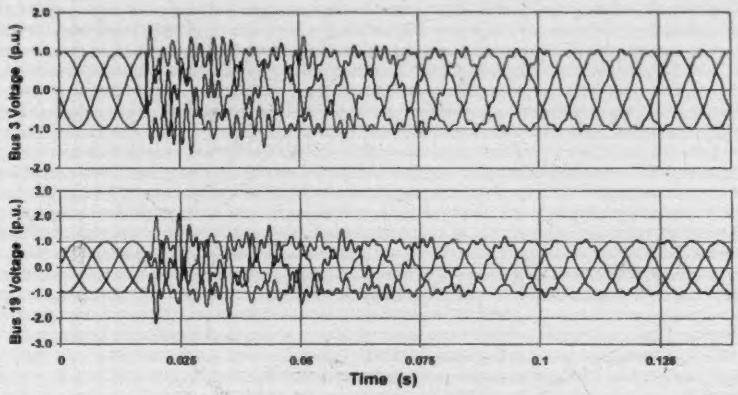

(a) Instantaneous Switching

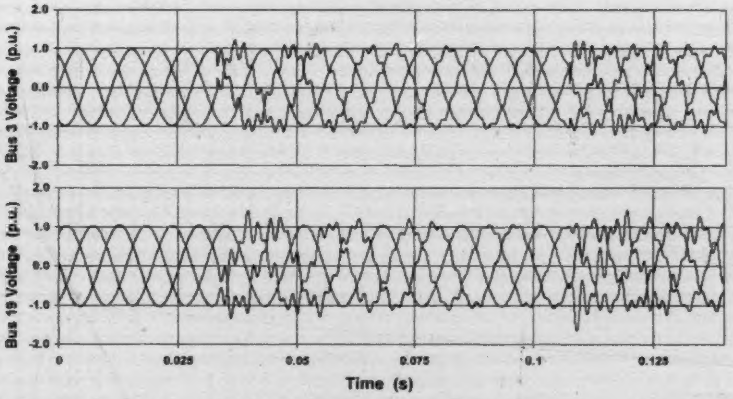

(b) Single Stage R-L Neutral Impedance

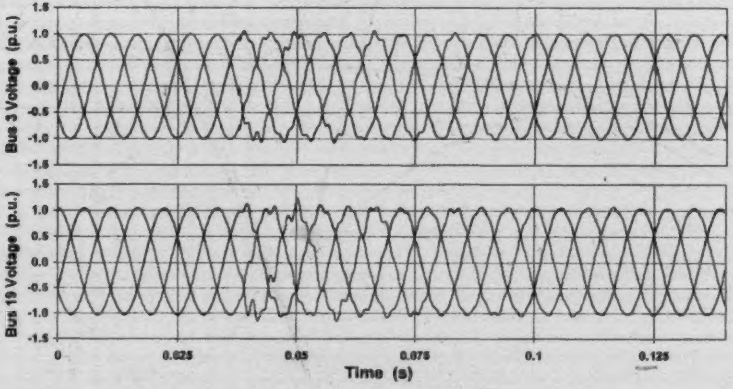

(c) Dual Stage Neutral Impedance

Figure 8.9 Voltage at the utility capacitor bus (top) and magnified voltage at customer bus 13 (bottom).

In the case loads were modeled using parallel R-L branches representing the load real and reactive power respectively, system damping will considerably increase resulting in less conservative results. Tables 8.1 and 8.2 summarize the performance of the three studied cases for the series and parallel load representations respectively.

TABLE 8.1: SUMMARY OF THE STUDIED SWITCHING SCHEMES WITH SERIES IMPEDANCE LOAD REPRESENTATION.

Switching Scheme	V_{ph} p.u.	V_d p.u.	Inrush kA	τ_d ms
Instantaneous	1.910	1.000	2.71	23
Single-Stage RL	1.402	0.470	1.45	31
Dual-Stage R-L	1.146	0.191	1.14	26

TABLE 8.2: SUMMARY OF THE STUDIED SWITCHING SCHEMES WITH PARALLEL IMPEDANCE LOAD REPRESENTATION.

Switching Scheme	V_{ph} p.u.	V_d p.u.	Inrush kA	τ_d ms
Instantaneous	1.675	0.943	2.19	4.0
Single-Stage RL	1.254	0.335	1.15	5.1
Dual-Stage R-L	1.064	0.170	0.83	6.3

As can be shown from Tables 8.1 and 8.2, the representation of the load will influence the evaluation of the transient over voltages generated due to capacitor switching by 24% to 8%. The representation of loads by their series equivalent impedance results in more conservative results which is more favourable. In terms of disturbance duration, the representation of the load will have more influence on the results.

8.6 Conclusions

This chapter presented the application of the sequential energization technique for mitigating the transient over-voltages occurring due to capacitor switching. The scheme's effectiveness is based on the reduction of the open circuit contact voltage during the sequential switching procedure. The main conclusions can be summarized as follows;

It was shown that the single-stage R-L neutral impedance arrangement leads to an optimized open circuit voltage of 0.677 p.u., which reduces the switching transient over-voltage level to as low as 1.27 p.u.. The dual stage R-L neutral impedance arrangement represents a self-synchronized switching mechanism where the open circuit voltages during the second and third switching stages can be brought to zero independently of the switching instant. It was also shown that this arrangement can reduce the local transient over-voltages at the switched capacitor's location to 1.07 p.u.. The scheme's performance in the presence of voltage magnification was also studied, showing that both neutral impedance arrangements can reduce the amount of voltage magnification at remote busses to 1.3 p.u., or low enough to help reduce the chances of the nuisance tripping of VSDs.

The proposed scheme's main limitation results from the requirement for a separate pole closure mechanism. Although this requirement is the same as for synchronous controlled-switching schemes, the simple delay requirement for the presented scheme makes it easier to implement in already installed gang-operated breaker mechanisms. It is also obvious that the scheme can be implemented only in capacitor installations with a Wye connection. In most cases, utility capacitors are usually Wye connected which makes the proposed scheme an effective transient over voltage mitigation technique for this application.

9.Conclusions and Recommendations

Power transformers are critical components in power systems. Transformer inrush transients have diverse effects on a transformer's lifetime and power quality and might negatively affect the protection equipment, leading to the reduced reliability of the power system's operation. The current trends in the electric power industry have reignited interest in finding new and effective means to control and limit inrush current due to transformer energization. The main focus of this thesis was on the investigation and the development of a sequential energization technique aided with a single neutral or series resistor for inrush-current mitigation.

The accurate and adequate representation of a transformer's non-linear characteristics plays an essential role in the modeling of transformers under inrush and highly nonlinear conditions. A new application of the Newton-Raphson iterative method for solving a three-phase non-linear transformer model was developed for the stable and accurate simulation of transformer behavior during inrush-current conditions. The introduction of the non-linear reluctances as a function of the system variables led to a stable, accurate and time-efficient simulation technique. Additionally, it was verified that either polynomial curve-fitting techniques or piecewise segments could be used to represent the transformer's nonlinear reluctance curves. The simulation technique's stability was proven throughout various simulations including simultaneous and sequential closing and energizing from the delta winding side. More importantly, the developed model could successfully handle transformers with either linear or non-linear neutral branches.

One of the biggest challenges in transformer modeling is the precise presentation of transformer nonlinear characteristics. A novel technique was developed for estimating transformer-saturation characteristics from measured terminal voltages and currents during transformer energization. The developed technique does not require special test equipment and/or modification of the transformer connection at the transformer's location, which are difficult to implement. A practical method for the estimation of nonlinear core reluctances of three-phase three-limb power transformers from inrush waveform data has been developed and was presented. The method could also be implemented to estimate the classical flux-current saturation curve. In addition, it was shown that the residual fluxes at each transformer limb could be estimated as if at least one point of the no-load curve, in the flux-current plane, is known. The use of inrush waveforms ensures the estimation of the nonlinear characteristics up to high saturation levels. The developed method provides an accurate, easily implemented means estimating transformer saturation characteristics. The estimated core nonlinear characteristics were used to simulate the energization of a three-phase transformer with Wye-Wye and with Wye-Delta connections. Simulations and measurements were performed for single-pole and simultaneous three-pole switching operations and were shown to be in close agreement. Moreover, it was shown that the obtained non-linear characteristics replicated the transformer's performance with different energization scenarios and arrangements. The close matching suggests that the method could be used for practical applications.

The single neutral resistor sequential energization arrangement was thoroughly investigated, and an improved neutral-resistor sizing criteria was developed. Extensive experimental, simulation and sensitivity analysis results for different transformer types and/or connections proved the scheme's effectiveness. A detailed study of the scheme's transient performance led to the development of a more precise neutral-resistor-sizing criterion. The following list summarizes the performance characteristics of the neutral-resistor-based sequential energization technique:

- ☐ The sequential energization technique is effective in reducing the inrush current level by more than 90% for all transformer types energized from the Yg side with a neutral resistor that is less than 10 times the total series reactance in the circuit.
- ☐ The maximum inrush current among the three phases decreases rapidly as the neutral resistor size is increased by small values. However, a sufficiently reasonable range of neutral resistor values capable of achieving an optimized inrush current reduction among all-three phases exists.
- ☐ For the second-phase energization, the inrush current magnitude is always lower than that for first-phase energization for the same neutral resistor value within the effective range of the neutral resistor values.
- ☐ The positive energization sequence was shown to be much less sensitive than the negative sequence to the variation of the neutral resistor's size. This decreased sensitivity leads to a wider range of effective neutral resistor values.
- ☐ For electrically or magnetically coupled transformers, the third-phase energization inrush current is directly proportional to the neutral resistor's size. Small neutral resistor values lead to an almost synchronous closing condition with minimal transients.

- For transformer banks with a Y-Y connection, the third energized phase behaves similarly to that of the second energized phase with an opposite sequence.
- Transformer-saturation characteristics play an important role in determining the maximum inrush current. However, within the range of typical saturation characteristics, the sequential energization scheme has close performance characteristics with respect to the maximum inrush current as affected by the neutral resistor size.
- It was shown that with a delta winding or an E-core structure, the zero sequence current leads the neutral resistor to be two times as effective in reducing the inrush current magnitude during second-phase energization.
- The scheme's main practical limitation was identified as the permissible rise of neutral voltage. A feasible application range for both dry-type and liquid-immersed transformers was proposed. The use of surge arresters to extend the scheme's application range was also presented.

The application of a single series-resistor scheme as an inrush-current-mitigation technique was presented. By using experimental, simulation and analytical studies, it was shown that the scheme is most applicable to transformers with un-grounded primaries. The scheme provides an effective solution to the problem of high inrush current magnitudes and, accordingly, presents a simple solution for independent power producers wishing to meet or exceed the requirements of the allowable maximum voltage sag level at the point of common coupling.

The scheme was shown to be capable of achieving 80% and 55% reduction in the inrush current magnitude for transformers energized from ungrounded-Wye and Delta connected primaries, respectively. For transformers energized from Wye-grounded primaries, the scheme is capable of reducing the inrush magnitude by 70% by using a single series resistor. For ungrounded primaries, a rapid energizing strategy of 5 cycles could be applied, which reduces the chances of developing the ferroresonance condition, without compromising the scheme's efficiency. The analytical-sizing procedures carried out for the sizing of the series resistor showed that a relatively small resistor size of 16 to 10 times the total series reactance in the energizing circuit was capable of achieving or exceeding the scheme's required performance. However, for transformers with grounded primaries, a rapid closing strategy could not be implemented with a small resistor size. Alternatively, the scheme could be applied for this connection with a simple point-on-wave closing after energizing the first phase with a small series resistor.

The appropriate sequential phase energization technique for inrush-current reduction could be applied based on the following conditions:

- ☐ For transformers with grounded-Wye primaries and sufficient insulation at the neutral, the simple neutral-resistor-based scheme could be directly applied based on the developed resistor-sizing criterion. Inrush-current reduction of more than 90% is achievable among the three phases. If an insulation limitation exists at the neutral or the neutral point is not accessible, a series resistor of the same size could be applied to the first energized phase with an achievable reduction of up to 70% compared to simultaneous closing. However, the last energized phase should immediately follow the second energized phase within a few cycles in order to minimize the chances of ferroresonance development.

- For transformers energized from Wye-ungrounded primaries, a single series resistor could be applied with sequential energization to achieve up to an 80% inrush-current reduction. For this application, the chances for ferroresonance development are low. However, within a few cycles, rapid closing could be implemented due to the fast equalization of the core flux after the first phase is energized. The resistor size is twice of that used for the neutral-resistor application.

- For delta-connected primaries, a single-series resistor could achieve an inrush-current reduction of up to 55%. The scheme in this case is applicable to single phase and core-type transformers due to the coupled electric circuit throughout the delta-connected primary.

The application of the sequential switching technique for transient-overvoltage mitigation due to capacitor switching was presented. The scheme's effectiveness is based on the reduction of the open-circuit contact voltage during the sequential switching procedure. The main conclusions can be summarized as follows;

- The single-stage R-L neutral impedance arrangement leads to an optimized open circuit voltage of 0.677 p.u., which results in a reduction of the switching transient overvoltage level to as low as 1.27 p.u..

- The dual stage R-L neutral impedance arrangement represents a self-synchronized switching mechanism where the open-circuit voltages during the second and third switching stages can be brought to zero independently of the switching instant. It was also shown that this arrangement can reduce the local transient over-voltages at the switched capacitor's location to 1.07 p.u..

- The proposed scheme's main limitation results from the requirement for an independent pole closure mechanism. Although requirement of a separate pole closure mechanism is the same as for synchronous controlled-switching schemes, the simple delay requirement for the presented scheme makes it easier to implement in already installed gang-operated breaker mechanisms.

An interesting subject for future research would be the methods for interfacing the developed transformer modeling technique with available simulation tools. The modeling of the magnetic circuit's behaviour by using reluctances results in the formation of an extended impedance-reluctance matrix that should be inverted at every time step. One of the possible ways to achieve the integration of such a model with readily available software would be to implement the model as a stand-alone independent algorithm and to integrate the model with the rest of the system through electrical nodes. Such a feature is already available in PSCAD/EMTDC. For simulation tools using the direct system formation through the Y or Z matrices, the R-Z matrix could be formed from initial solutions at the previous time step, and then reduced through nodal elimination into a Z matrix form. Afterwards, the reduced Z matrix or the inversion Y matrix could be directly used to represent the transformer as a simple three-phase element.

Another subject for future research would involve extending the developed transformer parameter estimation technique to multi-limb '4 and 5' core-type transformers. Moreover, the accuracy of the parameter-estimation technique increases the possibility of using a similar estimation technique for detecting and distinguishing of faults during transformer energization.

Although the sequential energization technique has been proved effective for inrush-current reduction, this technique has two main limitations. Because of the scheme's sequential energization, the possibility of ferroresonance development is high for some transformer connections. However, the scheme could be implemented with a simple point-on-wave energization for the second and third energized phases with a series resistor applied to the first energized phase. Only one voltage measurement with a suitable independent-pole breaker would be required for such an arrangement. For such a scheme, a considerable reduction in cost could be achieved for applications consisting of a large number of transformers to be energized. Potential applications already exist for wind farm transformers. These applications will, in turn, eliminate the requirement to measure the voltage and estimate the residual flux for each transformer independently.

10. References

[1] Westinghouse, "Electrical Transmission and Distribution Reference Book," Westinghouse, East Pittsburgh, Pennsylvania, USA, 1964.

[2] J. J. Winders, Jr. "Power Transformers Principles and Applications". Marcel-Decker, New York, 2002.

[3] Paul C. Y. Ling and Amitava Basak, "Investigation of Magnetizing Inrush Current in a Single-Phase Transformer", *IEEE Transaction on Magnetics*, vol. 24, No. 6, Nov. 1988, pp. 3217-3222.

[4] L. F. Blume, G. Camilli, S. B. Farnham and H. A. Peterson, "Transformer magnetizing inrush currents and influence on system operation" AIEE Transactions Power Apparatus Systems, vol. 63, pp. 366-375, Jan 1944.

[5] F. Huber, "Inrush Current of Distribution Transformers," Brown Boveri Review, Vol. 52, No.11/12, pp. 908-916, December 1965.

[6] G. Moraw, W. Richter , H. Hutegger and J. Wogerbauer, "Point-On-Wave Controlled Switching of High Voltage Ciruit Breakers," CIGRE paper 13-02, pp 1-6, September 1988.

[7] Allan Greenwood, Electrical transients in Power Systems, second edition, John Willey and Sons, 1991.

[8] James H. Harlow, Electric Power Transformer Engineering, CRC Press, 2004.

[9] Steurer, M.; Frohlich, K., "The Impact of Inrush Currents on the Mechanical Stress of High Voltage Power Transformer Coils," IEEE Transactions on Power Delivery, Volume: 17, Issue: 1, pp: 155 – 160, Jan. 2002.

[10] Adly, A.A.; "Computation of inrush current forces on transformer windings," IEEE Transactions on Magnetics, Volume: 37, Issue: 4, July 2001, Pages: 2855 – 2857.

[11] A.C. Franklin and D.P. Franklin, "The J&P Transformer Book 11th Edition," Butterworths, London, pp 549-641, 1988.

[12] N. Richard, N. Szylowicz, "Comparison Between a Permeance Network Model and a 2D Finite Element Model for the Inrush Current Computation in a Three Phase Transformer," IEEE Transactions on Magnetics, Vol. 30, Issue: 5, September 1994, Page(s): 3232–3235.

[13] L.F. Blume, Transformer Engineering, John Wiley and Sons, New York, London, 1957.

[14] AIEE Committee Report, "Report on Transformer Magnetizing Current and its Effect on Relaying and Air Switch Opertaion," AIEE Transactions, Vol. 70, pp 1733-1740, 1951.

[15] R.L. Bean, N. Chackan, H.R. Moore and E.C. Wentz, Transformers for the Electric Power Industry, McGaw-Hill, pp 80-110, 1959.

[16] P.M. Anderson, Power System Protection, John Wiley & Sons Canada, 1st edition November 1998.

[17] Westinghouse, "Applied Protective Relaying," Westinghouse Electric Corp., Relay-Instrument Division, 1982.

[18] H. Kan, "Reports Sponsored by study committees, Problems Related to cores of Transformers and Reactors, Report of the Discussion at the Colloquium of Study Committee 12 (Transformers), Electra No. 94, pp. 15-33, September 1983.

[19] N. Rajakovic, A. Semlyen, "Investigation of the inrush phenomenon: a quasi-stationary approach in the harmonic domain", IEEE Trans. Power Delivery, Vol. 4, Issue 4, pp: 2114 – 2120, Oct. 1989.

[20] P. Boss, J.L. Hermin, J.P. Uehlinger, G. Biasiutti, P. Muller, "Study on inappropriate transformer trippings by Buchholz relays", paper 12-102, CIGRE Paris session 1996.

[21] Bayless, R.S.; Selman, J.D.; Truax, D.E.; Reid, W.E.; "Capacitor switching and Transformer transients," IEEE Transactions on Power Delivery, Volume: 3, Issue: 1, Jan. 1988, Page(s): 349 –357.

[22] H.A. Khan, D.S. Johnson, J.H. Brunke, D.L. Goldsworthy, "Synchronous Closing Applications in Utility Transmission Systems", Paper 13-306 CIGRE session, Paris, France, pp 1-8, 1996.

[23] A. Hamel, G. St-Jean, M. Paquette, "Nuisance fuse operation on MV transformers during storms", IEEE Trans. Power Delivery, Vol. 5, Issue 4, pp:1866–1874, Oct. 1990.

[24] H.S. Bronzeado, P.B. Brogan, R. Yacamini, "Harmonic analysis of transient currents during sympathetic interaction", IEEE Trans. Power Systems, Vol. 11, Issue 4, pp: 2051-2056, November 1996.

[25] H. Bronzeado and R. Yacamini, "Phenomenon of sympathetic interaction between transformers caused by inrush transients", IEE Proceedings- Science, Measurement and Technology, Vol. 142, Issue 4, pp.:323–329, July 1995.

[26] M. Nagpal, T.G. Martinich, A. Moshref, K. Morison and P. Kundur, "Assessing and Limiting Impact of Transformer Inrush Current on Power Quality", IEEE Trans. Power Delivery, Vol. 21, No. 2, April 2006.

[27] E. Andersen, S. Bereneryd and S. Lindahl, "Synchronous Energizing of Shunt Reactors and Shunt Capacitors," CIGRE paper 1[illegible]12, pp 1-6, September 1988.

[28] R. Yacamini and A. Abu-Nasser, "The Calculation of Inrush Current in Three Phase Transformers", 17th Universities Power Engineering Conference, UMIST, paper 4A.6, pp: 31-40, 1982.

[29] Bellei, T.A., O'Leary, R.P., Camm, E.H., "Evaluating capacitor-switching devices for preventing nuisance tripping of adjustable-speed drives due to voltage magnification", IEEE Trans. Power Delivery, vol. 11, Issue 3, p.p. 1373 – 1378, July 1996.

[30] B. Holmgrem, R.S. Jenkins and J. Riubrugent, "Transformer Inrush Current", Cigre paper 12-03, Cigre, Paris, pp. 1-13, 1968.

[31] Slamecka, E. "Present and Future Designs of High-Voltage Circuit-Breakers and the Failure Rates Correlated Attempt of Survey and Outlook," Electra, No. 86, pp: 61-75.

[32] Alexander, R.W., "Synchronous Closing Control for Shunt Capacitors," IEEE PES, vol. PAS-104, no.9, pp 2619-2626, September 1985.

[33] Brunke, J.H., Schockelt, G.G., "Synchronous Energization of Shunt Capacitors at 230 kV", IEEE PAS A 78 148-9, 1978 IEEE Winter Power Meeting, New York, NY, pp: 1-4, 1978.

[34] CIGRE Working Group 13-07, Controlled Switching of HVAC Circuit-Breakers – Guide for Application, Part 1: ELECTRA, No. 183, April 1999, pp. 43-73. Part 2: ELECTRA, No. 185, pp. 37-57, August 1999.

[35] J. H. Brunke and J. Frohlich, "Elimination of Transformer Inrush currents by Controlled Switching – Part I: Theoretical Considerations," IEEE Transactions on Power Delivery, Volume: 16, No. 2, April 2001, Pages: 276-280.

[36] J. H. Brunke and J. Frohlich, "Elimination of Transformer Inrush currents by Controlled Switching – Part II: Application and Performance Considerations," IEEE Transactions on Power Delivery, Volume: 16, No. 2, April 2001.

[37] A. Mercier, E. Portales, Y. Filion and A. Salibi, "Transformer Controlled Switching Taking Into Account the Core Residual Flux, a Real Case Study," Cigre session 2002, 13-201.

[38] Koreman, C.G.A., "Determination of the magnetizing characteristic of three-phase transformers in field tests", *IEEE Transactions on Power Delivery*, vol.: 4, Issue: 3, July 1989, pp. 1779 – 1785.

[39] CIGRE WG A3.07, Controlled Switching of HVAC Circuit-Breakers: Guidance For Further Applications Including Unloaded Transformer Switching, Load And Fault Interruption And Circuit-Breaker Uprating, CIGRE Technical Brochure, January 2004.

[40] Boyle, D., "Interruption of Small Inductive Currents: Chapter 5: Switching of Unloaded Transformers, Part One: Basic Theory and Single-Phase Transformer Interruption without Reignitions", ELECTRA No. 133, pp. 99-107, December 1990.

[41] Harold A. Peterson, Transients in Power Systems, General Publishing Company, General Electric, 1951.

[42] S.G. Abdulsalam and W. Xu "A Sequential Phase Energization Method for transformer inrush current reduction, Transient Performance and Practical Considerations", IEEE Transactions on Power Delivery, vol. 22, No. 1, pp. 208-216, Jan. 2007.

[43] S.G. Abdulsalam and Wilsun Xu "Analytical Study of Transformer Inrush Current Transients and Its Application", Proceedings of the seventh International Conference on Power System Transients, June 19-23, Montreal, Canada. Paper No. IPST05-140.

[44] S.G. Abdulsalam, W. Xu, W. A. Neves and Xian Liu "Estimation of Transformer Saturation Characteristics from Inrush Current Waveforms", IEEE Transactions on Power Delivery, vol. 21, No. 1, pp. 170-177, Jan. 2006.

[45] S.G. Abdulsalam, W. Xu and V. Dinavahi "Modeling and Simulation of Three Phase Transformers for Inrush Current Studies", IEE Proceedings – Generation, Transmission and Distribution, vol. 152, No. 3, pp. 328-333, May 2005.

[46] W. Xu, S.G. Abdulsalam, Y. Cui, and X. Liu "A Sequential Phase Energization Method for transformer inrush current reduction, Part II: Theoretical Analysis and Design Guide", IEEE Transactions on Power Delivery, vol. 20, No. 2, Part 1, pp. 950-957, April, 2005.

[47] Y. Cui, S.G. Abdulsalam, S. Chen, and W. Xu "A Sequential Phase Energization Method for transformer inrush current reduction, Part I: Simulation and Experimental Results", IEEE Transactions on Power Delivery, vol. 20, No. 2, Part 1, pp. 943-949, April, 2005.

[48] S.G. Abdulsalam and W. Xu "Sequential Phase Energization Technique for Capacitor Switching Transient Reduction", IET proceedings - Generation, Transmission and Distribution, vol. 1, No. 4, pp. 596-602, July 2007.

[49] A. Boyajian, "Mathematical Analysis of Non-linear Circuits-Part I: Some Circuits Involving Saturation", General Electric Review (Schenectady, NY), September 1931, pp. 531-537.

[50] A. Boyajian, "Mathematical Analysis of Non-linear Circuits-Part II: Other Circuits Involving Saturation and Arc and Vacuum-Tube Circuits ", General Electric Review (Schenectady, NY), December 1931, pp. 745-751.

[51] T.R. Specht, "Transformer Inrush and Rectifier Transient Currents," IEEE Transactions on Power Apparatus and Systems, Vol. PAS-88, No. 4, pp. 269-279, April, 1969.

[52] T.R. Specht, "Transformer Magnetizing Inrush Current," AIEE Transactions, Vol. 70, pp. 323-327, 1951.

[53] M. Elleuch and M. Poloujadoff. "A Contribution to the modeling of Three Phase Transformers Using Reluctances". IEEE Transactions on Magnetics, Vol. 32, Mar. 1996, pp. 335-343.

[54] M. Elleuch and M. Poloujadoff, "New Transformer Model Including Joint Air Gaps and Lamination anisotropy," IEEE Trans. Magnetics, vol. 34, pp. 3701-3711, Mar. 1998.

[55] G. W. Ludwig and S. A. El-Hamamsy. "Coupled Inductance and Reluctance Models of Magnetic Components". IEEE Transactions on Power Electronics, Vol. 6, April 1991, pp. 240-250.

[56] M. Elleuch and M. Poloujadoff. "Anisotropy in Three-Phase Transformer Circuit Model". IEEE Transactions on Magnetics, Vol. 33, Sept. 1997, pp. 4319-4326.

[57] F. de Leon and A. Semlyen. "Efficient Calculation of Elementary Parameters of Transformers". IEEE Transactions on Power Delivery, Vol. 7, Jan. 1992, pp. 427-432.

[58] M. C. Williams, R. S. Vogelsong and K. S. Kundert. "Simulation and Modeling of Non-linear Magnetics". IEEE International Symposium on Circuits and Systems (ISCAS-1995), May 1995.

[59] L. O. Chua and K. A. Stromsmoe. "Lumped-Circuit Models for Non-Linear Inductors Exhibiting Hysteresis Loops". IEEE Transactions on Circuit Theory, Vol. 17, Nov. 1970, pp. 564-574.

[60] W. L. Neves; H. W. Dommel and Wilsun Xu; "Practical distribution transformer models for harmonic studies". IEEE Transactions on Power Delivery, Vol. 10, Apr 1995, pp. 906-912.

[61] B. A. Mork. "Five-Legged Wound-Core Transformer Model: Derivation, Parameters, Implementation and Evaluation". IEEE Transactions on Power Delivery, Vol. 14, Oct. 1999, pp. 1519-1526.

[62] Slow Transients Task Force of the IEEE Working Group on Modeling and analysis of Systems Transients Using Digital Programs, M. R. Iravani and Others. "Modeling and analysis Guidelines for Slow Transients-Part III: The Study of Ferroresonance". IEEE Transactions on Power Delivery, Vol. 15, Jan. 2000, pp. 255-265.

[63] H. W. Dommel, "Digital Computer Solution of Electromagnetic Transients in Single and Multiphase Networks". IEEE Transactions on Power Apparatus and Systems. Vol. 88, April 1969, pp. 388-399.

[64] H. W. Dommel. "Nonlinear and Time-Varying Elements in Digital Simulation of Electromagnetic Transients". IEEE Transactions on Power Apparatus and Systems, Vol. 95, 1976, pp. 1882-1891.

[65] W. L. Neves and H. W. Dommel; "On modeling iron core non-linearities", IEEE Transactions on Power Systems, Vol. 8, May 1993, pp. 417-425.

[66] M. J. Maron. "Numerical Analysis A Practical Approach"; Macmillan Publishing Company, 2nd ed., 1987.

[67] Leon O. Chua and Pen-Min Lin. "Computer aided analysis of electronic circuits: algorithms and computational techniques". Prentice-Hall, 1975.

[68] R J. Rusch and M. L. Good, "Wyes and Wye Nots of Three-Phase Distribution Transformer Connections," IEEE Conference Paper No. 89CH2709-4-C2, 1989.

[69] R. S. Bayless, J. D. Selman, D. E. Truax and W. E. Reid, "Capacitor Switching and Transformer Transients," IEEE Trans. Power Delivery, vol. 3, pp. 349-357, Jan. 1988.

[70] S. Calabro, F Coppadoro and S. Crepaz, "The Measurement of The Magnetizing Characteristics of Large Power Transformers and Reactors Through D.C. Excitation," IEEE Trans. Power Delivery, vol. 1 No. 4, Oct. 1986.

[71] E. P. Dick and W. Watson, "Transformer Models for Transient Studies Based on Field Measurements," IEEE Trans Power Apparatus and Systems. PAS-100, pp. 409-418, January 1981.

[72] J. Takehara, M.Kitagawa, T. Nakata and N. Takahashi, "Finite Element Analysis of Inrush Currents in Three Phase Transformers," IEEE Trans. Magnetics, vol. 23, No.5, sep. 1987.

[73] E. F. Fuchs, Y. You and D. J. Roesler, "Modeling and Simulation, and Their Validation of Three Phase Transformers with Three Legs Under DC Bias," IEEE Trans. Power Delivery, vol. 14, pp. 443-449, Apr. 1999.

[74] C. E. Lin, C. L. Cheng, C. L. Huang and J. C. Yeh, "Transient Model and Simulation in Three Phase Three-Limb Transformers," IEEE Trans. Power Delivery, vol. 10, No.2, APR 1995.

[75] E. F. Fuchs and Y. You. "Measurement of λ-I Characteristics of Asymmetric Three-Phase Transformer and Their Applications," IEEE Trans. Power Delivery, vol. 17, pp. 983-990, Oct. 2002.

[76] B. A. Mork. "Five-Legged Wound-Core Transformer Model: Derivation, Parameters, Implementation, and Evaluation," IEEE Trans. Power Delivery, vol. 14, pp. 1519-1526, Oct. 1999.

[77] A. Gaurdeau, P. Picher, L. Bolduc and A. Coutu, "No Load Losses in Transformer Under Overexcitation/Inrush Current Conditions: Tests and a New Model," IEEE Trans. Power Delivery, vol. 17, pp. 1009-1017, Oct. 2002.

[78] M. Elleuch and M. Poloujadoff, "Analytical Model of Iron Losses in Power Transformers," IEEE Trans. Magnetics, vol. 39, pp. 973-980, Mar. 2003.

[79] W. L. A. Neves and H. W. Dommel, "On Modeling Iron core Nonlinearities". IEEE Trans. Power Systems, vol. 8, pp. 417-425, May 1993.

[80] W. L. A. Neves and H. W. Dommel, "Saturation curves of delta-connected transformers from measurements", IEEE Trans. Power Delivery, vol. 10, pp. 1432-1437, Jul. 1995.

[81] M. A. Rahman and A. Gangopadhayay. "Digital Simulation of Magnetizing Inrush Currents in three phase transformers," IEEE Trans. Power Delivery, vol. 1, Oct. 1986.

[82] IEEE Std C57.12.00-2000, "IEEE standard general requirements for liquid-immersed distribution, power, and regulating transformers", 2000, pages 1-53.

[83] IEEE Std C57.12.01-1998, "IEEE standard general requirements for dry-type distribution and power transformers including those with solid cast and/or resin-encapsulated windings", 31 Dec. 1998.

[84] ANSI/IEEE Std 32-1972, "IEEE standard requirements, terminology, and test procedure for neutral grounding devices", 1972.

[85] British Columbia Transmission Corporation, "69kV to 500kV Interconnection Requirements for Power Generators", May 2004.

[86] BC Hydro, "35kV and Below Interconnection Requirements for Power Generators", June 2004.

[87] J.J. Lee and M.S. Cooper, "High-Energy Solid-State Electrical Surge Arrestor" IEEE Transactions on Parts, Hybrids and Packaging, Vol. PHP-13, No. 4, Dec. 1977

[88] Martinez, M.L.B.; Zanetta, L.C., Jr.; "A proposal to evaluate the energy withstand capacity of metal oxide resistors", High Voltage Engineering, 1999. Eleventh International Symposium on (Conf. Publ. No. 467) ,Volume: 2 , 23-27 Aug. 1999 Pages:309 - 312 vol.2

[89] Manuel Martinez and Luiz Zanetta, “On Modeling and Testing Metal Oxide Resistors to Evaluate The Arrester Withstanding Energy”, Dielectric Materials, Measurements and Applications Conference Publication No. 473, IEEE 2000.

[90] Ralph H. Hopkinson, “Ferroresonant Overvoltage Control Based on TNA Tests on Three-Phase Wye-Delta Transformer Banks”, IEEE Trans. Power Aparatus and Systems, vol. PAS 87, No.2, pp. 353-361 Feb. 1968.

[91] D. Kundu, “Technical Requirements to Connect Parallel Generators to the Ontario Hydro Distribution Electrical System”, IEEE Tans. On Energy Conversion, Vol.7, No. 1, p.p. 8-14, Mar. 1992.

[92] C. J. Mozina, “Interconnect Protection of Dispersed Generators”, IEEE Tans. On Industry Applications, Vol.37, No. 3, p.p. 681-688, May-June 2001.

[93] R. A. Walling, K. D. Barker, T. M. Compton, and L. E. Zimmerman,“Ferroresonant overvoltages in grounded wye-wye padmount transformers with low-loss silicon-steel cores,” IEEE Trans. Power Delivery, vol. 8, no. 3, pp. 1647–1660, July 1993.

[94] R.A. Walling, R.K. Hartana, and W.J. Ros, “Self-generated overvoltages due to open-phasing of ungrounded-wye delta transformer banks” IEEE Trans. Power Delivery, vol. 10, no. 1, pp. 526-533, Jan. 1995.

[95] R.A. Walling, “Ferroresonance in low-loss distribution transformers,” IEEE Power Engineering Society General Meeting, 2003, vol. 2, 13-17 July 2003.

[96] P. Ferracci, “Ferroresonance”, Group Schneider: Cahier no 190, pp. 1-28, March 1998.

[97] Adams, R.A., Middlekauff, S.W., Camm, E.H. and McGee, J.A., “Solving customer power quality problems due to voltage magnification”, IEEE Trans. Power Delivery, vol. 13, Issue 4, p.p.1515 – 1520, Oct. 1998.

[98] Bellei, T.A., O'Leary, R.P., Camm, E.H., “Evaluating capacitor-switching devices for preventing nuisance tripping of adjustable-speed drives due to voltage magnification”, *IEEE Trans. Power Delivery*, vol. 11, Issue 3, p.p. 1373 – 1378, July 1996.

[99] Dick, E.P., Fischer, D., Marttila, R. and Mulkins, C., “Point-on-wave capacitor switching and adjustable speed drives” *IEEE Trans. Power Delivery*, vol. 11, Issue 3, pp. 1367-1372, July 1996.

[100] A. J. Schultz, I.B. Johnson, and N. R. Schultz, "Magnification of Switching Surges," *IEEE Trans. Power Apparatus and Systems*, vol. 77, February 1959, pp 1418-1425.

[101] McGranaghan, M.F.; Zavadil, R.M.; Hensley, G.; Singh, T.; Samotyj, M.; “Impact of utility switched capacitors on customer systems-magnification at low voltage capacitors”, IEEE Trans. Power Delivery, vol. 7, Issue 2, p.p. 862 – 868, April 1992.

[102] Jasper J. Goedbloed, “Transients in Low-Voltage Supply Networks”, IEEE Trans. Electromagnetic Compatibility, vol. EMC-29, No.2, pp. 104-115, May 1987.

[103] IEEE Standard 399-1990, “IEEE Recommended Practice for Industrial and Commercial Power System Analysis”, IEEE, New York, 1990.

Appendix

Laboratory Transformer 30kVA, 208/208, Yg/Δ, 3-legged core

Open circuit and Short Circuit tests

Open Circuit Test:

V_{rms} (V)	I_{rms} (A)	I-peak	P (W)	S (VA)	Q (VAr)
10.1	0.731	0.159	0.49	0.73	0.55
20.65	0.110	0.221	1.74	2.29	1.49
30.27	0.147	0.279	3.46	4.44	2.77
39.9	0.181	0.300	5.77	7.2	4.32
50.05	0.221	0.310	8.88	11.1	6.6
59.7	0.268	0.376	12.7	16.1	9.9
70.1	0.327	0.457	17.4	22.9	14.9
81.2	0.441	0.705	23.6	35.8	26.9
90.4	0.75	1.275	30	67	60
94.9	1.054	1.791	34	100	94
100	1.492	2.238	40	149	144
105.3	1.926	3.081	40	203	199
109.8	2.495	4.241	50	272	267
115.8	3.018	4.828	8.3	351	351
118.6	3.625	5.437	52	434	431

Short Circuit Test:

V_{rms} (V)	I_{rms} (A)	pf	P (W)	S (VA)	Q (VAr)	R_{SC}	X_{SC} (Ω)	L_{SC} (H)
0.268	7.61	0.73	1.53	2.1	1.4	0.026419	0.024175	6.412E-05
0.354	10.05	0.73	2.48	3.5	2.4	0.024554	0.023762	6.303E-05
0.61	17.21	0.73	7.45	10.1	7	0.025153	0.023634	6.269E-05
0.805	22.63	0.73	13.09	18.2	12.5	0.025561	0.024408	6.474E-05
1.081	30.08	0.73	23.63	32.4	22.2	0.026116	0.024536	6.508E-05
1.232	34.43	0.73	31.7	43.7	30	0.026741	0.025307	6.713E-05